AN INVESTIGATION OF THE COMBUSTION KINETICS OF COAL-MICROALGAE COMPOSITE

BY

O. V. EJESIEME

(BSc. Hon. Ind. Chem., PgCert. Bus. Mgt., BSc. Hon. Form. Sci., MSc. (Research) Chem.)

Email: ejevit@yahoo.com , s211266744@mandela.ac.za

PhD Chemistry (Research), 2018

Nelson Mandela University, Port Elizabeth, South Africa

Promoter: The late Professor Ben Zeelie

Director of InnoVenton Institute for Chemical Technology and Downstream Station,

Nelson Mandela University

Promoter: Dr Gary Dugmore

Deputy Director of InnoVenton Institute for Chemical Technology and Downstream Station, Nelson Mandela University

Co-Promoter: Dr Nicole Vorster

Head of Formulation Science, InnoVenton Institute for Chemical Technology and Downstream Station, Nelson Mandela University

TITLE

AN INVESTIGATION OF THE COMBUSTION KINETICS OF COAL-MICROALGAE COMPOSITE

BY

EJESIEME VITUS OBIALO

Student number: 211266744

A thesis submitted to the faculty of Science, Nelson Mandela University,

Port Elizabeth South Africa in fulfilment of the requirements for the degree of

PHILOSOPHY OF SCIENCE, CHEMISTRY

December: 2018

Declaration

I declare that this thesis is my own original work and that it has not been submitted before for any degree or examination in any other University.

 ….. (Signature)

03/09/2018… (Date of signature)

Abstract

Coal mining and handling generate sizeable quantities of ultra-fine coal particles which are heaped as discard material. Use of the ultra-fine coal for co-firing with microalgae biomass appears to be a promising option that would improve combustion of the discard. There is no available traditional biomass binder that can be used to agglomerate, reclaim, and co-fire the discard ultra-fine coal to generate heat. In a recent research, microalgae biomass was identified as an effective natural binder for discard ultra-fine coal. Biomass is a renewable resource, and many have been co-fired on a large scale except microalgae biomass. Researchers have studied co-firing of dry mixed coal-microalgae, however, the kinetics of a wet mix of microalgae biomass and ultra-fine coal, "Coalgae®" patented recently by the Nelson Mandela University needs to be explored.

The study aimed at investigating in some detail the oxidation mechanism of coal-microalgae composites. The objective is to understand the impact of microalgae on the kinetic properties of coal which will inform on the application of "Coalgae®". It involves correlating the small and large-scale combustion properties that will establish the co-firing option on an industrial scenario. The goal is to utilize all grades of discard ultra-fine resource using microalgae biomass as binder and a renewable component which enhances the combustion of coal to supply heat and electricity. The use of microalgae for fuel preparation and upgrading is on the increase due to its high growth potential, reactivity, and ability to store energy more than other biomasses. This research hypothesized that blending of discard ultra-fine coal with live microalgae biomass would improve the kinetic properties of the coal more than expected from linear combination of the dry materials.

Thermogravimetric combustion of "Coalgae®" was studied under non-isothermal conditions from 40 °C to 900°C at a heating rate of 15 °C/min and air flow rate of 20 ml/min. The thermogravimetric combustion properties *i.e.* small-scale was related to the large-scale, John Thompson's fixed-bed reactor under the above condition. Thermal profiles were transformed into a differential function to reveal overlapped combustion events. The Coat-Redferns kinetic model was applied on the non-de-

convoluted reactions set to obtain some of kinetic parameters. The Fraser-Suzuki equation was used to de-convolute the overlapped combustion. Then, rate law combined with Arrhenius equation was used to derive the activation energy E_a and pre-exponential factor A, while the integral form of solid states reaction model, g ($\propto$) was applied to deduce the oxidation mechanism.

The composite formed a strong and partly renewable blend under controlled temperature conditions, unlike assorted dried biomass mixed with coal. Microalgae biomass upgraded the fuel and kinetics properties of ultra-fine coal more than what was expected from a linear combination. It released heat that promoted the oxidation mechanism of the discard coal. The main effect is that the “Coalgae®” is significantly ($p = 0.0570$) more reactive than the coal.

The co-firing approach is partly renewable and contributes to the utilization of high and low-quality available discard ultra-fine coal. It advances the combustion of coal resources and reduces carbon dioxide, CO_2 emission attributed to global warming as well as preserves the natural biomass sources. The combustion of “Coalgae® “will improve economy, environment, and health, heat, and electricity supply to the society.

Key words: Coalgae®, co-firing, deconvolution, ultra-fine coal, kinetics, mechanism, microalgae.

Acknowledgements

The joy of completion comes as I think of how I started, and remembered God, organisations, friends, families, and colleagues that helped me in one way or the other. Seven years of study at the Nelson Mandela University with all the hurdles added to the joy of developing the Coalgae Technology, was one of the most valuable experiences. It made me to sacrifice like the Mandela of Robin Island, with hope, faith, and patience to develop the combustion kinetics that can improve clean energy supply.

I give Jehovah all the glory for direction, grace, ideas, love, and His presence in the time of need. He guided and constructed this piece so that the audience can easily find what they need and understand what they find. With my hands, He carved and merged all the ideas into an art and chemical science masterpiece.

I thank Prof Andrew Leitch, Dealtry Gill Gerber, Campbell Eileen, Louis Vincent, Paul Watts, Tshentu Zeni, who supported me. Heartfelt gratitude, to my supervisors' Dr Nicole Vorster, Dr Gary Dugmore, and especially The Late Prof Ben Zeelie who have helped, trained, and mentored me for 7years. He taught me that everything is a process, we work to make things work, and he showed me how to upscale. Thank you so much Ben Zeelie, may your soul rest in peace. Thanks to Mr Bosma, for his patience, hardwork and time on data analysis. He taught me statistics and made to see numbers beyond their shapes. Thanks to the students and staff at InnoVenton.

I thank the Department of Science and Technology DST, National Research Foundation NRF, InnoVenton Institute for Chemical Technology, the Research Capacity Development RCD for funding. My thanks go to Mrs Noelene, the quality assurance manager of Aberdare Cables, for giving me the opportunity to use their laboratory. Thanks to Beth De Maagd and Joe D'Amico of the United States for helping me, and to my friends Engineer Peter Odedeyi and Dr Faith Akwi for great ideas.

I am grateful to my parents for their love and years of investment on me. Thank you, my father Mr Ejesieme Okorie for inculcating the spirit of determination. Thank you, mom Mrs Livina Ejesieme, my first chemistry teacher and for dedicating your business for my education. Thank you so much my beloved wife Amara for hard-work, prayers and support, and our son Ellis Chimeremeze David for being there while I write.

Table of contents

List of Figures

List of Tables

List of symbols

- A = Ash
- *A* = Microalgae biomass (Algae)
- Ad = Ash dry basis
- Al = Aluminium
- ANOVA = Analysis of variance
- ASTM = American standard test method
- AUD = Australian dollar
- A* = Pre-exponential factor (in equations)
- a_0 = Amplitude of curve
- a_1 = Centre of the curve
- a_2 = Width of curve
- a_3 = Shape of the curve
- $(\propto)$ = Degree of conversion
- B = Mass of sample after drying
- β = Constant heating rate, dT/dt
- β = Constant heating rate
- CO_2 = Carbon dioxide
- “Coalgae® “ = Coal-microalgae blend
- CO = Carbon monoxide
- CH_4 = Methane
- C=O = Carbonyl group
- C = Carbon
- c = Intercept
- Coal A = Eskom low quality ultra-fine coal
- Coal B = Exxarro high quality ultra-fine coal
- *C* = Coal
- C=C = Double bonds
- C-H = Single bonds
- C* = Mass of test sample after heating

- $C_v(n)$ = Heat capacity (J/^oC) of the vessel
- ccc or S – value = Comprehensive combustion characteristics index
- C #clusters/100 = Average # of Aromatic C's per cluster
- DST = Department of Science and Technology
- DSC = Differential scanning
- DTGA = Differential TGA
- DTG_{max} = $\left(\frac{dm}{dT}\right)$ at maximum combustion
- D1 = One dimensional diffusion mechanism
- D2 = Two-dimensional diffusion
- D3 = Three-dimensional diffusion
- D4 = Jander's or Ginstling–Brounshtein's equation
- da = Dry solid of algae
- dc = Dry solid of $c$oal
- $(\frac{dm}{dt})c$ = Rate of combustion of coal
- $(\frac{dm}{dt})b$ = Rate of combustion of biomass
- $\left(\frac{dm}{dt}\right)_{mix}$ = Rate of combustion of mix
- $\left(\frac{dm}{dt}\right)_{max}$ = Maximum combustion velocity
- $\left(\frac{dm}{dt}\right)_{mean}$ = Average combustion velocity
- $\left(\frac{d\alpha}{dt}\right)$ = Rate of degradation *i.e.* conversion of solid fuel
- DTG_{mean} = Mean burning velocity
- $(dm/dT)_c$ = Rates of combustion of coal
- $(dm/dT)_a$ = Rates of combustion of microalgae biomass
- da = % solid for microalgae biomass
- d b = Dry basis
- dc = % solid for coal
- $DA1$ = Area of trapezium for L
- $DA2$ = Area of trapezium for H
- df = Degree of freedom
- $\Delta T_{1/2}$ = Width of combustion at half temperature range
- δ+1 = # of Attachments per cluster

- E_a = Activation energy
- Euro = European currency
- $E_{TS\,(c)}$ = Energy based on thermodynamic model of calorimeter
- F = Mass of crucible and ash
- FC = Fixed carbon
- FM = Free moisture content
- FTIR = Fourier transform infra-red
- f (∝) = Temperature-independent function of conversion
- $f(\propto)$ = Differential model
- f_a = Fraction Aromatics
- f_a* = Corrected Fraction Aromatics (excl. CO)
- f_{al} = Fraction Aliphatic
- f_{al} o = Fraction Aliphatic C's bonded to Oxygen
- f_a co = Fraction CO
- $f_{a\,P}$ = Fraction Phenolics
- $f_{a\,S}$ = Fraction Alkylated Aromatics
- f_{al}^{N} = Fraction Non-Protonated C's in Aromatic region
- f_{al}^{H} = Fraction Protonated C's in Aromatic region
- f_a^{B} = Fraction Bridgehead C's
- f_{al}^{N*} = Fraction Non-Protonated C's + Methyl in Aliphatic
- f_{al}^{H} = Aliphatic CH+CH_2
- G = Mass of empty crucible
- g (α) = Integrated form of f (α)
- g $(\propto)$ = Solid states reaction model
- H = Hydrogen
- HHH = Higher heating value
- H = High temperature scheme Y_2
- 100 = 100 % Algae
- InnoVenton = Institute for Chemical Technology
- K-boilers = Parallel co-firing system
- kg/m^3 = Fuel density

- kg = Kilogramme
- kW/h/m^2 = Kilo watt hour per meter square
- K = Degree Kelvin
- K = Potassium
- $K_v b$ (n) = Thermal conductance (J/^oC)
- k-t = Kilo tonne
- k = Rate constant related to the Arrhenius
- L = Litres
- L = Low temperature scheme, *i.e.* Y_1
- (ln) = Natural log function
- $(\log_e)y$ = logs to base e, $= e^x \text{ or } y = e^{-x}$
- MJ/kg = Mega joules per kilogramme
- M_C = Mass of coal
- M_{mix} = Mass of theoretical mix
- Mg = Magnesium
- Mn = Manganese
- m = Slope
- m_0 = Initial mass of sample
- m_t = Mass of sample at time, t
- m_f = Final mass of sample
- m = Mass of sample
- m_0 = Initial mass at starting temperature T= 40 ^oC
- m_T = Mass at temperature T
- m_f = Final mass at temperature (T_f = 900 ^oC)
- Mm = Millimetre particle size
- Mt = Metric tonne
- MHz = Frequency in mega Hertz
- m_T = Total mass of mixture
- M = Moisture (%)
- MJ/ kg = Mega Joules per kilogramme
- µm = Micron meter
- N = Nitrogen

- NMU = Nelson Mandela University
- NRF = National Research Foundation
- NOx = Nitrogen oxide
- NMR = Nuclear Magnetic Resonance
- No. = Number of observations, (n)
- n = Reaction index, or order
- $\eta_{b,char}$ = Fraction of biomass char
- $\frac{\eta_b}{\eta_{coal}}$, = Fraction of coal that burnt completely
- O = Oxygen
- O1, O2, and O3 = First, second and third reaction order mechanism
- Obs. = Observed
- -OH = Hydroxyl group
- PP = Repowered pre-furnace
- PAH = Polyaromatic hydrocarbons
- P_c = Co-firing ratio (*i.e.* the share) of coal
- P_b = Co-firing ratio (*i.e.* the share) of biomass
- p = Dry mass of microalgae biomass
- Pred. = Predicted, (theoretical)
- % S = Solids in (moist) wet samples
- % wt. = Weight percent
- q = Dry mass of coal
- R = Molar gas constant = 8.314 J/mol. K
- RCD = Research Capacity Development
- RS = Raman spectroscopy
- RG = Biomass gasifier
- R2 = Phase boundary mechanism, contracting area
- R3 = Phase boundary mechanism contracting volume
- R^2 = Correlation co-efficient
- R c = Rate of combustion of composite
- $\left(\frac{R_{max}}{T_{ig}{}^2}\right)$ = Ignition index
- $\left(\frac{R_{max}}{T_{ig}T_f}\right) R_{max}$ = Comprehensive combustion characteristic index

- S = Sulphur
- SS = Sum of standard residuals
- SO_x = Sulphur oxide
- SCR = Selective catalytic reduction
- T = Temperature
- T_{ig} = Ignition temperature
- T_f = Burn-out temperature.
- TG = Thermogravimetry
- TGA = Thermogravimetric analysis
- t = Time
- TCD = Thermal conductivity detectors
- $T_v(n)$ = Calculated temperature (^oC) at time interval n
- $T_b(n)$ = Measured temperature (^oC) at time interval n
- T_{max} = Peak temperature
- T_h = Burn-out
- Theo. = Theoretical
- US$ = United States dollars
- V = Volatile
- Vd = Volatile dry basis
- VLOOKUP = An excel function
- $v\,m_b$ = Observed values of volatiles for biomass
- $v\,m_c$ = Observed value of volatiles for coal
- W = Mass (g) of sample
- x = Mass of microalgae biomass (slurry)
- XANES = X-ray absorption near edge structure
- XRD = X-ray diffraction
- X_b = Mole fraction of Aromatic Bridgehead C's
- y = Mass of wet coal
- y_{CR} = Coats and Redfern kinetic model,
- Y_1 = Devolatilization stage, L.
- Y_2 = Char combustion stage, H
- Y_{FS} = Frasier-Suzuki equation

- Y_G = Gaussian
- Y_L = Lorentzian
- Y_W = Weibull
- 0 (%) = 100 % coal

List of patents, manuscripts, and conferences

This work produced patents, manuscripts, conference papers and have been showcased in exhibitions under the “Coalgae Technology” trademark, based on the PhD research. The study is the outcome of my research at the Nelson Mandela University from October 2014 to September 2018. The pilot scale combustion was successful and some of the research outcome was presented in South Africa, United Kingdom, United States of America, and other papers are in progress.

Patents

1. Upgrading coal fines using microalgae - PCT/IB2014/061295

2. Processing Carbonaceous Materials - US20160289567A1

Dissertation

Evaluating the effect of microalgae biomass on the combustion characteristics of coal.

Vitus Ejesieme; Ben Zeelie., (2014)

Manuscript

1. Reclamation of discard ultra-fine coal with microalgae biomass, and combustion properties of the composite: Coalgae®
2. Kinetic study of Coalgae® fuel under non-isothermal condition in O_2/CO_2 atmosphere. Vitus Ejesieme; Ben Zeelie. In Progress (2018)

Conference presentations

Paper 1. Evaluating the effect of microalgae biomass on the combustion of coal. Vitus Ejesieme; Ben Zeelie, 5th Cofiring biomass with coal workshop, Drax Power Station, Selby, United Kingdom, (2015).

Paper 2. Evaluation of the combustion behaviour of coal-microalgae biomass blends, Vitus Ejesieme; Ben Zeelie, International Renewable Energy Conference, University of Fort Hare, South Africa. Fort Hare, (2016).

Paper 3. An investigation of Combustion kinetics of coal-microalgae biomass fuel “Coalgae®”, Vitus Ejesieme; Ben Zeelie, The 34th Annual International Pittsburgh Coal Conference, United States, (2017).

Exhibition – 1. “Coalgae” Technology”, Vitus Ejesieme; Ben Zeelie, International Renewable Energy Conference, Cape Town, South Africa (2015). 2. “Coalgae Technology”, Vitus Ejesieme; Ben Zeelie, Renewable Energy Conference, University of Fort Hare, South Africa (2016).

Chapter 1

1.0 Introduction and literature review

1.1 Introduction

The combustion of fuel for heat and electrical energy is fundamental for the development of all the countries in the world (1). Heat and electricity are identified as strategic commodities for sustainable economic advancement (2). The combustion of solid, liquid and gaseous fuels is a well-developed practice for household cooking, space heating, and for generating electricity (3). South Africa and many countries around the globe utilize large quantities of solid fuels such as biomass, and coal annually to generate heat and electricity (4). The consumption of coal may be declining in some countries, but the use of coal as fuel is expected to remain for several decades (5), (6), (7), and (8), until alternative energy sources completely replace coal. The combustion of coal is not a clean chemical process so it releases carbon monoxide CO, and dioxide CO_2, methane CH_4, nitrogen oxide NO_x, and sulphur oxide SO_x into the atmosphere (9), (10), (11). This is partly due its composition, and the inability of coal to achieve a complete combustion. Combustion of coal affects the environment, reduces health standard, and deprives users the access to clean air. On the other hand, biomass provides clean air, consumes CO_2 during growth, and releases same amount of CO_2 through combustion. The growing of biomass, and combustion of coal together with biomass is accepted worldwide to reduce CO_2 emission (12), (13), (14).

Combustion of coal-microalgae biomass have not been fully utilized for power generation. In conventional power stations, only coal is combusted to generate electricity, however, biomass co-firing has been confirmed to improve the combustion of coal (15), (16), (17). Co-firing is considered as the lowest risk and cost option for combustion of coal (18), (14). Combustion heat is used to produce steam in industrial boilers which drives turbines that generate most of the world's electrical power. This research explored the combustion kinetics of coal-microalgae biomass which was wet

blended as compared to the linear combination of the original materials, and to coal. The intention of the research was to introduce coal-microalgae biomass as one fuel in households and utility boilers, unlike dry mixed coal-biomass usually co-fired. This chapter reviews the available literature, and describes the aims and objectives, structure, problem statement, hypothesis, and scope of the research.

The literature review provides an overview on the combustion of coal with biomass. First, it describes the concept of co-firing, driving forces for the practice, biomass properties, advantages, and challenges. Second, it explains the combustion of coal, properties of coal that makes co-firing effective, effects of biomass on coal and the influence of co-firing on the combustion characteristics of coal. Third, it considers how biomass affects the ignition temperature, comprehensive combustion index, reaction rate, and activation energy of coal. Fourth, the chapter describes how to investigate the effects of biomass on the combustion of coal and how to derive combustion characteristics. It provides an overview on thermogravimetry, kinetic modelling, deconvolution processes and solid states oxidation mechanisms.

Biomass and coal are among the oldest materials used to generate household heat. Heat production is a component of the energy system that drives modern societies. Biomass and coal may be combusted in utility boilers to generate steam that drives turbines to produce electricity. Recently, the combustion of biomass together with coal, simply known as co-firing, have become the method of choice in power stations to reduce the environmental impact of coal (15), (16). A novel fuel mixture of discard ultra-fine coal and microalgae biomass, prepared at InnoVenton, Nelson Mandela University in earlier research, indicated improved combustion behaviour as compared to the parent coal (19). In this research, '**microalgae biomass'** was referred to as **algae** while all composites of coal with algae referred to as **Coalgae®**. The work reported in this thesis is aimed at exploring the combustion behaviour of Coalgae® with the view to evaluate whether the treatment of ultra-fine coal with live microalgae resulted in a fuel with an improved combustion behaviour compared to a fuel with a simple blend of coal and biomass.

Combustion is a natural phenomenon where a combustible material is ignited in the presence of oxygen to produce heat, water, flue gas and a solid residue (ash). The combustion of liquid, gaseous and solid fuels provides heat as the most important

product whereas water, flue gas, carbon dioxide and ash are byproducts(20). In some cases, the combustion of fuel produces a flame at the point of ignition, proceeds as a continuous event and terminates at burn-out. Combustion rarely occurs in a single step, but rather as a series of steps that are defined by the nature of the fuel and the actual mechanism of combustion. Generally, the terms combustion and burning of materials have different interpretations. Though both events comprise a series of complex and overlapping chemical reactions, burning is generally used to refer to combustion in an uncontrolled environment, while the term combustion describes a controlled thermal reaction.

Combustion involves one or more rapid thermal events that strive to achieve a stable kinetic state. The composition of a fuel and the rate it approaches kinetic equilibrium, during combustion determines the completeness of the process and its level of pollution.

The development and design of efficient combustor systems require a detailed knowledge of the complete combustion kinetics of specific fuels. Combustion kinetics explains how fast a series of steps progress across the entire temperature range of the process from ignition through to burn-out (21). The development of a reaction mechanism does not only assist in the formulation of optimal fuels, but also allows prediction of emissions over a wide range of combustion conditions that are appropriate to various types of combustors.

Coal is a combustible rock formed from the accumulation and partial decomposition of vegetation under pressure. Coal stores a large amount of energy, which is released on combustion to produce heat for heating, cooking, and to generate electricity. Microalgae are microscopic and photosynthetic organisms that have the potential to store solar energy in the form of biomass more efficiently than any other photosynthetic plants or organisms (22). This research focused on the action of microalgae biomass on the combustion behaviour of discard ultra-fine coal. The discard ultra-fine coal is generated in large quantities (19), (23). The research motivation includes to use microalgae biomass to upgrade abundant waste coal (19), and low ranked coal, and to grow this biomass with carbon dioxide CO_2, from air or from the combustion of coal-microalgae. The waste and low ranked coal presents a significant economic loss and environmental hazard. The discard ultra-fine is dusty,

can be blown into air, washed into rivers, burns spontaneously, releases emission (24), (25) and low ranked coal accounts for 47 % of global reserve (26).

Apart from recovering the resources, to blend microalgae biomass with coal offers a potential low cost, low risk option to reduce the impact of coal combustion (26). At the same time, extending the lifetime of coal as a viable energy resource is required to meet the world's demand for energy. The co-firing of coal together with microalgae biomass and the expected benefits through reduced environmental effect of firing coal, may impact significantly on the use of coal as energy resource. The increasing world population results in a considerable increase in demand for energy. The Royal Dutch Shell Oil and Gas Company predicts that by 2050 the number of people on the planet would grow to about 9 billion, *i.e.* about 2 billion more than today (27). The renewable and nuclear energy sources would not be able to completely replace fossil fuels whilst meeting the ever increasing demand for energy (28).

1.2 Concept of co-firing biomass (microalgae biomass) with coal

For energy generation, co-firing is widely accepted as an option to improve the combustion, and reduce the emission from coal (17). The combustion of coal with any kind of biomass is known as co-firing (15).

There are more than 200 co-firing operations , Table 1.1, worldwide (29). In the United States, about 80 power plants with high potential to expand the technology have been reported (18).

Table 1.1: A summary of biomass co-firing worldwide (29)

Worldwide biomass co-firing power plant (29)							
-	**BFB**	**CFB**	**CFB/BFB**	**Grate**	**PF**	**unknown**	**Total**
Australia	0	0	0	0	8	0	8
Austria	0	3	0	1	1	0	5
Belgium	0	0	0	0	1	0	1
Canada	0	0	0	0	7	0	7
Denmark	0	1	0	4	7	0	12
Finland	42	13	6	4	10	6	81
Germany	0	0	0	1	4	22	27
Indonesia	2	0	0	0	0	0	2
Italy	0	0	0	0	6	1	7
Netherlands	0	0	0	0	6	0	6
Norway	0	1	0	0	0	0	1
Spain	0	1	0	0	0	0	1
Sweden	3	7	0	2	3	0	15
Taiwan	0	1	0	0	0	0	1
Thailand	0	1	0	0	0	0	1
UK	0	2	0	0	16	0	18
USA	1	5	0	5	29	0	40
Total	48	35	6	17	98	30	234

CFB = circulating fluidised bed, FBC = fluidised bed combustion, GF = grate fired, PF = pulverized fuel

Co-firing means to blend biomass with coal at different ratio and a global review of the activity has been reported (18). It also describes the blending of biomass (including macro and microalgae) with coal at various ratio to generate clean electricity relative to coal. The practice reduces the consumption of coal, emission and improves combustion of coal (15), (16). The concept of microalgae biomass co-firing (30) in coal fired power station could be illustrated as in Figure 1.1 (30).

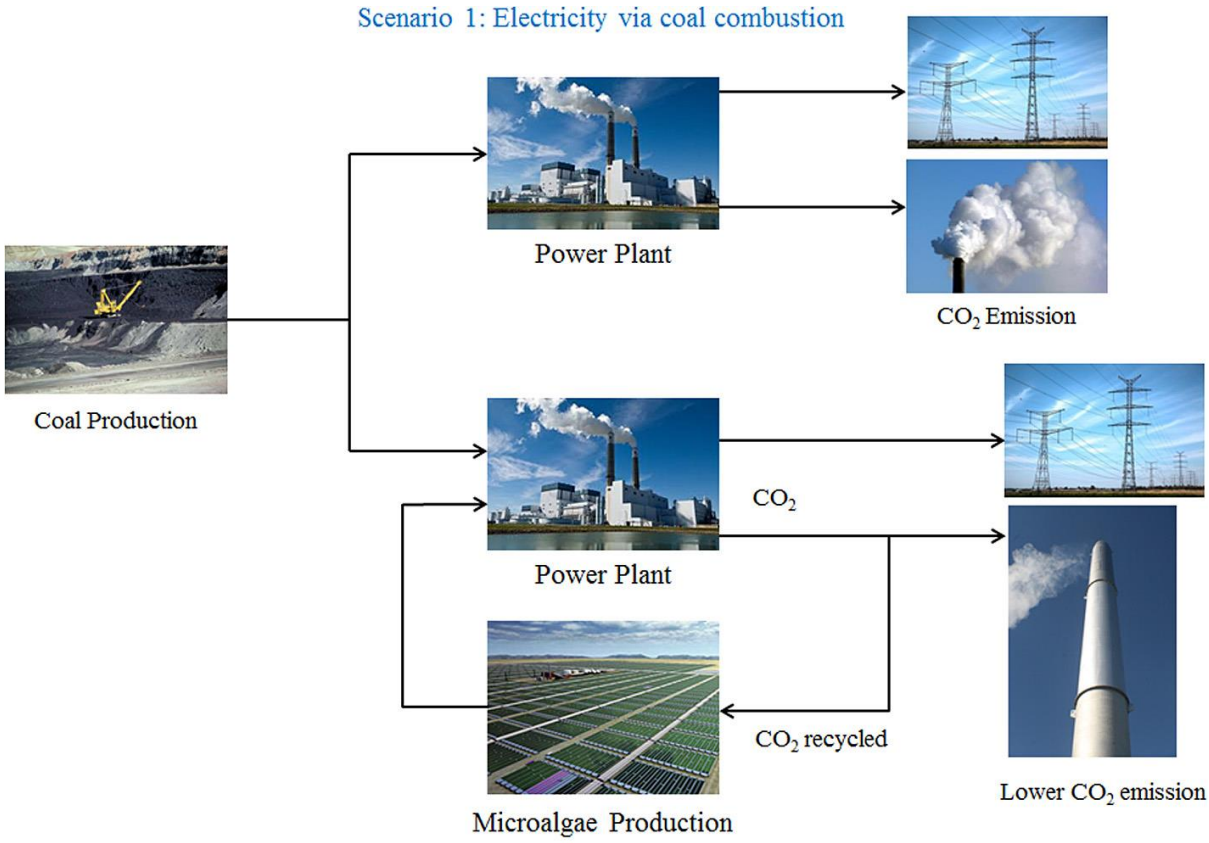

Figure 1.1: The use of coal-microalgae biomass to generate electricity (30)

The Figure 1.1 shows a second scenario that used coal-microalgae biomass in coal power plant to generate electricity. Most microalgae biomass blending with coal, and co-firing operations reported was with the dried biomass (5), (26), (30), (31), (32), (33) unlike this work that used wet method and discard ultra-fine coal. Co-firing is an economical and efficient means to reduce CO_2 gas emission in the energy sector (34). Microalgae biomass can offer a great solution to deforestation and greenhouse gas GHG, emission (18) compared to other biomass. It is renewable, sustainable, and offers both short and long term solution to greenhouse gas emission (33), (35). The adsorption of microalgae biomass unto coal can produce "one" coal-biomass material that can be fired for heat. There are over 100 field demonstrations and power plants worldwide that uses coal-biomass (16), (36), however, none of the fuels was co-fired as "one material". Co-firing reduces NO_x by 10 – 30 % as well as SO_x and CO (37), (38), (3) based on the boiler type, coal and co-firing technique used. The success of co-firing depends on the quantity, physical properties and chemistry of the biomass, though several research projects are in progress to improve the co-firing (39). The

practice of co-firing has been reported to be effective with up to 20 % biomass mix (15), (13), (29), but it has some problems associated with run-off and dirtiness in the boilers (40).

The term biomass includes all organic raw materials of plant origin that store solar energy, which includes agricultural wastes, wood, microalgae biomass, and several others (41). Biomass contains lignocellulose which is responsible for its energy content. The main constituents (Figure 1.2) are (a) cellulose, (b) hemicellulose, (c) lignin (42), (43), (44), lipids, starch, and protein(45).

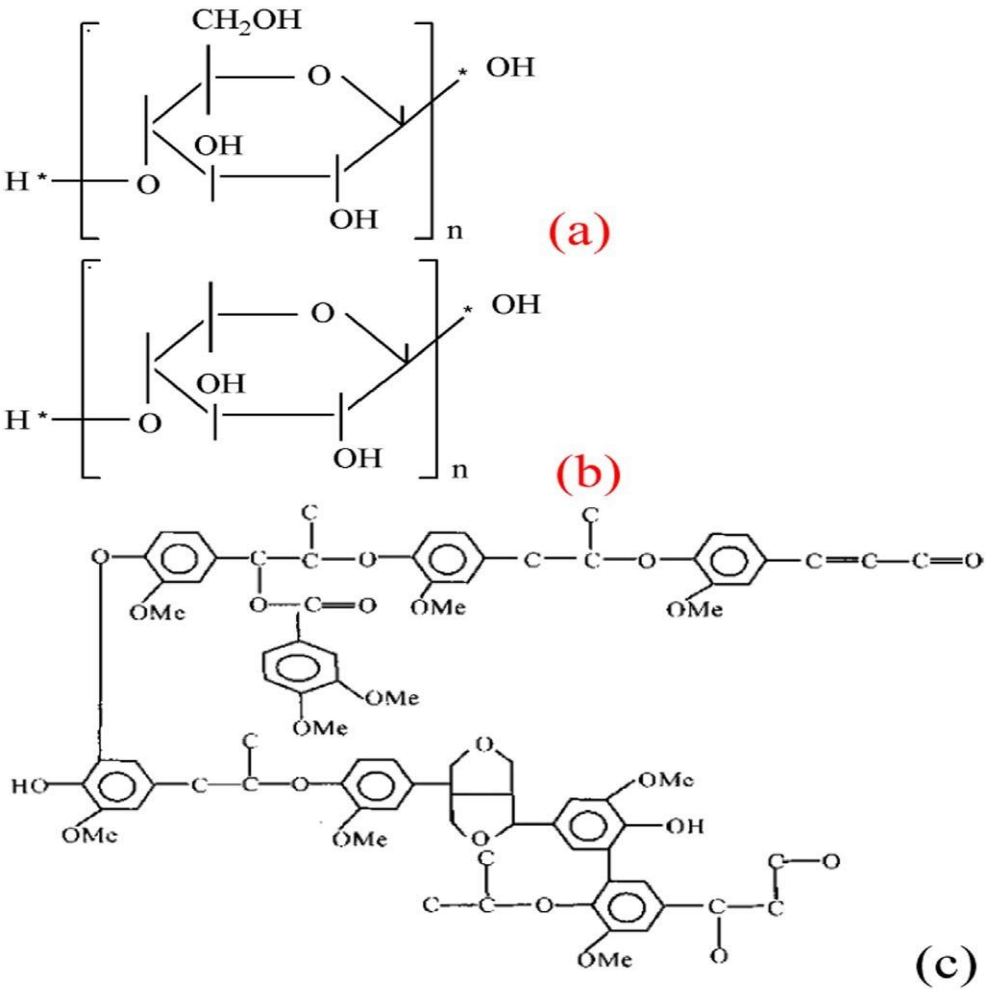

Figure 1.2: Main components of biomass (a) cellulose; (b) hemicellulose; (c) lignin

Biomass is the oldest and most abundant material source of energy in nature which represents the best, economical, low-risk, renewable and sustainable energy option

for power producers. The use of biomass contributes 65 % of the European Union renewable energy (36) and it accounts for 15 % of primary energy consumption worldwide (46). Biomass is the only renewable substitute for petroleum that could supply about 38 % direct fuel and 17 % electricity by 2050 (47).

The abundant supply of biomass, competitive cost relative to coal, and the cost of transportation are a few drivers for co-firing. The decision to engage in co-firing is frequently delayed by the issues around biomass source and transport distance to power stations. One factor that influences feasibility of large scale co-firing is the network of local suppliers of biomass, followed by an established transport system (48). Thus, biomass supply, operational and investments cost, environmental restrictions, and company commitments to the practice have been identified to affect the decision to co-fire (49).

There are assumptions associated with co-firing as an alternative source for energy production. These are availability and characteristics of the biomass that would replace 10 % coal on energy basis because high percentage biomass co-firing would reduce efficiency and power output (50). Another postulation is that the energy effectiveness of utility boilers decreases by 1 % for every 10 % less coal (51). The assumptions include pre-treatment, moisture content, biomass size, and investment associated with retrofitting existing infrastructure to accommodate biomass (51).

There are advantages, disadvantages, and properties of biomass including microalgae compared to coal as detailed in literature which relates to co-firing with coal (52). These are high volatility and high reactivity, the proportion of fixed carbon, alkali metal, and high reactivity of its char (39), (53). Also, biomass produces nearly CO_2 free electricity as it is considered CO_2-neutral because it absorbs an almost equal amount of CO_2 from the atmosphere during growth which is equivalent to the amount liberated on combustion (54), (55), (47), (49), and (51).

The co-firing of coal with traditional biomass has many challenges, which include substantial costs to retrofit power plants to accommodate various biomass, and many more (18). There are technical hitches associated with biomass co-firing in terms of the preparation, storage, and delivery system of biomass fuel (18). The milling of biomass to the same size and shape as coal is very difficult. Biomass has low bulk energy density, is moist and hydrophilic, and non-friable (56). The low heating value,

particle, and bulk densities relative to coal reduce the fuel density by about one tenth of coal. The formation and deposition of ash influence fuel and boiler selection. Ash deposition varies largely with the herbaceous biomass producing a high residue compared to woody biomass. The formation of pollutants and release of emission from coal, as well as from biomass combustion is complex. Co-firing deactivates selective catalytic reduction, SCR system and forms striated flows (17). The mineral content of biomass, for example potassium, aluminium, sodium, calcium and iron, causes corrosion of utility boilers (35).

There are three co-firing options used in utility boilers (57), (Figures 1.3 – 1.5) and three combustion systems are identified, (Table 1.2) in the use of coal, biomass and coal-biomass in power production(36), (48), (58). The co-firing options are not implemented to save energy, but to reduce operation cost, and greenhouse gas emissions (57).

Table 1.2: Co-firing options and combustion systems

No.	Co-firing options	Combustion systems
1	Direct	Fixed bed (stoker or grate)
2	Indirect	Fluidized bed (bubble and circulate)
3	Parallel	Pulverized fuel (dust)

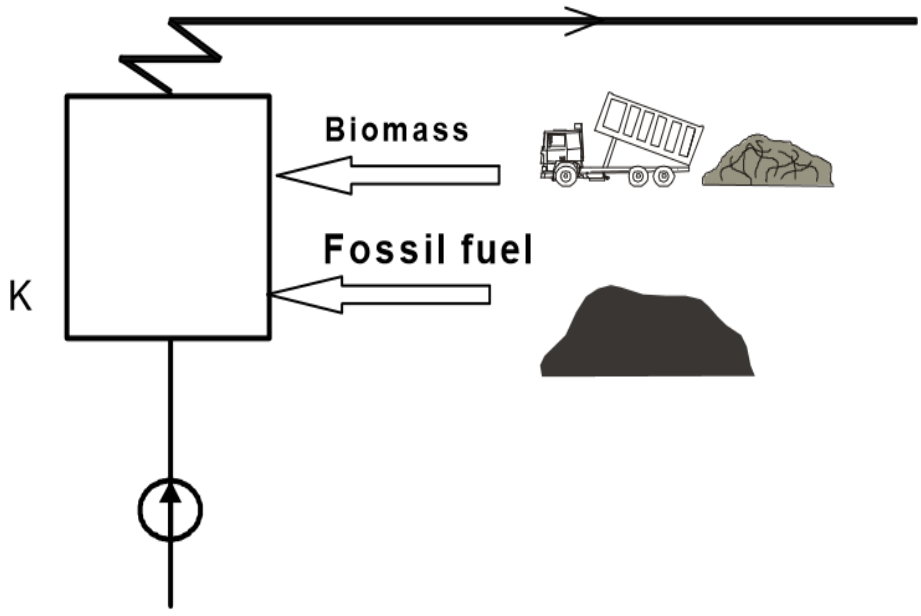

Figure 1.3: Direct co-firing (36)

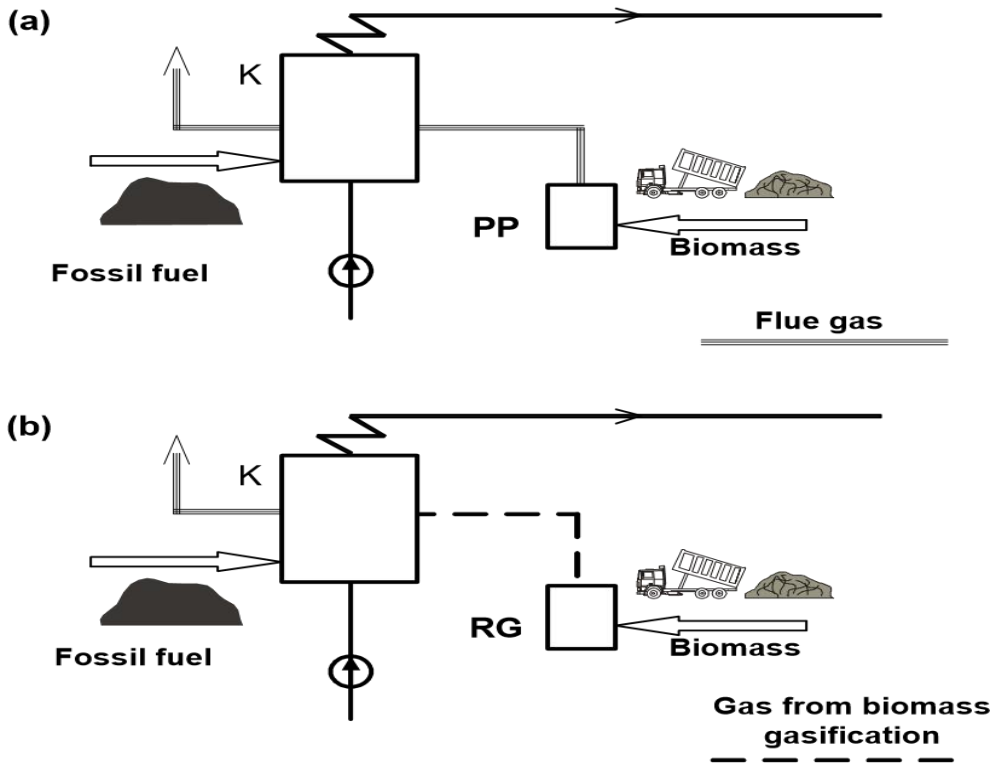

Figure 1.4: Indirect co-firing (repowered pre-furnace, PP and biomass gasifier, RG) (36)

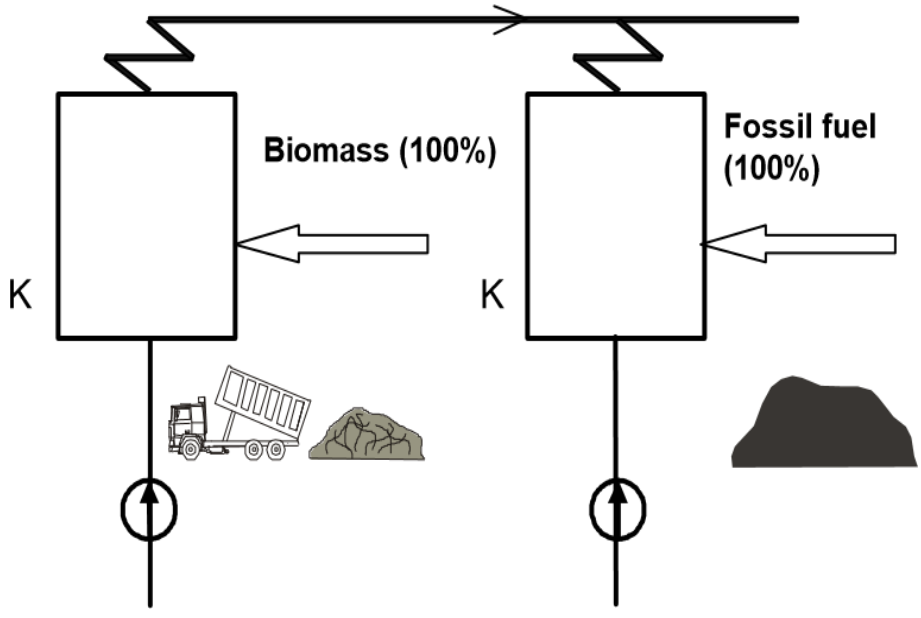

Figure 1.5: Parallel co-firing system (K-boilers) (36)

With direct co-firing, (Figure 1.3), the coal and biomass enter the boiler together for combustion. Although this is the most popular and economical of the options, direct co-firing is associated with problems such as,

- Milling, crushing and combustion difficulties due to differences in characteristics of biomass and coal.
- High investment in separate milling and mixing of feedstocks.
- High cost of installation of new biomass mill and combustion equipment.

The indirect co-firing option involves combustion of biomass in a separate combustor with resultant gas transferred into a coal boiler. The biomass and coal ashes are separated, (Figure 1.4) but the investment cost is relatively high.

For parallel (hybrid) co-firing, (Figure 1.5), the coal and biomass are combusted in two different units but are fed to a common header. The benefits include optimization of the combustion process and having the ash residues separately. The limiting factor with this option is the challenge in calculating the amount of biomass that would be fed to meet the capacity of the retrofitted steam generator, thus the investment for parallel co-firing is quite high (36).

Some advantages of biomass make co-firing feasible while a number of limitations, Table 1.3, affect the practice (58).

Table 1.3: Advantages and disadvantages of biomass (58)

S/No.	Advantages	Disadvantages
1	Relatively cheap, abundant, and renewable source	Lack of worldwide standard, classification system and terminology
2	Low ash, sulphur, nitrogen, and trace	Low carbon, energy and fuel density
3	High calcium, Magnesium, hydrogen, phosphorus, oxygen	Competition with food and feed production
4	High volatile and very reactive on combustion(59)	High investment in harvesting, transportation, and storage cost
5	Moderate emission of CO_2, SO_X, NO_X, CH_4,	Contributes to global warming and particulate emission on direct combustion
6	Retention of hazardous components in ash	Quantity of biomass are not easily predicted. Diverse, one source may not be enough for national electricity supply
7	Diversity of biomass fuel supply	Offensive odour, emission and leaching of hazardous components
8	Reduction of landfill wastes, soil, water, and air pollution	High moisture and flame stability issues
9	Increased boiler efficiency	Less fixed carbon
	Microalgae biomass*****	
10	Improved handling – (“Coalgae”)	Low density
11	Forms single co-fired fuel - Coalgae	Combustor fouling and corrosion – due to alkali & chlorine
12	High oxygen, and growth rate – microalgae (60)	May have reduced yield in winter
13	Potential use of ocean, poor quality soil and restoration of degraded lands	-

Biomass is a cheap feedstock but there is no standard classification that is globally accepted for it (61), although it has the potential to substitute fossil fuel for energy generation(62). Biomass is viable for power generation, and it is competitive with coal (61). On a dry ash-free basis, the heat content of all plant species lies between 17–21 MJ/kg (53), and this includes microalgae biomass. The principal selection criteria for biomass species are growth rate, ease of management, harvesting and intrinsic material properties like moisture, ash, and alkali content (53). One of the benefits of microalgae biomass is the potential of using the ocean resource for its cultivation (53). Also, it can be transported using drums, and through pipelines unlike other biomass forms.

1.3 An overview of coal combustion

This section provides an outline on the complex chemical structure of coal, (Figures 1.6a – b), combustion, rank, and properties of coal. It describes some effects of biomass on coal, and the influence of co-firing on the combustion characteristics of coal.

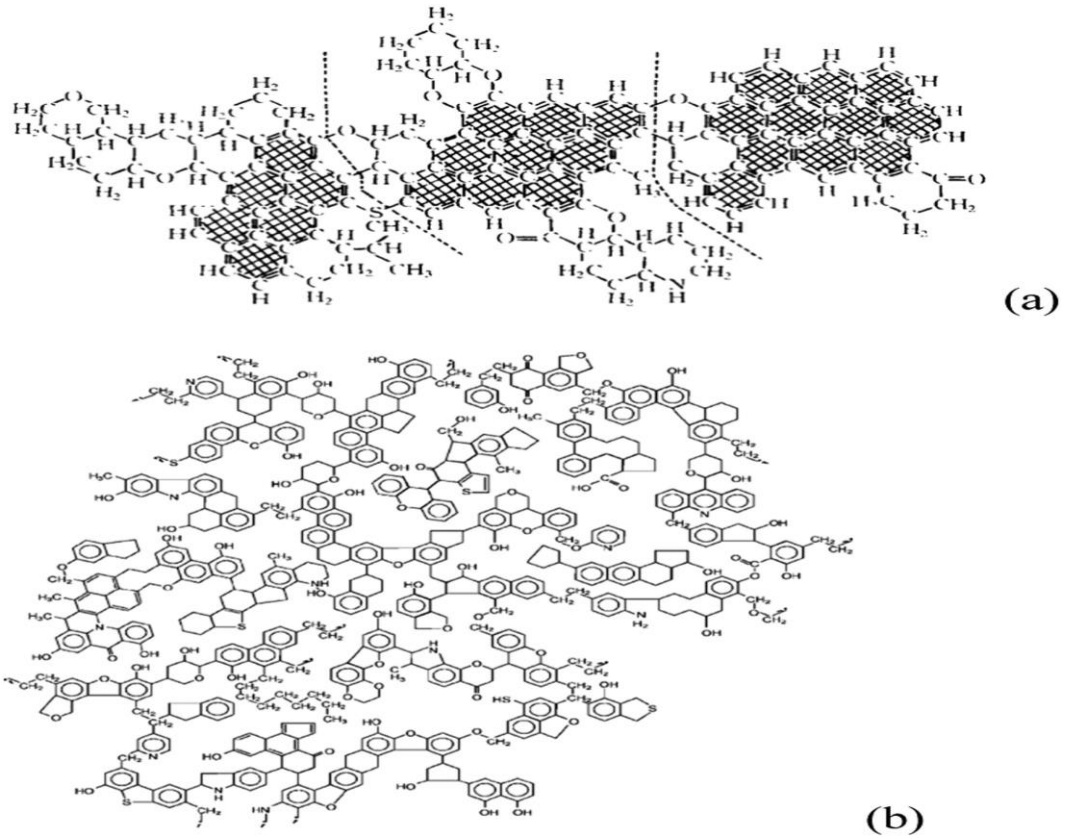

Figure 1.6: Typical structure of coal (42), (63),(64)

Coal is a complex polymer with many aromatic bonds, (Figure 1.6a – b) (65) formed over millions of years by aged compact biomass (42). The principal components of coal are carbon, hydrogen, nitrogen, sulphur, and oxygen *i.e.* CHNS and O (63), (64). The breaking of chemical bonds involving carbon atoms is the main source through which the energy in coal is released as heat content (66). The hydrogen provides energy that continues the oxidation whereas the oxygen content sustains progress, and detailed oxidation of coal has been reported (67). Coal contains moisture, intrinsic minerals, (from dissolved salts in water) and extrinsic mineral (due to contact with soil) (64).

About 27 % of recoverable coal worldwide is used for commercial heat production while 34 % is utilized in generating electricity (68). Coal provides warmth to households and simultaneously allows for cooking on the same stove which is economical to the rural dwellers (69). The oxidation of coal commences once it is ignited by a source and exposed to air, which at a rapid rate produces useful heat (70). An instant and uncontrolled oxidation is termed burning, but under controlled conditions, it is known as combustion. Oxidation is a complex phenomenon that involves simultaneous heat and mass transfer with chemical reaction and fluid flow. The prediction of combustion is for the purposes of design and control. It requires knowledge of fuel properties and the way the properties changes the outcome of the process (71). Combustion reactions depend directly on air-fuel mixing, chemistry of the fuel, and humidity in the air. The rate of diffusion of oxygen into solid fuel determines the degree of combustion. Since air diffuses faster in biomass than coal, it is more reactive than coal so diffusion will affect the combustibility of coal-biomass blend (59). Therefore, diffusion is always the rate limiting step in solid state reactions (72), (73). In turbulent mixing, diffusion controls fast combustion, but slow mixing is limited by chemical kinetics (73).

The term combustion kinetics is expressed as the dynamics of a reaction, illustrated by mathematical equations known as models (74). Combustion kinetics describes the extent of a thermal event in solid state reactions (74). It is measured as a change in concentration (conversion) of reactant or product with time (74), (75). Kinetic parameters can be determined at different times for each stage of a combustion process. Combustion kinetics is required for design, adjustment, and modelling of processes in reactors. The combustion of solid states is an oxidation reaction and can

be explained with different solid state kinetic models (76). Optimization of the model is required for manufacturing of combustors that reduce fuel emissions.

The mechanism of combustion comprises of all overlapped elementary reaction steps or pathways (74), (77). Reaction mechanisms are used to work out the rate law which agrees with the observed laws. They are theoretical explanations of a real-time combustion process. At the macroscopic level, the mechanism defines the rate, order, and rate law of the reaction. These three aspects of combustion kinetics are used to describe the mechanism. An acceptable mechanism must be consistent with stoichiometry of the overall reaction and be determined experimentally by rate law (78). The rate law is used to establish ignition conditions of fuel, characteristic reactivity (activation energy) and to optimize emission. The best option to achieve the highest efficiency with lowest emission is to optimize the entire fuel–engine–after – treatment system (79). The extent of combustion depends on the kinetic equilibrium of the process while the degree of the equilibrium controls the volume of emission.

Several types of coal are classified by rank which is based on the degree of its transformation from the original source. The rank of coal is a measure of age of the coal. As the coal is aging, its heating value and the fixed carbon increases and the amount of volatile matter is decreases (80). Thus, the “rank” of coal, Table 1.4, shows the grades the heat content, economic value, and the degree of combustion expected of the coal. The simple ranking of coal starting from the precursor (*i.e.* biomass) can be in the order of peat (lowest) to lignite (low) and anthracite the highest quality (81). Coal exists in numerous categories but ASTM ranked based on the relative proportions of fixed carbon content, heating value and volatile matter (81).

Table 1.4: The ASTM ranking of coal (80)

No.	Class or Rank	Group	Fixed Carbon [a] (wt. % dry mmf)		Volatile Matter [b] (wt. % dry mmf)		Gross Heating Value [c] (wt. % dry MJ/kg moist mmf)	
			= or >	<	>	= or <	= or >	<
1	**Anthracitic**	Meta-anthracite [d]	98			2	-	-
		Anthracite [d]	92	98	2	8	-	-
		Semi-anthracite [d]	86	92	8	14	-	-
2	**Bituminous**	Low-volatile bituminous [d]	78	86	14	22	-	-
		Medium-volatile bituminous [d]	69	78	22	31	-	-
		High-volatile bituminous **A**	-	69	31	-	32.55	-
		High-volatile bituminous **B**	-	-	-	-	30.23	32.55
		High-volatile bituminous **C**	-	-	-	-	26.74	30.22
		High-volatile bituminous **C**	-	-	-	-	24.41	26.74
3	**Subbituminous**	Subbituminous **A**	-	-	-	-	24.41	26.74
		Subbituminous **B**	-	-	-	-	22.09	24.41
		Subbituminous **C**	-	-	-	-	19.30	22.09
4	**Lignite**	Lignite **A**	-	-	-	-	14.65	19.30
		Lignite **B**	-	-	-	--	-	14.65

a = excludes coal with unusual properties within the fixed carbon and heating value ranges of high volatile bituminous and subbituminous ranks, b = % weight on dry and mineral matter ash free basis, c = gross heating value on mineral matter free basis, d = coal containing 69 % and above fixed carbon are ranked according to the fixed carbon content regardless of the gross heating value, e = may be agglomerating or non-agglomerating, f = agglomerating, tends to be sticky and cakes when heated.

The precursor of coal is biomass (*i.e.* vegetation) and it behaves slightly like low ranked coal. The low rank coal, peat is composed of brown decomposed biomass which can be used as fuel if adequately dried. In terms of geological characteristics, lignite, another low rank coal is the soft and youngest whereas anthracite is the highest rank, hardest, and oldest form which is composed of almost pure carbon.

1.4 Chemical, physical and combustion properties of coal and biomass

The chemical, fuel and physical properties of some biomass, Table 1.5, and the ash composition from a co-fired sample have been detailed by some research (71).

Table 1.5: Some co-fired biomass and the properties (71)

Properties	**Alfalfa stems**	**Wheat straw**	**Rice hulls**	**Rice straw**	**Switch grass**	**Sugar cane bagasse**	**Willow wood**	**Hybrid poplar**
Proximate analysis (% dry fuel)								
Fixed carbon	15.81	17.71	16.22	15.86	14.34	11.95	16.07	12.49
Volatile matter	78.92	75.27	63.52	65.47	76.69	85.61	82.22	84.81
Ash	5.27	7.02	20.26	18.67	8.97	2.44	1.71	2.70
Ultimate analysis (% dry fuel)								
Carbon	47.17	44.92	38.83	38.24	46.68	48.64	49.90	50.18
Hydrogen	5.99	5.46	4.75	5.20	5.82	5.87	5.90	6.06
Oxygen diff.	38.19	41.77	35.47	36.26	37.38	42.82	41.80	40.43
Nitrogen	2.68	0.44	0.52	0.87	0.77	0.16	0.61	0.60
Sulfur	0.20	0.16	0.05	0.18	0.19	0.04	0.07	0.02
Elemental composition of ash (%)								
SiO_2	5.79	55.32	91.42	74.67	65.18	46.61	2.35	5.90
Al_2O_3	0.07	1.88	0.78	1.04	4.51	17.69	1.41	0.84
TiO_2	0.02	0.08	0.02	0.09	0.24	2.63	0.05	0.30
Fe_2O_3	0.30	0.73	0.14	0.85	2.03	14.14	0.73	1.40
CaO	18.32	6.14	3.21	3.01	5.60	4.47	41.20	49.92
MgO	10.38	1.06	-0.01	1.75	3.00	3.33	2.47	18.40
Na O_2	1.10	1.71	0.21	0.96	0.58	0.79	0.94	0.13
K O_2	28.10	25.60	3.71	12.30	11.60	0.15	15.00	9.64
SO_3	1.93	4.40	0.72	1.24	0.44	2.08	1.83	2.04
P_2O_5	7.64	1.26	0.43	1.41	4.50	2.72	7.40	1.34
HHV, MJ/kg	18.67	17.94	15.84	15.09	18.06	18.99	19.59	19.02

The proximate, ultimate, and elemental properties of coal and biomass, Tables 1.5 – 1.7 are related which make co-firing possible (47). Such similarities could apply to the ultra-fine which is a grade of coal, and microalgae that is a class of biomass.

Table 1.6: Relationship between properties of biomass and coal (47)

Properties		**Biomass** (microalgae)	**Coal** (ultra-fine)	**Units**
Physical	Friability	Low	High	-
	Fuel density	~ 500	~ 1300	kg/m^3
	Particle size	~ 3	~ 100	mm
Chemical	Carbon	42 – 54	65 – 85	% wt. dry fuel
	Oxygen	35 – 45	2 – 15	“
	Sulphur	0.5 (max)	0.5 – 7.5	“
	SiO_2	23 – 49	40 – 60	% wt. dry ash
	K_2O	4 – 48	2 – 6	“
	Al_2O_3	2.4 – 9.5	15 – 25	“
	Fe_2O_3	1.5 – 8.5	8 – 18	“
Fuel (combustion)	Ignition	418 – 426	490 – 595	K
	Peak temperature	560 – 575	–	K
	Heating value	14 – 21	23 – 28	MJ/kg

Generally, biomass differs from coal in term of organic, inorganic, and heat content, as well as physical properties. Junmeng Cai *etal* detailed the physicochemical and the several analytical characteristics of biomass (56), and (82). Biomass has less carbon, more oxygen, more silica, and potassium, less aluminium and iron relative to coal. It has low ignition temperature, and heating value, high moisture content, and low density and friability (47). The composition varies more in biomass fuels than among coals, but each class of biomass has more oxygen and less carbon than coal. Nitrogen

content, chlorine, and ash content differ remarkably among biomass. The nitrogen forms NO_x while sulphur is responsible for SO_x, though biomass has low sulphur content relative to coal. The chlorine content in biomass forms acid that causes corrosion. The particle size of microalgae is smaller (47) compared to coal, which makes it diffuse into the coal. The carbon content of biomass is less as compared to coal, so the blending will not increase the content. Unlike other biomass, live microalgae would introduce more oxygen on penetrating into the coal thereby improving oxidation(19), (23).

The combustion stages in biomass, and coal are related as in Figures 1.7 - 1.8 below. It illustrates the dewatering, devolatilization, and the char combustion stages. The figures show that carbon dioxide CO_2, carbon monoxide CO, methane CH_4, nitrous oxides NO_x, sulphur oxides SO_x and polyaromatic hydrocarbons PAH are released (42), (54). An optimal coal-biomass, combustor design and operation procedure would reduce SO_x, NO_x, CO_2 and CH_4 emissions (17). The combustion stages of cellulose, hemicellulose, lignin of biomass particles, Figure 1.7, have been reported to be similar to that of coal, Figure 1.8, (64).

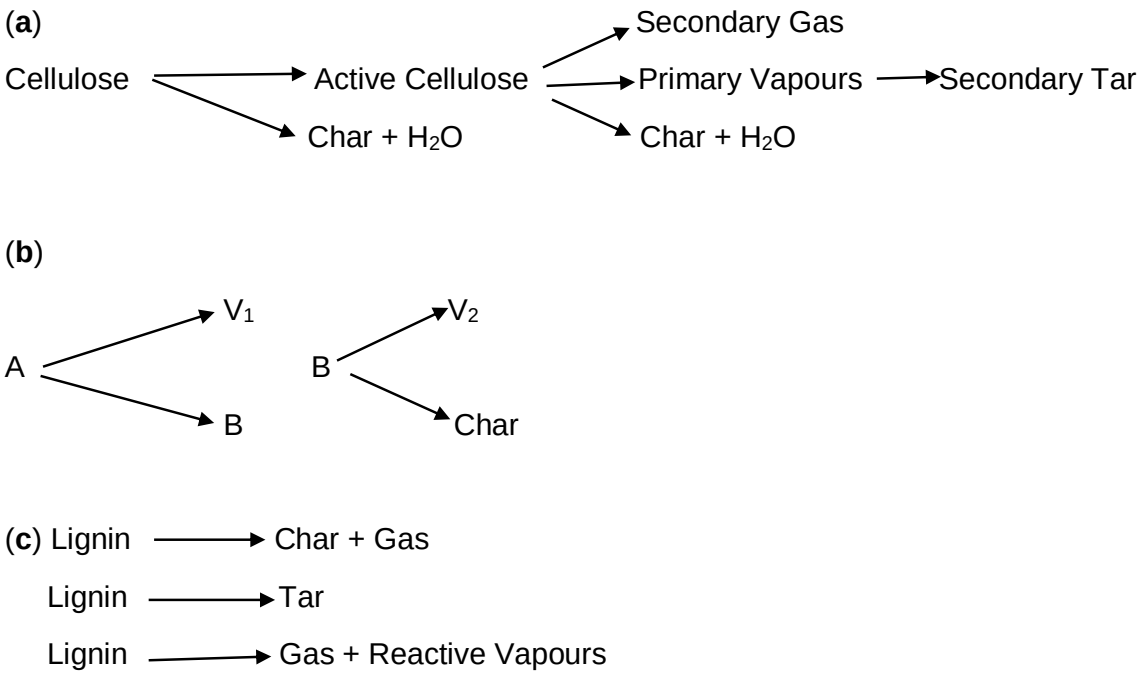

Figure 1.7: Decomposition mechanism of biomass components (64)

Also, the three stages in biomass i.e. drying, devolatilization and char combustion, are identified in the combustion of coal, Figure 1.8 below.

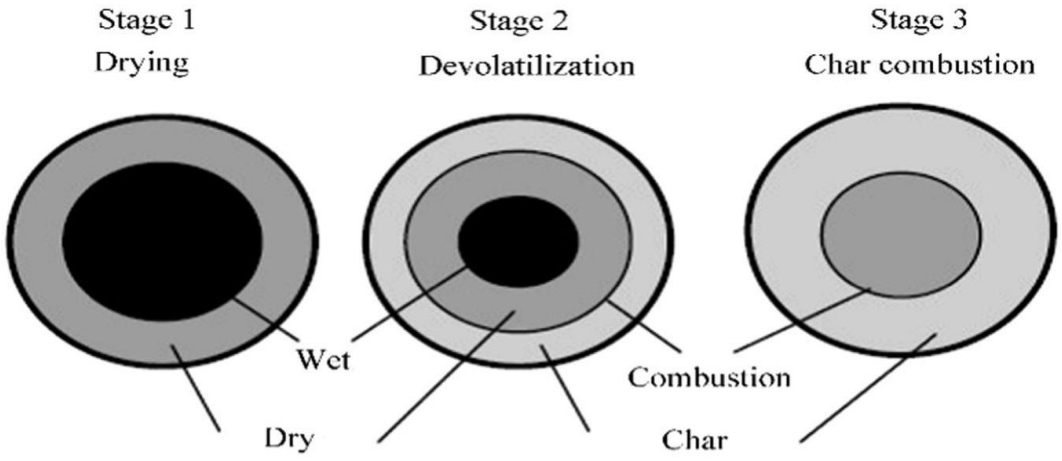

Figure 1.8: Stages of combustion of coal particle (64)

1.5 Microalgae and discard ultra-fine coal

Using discard ultra-fine coal, and microalgae biomass could be of advantage to the South African small-scale boilers operators, because the discard could be collected for free. Of about 255 Mt of coal produced per annum in South Africa, 60 Mt was discarded due to poor quality and particle size, <500µm, whereas the heating value was about 16 MJ/kg and some 23 – 28 MJ/kg which could be utilised (83). In Australia such discard coal was converted to briquettes using synthetic binders to obtain 70 K-t quantity of briquettes per year (83).

At InnoVenton, the Nelson Mandela University Institute for chemical technology and downstream station, microalgae biomass was found to be an effective binder for discard ultra-fine coal (19). Microalgae biomass consume three primary components – sunlight, carbon dioxide and water (84). South Africa receives large quantity of solar radiation per annum (85), with the lowest value as 4000 Kw/h/m^2 and the highest as 6000Kw/h/m^2 (86). This makes South Africa suitable for commercial microalgae biomass production. The commercial scale production of microalgae biomass started in Japan in 1960 (87). Commercial production, (Figure 1.9) of about 15,000 tons per year in Fraunhofer-Gesellschaft, Germany, (88) is feasible and could use flue gas, (89), (90), (91), (92), (87), (93), (94), and (95), from coal-microalgae combustion at

power stations. More than 70 companies worldwide produce microalgae (biomass) (96).

Figure 1.9: Commercial photo-bioreactor for Microalgae cultivation (97)

Similar to wood, this biomass has synergistic effect on the comprehensive combustion property of coal (23). Microalgae biomass have the potential to sequester carbon dioxide from stack gas, (92) and (41), as biological processes are the best known method for direct conversion of CO_2 from stationary point source emission (89). There are about 300,000 species of microalgae that can double their biomass within 24 hours, and with 3.5 hours as the shortest doubling time for growth which makes the biomass ideal for fuel production(41). The characterisation of some microalgae biomass, Table 1.7, which include specie grown at InnoVenton have been illustrated (41), (98).

Table 1.7: Characterisation of Microalgae biomass (99), (98)

Chlorella vulgaris (CV), Scenedesmus almeriensis* (SC), *Nannochloropsis gaditana (NG) (99), ***Spirulina platensis (SP)***										
Microalgae	***CV***	***SC*)**	***NG***	***CV*** *ar*	*dry*	*daf*	***SP*** *ar*	*dry*	*daf*	–
Parameters (%)/Reference	(99)			(98) ECN #2333			(98) ECN #1450			–
Inherent moisture (M)	4.4	2.9	3.5	71.87	–	–	6.70	–	–	–
Ash (A)	15.9	19.4	6.4	1.67	5.94	–	7.18	7.70	–	–
Volatile matter (VM)	67.2	67.9	79.8	22.61	80.38	85.46	–	–	–	–
Fixed carbon (FC)	12.4	9.7	10.2	3.85	13.68	14.54	–	–	–	–
Carbon (C)	42.8	40.7	47.7	12.92	53.03	56.38	41.00	43.94	47.61	–
Hydrogen (H)	6.5	6.5	7.4	2.02	7.18	7.63	6.40	6.86	7.43	–
Nitrogen (N)	6.7	5.7	6.8	3.18	11.30	12.20	6.10	6.54	7.08	–
Sulphur (S)	1.0	0.8	1.1	0.19	0.69	0.73	0.40	0.43	0.46	–
Oxygen (O) [a diff]	43.1	46.3	37.0	5.79	20.57	21.87	32.22	34.53	37.41	–
Elemental analysis (ppm)	Elements									
Microalgae	Al	Ba	Ca	Cu	Fe	K	Mg	Na	Mn	Zn
CV (99)	107.3	129.5	10397	144.2	711.6	3116	3577	5277	121.8	177.8
SC (99)	106.1	–	7297	–	2768.6	21038	22455	4402	469.5	83.9
NG (99)	433.1	–	7493	–	2414.9	2689	3123	41620	339.6	77.9
CV (98) ECN #2333, (mg/kg) dry	6.0	–	1 042.3	22.5	5 685.1	5 389.4	3 676.8	652.9	336.8	57.6
ECN #2333	Ti	As	Cd	Co	Cr	Se	Mn	Sb	*Cl*	*F*
	3.5	0.3	0.1	1.3	7.4	0.1		0.8	*30.9* *ar*	*6.8* *ar*
ECN #2333	Ni	Sr	V	Ni	Ba	P	Si	Mo	*110.0* *dry*	*24.0* *dry*
	12.7	0.5	1.7	12.7	0.7	12 668.9	12.1	6.7	*116.9* *daf*	*25.5* *daf*

ar = as recieved, daf = dry ash free, ppm = part per million, diff = difference, # = ECN Phyllis standard number, ultimate analysis

The production of 1 kg of microalgae biomass consumes about 1.8kg of carbon dioxide (100). The chemical and nutritional properties of microalgae biomass has been reported (96), (91), (101), as well as the productivity (102), and the direct cost of about US$5 – 20, kg dry weight $^{-1}$ (92). The cost of production was also estimated at Euro 0.68 per kg (103). Relative to traditional energy crops, microalgae biomass has,

- Fast growth rate
- Short growth time
- High lipid content
- High photosynthetic production
- Low energy consumption
- Adaptation to different water sources
- Areas that are not suitable for traditional crops (104), (105).

Microalgae biomass could be produced in ponds, tanks, tubes, fermenters, and raceways *etc.* (94). Its high cost of production relates to the need for light and some slow growth rate are due to inadequate sunlight (87). The cultivation cost is low in areas with enough sunlight (106) and for systems with optimized growth conditions. Although coal and woody biomass are mainly combusted to produce heat, microalgae can be converted to heat as well (107). Carbonaceous resources like coal absorb tiny molecules of other substances into its pores. Microalgae could penetrate pores of carbonaceous resources and breaking them down to arable soil. Microalgae serves as a natural binder (23), it is a renewable and sustainable fuel. Microalgae biomass is the fastest biomass producing species known to man that does not necessarily require arable land for cultivation. Microalgae can be used to recover, and upgrade dumped coal to produce a composite (19). The composite can be used as a substitute fuel for coal in industrial boilers, and to produce a biofuel blend. Microalgae has significantly higher activation energy of about 71.63kJ/mol. (32) compared to other types of biomass, and it does not compete with food production. Coalgae® could be used as feed stock for bio-crude oil, liquefied natural gas, and the ash modified as organic fertilizer. Coalgae® fuel is partly renewable and sustainable. Its use would improve energy supply, economy, health, and environment.

Coal and microalgae biomass have a structure that makes them compatible and co-firing feasible. The structure of coal represented by Smith *et al* (63) and microalgae -

(a) β-Carotene, (b) astaxanthin, (c) phycoerythrin depicted by Spolaore *et al* (96) have functional groups such as -OH, C=O, *etc* (Figure 1.2) capable of initiating chemical reaction between the two molecules. The addition of microalgae to coal could close the reactive sites in coal to form interlocks - “bonds”, but this needs to be explored. The structure of coal and microalgae defines the thermal reactivity and mode of interaction with one another. Our previous research showed that coal-microalgae agglomerates to form a blend comparable to coal (23). Microalgae biomass has been used to improve the mechanical strength of paper material (108), thus, it could enhance the drop resistance of pelleted coal-microalgae composite.

The discard ultra-fine coal is the by-products of commercial coal processing. Commercial processing of coal generates million tons of ultra-fine particulates that are normally discarded (109). For instance, Eskom provided the discard ultrafine coal sample for this study from one of its dump sites. Since the coarse or lump coal could be pulverised and in the same way be treated as the discard, therefore both ultra-fine coal and lump coal were referred to coal in this study. The properties of South African discard coal, Table 1.8, has been reported, (110).

Table 1.8: Fuel and chemical properties of discard coal and other coal (110)

Parameters (%)	**Discard coal**	**Anker Diversen coal***** (ar)	dry	daf	**Pitts coal** (ar)	dry	**coal**	**Anthracite**	**Hard coal**	**Brown coal**
Reference	(110)	(98)	-	-	(98)	-	(110)	(110)	(29)	(29)
Inherent moisture	4.0	1.06	-	-	-	-	6.49*	4.87*	5.1	50.4
Ash	29.4	20.20	20.42		13.70	-	27.49	20.80	8.3	5.1
Volatile matter (VM)	24.4	37.30	37.70	47.37	34.40	39.86	51.75	5.80	34.7	52.1
Fixed carbon (FC)	42.2	41.44	41.88	52.63	51.90	60.14	20.76	73.40	57.1	42.8
Gross calorific value (CV) MJ/kg	20.2	-	-	-	-		19.44	23.10	28.0 $_{L}$	9.0 $_{L}$
Carbon (C)	85.6	64.59	65.28	82.03	71.90	83.31	52.70	67.60	72.5	65.9
Hydrogen (H)	3.6	3.50	3.53	4.44	4.70	5.45	3.53	1.00	5.6	4.9
Nitrogen (N)	1.7	1.60	1.62	2.03	1.36	1.58	1.36	0.85	1.3	0.69
Sulphur (S)	1.2	9.87	9.97	12.53	6.98	8.09	0.71	0.30	11.1	23
Oxygen (O)	7.9	0.91	0.92	1.16	1.36	1.58	9.5	5.60	0.94	0.39

ar = as received, daf = dry ash free, Pitts = Pittsburgh, $_{L}$ = low heating value, *** = low quality coal, * = inherent moisture

There are literature reports on microalgae co-firing, but those studies used the dried biomass together with coal, wood, municipal waste, etc (111), (31) and (32).

1.6 Influence of biomass co-firing on combustion properties of coal

Biomass co-firing lowers the ignition and burn-out temperatures, comprehensive combustion index, activation energy, ash residue, and emission (45), (71), (14), (43), (112), (113) of coal. Co-firing has synergistic effect that improves the reactivity and fuel properties of coal (14), (112), (110). The ignition index, $c = \left(\frac{\mathrm{R_{max}}}{T_{ig}{}^{2}}\right)$ and the comprehensive combustion characteristic index, $S = \left(\frac{\mathrm{R_{max}}}{\mathrm{T}_{ig}\mathrm{T_f}}\right)$ could be used to evaluate co-firing and to represent characteristic ignition and whole combustion processes (45). Where, $\mathrm{R_{max}}$ is the maximum combustion temperature, $\mathrm{T_{ig}}$ is the ignition temperature and $\mathrm{T_f}$ is the burn-out temperature. High S values indicates a superior burning behaviour (114). Activation energy, E_a is the best way to differentiate between the reactivity of two or more coals as well as other solid fuel samples. Thus, the reaction rate of solid states can be evaluated from oxidation reaction models $\mathrm{g}(\alpha)$, by considering the model of the controlling reaction mechanism and its slope m.

The rate of collision between reacting particles in the low and high temperature scheme are obtained by calculating the frequency factor, A, from the intercept of the graph of the controlling reaction.

The co-firing ratio (*i.e.* the share) of coal, P_c and biomass, P_b as indicated in the formula can be calculated (50).

Also, Falcon *et al* assumed that the observed rate of combustion of a composite fuel would be equal to the theoretical sum of the weight loss rates of the individual components (110). According to Falcon *et al,* the additive or interactive behaviour between coal and biomass could be evaluated (predicted) by overlaying $(\frac{dm}{dt})$c versus T with mass of composites, M_C versus T for all the composites, M_{mix}. A graph of M_{mix} and $(\frac{dm}{dt})$ together against T (in K) for non-isothermal combustion would indicate either an additive or interactive behaviour. An interaction occurs when the combustion of

theoretical M $_{mix}$ is parallel to the experimental ($\frac{dm}{dt}$) graph. Alternatively, an overlap of mass loss rates of composite $\left(\frac{\mathrm{dm}}{\mathrm{dt}}\right)_{mix}$, proportion of coal multiplied by mass loss rate of coal $\mathrm{P\,c}\left(\frac{\mathrm{dm}}{\mathrm{dt}}\right)_{c}$, and proportion of biomass multiplied by mass loss rate of biomass $\mathrm{P\,b}\left(\frac{\mathrm{dm}}{\mathrm{dt}}\right)_{b}$ graphs confirms an additive behaviour between coal and the biomass.

The combustion efficiency of a solid state could be investigated as a function of the volatile and char combustion. The volatile content is completely burnt during combustion before char oxidation. Thus, the burning efficiency is commonly restricted by the extent of char combustion. The volatile matter of biomass is higher than that of coal. Hence, with the same TGA analyser *i.e.* combustor, it is assumed that parallel mass or similar fraction of coal and biomass char $\eta_{\mathrm{b,char}}$ are completely burnt. Hence, the overall efficiency becomes fraction of biomass that burnt completely divided by fraction of coal that burnt completely $\frac{\eta_{\mathrm{b}}}{\eta_{\mathrm{coal}}}$, (65). If we substitute the observed values of volatiles for biomass v m $_{b,}$ and for coal v m $_{c}$, and for each blend, we have similar fraction of biomass char that burnt completely, $\eta_{\mathrm{b,char}}$, then, $\frac{\eta_b}{\eta_{coal}} = (1 + 0.16458P_b)$ (65).

1.7 Characterisation of the fuel properties of coal-microalgae

The fuel properties of coal and microalgae biomass have been studied and reported in literature (32), (115). The proximate parameters are fundamental in rating fuel quality and these are the moisture, ash, volatile matter, and fixed carbon. Proximate parameters are used to correct other analytical results, which in turn determine the market value of the fuel. The bulk parameters can be determined with automatic proximate analysis method (116), (117). The proximate values are useful in negotiating and dictating fuel price.

The moisture of coal is the water inherently contained in the coal when the sample exist in its natural state of deposition(80). The moisture of a sample is determined as received and used to re-calculate the analytical results to dry basis. The total moisture is used to compute results for as received basis. Ash is the remaining inorganic residue after coal is completely burned. The ash is composed of compounds of aluminium, calcium, iron, magnesium, silica, and others (80). Ash content is used to consider the

cleaning and sampling procedures, to calculate the oxygen content, and it provides details on the degree of conversion of fuel. The ash content can be used to compute for the material balance. It provides information on the fly ash and bottom ash disposal. It is used to predict the erosion rate on boilers and to estimate the loading on electrostatic precipitator. The volatile matter is the gas released when coal is heated in the absence of air under set conditions (80). These include carbon dioxide, volatile organic and inorganics that contains sulphur and nitrogen. The volatile matter of coal comprises of the methane, hydrocarbons, hydrogen, carbon monoxide, and incombustible gases (118). The volatile matter provides the basis for purchase and sales of solid fuel and predicting coke yield on carbonization (119). The fixed carbon is the remaining organic material after the volatile matter and moisture have been released. Thus, the baseline proximate parameters for Coalgae® are required. Low ash, less fixed carbon, negligible sulphur and more volatiles favours clean fuel combustion (120).

The heating value is the energy released as heat when fuel undergoes complete combustion with oxygen (80). Heating value of coal, microalgae and the composites could be determined at 25 °C with the bomb calorimeter, by using the ASTM-D5865-07 method for coal and the ASTM-D4809-09a (121). The heat of combustion per unit mass could be expressed as gross heat (at constant volume) or the net heat (at constant pressure of 0.101MPa) at 25 °C (121).

The ultimate parameters give indications of the expected gaseous pollutants. The elementar analyser could be used to evaluate the carbon C, hydrogen H, nitrogen N, sulphur S (122), while the oxygen O content could be calculated using difference method. Sulphur and nitrogen are the sources of SO_x and NO_x. The X-ray fluorescence is used to quantify elements in solid states materials (123), (124), (125). The oxides of magnesium (Mg), manganese (Mn), potassium (K), and aluminium (Al) *etc*. catalyse combustion reactions (45). Also, the chlorides content of biomass contributes to corrosion of utility boilers (45). The ash composition of microalgae biomass has metals withcatalytic potentials as those of other co-fired biomass, Table 1.9, (29).

Table 1.9: Ash composition from Studstrup co-firing (29)

Constituents	**Coal** (%)	**Coal-straw** (min %)	**Coal-straw** (max %)	**Coal-wood Typical** (%)
SiO_2	59.8	19.70	38.9	10
Al_2O_3	19.1	0.24	0.52	2
Fe_2O_3	8.1	0.13	0.19	1
CaO	2.0	6.35	8.45	35
MgO	1.7	1.50	1.90	5
Na_2O	0.6	0.29	1.00	3
K_2O	2.2	28.70	34.60	20
P_2O_5	0.2	2.45	3.00	12
SO_3	2.1	3.40	5.00	12
Cl	<0.1	4.55	7.06	-

1.8 Kinetic parameters of microalgae and coal-microalgae biomass

The study of combustion kinetics is useful for the optimization of fuel properties required for reactor design (126). The firing of coal is limited by chemical kinetics and external diffusion (127).

There are reports on kinetic parameters such as ignition, peak and burnout temperatures, and rate of reaction of dry blended coal-microalgae biomass (32). None of such parameters was cited for wet blended discard ultra-fine coal-microalgae biomass. The combustion of microalgae which showed three kinetic stages for different reaction rates was reported, Table 1.10, (128).

Table 1.10: Combustion parameters of some microalgae (128)

Heating rate	**T_i** (K)	**T_p** (K)	**DTG** max	**%/K**	**HT_Z** (K)	**M_L** (%)		**T_i** (K)	**T_p** (K)	**DTG** max	**%/K**	**HT_Z** (K)	**M_L** (%)
C/min	Chlorella *pyrenoidosa (CP)* Stage 1							Spirulina *platensis (SP)* Stage 1					
10	298	401	338	0.067	78	5.975		298	402	349	0.056	106	5.346
20	298	418	350	0.069	82	6.604		298	405	354	0.061	110	5.460
Stage 2								Stage 2					
10	419	672	556	0.340	124	47.16		421	703	553	0.312	120	45.18
20	437	709	567	0.347	122	47.39		435	715	565	0.331	125	46.86
Stage 3								Stage 3					
10	685	1039	813	0.265	177	38.36		714	1020	842	0.410	78	39.31
20	714	1048	842	0.276	161	37.42		723	1027	855	0.324	108	38.99

T = temperature; T_i: initial ignition at any stage, K; T_f: final burnout at any stage, K; T_p: temperature of the maximum rate of mass loss, K; DTG_{max}: maximum mass loss rate at any stage, %/K; HT_Z: full temperature width at half-maximum of the value of DTG_{max}, K; M_L: total mass loss at any stage, %.

The combustion kinetics studies of microalgae, coal, (Table 1.9), and blends was reported based on the following analytical techniques (76), (129), (130), (131), (132),

- Differential scanning, DSC
- Fourier transform infra-red, FTIR
- Raman spectroscopy
- Thermogravimetry analysis, TGA
- X-ray absorption near edge structure, XANES
- X-ray diffraction, XRD, *etc.*

1.8.1 Combustion kinetics of coal-biomass and relevance

The conventional parameters frequently used to describe the combustion of coal, biomass, and their blends were illustrated with macadamia nut shell, high ash coal, and anthracite, Table 1.11, (110). The combustion properties can be evaluated at any heating rate (β) for coal-microalgae biomass. The relevant parameters include ignition, burn-out, and DTG peak temperatures, minimum and maximum reaction rate (133). It also includes detailed parameters such as the activation energy, pre-exponential factor, reaction order *etc*, (133), (134), (135), and (136).

Table 1.11: Combustion properties of biomass, high ash coal and anthracite

Parameters	**β**	**T_{ig}**	**PT**	**PT** wt loss	**BT**	**Final** wt loss	**DTG** max
Samples	(°C/min)	(ºC)	(°C)	(%)	(°C)	(%)	(%/min)
Macadamia	10	160.22	320.70	56.30	520.52	99.90	9.11
	20	169.00	323.20	59.80	556.40	99.98	17.60
High ash coal*	10	231.32	390.00	25.10	632.20	72.13	4.50
	20	225.10	469.00	51.12	650.00	72.44	6.14
Anthracite	10	415.00	502.85	27.81	677.80	80.20	6.40
	20	428.13	609.52	53.30	778.23	79.85	9.75

β = heating rate; T_{ig} = ignition temperature; PT = T_{max} = peak temperature; BT = burnout temperature; DTG_{max} = reactivity, high-ash coals* = sourced from the KwaZulu-Natal province, South Africa.

The reactivity of a fuel material is measured by these combustion parameters. For instance, a low ignition, DTG peak, and burnout temperature and activation energy *etc*, indicate a very reactive fuel and vice versa (136). The comprehensive combustion index (137), and the kinetic parameters (138), *etc.* are used to describe the combustion performance (139), (140). With the TGA technique, several mathematical approaches, Figure 1.10, were reported to have been applied on observed data to calculate the combustion parameters (141).

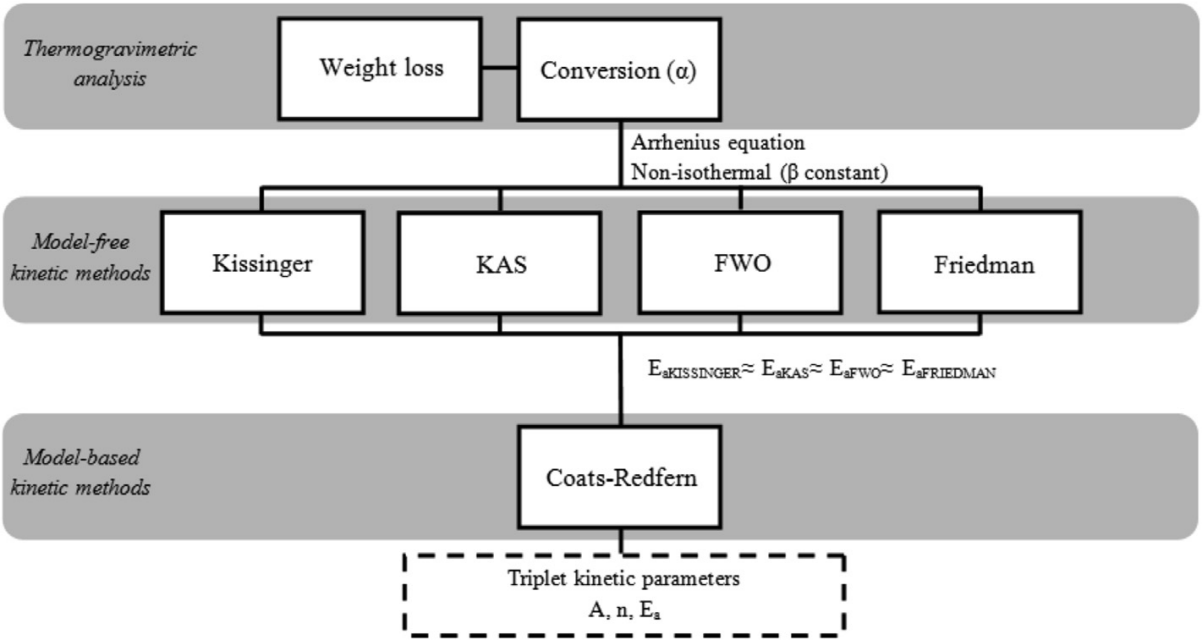

Figure 1.10: Some methods for determination of kinetic parameters (141)

- Arrhenius equation: is often applied to determine the activation energy and pre-exponential factor, because the reactivity of fuel is characterised by the reaction rate constant (142). The reaction rate constant is factored in the activation energy E_a (143), (142), (144) which is unique, and relevant to differentiate the reactivity of materials (86).
- Model-free methods: this includes Flynn-Wall-Ozawa (143), Friedman, and the Kissinger-Akahira-Sunose. The later provides an exact result if the reaction order is one (141), (145), and (146). The methods are also significant in calculating the activation energy (33).
- Model-based methods: the Coats and Redfern's model (146) is considered more appropriate in calculating the apparent reaction order n, frequency factor

and activation energy of fuels (141). The reaction order describes the effect of concentration on the rate of conversion of fuel.

- Solid states oxidation model: specifies the reaction order, and possible mathematical equation that describes the process. The model describes air diffusion processes, phase changes, and relevant in differentiating the controlling mechanisms from others (146).

Some of the methods were applied in literature to determine the combustion parameters of dry mixed coal-microalgae, Table 1.12, (32).

Table 1.12: Characteristic parameters of dry mixed and co-fired coal-microalgae biomass (32)

Fuel-Air (O_2/N_2 = 21/79)	**Mix**	**T_i** (ºC)	**T_{p1}** (ºC)	**T_{p2}** (ºC)	**T_{p3}** (ºC)	**DTG_{max}** (%/ºC)	**W_R** (%)	**E a FWO** (kJ/mol)	**Corr.** R2	**E a KAS** (kJ/mol)	**Corr.** R2
Coal	1	256.8	–	366.3	–	0.762	8.57	37.83	0.99659	36.73	0.99907
Coal-microalgae	9/1	249.1	–	366.5	480.7	0.695	11.95	41.65	0.99294	39.91	0.99932
Coal-microalgae	7/3	237.1	267.3	368.1	482.9	0.535	13.89	44.86	0.99404	40.37	0.99852
Coal-microalgae	5/5	228.7	265.4	370.9	483.6	0.398	16.56	48.38	0.98139	44.28	0.99360
Coal-microalgae	3/7	224.4	264.5	372.3	484.4	0.293	19.2	59.35	0.995951	58.22	0.98695
Microalgae	1	216.8	263.1		485.1	0.406	22.58	76.96	0.99409	71.63	0.96617

T_i = ignition temperature., T_p = peak temperature., DTG_{max} = maximum weight loss rate. W_R = residual mass, Ea = activation energy, FWO = Flynn-Wall-Ozawa, KAS = Kissinger-Akahira-Sunose.

Thermogravimetric analysis TGA, is accepted as an inexpensive and reliable technique to characterise kinetic parameters and the method simulates industrial combustion (147), (148), (149), and (150). TGA is the simplest and the most effective method to observe the combustion profile of a fuel (151). It was used to assess the decomposition, and combustion characteristics required for predicting the coal-biomass (microalgae, (152)) combustion efficiency (153). A slow heating rate <10K/min does not model rapid combustion process of coal in an industrial boiler of up to 1000K/min (142). The TG data can be applied to determine the effect of biomass on the combustion of coal. Thermogravimetric analysis, TGA, describes mass loss as a function temperature while the, DTGA, depicts the differential of the mass loss (147), (154). A combination of TGA and DTGA, are used in the thermochemical study of biomass, crude oil, coal, polymers, and blends. The TGA is used to determine the kinetic triple, discussed below, which is applied to explain the reaction mechanism (76), (155). The fundamental rate equation, Arrhenius equation, and TGA – DTGA data are used in all kinetic studies (20), (33), (55), (68), (156), (157), (158), (159), (160), (161), (162). An equation that models chemical behaviour is not always a straight-line function, therefore, linear functions are plotted as partial evidence that the original non-linear model agreed with observed data. Galway and Brown have confirmed that the use of Arrhenius equation in heterogeneous kinetics is theoretically well established and practically sound (141).

Thus, the Arrhenius equation can be rearranged to obtain a linear function capable of explaining a natural event such as combustion by using natural log function ($\ln$) or logs to base e, ($\log_e$). When rearranged into a linear model, $y = e^x$ or $y = e^{-x}$ relative to $y = -mx + c$, the Arrhenius equation provides a model which agrees with the observed experimental data. Where, intercept $c = 0$ and, the slope $m = -k$, described in the Arrhenius equation which can be inverted to obtain a positive slope $m = +k$.
Coats and Redfern kinetic model has been generally applied to describe combustion reactions (114), (155), (163), (164), (165), (166), (167), (168), (169), (170), (171). This model, together with TGA – DTGA methods, are applied to evaluate the combustion kinetic parameters. The TGA methods are isothermal model-fitting, isothermal model-free fitting and non-isothermal (76) which are used to evaluate the combustion triple kinetic parameters highlighted and described below.

- Kinetic model g (∝): A model is a theoretical and mathematical description of what occurs experimentally. The kinetic model g (∝) is a mathematical equation that describes the true or real-life combustion observation.

- Arrhenius pre-exponential factor, A*: The Arrhenius pre-exponential factor describes the frequency that collisions would occur with proper orientation in a combustion reaction space.
- Activation energy, E_a: The activation energy describes the minimum amount of energy in kJ/mol required to make the reaction happen which is the best way to differentiate the rate of reaction in solid states.

The A*, E_a and g (∝) are used to explain rate of oxidation of solid fuel. The rate of degradation *i.e.* conversion of solid fuel, $\left(\frac{d\alpha}{dt}\right)$ is a linear function of temperature-dependant rate constant, k (T). Also, it is a linear function of the temperature-independent function of conversion f (∝), (172). The rate constant k(T) is related to the Arrhenius equation as $\mathrm{k} = \mathrm{A}\exp\left(-\frac{\mathrm{Ea}}{\mathrm{RT}}\right)$. With equation, k can be established by fitting the "best" model of g (∝) versus t, to the experimental data and, k can be substituted into the Arrhenius equation to calculate pre-exponential factor and activation energy. When TGA is used, T is proportional to t and 100 % correlated and then for non-isothermal *i.e.* linear heating rate with change in temperature β at constant time interval, the degree of conversion (∝) of sample (163) during the combustion process is $\alpha = \left(\frac{\mathrm{m_0} - m_t}{m_0 - m_f}\right)$, where $\mathrm{m_0}$ represents the initial mass of sample, m_t equals the mass of sample at time, t and m_f is the final mass of sample.

For non-isothermal combustion where the temperature changes by a constant heating rate, $\beta = \mathrm{dT/dt}$ (ºC/min), the rate equation combined with the Arrhenius equation gives $\frac{\mathrm{d}\alpha}{\mathrm{dT}} = \frac{\mathrm{A}}{\beta}\exp\left(-\frac{\mathrm{Ea}}{\mathrm{RT}}\right)\mathrm{f}(\alpha)$ (173). An integrated solution for this equation is written as, $\mathrm{g}(\alpha) = \int_0^{\alpha}\frac{\mathrm{d}\alpha}{\mathrm{f}(\alpha)} = \frac{\mathrm{A}}{\beta}\int_{\mathrm{T_0}}^{\mathrm{T}}\exp\left(-\frac{\mathrm{Ea}}{\mathrm{RT}}\right)\mathrm{dT}$, where, $\mathrm{g}(\alpha)$ is the integrated form of the conversion dependence function, $\mathrm{f}(\alpha)$ (174). The approximate integrated value of the model equation $\mathrm{g}(\alpha)$ using the Coats and Redfern's $\mathrm{y_{CR}}$, integral method results in two possible solutions, $\ln\left[\frac{\mathrm{g}(\propto)}{\mathrm{T}^2}\right] = \ln\left[\frac{-\ln(1-\propto)}{\mathrm{T}^2}\right] = ln\frac{\mathrm{AR}}{\beta\mathrm{Ea}}\left[1 - \frac{2RT}{\mathrm{E}}\right] - \left[\frac{Ea}{\mathrm{RT}}\right]$, if n = 1 and,

$\ln\left[\frac{g(\propto)}{T^2}\right] = \ln\left[\frac{-\ln(1-\propto)^{1-n}}{(1-n).T^2}\right] = ln\frac{AR}{\beta Ea}\left[1-\frac{2RT}{Ea}\right] - \left[\frac{Ea}{RT}\right]$, if n ≠ 1 (175). The application of Coats and Redfern's requires three parameters search, i.e. reaction order, activation energy and Arrhenius constant (133), and since the value of $\frac{2RT}{Ea}$ is negligible *i.e.* << 1, the two equations of Coats and Redfern can be approximated as, $y_{CR} = \ln\left[\frac{-\ln(1-\propto)}{T^2}\right] = \ln\frac{AR}{\beta Ea} - \left[\frac{Ea}{RT}\right]$ if n = 1 and $y_{CR} = \ln\left[\frac{-\ln(1-\propto)^{1-n}}{(1-n).T^2}\right] = \ln\frac{AR}{\beta Ea} - \left[\frac{Ea}{RT}\right]$ if n ≠ 1, from which n can be calculated (173), (174), (175). Thus, for reaction order, n = 1, see Table 1.13 below, $\ln\left[\frac{-\ln(1-\propto)}{T^2}\right]$ versus 1/T gives a straight-line graph. Also, for the correct choice of the reaction index, n ≠ 1, $\ln\left[\frac{-\ln(1-\propto)^{1-n}}{T^2}\right]$ versus 1/T is equal to a straight-line graph. The parts of reaction in the graph which follow the same mechanism will always give straight-lines. The graph with highest correlation co-efficient for the correct value of $g(\propto)$, (see Table 1.5, section 1.8) is the mechanism controlling the combustion reaction. The correct mechanism and model also depend on shape and size of particles. The slope of the straight-line, $\left(-\frac{Ea}{RT}\right)$ equals apparent activation energy E_a, and intercept represents the pre-exponential factor A which is calculated by considering the temperature at which $m_t = \frac{(m_0 - m_f)}{2}$.

Also, the general expression for the isothermal reaction ($\ln\ln$-method, Sharp-Hancock) is used to investigate conversion kinetics (76). Combustion reaction of solid state is explained by an empirical kinetic model simplified from the Sesktak-Berggren equation (176). Furthermore, a non-isothermal method can be used to achieve the integrated model to determine the kinetic triple parameters (76). The non-isothermal method includes - Model-fitting e. g Freeman-Carroll, model-free fitting *e. g* Kissinger, Iso-conversional *e.g.* Ozawa-Flynn-Wall. One step global model $\left(\frac{d\propto}{dT}\right) = \left(\frac{A}{\beta}\right)e^{-E/RT}(1-\propto)^n$, is the simplest kinetic model used to explain combustion process of carbonaceous materials (177). This global model assumes that the rate of combustion can be expressed in one kinetic scheme. The Coats and Redfern model has been widely used to provide the kinetic description when n = 1, and n ≠ 1.

1.9 Oxidation mechanisms and models

The combustion of coal, biomass, and coal-biomass are examples of oxidation reactions. There are four basic mathematical models – nucleation, geometrical contraction, diffusion and reaction order used to explain the chemical kinetics of solid states (33), (76), (155), (156), (158), (178), (179), (180), (181), (182), (183), and (99). The geometrical contraction model explains the effect of shape and particle size. The models were generated by differentiation and integration using mechanistic assumptions (155).

The Table 1.13 shows the basic model used for the kinetic study of solid-state reactions. It is possible to estimate the reaction mechanisms that controls the thermal oxidation of the fuel samples as described in the TG curves (156), (172), (184), (185).

Table 1.13: Solid states oxidation mechanisms

Mechanisms	Description	Symbols	Models $\mathbf{g}(\propto)$
Reaction Order	First-Order	O1	$-\mathbf{ln}(\mathbf{1}-\propto)$
	Second-Order	O2	$(\mathbf{1}-\propto)^{-\mathbf{1}}$
	Third-Order	O3	$(\mathbf{1}-\propto)^{-\mathbf{2}}$
Phase boundary controlled reaction	Contracting area	R2	$\mathbf{1}-(\mathbf{1}-\propto)^{\mathbf{1/2}}$
	Contracting volume	R3	$\mathbf{1}-(\mathbf{1}-\propto)^{\mathbf{1/3}}$
Diffusion controlled reaction	1-D Diffusion	D1	$(\propto)^{\mathbf{2}}$
	2-D Diffusion	D2	$(\mathbf{1}-\propto)\mathbf{ln}(\mathbf{1}-\propto)+\propto$
	3-D Diffusion	D3	$[\mathbf{1}-(\mathbf{1}-\propto)^{\mathbf{1/3}}]^{\mathbf{2}}$
	Ginstling-Brounshtein's	D4	$\mathbf{1}-\frac{\mathbf{2}\propto}{\mathbf{3}}-(\mathbf{1}-\propto)^{\mathbf{2/3}}$

$\propto$ = conversion, 1-D, 2-D, and 3-D = one, two and three dimensions

The reaction order mechanism O1, O2 and O3 – describe a reaction in which the rate depends on concentration of the reactants. The phase boundary mechanism R2 – refers to a circular disc reacting from the edge inward and R3 – explains a sphere which reacts from the surface inward and it is assumed to be the central conversion model in combustion of carbonaceous molecules. Diffusion mechanism D1 – describes one-dimensional diffusion ruled by a parabolic law which has a constant diffusion coefficient whereas D2 – shows a two-dimensional diffusion-controlled combustion in a cylinder. The D3 – illustrates diffusion-controlled in a sphere with all three directions being important, while the Jander's equation and D4 – defines diffusion that begins from the outside of a spherical particle which is also known as Ginstling–Brounshtein's equation (156), (172), (184), (185).

A linear graph of the models with highest correlation co-efficient (R^2) indicates the mechanism, (Table 1.12) that best describes the combustion. The model that belongs to the controlling mechanism is required to adjust an existing combustor and to design a new one for efficient combustion.

1.10 Deconvolution

Combustion is comprised of overlapped processes which can be appropriately deconvoluted with the mathematical functions stated below (186), (187).

- Gaussian $Y_G = a_0 \exp\left[-\frac{1}{2}\left[\frac{(x-a_1)}{a_2}\right]^2\right]$
- The Lorentzian $Y_L = \left[\frac{a_0}{1+\left(\frac{x-a_1}{a_2}\right)^2}\right]$
- Weibull $Y_W = a_0\left(\frac{a_3-1}{a_3}\right)^{\frac{1-a3}{a3}}\left[\frac{x-a_1}{a_2}+\left[\left(\frac{a_3-1}{a_3}\right)^{\frac{1}{a3}}\right]\right]\exp\left[-\left[\frac{x-a_1}{a_2}+\left(\frac{a_3-1}{a_3}\right)^{\frac{1}{a3}}\right]^{a_3}\frac{a_3-1}{a_3}\right]$
- Frasier-Suzuki equation $Y_{FS} = a_0 \exp\left[-\ln 2\left[\frac{\ln\left(1+2a_3\frac{x-a_1}{a_2}\right)}{a_3}\right]^2\right]$

Where a_0 represents the amplitude, a_1 is centre of the curve, a_2 equals width, and a_3 is shape of the curve. These function are used to deconvolute reactions into individual processes, however, the Frasier-Suzuki has been reported to be efficient for multiple thermal events (186).

The application of the solid states oxidation models on the deconvoluted thermal processes provides activation energy E_a, pre-exponential factors A and the correct model $g(\propto)$ to describe combustion mechanism.

Though several research have been carried out on using microalgae biomass for biofuel, and there are few on coal-microalgae biomass blend (115). At the moment there is no report on agglomerate of discard ultra-fine coal and live microalgae biomass, as prepared using wet mixing approach except the attempts at InnoVenton (19), (23). This work is centred on co-firing live microalgae biomass prepared through wet blending with coal.

1.11 Aims and objectives

The aim of the research is to investigate the effect of live microalgae on the combustion kinetics of coal-microalgae composite. It includes to study the oxidation reaction mechanism of the composite as an agglomerated (pelletized or briquetted) product. In so doing, an understanding of the existence of the interaction between the coal and microalgae biomass will be developed. The study will not explain the economics of producing microalgae biomass, Coalgae production, and the quantity of power generated which can be found in the Infinergy unpublished report (188). To achieve the research aim, however, the following objectives must be reached –

- To produce different blends (Wt. %) of ultra-fine coal-microalgae biomass.
- To understand the effect of the microalgae biomass on the proximate and ultimate properties of the blends.
- To study in detail the effect of the microalgae biomass on the combustion kinetics of coal.
- To compare the lab scale (TG) to the pilot scale (fixed-bed) and to recommend on large-scale (industrial) combustion of the blend.

Thus, comparing the combustion kinetics of coal-microalgae biomass with coal could add knowledge on the potential of incorporating live microalgae biomass into coal to form single agglomerate unlike a linear combination of coal with traditional biomass. Microalgae biomass stores more energy than other biomass. It serves as a natural binder for discard ultra-fine coal, which has no market value. This approach will improve the economy, environment, and the health of coal users in South Africa.

1.12 Research structure

The structure of this research is summarized, (Figure 1.11) in the flow diagram below.

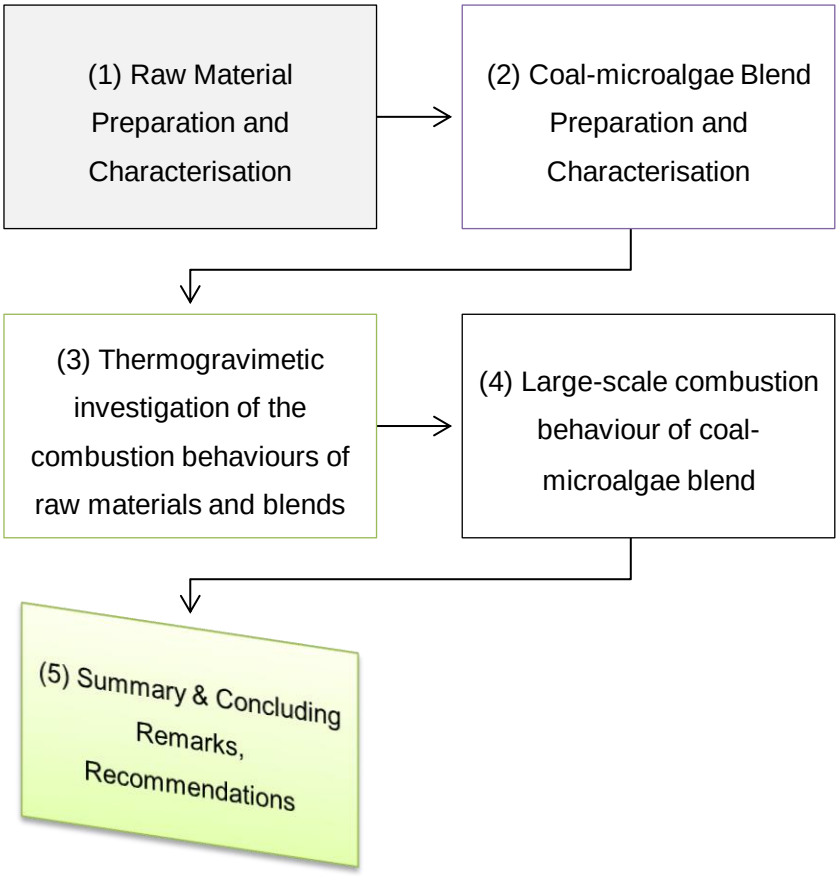

Figure 1.11: Research Flow Diagram

1.13 Problem statement

The combustion of coal together with biomass is recognised as an approach with low risk and low cost that significantly reduces the environmental impact of coal. Despite many examples of large coal-firing power stations successfully co-firing biomass and coal, the supply of sufficient biomass to such co-firing utilities remains a significant challenge. Though biomass is associated with corrosion, fouling or slagging based on the alkali metals content of biomass, there could be synergistic reaction between coal/algae biomass. Provided it can be produced cost-effectively, microalgae biomass is recognised as a viable source of biomass in view of its potential advantages over traditional land-based plants, including:

- Microalgae does not require arable land for cultivation.
- Microalgae is the fastest biomass producing species known to man.
- Microalgae has higher energy density compared to other types of biomass.
- Microalgae does not compete with food production.

Previous study at the Nelson Mandela University Institute for Chemical Technology, InnoVenton showed the viability of recovering, upgrading, and agglomerating waste coal (fine and ultra-fine) by treating it with live microalgae. A new integrated microalgae cultivation system developed by the Institute promises to significantly reduce the costs of microalgae cultivation. To exploit these advances, a thorough understanding of the combustion behaviour of blends of coal and microalgae biomass is required.

1.14 Research Hypothesis

The treatment of ultra-fine coal with live microalgae will improve the combustion behaviour of the resultant blends of coal and microalgae biomass to an extent that is greater than what could be expected from a simple linear combination of the two separate raw materials.

1.15 Scope of thesis

The scope of this thesis includes the detailed investigation of the effect of treating ultra-fine coal with live microalgae by studying the impact on the chemical properties of the coal-algae blends compared to the parent coal, the effect on the kinetics of the combustion of blends of microalgae and coal, and finally the investigation of actual larger-scale combustion processes. Now, there is no literature report which describes the process by which microalgae biomass forms a fuel with discard ultra-fine coal (waste) and the effect on the combustion kinetics of coal.

Combustion is a natural chemical process which proceeds to achieve kinetic equilibrium. It can be characterised using reaction order, kinetic model, mechanism, and activation energy which defines the reactivity of a fuel. This can be done by using thermogravimetry, which is widely accepted in combustion studies. The Frasier-Suzuki equation can deconvolute combustion process into primary schemes, after which the rate and Arrhenius equations, Coats and Redfern model, and solid states oxidation mechanism are used to describe the combustion as were applied in this study.

Chapter 2

2.0 Experimental

2.1 Introduction

This chapter describes the raw materials, preparation procedures for raw materials and blends, analytical techniques, mathematical calculations, thermogravimetric and fixed bed combustion carried out in this study.

2.2 Raw materials

The materials utilized are discard ultra-fine coal supplied by Eskom and labelled Eskom coal A (Figure 2.1), and microalgae biomass (Figure 2.2) harvested at Innoventon and another discard ultra-fine coal supplied by Exxarro and labelled Exxarro coal B (Table 2.1) for comparison purposes.

Table 2.1: Raw materials

S/No	Materials	Characteristics
1	Eskom coal (A)	Discard ultra-fine coal, no market value
2	Exxarro coal (B)	Discard ultra-fine coal, no market value
3	Microalgae biomass (mixed specie)	Renewable, sustainable

2.2.1 Coal

The Eskom coal sample was stored in 200 L drums and was obtained from the Izibulo coal mine, Mpumalanga.

(a) (b)

Figure 2.1: (a) Coal lumps (b) discard ultra-fine coal

2.2.2 Microalgae biomass

Microalgae used in this study was cultivated in the integrated vertical column photo-bioreactor–raceway cultivation system developed at InnoVenton, (Figure 2.2) and comprised a mixed colony of various strains of *scenedesmus*.

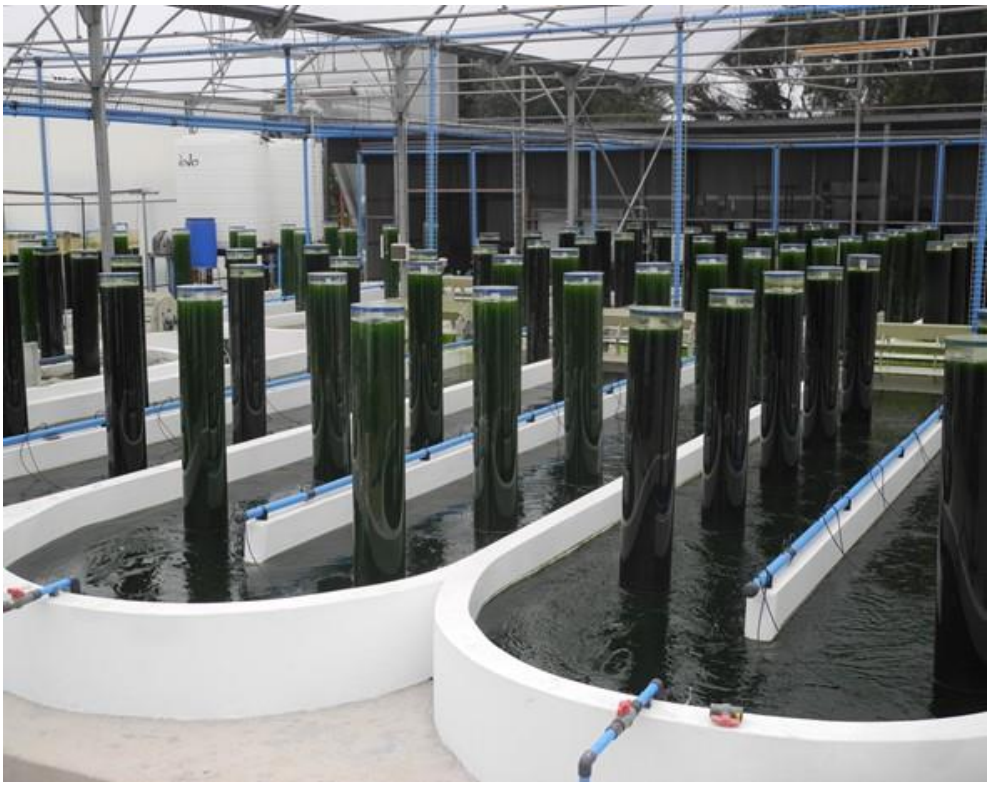

Figure 2.2: Photobioreactor for cultivation of microalgae, InnoVenton

2.3 Sample preparation

2.3.1 Milling, sizing, and conditioning of coal

A gross sample was taken according to ASTM D-2234 from various points, and at various depths of the 200 L drums with a cylindrical pipe. The sample was then placed on a rectangular wooden tray and allowed to air-dry for 24 hours to remove the surface moisture. The raw coal sample was prepared according to ASTM D-2013, on a Keegor Vertical Spindle pulveriser to a particle size of <250 µm, and further milled to <150 µm size fraction. The fraction <150 µm was suitable for chemical and thermal analysis as well as forming coal-microalgae agglomerates. The pulverised coal sample was air-dried for 2 to 3 days and thoroughly mixed, after which the sample was transferred to an airtight container.

2.3.2 De-watering of microalgae biomass

Fresh microalgae biomass was harvested from the growth system by natural settling. Growth medium was transferred into a settling dam in the evenings and allowed to settle overnight before returning the supernatant growth medium back to the growth system the next morning. The slurry sample obtained from the growth system was dried, (Table 3.2b) and used to calculate the percentage mass of dry microalgae per litre of the settled slurry. Microalgae slurry of about 40 – 50 g/L, was then transferred into a mixing tank to await further processing. For the preparation of coal-microalgae mixtures, freshly harvested microalgae biomass was centrifuged using a Hermle centrifuge Z-383. An approximate volume of 200 ml each was transferred into tubes (cups) and centrifuged at 4500 rpm for approximately 10 minutes. The sample was removed, and the supernatant was decanted and replaced with distilled water. The microalgae “pellet”, (see cups in Figure 2.3) was re-suspended by stirring with a glass rod, and re-centrifuged. The process was repeated 3 times in all to ensure that the resultant slurry was properly separated from residual nutrients and excess water.

Figure 2.3: Dewatering and cleaning of microalgae biomass with centrifuge

2.3.3 General procedure for preparation of blend

The D-Optimal experimental design was used to construct, (Table 2.2) the blends.

Table 2.2: Mixtures Experimental Design

S/No.	Coal (%)	Algae (%)	Coalgae™ (formula)	Sample ID (%)
1	100	00	100C-00A	0
2	90	10	90C-10A	10
3	80	20	80C-20A	20
4	70	30	70C-30A	30
5	60	40	60C-40A	40
6	50	50	50C-50A	50
7	00	100	00C-100A	100

A = microalgae biomass, C = discard ultra-fine coal, ID = identification

The identity of each blend denotes the quantity of microalgae biomass contained in the sample. In some instance, the blends were expressed as ratios of raw materials. Microalgae biomass was labelled as 100 %, coal as 0 %, and the blends as 10, 20, 30, 40, 50, and 5, 15, 25, 35, 45 % of microalgae biomass etc.

2.3.4 Dry solid of Coal and Microalgae for blend

The dry solid in microalgae biomass slurry as well as wet coal was obtained by considering the moisture of the original materials, (see Tables 3.1 – 3.2, chapter 3), which was used to work-out the material ratio (see Table 3.3, chapter 3) for blends. Average moisture content for 1.47g, 1.67g, and 1.26 g of microalgae biomass pellets was obtained using, a conventional oven and an Eltra TG-Proximate was ~ 83.27 %. Thus, the average dry solid in the microalgae biomass pellets was then calculated using equation 3.2 of the mathematical section and the result was ~ 16.73 % as indicated, (see Table 3.1), in chapter 3. The procedure was used to obtain the moisture content and the percent dry solid in coal (see Table 3.2 – Moisture for the Eskom Coal "A"). The average moisture content for 1.23 g, 1.26 g, and 1.33 g of coal was ~ 5.89 % and dry solid was ~ 94.11 % as represented in Table 3.2 of chapter 3.

2.3.5 Preparation of Coalgae® from wet feedstock

The co-firing share of dried samples of coal, and dried traditional biomass is normally calculated with equations like, $Fb = cW + bW$, where *Fb* represents fuel blend, *c* and *b* are coal, and biomass ratio, *W* is weight of individual dried raw material (32), (50), (see equations 2.21 and 2.2). This is not the same when a liquid feedstock like microalgae biomass is used.

First, the observed moisture for microalgae biomass, (section 2.3.4 above) was subtracted from 100 %, to achieve dry solid da of, ~ 16.73 %. Then, the moisture for coal, was also subtracted from 100 %, to achieve dry solid dc of, ~ 94.11 %, see results, chapter 3. The, da and dc were used to calculate the actual mass of microalgae biomass and coal required for each composite as detailed in the mathematical procedures, equation 2.1 – 2.8 in section 2.5.1. The total mass of mixture was then scaled up or down as required and the feedstock ratios in composite were constructed, (see Table 3.3 – material ratio in composites, chapter 3).

Then, using 10 % coal-microalgae biomass composite as an example, ~ 19.2 g of freshly prepared microalgae biomass of solids da ~16.73 % and moisture ~ 83.27 % was added to 30.8g of coal of solids dc ~ 94.11 % and moisture ~ 5.89 %. The mixture was either scaled up or down as required. Wet coal of mass, y was added to slurry of microalgae biomass of mass, x (see result in section 3.3 – Material ratio in Composites). Each of the composites was homogenised for 15 minutes separately, with mixer and dried at 35 ±5 ^{o}C overnight to ~ 5 - 10 % moisture. The resultant agglomerate known as Coalgae® powder was then blended as described in the experimental procedure, section2.3.6 and the same procedure was repeated for all other blends.

2.3.6 Pelletization of powdered blends

The powdered agglomerate, section 2.3 was dried to 8 – 10 % moisture under controlled temperature of 107 ± 3 ^{o} C, the temperature designated for moisture analysis. About 6.0g was then weighed into sample cups. The weighed mass was pressed at about 2500 psi for a minute using a Difftech-USA press machine RC104. A large amount of the moisture was lost on pressing. The pellets, (see Figure 3.4 in chapter 3 – picture of Coalgae) were dried for 2hrs under controlled temperature of 105 ^{0}C with conventional oven to a constant mass of ~ 4.0g, cooled in desiccator for about 15 minutes and packaged for combustion.

2.4 Instrumental methods

2.4.1 Proximate analysis by bulk TGA

The proximate analysis was carried out in a conventional oven using ASTM D-3172 for the moisture, and ASTM D-3174 for the ash, ASTM D-3175 for the volatile matter in a furnace. While the automatic bulk proximate analysis was carried out with an Eltra Thermostep macro TGA.

The dry solids in the wet coal and microalgae biomass (pellet) was obtained using a Smart Trac CEM system – 5, for 5 minutes. Confirmation of bulk proximate analysis result was carried out with the conventional oven at 107 ± 3 ^{o}C for 1 hour and the dry solids calculated as in section 2.3.4.

The samples were pulverised one after another with mortar and pestle to <150 µm size. Samples were analysed according to ASTM D7582– $10^{\varepsilon 1}$ with the Eltra Thermostep macro TGA, (Figure 2.4) which has 19 sample crucibles plus one blank crucible. Measurements were carried out in the sequence of moisture, volatile, ash and fixed carbon. The instrument was supplied with nitrogen of > 99.99% purity and oxygen >99.99 %. The progress of analysis was graphically displayed, and each parameter was completed when the specimen reached a constant mass.

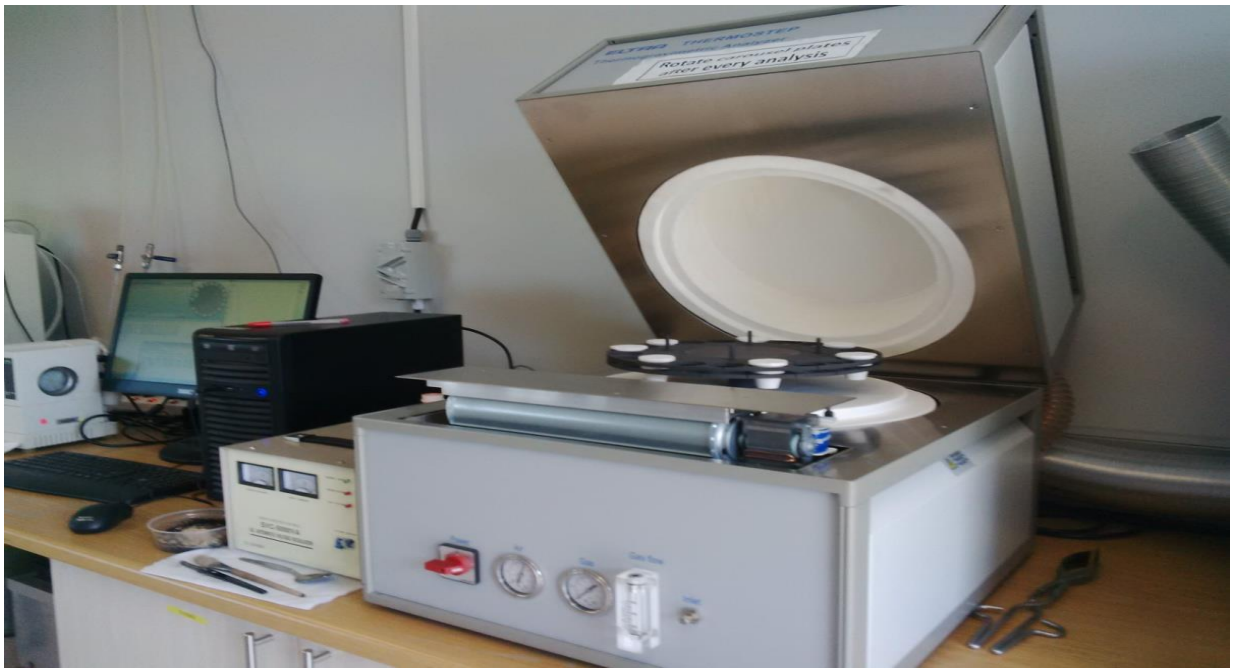

Figure 2.4: Eltra automatic thermogravimetric TG-Proximate analyser

Sample mass of 1.1 g ± 0.1 g each was added into separate crucibles and covered with lids. The instrument software records the initial mass. The moisture analysis was first carried out at 107 ± 3 ^{o}C for 1 hour with dry nitrogen gas of flow rate 0.4 – 1.4 cm^{3}/min. The test is completed when the mass at that temperature remains constant and the moisture, section 2.5.3 was calculated.

The program re-weighs the crucible at the end of moisture analysis to continue for volatile determination, section 2.5.3 with nitrogen at a flow rate of 0.7 – 1.4 cm^{3}/min. The temperature was raised from 107 ^{o}C to 950 ± 10 ^{o}C but was held at 950 ± 10 ^{o}C for 7 minutes, to obtain the volatile.

The mass after volatile determination was re-weighed as well as the crucible content, and the dropped temperature went to 950 ^{o}C ± 10 ^{o}C for ash analysis. Then, oxygen was allowed through at flow rate of 0.4 – 0.5 cm^{3}/min for 2 hours. The final mass at the end of the 2 hours of combustion was recorded as the ash content. The percent fixed carbon FC was calculated as the difference of moisture, volatile and ash from one hundred, as described in section 2.5.3

2.4.2 Ultimate analysis – CHNS and O

About 5 g of each fuel sample prepared as per section 2.3 was individually homogenised in a mortar. An accurate micro-sample of 5 mg was weighed into silver vessels of 6.0 µm thickness, according to ASTM D-3177 – 79 methods. The samples were transferred automatically into the combustion tube. One at a time, each sample was flushed with helium and oxygen was introduced at about 20ml/min for combustion. Catalytic combustion of sample was carried in the Vario EL Cube elementar furnace, at a steady temperature of 1200 °C. The reduction of CO_2, SO_x, NO_x and H_2O were done in another tube furnace, and the N2, CO_2, H_2O, and SO_2 gases were released to the corresponding adsorbers. The gases were separated individually by adsorption through three columns in purge and trap chromatography. The combustion gases was passed on to the thermal conductivity detectors linked to the computer which calculated the concentrations of each gas as peak signal, and sample weight with a known reference standard (122). The sample weight was then converted to percent and recorded on dry ash free basis. The O oxygen content was calculated according to ASTM D-3176 method (189), using equation (2.13).

2.4.3 Elemental analysis of composites and residual ash

Fuel samples prepared as per section 2.3.3 was analysed using the XRF, and according to the ASTM D-4326 method. Each fuel sample was homogenised separately with mortar & pestle. Then, sample cups were constructed using, sharp-nosed forceps, sample cup mould, spatula, labelled, and weighed on the analytical balance. With the aid of spatula about 5g was transferred into the cups, and the mass was recorded. Each sample cup was placed into the instrument and sample details were recorded. The sample was automatically analysed for elemental composition on an Epsilon 3 XRF system X-ray fluorescence instrument (190). Similarly, the ash

residue from proximate determination, section 2.4.1 was analysed, but the XRF result was semi-quantitative. Thus, it may not provide enough information for appropriate conclusion due to the measurement error.

2.4.4 Energy value of fuel – Bomb calorimetry

About 1.0 g of the sample was prepared as in section 2.3.1, and 0.5g sample was loaded into combustion crucible of the Leco AC6000 bomb calorimeter and according to ASTM-D5865-07 (121). The crucible was inserted into the holder, tied with thread onto the ignition wire, and allowed contact with the sample. The bomb was closed tightly, and oxygen was supplied at about 3200 k P or 450 psi pressure. The bomb was inserted onto the calorimeter vessel and it was given time to equilibrate with water at about 3 - 5 °C for 1.5 min. The mass was recorded, sample pre-fired for 0.5 minutes and ignited at 25 °C. The firing temperature changed by 7.5 °C for every 4.75 minutes' increase in time. The heat of combustion per unit mass was calculated, (see later in the mathematical section 2.5.4, (2.14)) and given as the gross heat at 25 °C in (MJ/ kg).

2.4.5 Solid state nuclear magnetic resonance

The samples prepared as described in the sample preparation section 2.3, were analysed in the Sasol research and development facility at Stellenbosch University, Cape Town. The analysis was carried out at room temperature with 500MHz Varian Inova spectrometer at 125MHz for ^{13}C using a 4-mm Magic Angle Probe for VT CP/MAS. The quantitative data are obtained with DP-MAS solid state NMR method using 13 kHz spinning speed and 4 μ s 90° ^{13}C pulse length. The CP/T1/total sideband suppression method was used to ensure that all carbon sites are relaxed by N95%. The recycle delay was adjusted as 30 s, to allow all carbon centres to be relaxed by more than 95%. The number of scans for DP/MAS was 3000 for all samples. Phase correction was applied before integration of peak area on the spectrum using the device's program Varian NMR analysis auto phase correction function. A small phase correction was done to flatten the baseline with no additional baseline correction. Using a spinning speed of 13 kHz, the total sidebands of the aromatic groups were reduced and easily integrated outside the region of integrated functional groups. The

integrated sideband was multiplied by two and added to centres band of aromatic C=C and C-H region and the structural changes were recorded (191).

2.4.6 Non-isothermal – TGA combustion

Combustion of samples was investigated using non-isothermal thermogravimetry, TGA and differential DTGA technique. About 10 g samples from section 2.3.1 were pulverised with mortar and pestle for 10 minutes. The prepared sample was dried at 35 °C for 2 hours in the oven and cooled for 15 minutes in a desiccator. About 5 mg of the sample was then weighed into the microbalance (furnace) of the Perkin Elma STA 6000 TG (Figure 2.5). The initial weight was recorded by Pyris software. The instrument was first set to isothermal at 40 °C for 5 minutes and thereafter non-isothermal from 40 °C to 900°C at a heating rate β of 15 °C/min under oxygen atmosphere of steady flow rate of 20 ml/min.

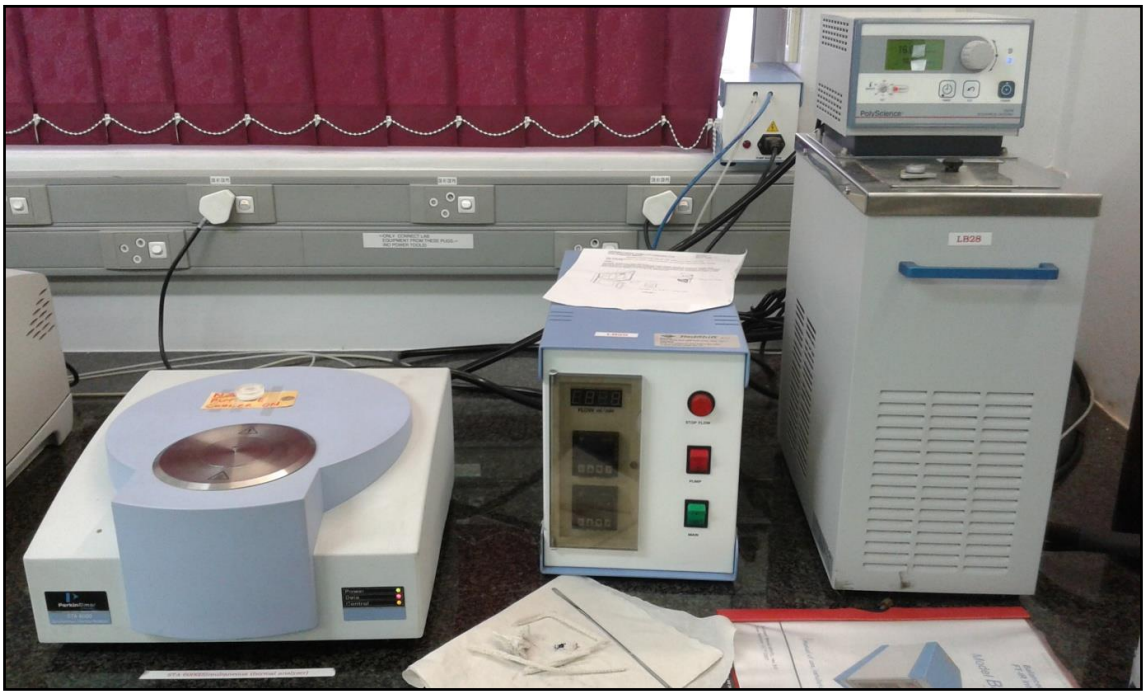

Figure 2.5: Perkin Elma STA 6000 TG - analyser

The TG and DTG curves, (Figure 2.6) below were generated automatically by the Perkin Elma STA 600 TG analyser instrument software.

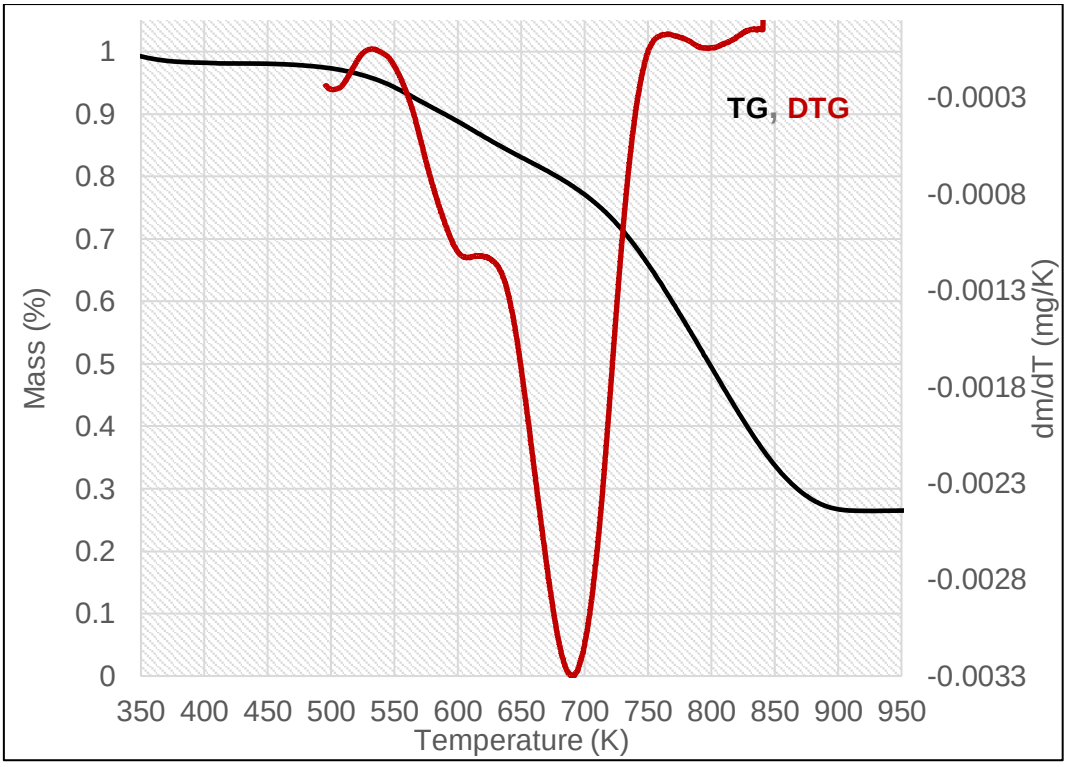

Figure 2.6: Typical TG and DTG profile for samples

The combustion characteristics were first investigated *via* graphical construction, (Figure 2.7), but later calculated with the Coats and Redfern's model as described in the section 2.5.5 of the mathematical procedures.

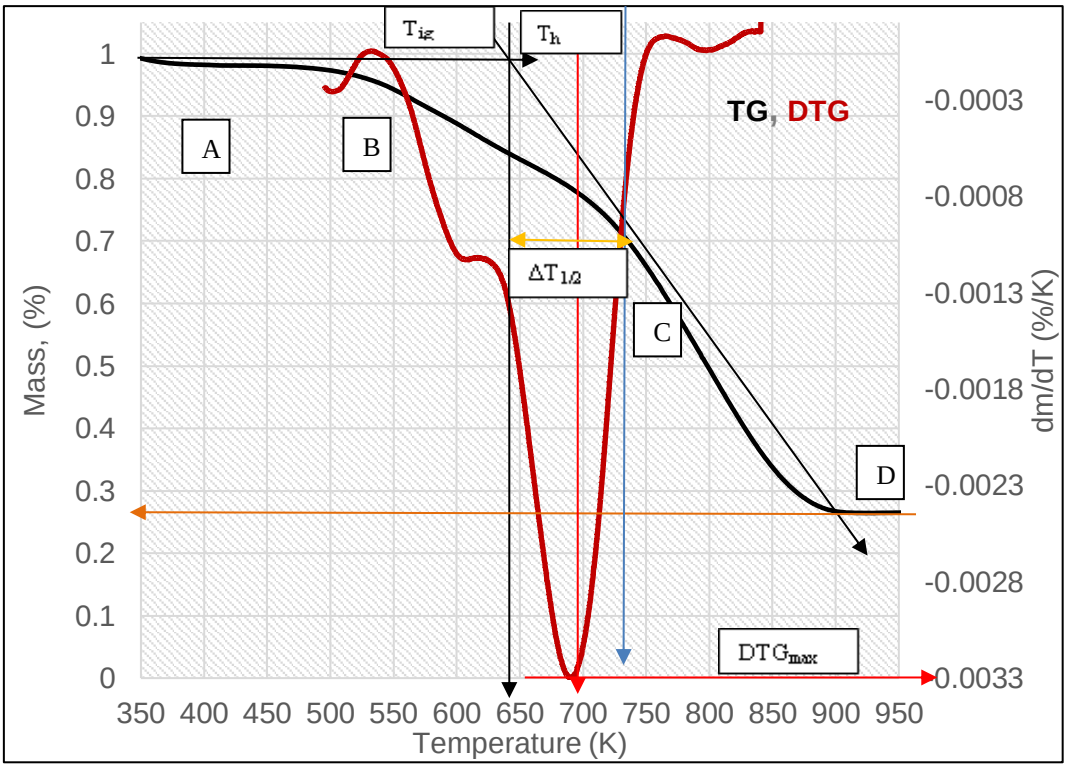

Figure 2.7: The graphical derivation of combustion characteristics

The combustion characteristics were investigated using TG and DTG plot (Figure 2.7). Four distinct stages, A – de-watering, B – de-volatilization, C – char combustion, and D – burn-out were identified. A horizontal straight line indicated by the black arrow was constructed tangentially along the de-volatilizing stage (B) towards T_h and another straight line crossing the ignition point down to the region D was drawn tangent on the TG curve, (Figure 2.7) along stage (C). Then, the point of intersection of the two straight-lines was considered as the ignition point. Through this ignition point, a straight-line was drawn downwards to obtain the ignition temperature (T_{ig}) on x-axis. The burn-out temperature was obtained by drawing a horizontal line to touch the stage D on the base of the TG. The point where this line meets the tangent drawn from stage (C) was considered as the burn-out temperature read from x-axis. The point where this horizontal line touched the secondary y-axis was read ass the rate of reaction. Another straight-line was drawn through the minimum point on the DTGA curve to the x-axis to obtain the maximum combustion temperature, Th. The values of $(dm/dt)_{max}$ and $(dm/dt)_{mean}$ were considered as the rate of reaction at maximum temperature and mean rate of reaction respectively between the ignition and burn-out temperatures. Similar construction was used for each sample, though mathematical procedure described in section 2.5.5 provided improved values which was applied to calculate the comprehensive combustion characteristics.

2.4.7 Bulk combustion in fixed-bed reactor

The bulk combustion of sample was carried out in a fixed bed reactor at John Thompson research and development facility (Cape Town). The facility was designed to test the ignition time, vertical burn down rate and to measure the quantity of ash of test sample relative to the reference coal. The aim was to evaluate the large-scale performance of Coalgae® relative to coal. Also, the O_2 and CO levels were monitored and trended. The samples were prepared with regards to foreign material and particle size to ensure an unbiased result and sieved to ensure that there were no fines in the test sample. Particle size distribution analyses were carried out to ensure similar size distributions for the raw materials. Combustion chamber of the fixed reactor, (Figure 2.8) was loaded with 10kg of each fuel sample and the top 20mm was ignited. The

time the bed was ignited, the weight, gas composition, and temperature were logged on a data logger, (Figure 2.8) and trended.

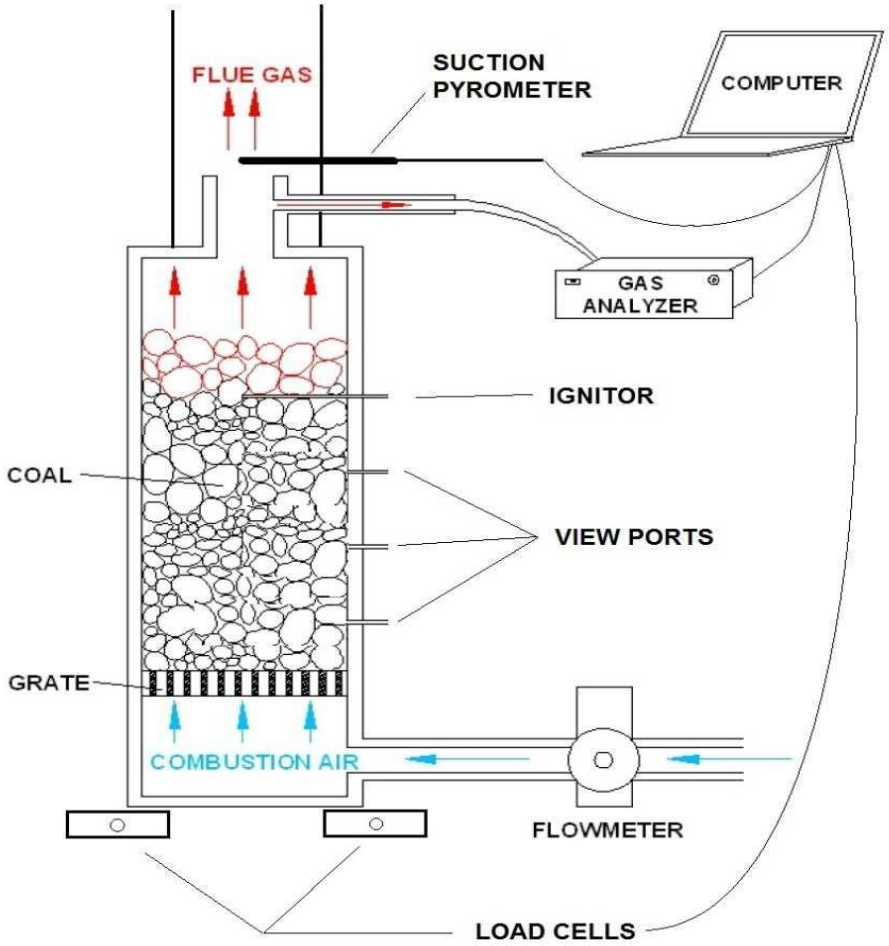

Figure 2.8: Vertical down fixed bed reactor

2.5 Mathematical procedures

2.5.1 Solids and mass of wet microalgae biomass and coal

The dry solids content of the freshly harvested microalgae biomass and the cleaned microalgae biomass pellets, and wet coal was calculated to ensure correct dry w/w blend, equation (2.1).

$\%\,S = (100 - \mathrm{FM})\%$..... (2.1)

Where, FM = moisture content and,

% S = solids in (moist) wet samples, represented as da for microalgae biomass and dc, for coal. The resultant mass, x of wet microalgae biomass blended as in section 2.3.5 was obtained with equations (2.2),

$$x = \frac{p\ dc\ m}{da\ (1-p)+pdc}$$ 2.2

Where, x = mass of microalgae biomass pellet (g).

Then, the mass y of wet coal was calculated with equation (2.3),

$$y = \frac{q\ da\ m}{dc\ (1-q)+q\ da}$$.....2.3

Where, y = mass of coal (g) and,

$q = (1 - p)$ or $(100 - p)$,

p = dry mass of microalgae biomass,

q =dry mass of coal,

m = total mass of mixture**.**

2.5.2 Mass of dry coal and microalgae biomass in blend

The mass (%) of feedstocks expressed in formula, (see result, Table 2.2 – Mixture experimental design) was translated to the actual dried mass w/w in the blend. The dry microalgae biomass (*i.e.* mass of the pellet) represented in each formula, (see result, Table 3.3) was computed using, equation (2.4),

$$\% \, p = \frac{da \, x}{da \, x + dc \, y} \quad \text{..... (2.4)}$$

Where, p = dry mass of microalgae biomass (%) and,

da and dc = solids in wet microalgae biomass (pellet) and coal (%) respectively.

x and y = mass of wet microalgae biomass (pellet) and coal (mg) respectively.

Similarly, the dry mass of moist coal in each formula, (see result, Table 3.2, chapter 3) was calculated with equation (2.5),

$$\% \, q = \frac{dc \, y}{da \, x + dc \, y} \quad \text{..... (2.5)}$$

Where, q = dry mass of wet coal (%).

$$\% \, p = \frac{da \, x}{da \, x + dc(m - x)} \quad \text{..... (2.6)}$$

Substituting p into equation (2.7), gave the mass of wet microalgae biomass as described by equations (2.8),

$$da \, x = p(da \, x) + p \, (dc \, (m - x)) \quad \text{..... (2.7)}$$

$$x = \frac{p \, dc \, m}{da - p \, da \, p \, dc} = \frac{p \, dc \, m}{da \, (1 - p) + p \, dc} \quad \text{..... (2.8)}$$

Where, m, p, and q = dry mass (mg) of mixture, microalgae, and coal respectively.

2.5.3 Proximate and ultimate – C H N S and O

The proximate parameters were determined using the bulk TGA proximate method and computed automatically by the instrument software. The moisture content of each sample was calculated, equation (2.9),

$$M = \left[\frac{(W-B)}{W}\right] x\ 100 \quad \text{..... (2.9)}$$

Where, M = moisture (%) and,

W = mass (g) of sample,

B = mass (g) of sample after drying.

The volatile released was computed, equation (2.10),

$$V = \left[\frac{(B-C*)}{W}\right] x\ 100 \quad \text{..... (2.10)}$$

Where, V = volatile (%)

C* = mass (g) of test sample after heating

The ash A was calculated, equation (2.11),

$$A = \left[\frac{(F-G)}{W}\right] x\ 100 \quad \text{..... (2.11)}$$

Where, A = ash (%) and,

F = mass (g) of crucible and ash,

G = mass (g) of empty crucible.

The fixed carbon, FC was computed, equation (2.12),

$$\mathrm{FC} = 100 - (\mathrm{M} + \mathrm{A} + \mathrm{V}) \quad \text{..... (2.12)}$$

Where, FC = fixed carbon (%) and,

M = moisture (%),

A = ash (%),

V = volatiles (%).

The C H N S was determined using the Elementar analyser whereas the oxygen, was calculated in percentage by difference using equation, equation (2.13),

$$\%\,\mathrm{O} = 100 - (\mathrm{A} + \mathrm{C} + \mathrm{H} + \mathrm{N} + \mathrm{S})\% \text{..... (2.13)}$$

Where, A = ash (%) and,

C = carbon (%),

H = hydrogen (%),

N = nitrogen (%),

S = sulphur (%).

2.5.4 Heat content of fuel samples

The higher heating value (gross calorific value), *i.e.* amount of heat released on combustion of fuel samples using the bomb calorimeter and allowing the products to return to 25 ^{o}C, was obtained using equation (2.14) below,

$$\mathrm{E_{TS}(c)} = \sum \mathrm{K_v b} \times (\mathrm{T_v\,(n)} - \mathrm{T_b\,(n)}) + \mathrm{C_v} \times (\mathrm{T_b\,(n+1)} - \mathrm{T_v\,(n)}) \quad \text{..... (2.14)}$$

Where, $E_{TS\ (c)}$ = calculated energy of sample based on thermodynamic model of calorimeter in Celsius heat unit (MJ/ kg) and,

$K_{v}b$ (n) = thermal conductance (J/ ^{o}C) of the combustion vessel to the bucket,

T_{v}(n) = calculated temperature (^{o}C) of the combustion vessel at time interval n,

C_{v} (n) = heat capacity (J/ ^{o}C) of the vessel,

T_{b} (n) = measured temperature (^{o}C) of the bucket at time interval n,

m = mass of sample (g)

n = time interval in minutes,

2.5.5 Combustion characteristics and reactivity

In addition to the graphical determination of combustion characteristics described in section 2.4.6, the ignition temperature (T_{ig}), was calculated by using the peak temperature (T_{max}), rate $\left(\frac{dm}{dT}\right)$ at maximum combustion i.e. DTG_{max} and the resultant value of Coats and Redfern kinetic model, y_{CR}. This was done by using the VLOOKUP in excel to obtain the most appropriate y_{CR} description, equation, (2.15) with correlation closest to the best suitable explanation of the thermal event.

$$y_{CR} = \ln\left[\frac{1-(1-\propto)^{1-n}}{T^{2}\,(1-n)}\right] \quad \text{……………………………………………………………….. (2.15)}$$

Where,

T = temperature

n = reaction index,

α = conversion

The reaction index, n was obtained by considering the maximum correlation of the linear graph y_{CR}. The combustion characteristics were computed in the mathematical procedure section, 2.5.5 as would be seen later. The activation energy $E_{a.}$ was

computed by using the observed slope, m of the graph of y_{CR} versus 1/T. The DTG_{mean} was calculated as sum mean of velocities divided by number of observations. Width of combustion $\Delta T_{1/2}$ consistent with the graphical values was obtained as half the temperature range of the combustion interval and fuel conversion $\propto$ was calculated in the mathematical procedures section 2.5.8, as fractional mass loss.

The ignition temperature T_{ig}, was obtained mathematically, as in equation (2.16),

$$T_{ig} = \frac{(1 - y_{CR})}{DTG_{max} + T_{max}} \quad \text{..... (2.16)}$$

While the burn-out T_h was read from the graph through peak of combustion.

$$DTG_{mean} = \frac{(DTG_1 + DTG_2 + DTG_3 \ldots\ldots\ldots + DTG_n)}{n} \quad \text{..... (2.17)}$$

Where, DTG_{mean} = mean burning velocity and,

n = number of observations.

The comprehensive combustion characteristics index, ccc or S – value, equation (2.18) was computed (114), (137), (192), (193), and (194),

$$S = \frac{R}{Ea}\frac{d}{dT}\left(\frac{dm}{dt}\right)_{T=T_{ig}} \frac{dm/dT_{max}}{dm/dt_{T=T_{ig}}} \frac{dm/dT_{mean}}{T_h} \quad \text{..... (2.18)}$$

$$S = \left[\frac{\left(\frac{dm}{dt}\right)_{max}\left(\frac{dm}{dt}\right)_{mean}}{(T^2{}_{ig})(T_h)10^{14}}\right] \quad \text{..... (2.19)}$$

Where, S = ccc or S -value and,

$\left(\frac{dm}{dt}\right)_{max}$ = maximum combustion velocity,

$\left(\frac{dm}{dt}\right)_{mean}$ = average combustion velocity,

T_{ig} = ignition temperature

T_h = burn-out temperature.

The activation energy E $_a$ was computed, equation (2.20),

$$Ea = \frac{m\,R}{1000} = \frac{m\left(8.314\,\frac{J}{mol}K\right)}{1000} \quad \text{..... (2.20)}$$

Where, R = Universal gas constant = 8.314 J/mol. K and,

E a = activation energy (kJ/mol.);

m = slope of the Coats and Redfern model $Y_{CR} = mx + c$ (i.e. mathematical description of the solid states kinetics),

Where, $m = \frac{R}{Ea}$, defines the reactivity of composites and on combustion, a small value of activation energy means high reactivity. Thus, $\frac{R}{Ea}$ can also be related to $k = A\exp\left(-\frac{Ea}{RT}\right)$, where, exp = exponential and, the results were presented and discussed as in chapter 4, section 4.1.5 – Coats and Redfern's combustion parameters.

2.5.6 Characteristic interaction

The DTG plots obtained from the non-isothermal combustion of fuels at different weight proportions were used to study the interaction between coal and microalgae biomass. The theoretical and observed curve of blends were overlaid to investigate for synergistic interaction and formation of new substance (195), (196), (197), and (198). The observed curve of blend M $_{mix}$ was also superimposed on the theoretical sum of curve, to check if both are similar by using equation (2.21),

$$M_{mix} = P_c . M_c + P_a . M_a \quad \text{..... (2.21)}$$

Where, M_{mix} = mass of composites and,

P_c = fractions of coal

P_a = fraction of microalgae biomass

M_c = mass of coal

M_a = mass of microalgae biomass,

Theoretical rate of combustion was overlaid on the observed rate of combustion using the additive rule (142), (199), (200), (201). The theoretical DTG for each blend was calculated by adding the weight loss rate of individual raw material and compared with the observed DTG plots. Theoretical and observed rates, (result, Table 3.4) were overlaid both against the standard temperature T (K), equation (2.22),

$$\left(\frac{dm}{dT}\right) = P_c . \left(\frac{dm}{dT}\right)_c + P_a . \left(\frac{dm}{dT}\right)_a \quad \text{..... (2.22)}$$

Where, $(dm/dT)_c$ = rates of combustion of coal and,

$(dm/dT)_a$ = rates of combustion of microalgae biomass, (T Corr. ~99.99% with t).

2.5.7 Rate of reaction

The observed TGA data, (Table 3.7a) was used to calculate the rate of combustion, Rc, (*i.e.* change in mass over change temperature (T) as in non-isothermal condition, time and temperature are ~ 99.9 % correlated). The rate of reaction obtained as equation (2.23),

$$Rc = \left(\frac{\mathbf{dm}}{\mathbf{dT}}\right) \quad \text{……..…….. (2.23)}$$

Where, R c = rate of combustion and,

m = mass of fuel,

T = temperature.

A graph of decrease in mass (m) on primary y-axis and $\left(\frac{\mathrm{dm}}{\mathrm{dT}}\right)$ (on secondary y-axis was plotted against temperature T, on x-axis. From the graph, rate at the peak temperature (DTG_{max}), was considered as the rate of the reaction. The rate at DTG_{max} for 0 – 50 % and 100 % was first deduced, as from the graphical construction, (section 2.4.6, Figure 2.7), on the rate - axis. The theoretical and observed rates at the peak combustion temperature for the samples were then (see section 4.1.3 and Table 4.13 – Theoretical and Observed rate) compared.

2.5.8 Kinetic modelling

For combustion under non-isothermal TGA conditions with fractional mass loss (197), equation (2.24),

$$\propto = \frac{\mathrm{m_0 - m_T}}{\mathrm{m_0 - m_f}} \quad \text{..... (2.24)}$$

Where, $\mathrm{m_0}$ = initial mass at starting temperature (T = 40 ºC) and,
$\mathrm{m_T}$ = mass at temperature T,
$\mathrm{m_f}$ = final mass at temperature (T_f = 900 ºC)
The rate at which the $\propto$ changes needs to be modelled, thus from the rate law,

$$\frac{\mathrm{d}\propto}{\mathrm{dt}} = kf(\propto) \quad \text{..... (2.25)}$$

Where, $f(\propto)$ = differential model, and
t = time, $k =$ rate constant, related to the Arrhenius equation,

$$k = \mathrm{A}\exp\left(-\frac{\mathrm{Ea}}{\mathrm{RT}}\right) \quad \text{(2.26)}$$

A = pre-exponential factor

$\mathrm{E_a}$ = activation energy,

T = Temperature (K),

R = molar gas constant = 8.314 J/mol. K

The differential model relates to the decrease in mass, equation (2.27),

$$\mathrm{f}(\propto) = (1-\propto)^{\mathrm{n}} \quad \text{(2.27)}$$

Where, $n =$ index of reaction.

By substituting the model equation (2.27) for $\mathrm{f}(\propto)$ in equation (2.25), we have equation (2.28),

$$\frac{\mathrm{d}\propto}{\mathrm{dt}} = k\,(1-\propto)^{\mathrm{n}} \quad \text{(2.28)}$$

By substituting for k in equation (2.26) into equation (2.28) we obtain equation (2.29),

$$\frac{\mathrm{d}\propto}{\mathrm{dt}} = \mathrm{A}\exp\left(-\frac{\mathrm{Ea}}{\mathrm{RT}}\right)(1-\propto)^{\mathrm{n}} \quad \text{(2.29)}$$

(Note: Temperature T and time t are ~100 % correlated, t and T may be used interchangeably, as in some graphs*). Since temperature increases linearly ($T = T_0 + \beta t$),

Where, β = constant heating rate. $\beta = \frac{\mathrm{dT}}{\mathrm{dt}}$, $dt = \frac{\mathrm{dT}}{\beta}$,

$$\frac{\mathrm{d}\propto}{\mathrm{dt}} = \frac{\mathrm{d}\propto}{\mathrm{dT}} . \frac{\mathrm{dT}}{\mathrm{dt}} = \frac{\mathrm{d}\propto}{\mathrm{dT}} . \beta$$

A substitution of β into the Arrhenius equation, equation (2.29) transforms the equation to non-isothermal rate expression, equation (2.30),

$$\frac{\mathrm{d}\propto}{\mathrm{dt}} = \left(\frac{1}{\beta}\right) \mathrm{Aexp}\left(-\frac{\mathrm{Ea}}{\mathrm{RT}}\right) (1-\propto)^{\mathrm{n}} \quad \text{..... (2.30)}$$

The approximate integration of equation (2.30) using the Coats and Redfern's indicated as $\mathrm{y_{CR}}$, integral method resulted in two possible solutions, (equations 2.31 and 2.32),

$$\mathrm{y_{CR}} = \ln\left[\frac{-\ln(1-\propto)}{\mathrm{T}^2}\right] = ln\frac{\mathrm{AR}}{\beta\mathrm{Ea}}\left[1 - \frac{2RT}{\mathrm{E}}\right] - \left[\frac{Ea}{\mathrm{RT}}\right] \quad \text{if n = 1 ..... (2.31)}$$

And,

$$\mathrm{y_{CR}} = \ln\left[\frac{-\ln(1-\propto)^{1-\mathrm{n}}}{(1-\mathrm{n}).\mathrm{T}^2}\right] = ln\frac{\mathrm{AR}}{\beta\mathrm{Ea}}\left[1 - \frac{2RT}{\mathrm{E}}\right] - \left[\frac{Ea}{\mathrm{RT}}\right] \quad \text{if n ≠ 1 ..... (2.32)}$$

Since the value of $\frac{2RT}{\mathrm{Ea}}$ is negligible i.e. << 1, therefore, the two equations of Coats and Redfern can be approximated, equations (2.33 and 2.34),

$$\mathrm{y_{CR}} = \ln\left[\frac{-\ln(1-\propto)}{\mathrm{T}^2}\right] = ln\frac{\mathrm{AR}}{\beta\mathrm{Ea}} - \left[\frac{Ea}{\mathrm{RT}}\right] \quad \text{if n = 1 ..... (2.33)}$$

And,

$$y_{CR} = \ln\left[\frac{-\ln(1-\propto)^{1-n}}{(1-n).T^2}\right] = ln\frac{AR}{\beta Ea} - \left[\frac{Ea}{RT}\right] \quad \text{if } n \neq 1 \text{ ……..……..……... (2.34)}$$

Thus, for reaction order, n = 1, $\ln\left[\frac{-\ln(1-\propto)}{T^2}\right]$ versus 1/T gave a straight-line graph and for the correct choice of the reaction index, n ≠ 1, $\ln\left[\frac{-\ln(1-\propto)^{1-n}}{T^2}\right]$ versus 1/T is equal to a straight-line graph with slope = activation energy, Ea., and intercept = pre-exponential factor A.

Also, a graph of the Coats and Redfern kinetic description (see detail later, Figures 4.13, 4.15, 4.21 - 4.22 and appendix Figure 1 - Coats and Redfern model for coal), y_{CR} versus $\frac{1}{T}$ was constructed for 0, 10, 20, 30, 40, 50 and 100 % composites.

The slope $\boldsymbol{m}$ was obtained from $yCR = mx + c$ where, $m = \frac{Ea}{R}$ from which the activation energy Ea for the Coats and Redferns description was calculated. The universal gas constant R = 8.314 J/mol. K and intercept c indicated the collision frequency i.e. pre-exponential factor A.

2.5.9 De-convolution of DTG profiles

The Fraser-Suzuki equation Y_{FS} was used to deconvolute the overlapped reactions into low and high temperature scheme, *i.e.* stages A, and B (186). This separated the combustion process into two major steps (202), Y_1 – devolatilization and Y_2 – char combustion using equation (2.35) (186).

$$Y_1 = a_0 \exp\left[-\ln 2\left[\frac{\ln\left(1+2a_3\frac{x-a_1}{a_2}\right)}{a_3}\right]^2\right] \text{ ……..……..…… (2.35)}$$

Where,

a_0 = amplitude,

$a_1 =$ center or position,

$a_2 =$ half width,

$a_3 =$ asymmetry or shape of the curve.

The area DA1, equations (2.36) and DA2, (2.37), under the de-convoluted curve was computed and recorded as illustrated in chapter 2 appendix, (Table 5 and Figure 4 – Deconvolution and area under curve).

The graphs of $\left(\frac{d\propto \mathbf{1}}{dT}\right)$ corresponding to Y_1 and $\left(\frac{d\propto \mathbf{2}}{dT}\right)$ representing Y_2 versus T deconvolutes the oxidation into low and high temperature schemes, Y_1 and Y_2 . Where the Y_1 and Y_2, depicts devolatilization and combustion respectively, (details in Figures 3, 4 and 5, and Tables 7 and 8 of chapter 2 appendix), as derived from, (Figure 2, appendix) the original DTG graphs.

The numerical integration of area under each curve was calculated as area of trapezium $DA1$ for low temperature scheme, *i.e.* devolatilization Y_1 equation (2.36).

$$DA1 = \frac{1}{2}\left(Y_{1_2} + Y_{1_1}\right)T_{1_2} - T_{1_1} \quad \text{..... (2.36)}$$

Also, the area $DA2$ under the high temperature combustion Y_2, equation (2.37) was computed,

$$DA2 = \frac{1}{2}\left(Y_{2_2} + Y_{2_1}\right)T_{2_2} - T_{2_1} \quad \text{..... (2.37)}$$

The conversion *i.e.* total area $\propto_{\mathbf{1}}$ and $\propto_{\mathbf{2}}$ under each curve was obtained as the sum of numerical integration for area of all trapeziums under each curve, equation (2.38 – 39) and (Figure 4) – chapter 2 appendix, graph of area under deconvolution.

$\propto_1 = (\mathrm{DA1})1 + (\mathrm{DA1})2 + (\mathrm{DA1})3 + \ldots\ldots\ldots + (\mathrm{DA1})_n$ ..... (2.38)

$\propto_2 = (\mathrm{DA2})1 + (\mathrm{DA2})2 + (\mathrm{DA2})3 + \ldots\ldots\ldots + (\mathrm{DA2})_n$ ..... (2.39)

Then, $\propto_{\mathbf{1}}$ and $\propto_{\mathbf{2}}$ were substituted into the solid states oxidation model g $(\propto)$, described in section 1.8, *i.e.* reaction order O1 – O3, phase boundary R2 – R3 and diffusion-controlled reactions D1 – D4, (Table 6,) for both the devolatilization stage A, and char combustion stage B, (Tables 7 and 8) of the coal combustion in chapter 2 appendix.

The graphs of each model g $(\propto)$ *i.e.*, O1, O2, O3, R2, R3, D1, D2, D3, and D4 versus 1/T was plotted, (Table 3.7, and see mechanism graph for coal, Figure 5, and Tables 7 and 8, chapter 2 appendix), one model or more for each of Y1 and Y2 produced the best linear fit.

The activation energy E $_{\mathrm{a}}$ for each mechanism, low and high combustion was calculated as in section 2.5.8, with the slope (m), from the oxidation models, (detail in appendix, Table (9) Activation energy – stages A and B, and Figure (5): Mechanisms – Low and high temperature schemes, $(\mathrm{y} = \mathrm{mx} - \mathrm{c})$.

$m = \frac{Ea}{R}$ ..... (2.40)

$\mathrm{Where,}\ \mathrm{Ea} = \mathrm{mR}$ and,

$\mathrm{R} = 8.314\ \mathrm{J/mol.K}$

The frequency of collision A was deduced from intercept, (Figure 5 of the Mechanisms – Low and high temperature schemes) and, recorded as in appendix, Table (9) Activation energy – stages A and B

2.5.10 Combustion mechanism

The oxidation reaction mechanism for each sample was deduced from the plots of the reaction order, phase boundary and diffusion reaction models $\mathrm{g}(\propto)$ against $\left(\frac{1}{\mathrm{T}}\right)$ for each stage of the combustion. A linear plot with highest correlation (R^2) was

considered as the best model, (Table 2.4) that described the mechanism. The reaction order, O1, O2, O3 and the corresponding model $g(\propto)$ were fitted and plots for phase boundary controlled – R2 and R3 and diffusion models – D1, D2, D3, and D4 were made. Typical mechanism that described the oxidation reaction for coal is illustrated for low temperature scheme, (see result, section 4.6, Tables 4.17 – 4.23 for mechanism) and for high temperature scheme, (see result, section 4.6, Table 4.9 – 4.12, for mechanism).

The model with the highest correlation R^2 is considered the controlling reaction for the stage. But the linear models with the highest correlation combined gave the overall oxidation mechanism of the combustion and one with the highest R^2 controls the entire combustion for that fuel.

The theoretical and observed rate of reaction were determined using the resultant solid states oxidation mechanisms on each of the deconvoluted combustion stages A and B. While the activation energy of samples was calculated for the single event using the Coats and Redfern's. Finally, the activation energy for the Frasier-Suzuki's de-convoluted event, was determined and both outcomes for samples were compared with the activation energy of coal reported in literature.

Chapter 3

3.0 Results and discussion – Characterisation of fuel properties

This chapter discusses the results for raw material and coal-microalgae biomass preparation. The discussion includes characterisation of the raw materials and their blends, which comprises of the proximate, ultimate, elemental, and solid states NMR properties. The properties of the observed, and the theoretical linear combination of coal and microalgae biomass were compared.

The experimental procedures described in section 2.3, subsection 2.3.1 – 2.3.6, were used to obtain the moisture, and the dry solid content (Table 3.1 – 3.2). The Figure 3.1 shows the fuel (pellets) of coal-microalgae composite from sample ratio of materials, (Table 3.3).

Table 3.1: Moisture of microalgae biomass

(a) Algae (slurry)		**Test**	**Test**	**Test**
	Weight	1	2	3
Pre-oven	M crucible (g)	28.03	27.05	27.45
	M sample (g)	01.47	01.67	01.26
Post oven	M crucible + sample	28.27	27.33	27.66
	M dry sample	00.24	00.28	00.21
	Moisture (%)	83.28	83.19	83.31
	Solid (%)	16.71	16.80	16.68
Moisture of Algae			-	83.27
Dry solid of Algae, da			-	16.73

Table 3.2: Moisture for Eskom coal "A"

(b) Eskom Coal 'A'		**Test**	**Test**	**Test**
	Weight	1	2	3
Pre-oven	M crucible (g)	26.55	26.31	24.62
	M sample (g)	01.23	01.26	01.33
Post oven	M crucible + sample	27.71	27.50	25.87
	M dry sample	01.15	01.19	01.25
	Moisture (%)	05.90	05.94	05.82
	Solid (%)	94.09	94.05	94.17
Moisture of Coal			-	05.89
Dry solid of Coal, dc			-	94.11

Table 3.3: Material ratios and mass blended for composites

Eskom "A"	**Solid** (%)	**Solid** (%)	**Formula** (%)	**Formula** (%)	**Weighed Algae x** (g)	**Weighed Coal y** (g)	**Total** m_T (g)
S/No	**Algae**	**Coal**	**Coal**	**Algae**	**mixed**	**mixed**	**Mass**
1	da	dc	**100**	**0**	0.0	50.0	50
2	16.73	94.11	90	10	19.2	30.8	50
3	16.73	94.11	80	20	29.2	20.8	50
4	16.73	94.11	70	30	35.3	14.7	50
5	16.73	94.11	60	40	39.5	10.5	50
6	16.73	94.11	50	50	42.5	07.5	50
7	16.73	94.11	**00**	**100**	50.0	00.0	50
Sum					215.7	134.3	350

da = % solid for algae biomass, dc = % solid for coal

From the Table 3.1, microalgae biomass and coal at a moisture level of 83.27 % and 5.89 %, and dry solid of 16.7 %, and 94.1 %, Table 3.2, required 19.2 g of coal and 30.8 g of the biomass respectively, Table 3.3, to make a 10 % blend. The resultant 10 % blend amounts to a total mass of 50 g moist powder. The sum indicated that the

right quantities of coal and microalgae biomass were blended. The final mass was scaled up as required, and for household combustion the fuel can be turned into briquettes. The pelletization of the Coalgae® powder, as in section 2.3.6 produced a blend, (Figure 3.1) known as Coalgae® fuel.

Figure 3.1: Coal-microalgae biomass pellet, "Coalgae®" from blends

3.1 Proximate Properties of Coal, Microalgae, and Blends

With the experimental procedures described in section 2.4.1, the bulk proximate properties for six replicates each of coal, microalgae biomass, and blends were achieved as shown, (Table 3.4) below.

Table 3.4: Observed proximate properties of coal, microalgae biomass and blends

Algae	**Moisture**		**Volatile matter $_{A}$**		**Ash $_{A}$**		**Volatiles $_{d\ b}$**		**Ash $_{d\ b}$**		**FC_{A}**	
(%)	(%)	±	(%)	(±)	(%)	(±)	(%)	(±)	(%)	(±)	(%)	(±)
0	3.99	0.02	24.26	0.11	25.99	0.03	25.22	0.12	27.02	0.03	45.76	0.11
10	4.96	0.02	28.50	0.15	23.85	0.02	29.91	0.16	25.03	0.12	42.69	0.16
20	5.05	0.05	33.20	0.23	21.83	0.02	34.88	0.23	22.93	0.02	39.92	0.20
30	5.03	0.02	38.23	0.27	19.85	0.02	40.15	0.28	20.85	0.02	36.89	0.25
40	5.52	0.04	42.36	0.15	17.93	0.04	44.70	0.15	18.92	0.03	34.19	0.14
50	5.21	0.03	48.25	0.17	15.71	0.01	50.76	0.18	16.53	0.01	30.83	0.17
100	2.62	0.20	76.01	0.22	6.26	0.06	78.01	0.16	6.42	0.06	15.10	0.12

0 (%) = coal only, 100 (%) = microalgae only, A = wet basis; d b = Value on a dry basis

The volatile content of microalgae biomass, Table 3.4, is in the range reported for co-fired biomass (71) section1.4, Table 1.5, but almost three times more than the amount in discard ultra-fines (110), Table 1.8. This amount of volatile is equivalent to the values reported for microalgae biomass, Table 1.7, (99), (98), and greater than the quantity in several biomass used for co-firing (203). The high volatile matter of microalgae biomass improved the conversion of discard ultra-fine coal. The ash of this microalgae biomass is similar to ash report for Nannochloropsis *gaditana* (99), Chlorella *vulgaris*, and Spirulina *platensis*, Table 1.7, (99), (98), and (204). It is about four times less than the ash of coal, and comparable to many biomass, Table 1.5, (71), (203). This will reduce the amount of deposited on boiler components (56). There is less quantity of fixed carbon in microalgae biomass as compared to coal, and to some biomass (56). The volatile matter content increases as the quantity of microalgae biomass in the blend increases. There is noticeable decrease in ash content of 10 – 50 % microalgae co-fired samples, which is low relative to some coal-biomass (205) (Table 1.7 and 1.8), and wastes such as sewage and coal gangue (206).

The observed and predicted (linear) proximate properties were compared as shown in Table 3.5, and Figures 3.4 – 3.6.

Table 3.5: Observed and predicted Proximate properties

Fuel (%)	**Coal** (ratio)	**Algae** (ratio)	**Obs. Vd** (%)	**Pred. Vd** (%)	**Obs. Ad** (%)	**Pred. Ad** (%)	**Obs. FC a** (%)	**Pred. FC a** (%)
10	0.9	0.1	29.91	30.50	25.03	24.96	42.69	42.70
20	0.8	0.2	34.88	35.78	22.93	22.90	39.92	39.63
30	0.7	0.3	40.15	41.06	20.85	20.84	36.89	36.57
40	0.6	0.4	44.70	46.34	18.92	18.78	34.19	33.50
50	0.5	0.5	50.76	51.62	16.53	16.72	30.83	30.43

0 (%) = 100 % coal, 100 = 100 % Algae, Obs. = observed, Vd = volatile dry basis, Pred. = predicted, Ad = ash dry basis, FC = fixed carbon, a = as received.

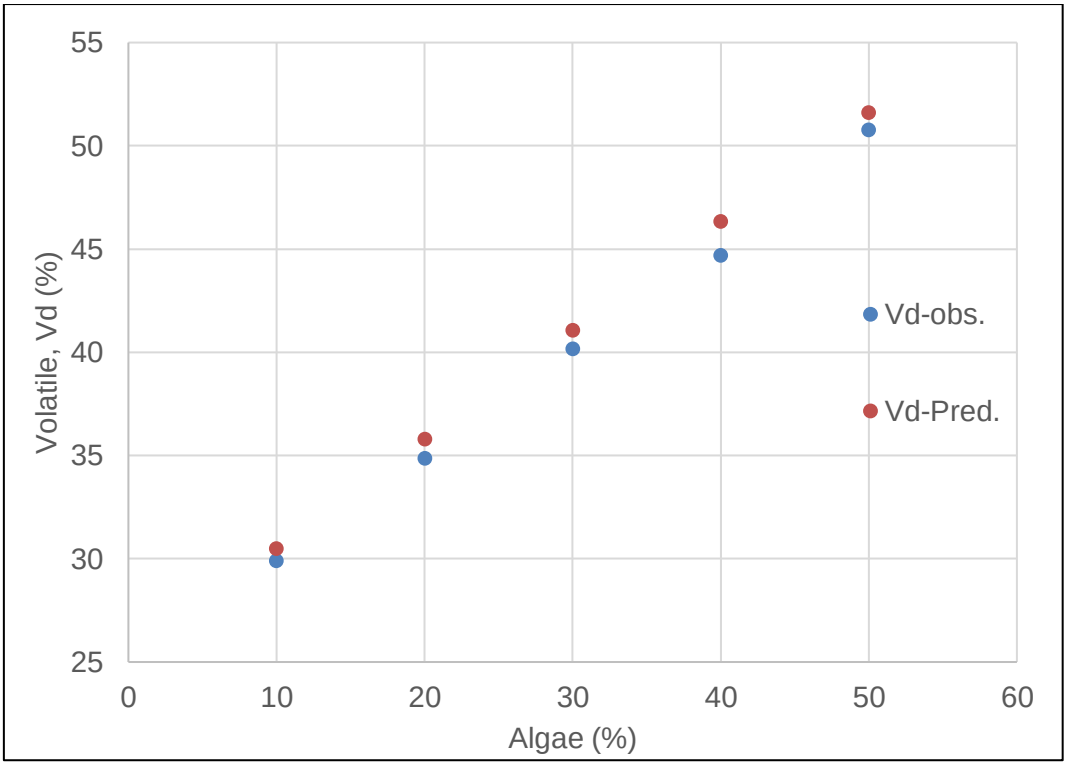

Figure 3.2: Change in observed and predicted Volatile matter with Microalgae content

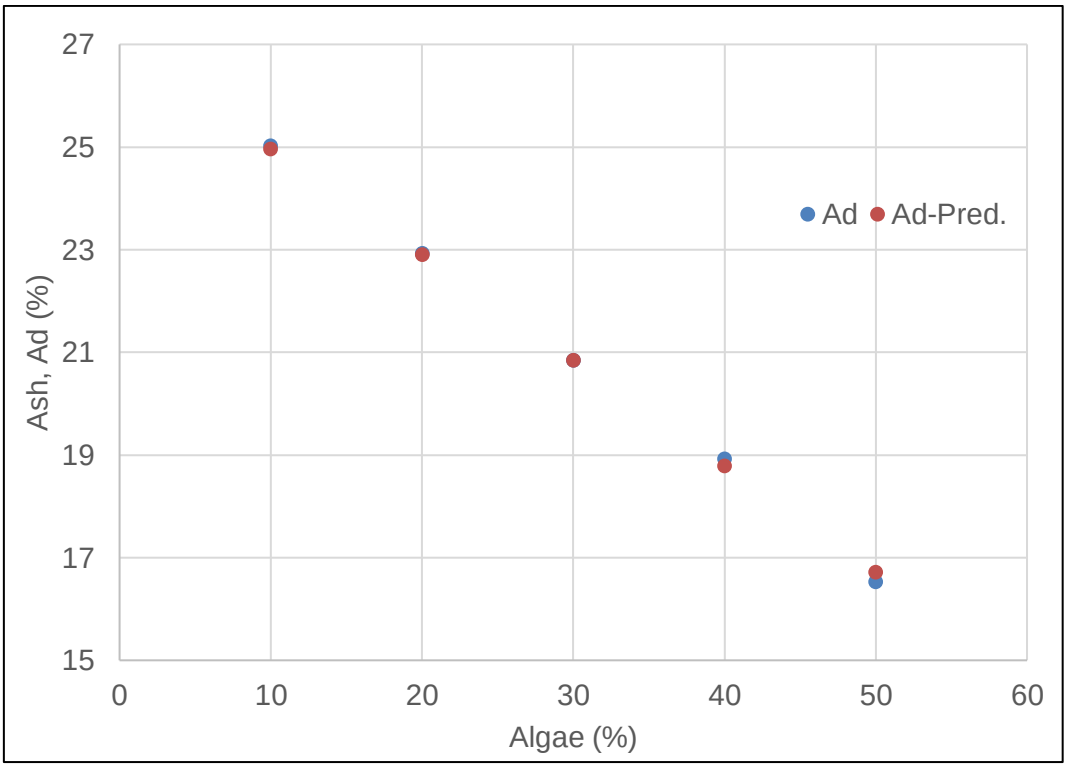

Figure 3.3: Change in observed and predicted Ash with Microalgae content

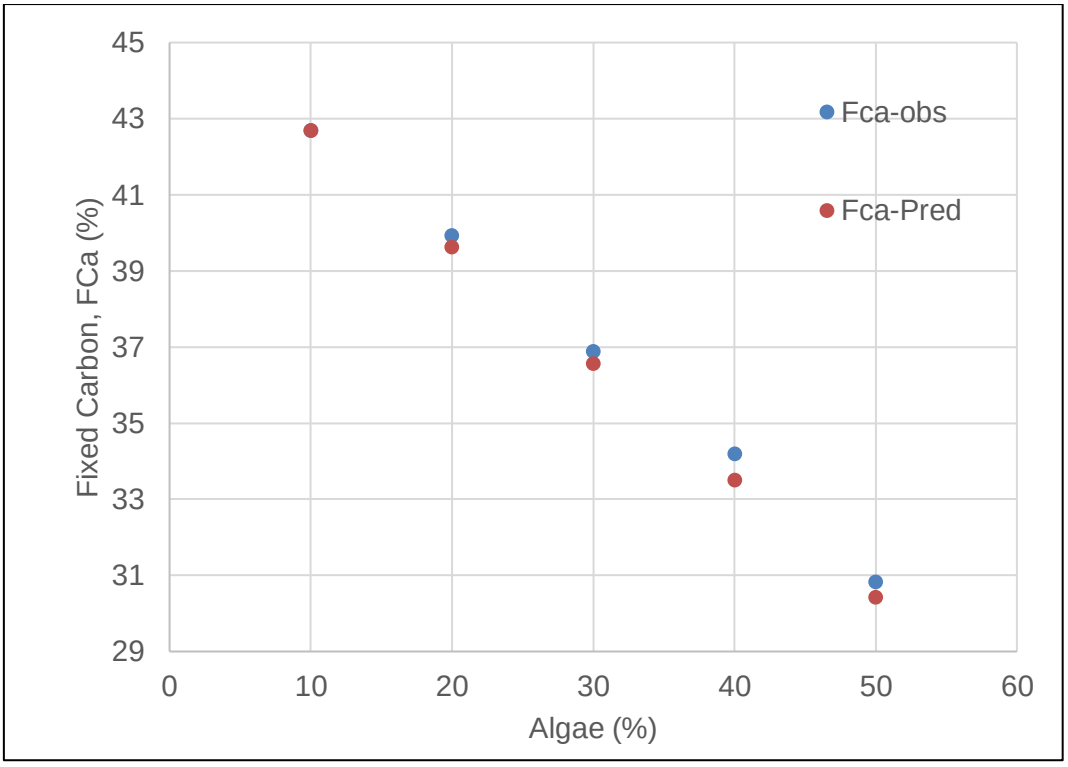

Figure 3.4: The observed and predicted Fixed carbon versus Microalgae content

The graphs, (Figures 3.2 – 3.4) indicated similar linear variation in proximate properties for the observed and predicted due to the increase in microalgae biomass. The increased volatile, Figure 3.2, with biomass could be attributed to the demethoxylation reactions reported in the presence of aliphatic compounds, and inorganic elements (40). It has been reported that this reaction decreases the formation of char, and favors the generation of more volatiles relative to coal (40). Thus, for every 10 % increase in biomass the volatile content of the blend increases by about 5.1 %, and the ash content decreases by about 2.1 %. The average predicted volatile is significantly higher than the average observed volatile (paired t-test, p = 0.005). The relative difference between the observed and predicted averages is 2.38%. So, there is a substantial increase in volatile matter content as microalgae biomass increases. The composite appeared to be a good raw materials from which organic chemicals could be produced as reported of coal samples with high volatile matter (207). The observed variation in proximate properties could change fuel properties (144). The average predicted ash is equal to the average observed ash, (paired t-test, p = 0.838). However, there is a negligible relative difference of 0.05 % between the observed and predicted averages due to experimental error. The predicted and observed ash contents are equal and decreased as expected with more

biomass, though the physical appearance of ash from composites differs as compared to ash from coal. The difference of 0.92% between the observed and predicted average fixed carbon could be due to experimental error.

3.2 Ultimate Properties – CHNS and O

Using the experimental procedure, section 2.4.2, the ultimate properties of coal, microalgae biomass, and blends were obtained, Table 3.6, on ash free basis and tabulated.

Table 3.6: Ultimate properties of Coal, Microalgae biomass and their blends

Algae (ratio)	**Coal** (ratio)	**C** (%)	**H** (%)	**N** (%)	**S** (%)	**O** (%)
1	0	47.95	7.65	5.63	0.57	31.78
0	1	57.07	3.84	1.66	0.64	9.77
0.05	0.95	56.79	3.77	1.76	0.43	11.26
0.15	0.85	56.85	3.63	1.74	0.47	13.38
0.25	0.75	55.57	3.59	1.94	0.49	16.54
0.35	0.65	55.91	3.87	2.14	0.44	17.83
0.45	0.55	54.41	3.9	2.35	0.45	21.14
0.55	0.45	55.89	4.36	2.86	0.51	20.69

C = carbon, H = hydrogen, N = nitrogen, S = sulphur, coal ash = 27.02, algae ash = 6.42, $\text{Oxygen} = \text{O} = 100 - (\text{A} + \text{C} + \text{H} + \text{N} + \text{S})\%$

The Table 3.6 displays ultimate properties of microalgae biomass, coal, and the blends. There is a decrease of about 8.37 % carbon content which could be attributed to the addition of microalgae biomass. Contrarily, hydrogen and nitrogen increased by about 3.63 %, and 3.94 % respectively. Approximately, 0.08 % increase in sulphur was obtained whereas the oxygen content was improved by about 21.47 % as deduced from gradient of a plots of these properties versus microalgae biomass.

The observed ultimate properties, Table 3.6, were compared to the predicted, as shown, Table 3.7, and Figures 3.5 – 3.9.

Table 3.7: Comparing observed and predicted ultimate properties

Algae (ratio)	**Coal** (ratio)	**Obs.** C (%)	**Pred.** C (%)	**Obs.** H (%)	**Pred.** H (%)	**Obs.** N (%)	**Pred.** N (%)	**Obs.** S (%)	**Pred.** S (%)	**Obs.** O (%)	**Pred.** O (%)
0.05	0.95	56.47	56.61	3.78	4.03	1.73	1.86	0.43	0.64	11.26	10.87
0.15	0.85	57.06	55.70	3.63	4.41	1.74	2.26	0.47	0.63	13.38	13.07
0.25	0.75	55.56	54.79	3.66	4.79	1.94	2.65	0.49	0.62	16.54	15.27
0.35	0.65	55.86	53.88	3.86	5.17	2.13	3.05	0.44	0.62	17.83	17.47
0.45	0.55	54.57	52.97	3.97	5.55	2.38	3.45	0.45	0.61	21.14	19.67
0.55	0.45	55.16	52.05	4.38	5.94	2.86	3.84	0.51	0.60	20.69	21.88

C = carbon, H = hydrogen, N = nitrogen, O = oxygen $= 100 - (\mathrm{A} + \mathrm{C} + \mathrm{H} + \mathrm{N} + \mathrm{S})\%$

The Table 3.7, and Figures 3.5 – 3.9, showed the predicted and observed ultimate properties versus microalgae biomass. The observed and predicted quantities of CHNS and O showed some similarities. The observed and predicted quantity of hydrogen, nitrogen and sulphur contents were slightly different, which could either be due to experimental error or interaction. The oxygen contents for the observed and predicted blend were equivalent. These indicates that the amount of coal and microalgae in the observed and predicted blends were equivalent.

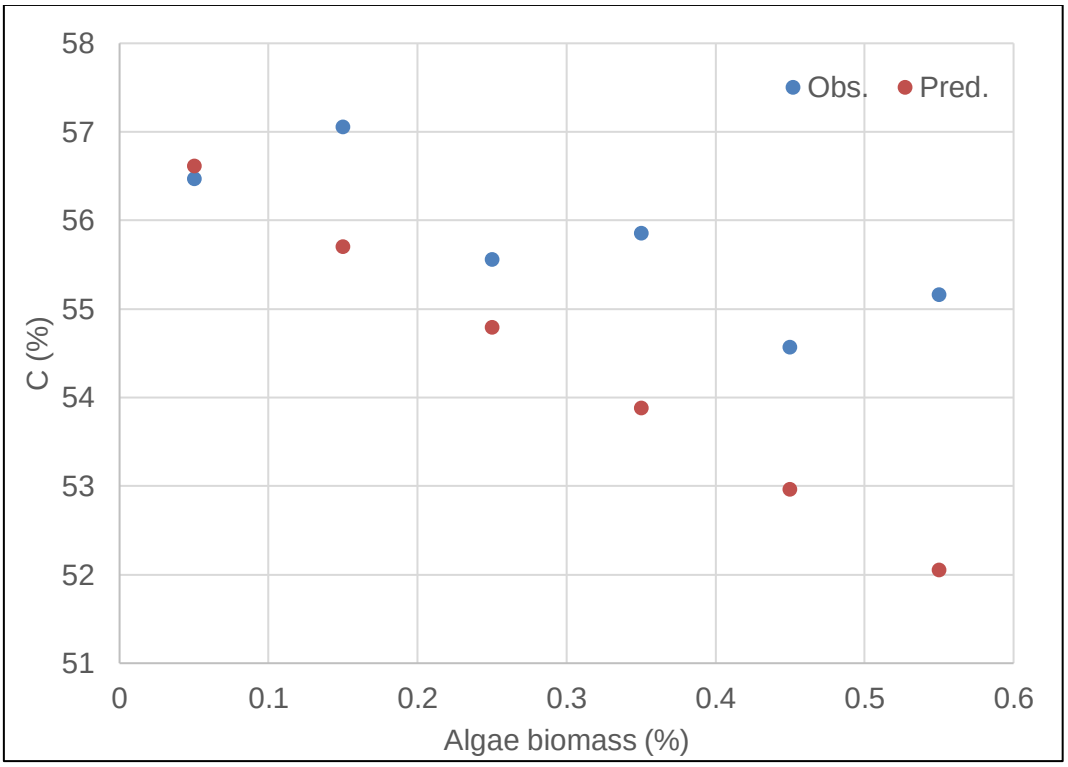

Figure 3.5: Observed and predicted change in Carbon with Microalgae content

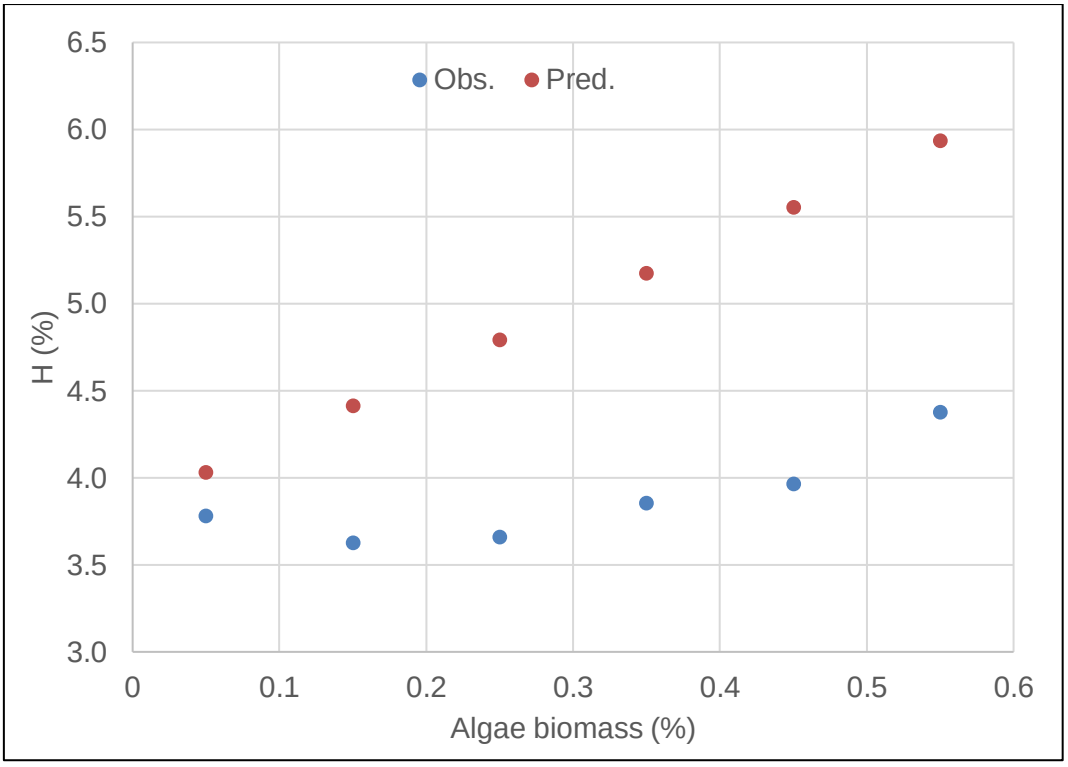

Figure 3.6: Observed and predicted change in Hydrogen with Microalgae content

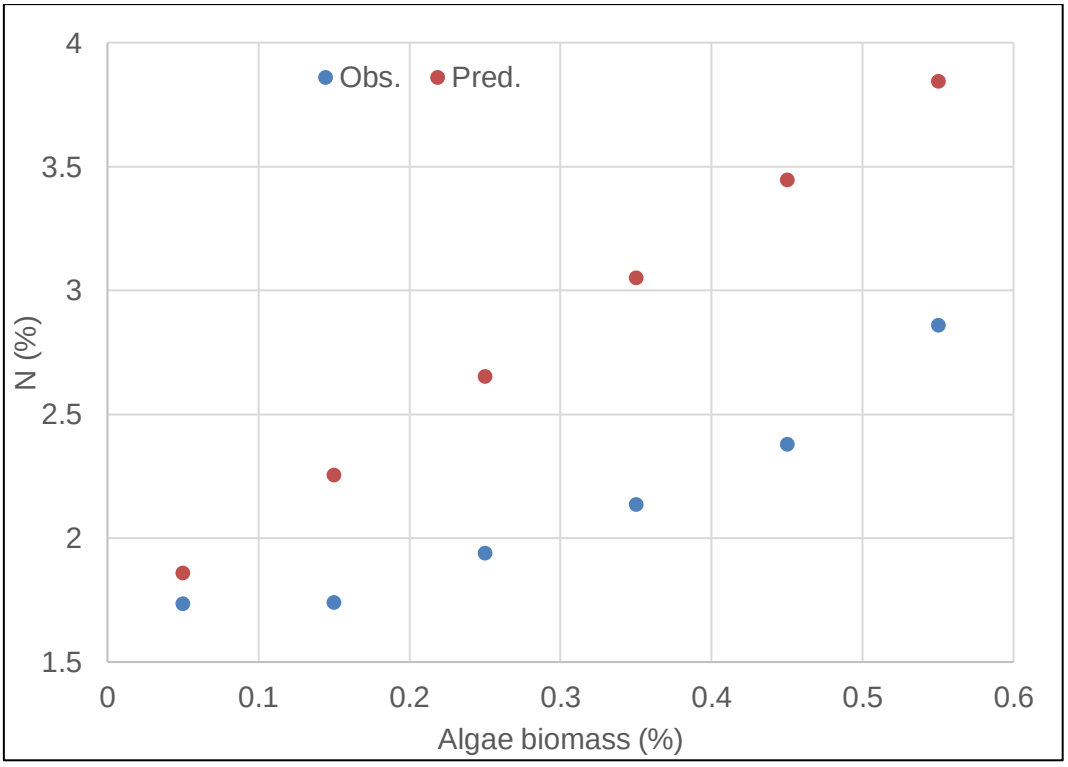

Figure 3.7: Observed and predicted change in Nitrogen with Microalgae content

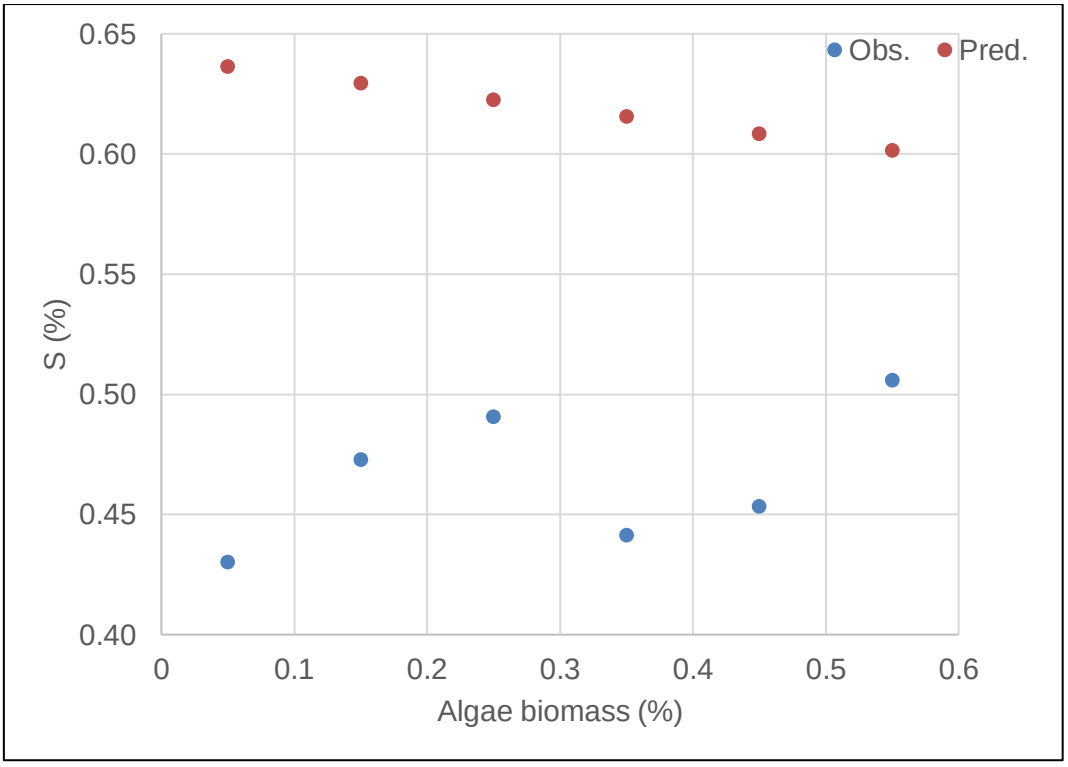

Figure 3.8: Observed and predicted change in Sulphur with Microalgae content

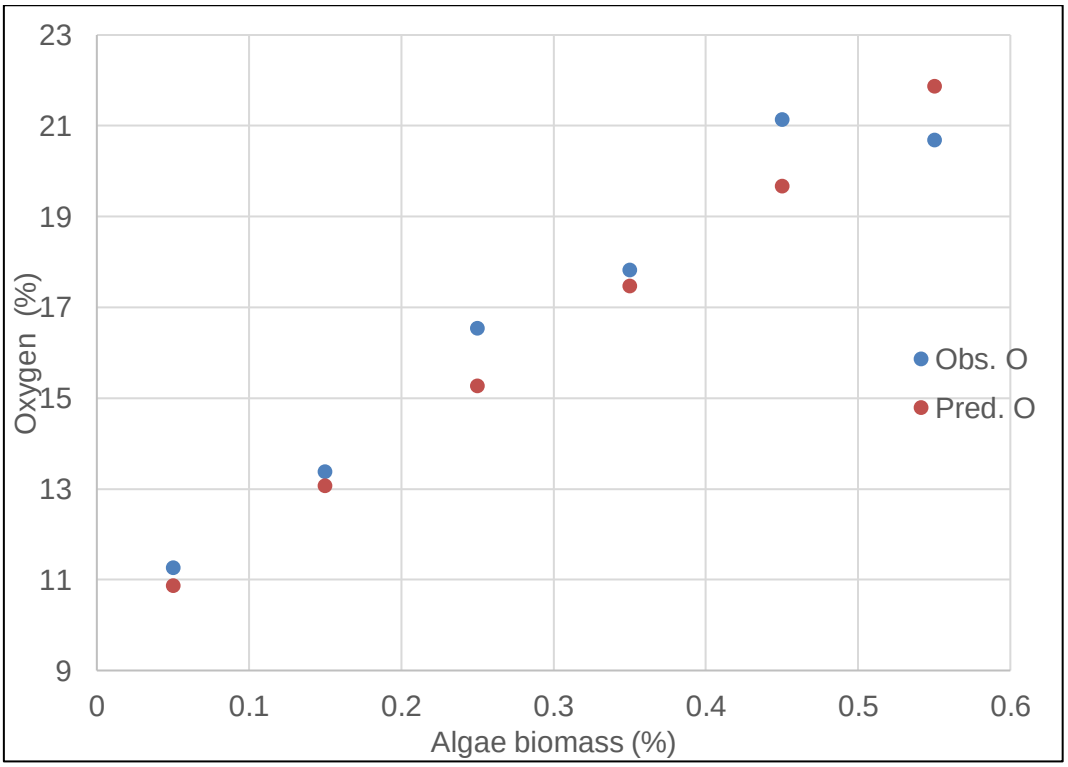

Figure 3.9: Observed and predicted change in Oxygen with Microalgae content

Figures 3.5 – 3.9 illustrated the relationship between predicted and observed average ultimate properties. The observed average for carbon, hydrogen, nitrogen, and sulphur

content slightly differs from the predicted content. These differences are rare to linear combination of dried coal and biomass as described in literature (144), (199), (142). If the differences are not due to the measurement error, then further studies would be required here.

3.3 Elemental properties of Coal, Microalgae, and Blends

Using the procedure as per section 2.4.3, chapter 2, other observed elements in the composites was obtained and tabulated, Tables 3.8. A comparison of the predicted and observed elements was shown in Table 3.9, while the resultant elemental composition of the corresponding ash was presented in Table 3.10.

Table 3.8: Elemental properties of Coal, Microalgae, and the blends

Elements in Composites (%)									
% Algae	**Mg**	**Al**	**Si**	**P**	**S**	**K**	**Ca**	**Mn**	**Fe**
100	0.250	0.123	0.000	2.022	1.433	3.400	0.678	0.029	0.418
0	0.109	2.312	2.857	0.027	0.418	0.050	1.045	0.010	0.722
10	0.105	2.411	2.937	0.035	0.390	0.056	0.998	0.010	0.704
20	0.117	2.235	2.768	0.066	0.425	0.064	0.987	0.009	0.665
30	0.116	2.203	2.798	0.090	0.434	0.078	1.019	0.010	0.674
40	0.117	1.944	2.408	0.106	0.385	0.088	0.890	0.009	0.600
5	0.112	2.484	3.098	0.032	0.436	0.054	1.049	0.010	0.731
15	0.101	2.303	2.819	0.047	0.414	0.062	0.964	0.009	0.653
25	0.120	2.207	2.734	0.095	0.433	0.078	0.977	0.010	0.681
35	0.124	2.002	2.483	0.121	0.430	0.089	0.916	0.009	0.632
45	0.113	1.868	2.362	0.154	0.438	0.109	0.919	0.009	0.616

100 = 100 % Microalgae biomass, 0 = 100 % coal, 10 – 45 % = blends, Mg – Fe = Elements in the periodic table, note: coal = discard ultra -fine, and contains some silica

Table 3.9: Observed and predicted elemental properties of Coal, Microalgae, and their blends

(%) **Observed and predicted elements**																			
Algae (ratio)	**Coal** (ratio)	**Obs Mg**	Pred. Mg	**Obs Al**	Pred. Al	**Obs Si**	Pred. Si	**Obs P**	Pred. P	**Obs S**	Pred. S	**Obs K**	Pred. K	**Obs Ca**	Pred. Ca	**Obs Mn**	Pred. Mn	**Obs Fe**	Pred. Fe
1	0	0.250	0.250	0.123	0.123	0.000	0.000	2.022	2.022	1.433	1.433	3.400	3.400	0.678	0.678	0.029	0.029	0.418	0.418
0	1	0.109	0.109	2.312	2.312	2.857	2.857	0.027	0.027	0.418	0.418	0.050	0.050	1.045	1.045	0.010	0.010	0.722	0.722
0.1	0.9	0.105	0.123	2.411	2.093	2.937	2.571	0.035	0.226	0.390	0.519	0.056	0.385	0.998	1.008	0.010	0.011	0.704	0.691
0.2	0.8	0.117	0.137	2.235	1.874	2.768	2.285	0.066	0.226	0.425	0.621	0.064	0.720	0.987	0.971	0.009	0.013	0.665	0.661
0.3	0.7	0.116	0.151	2.203	1.655	2.798	1.999	0.090	0.625	0.434	0.722	0.078	1.055	1.019	0.934	0.010	0.015	0.674	0.630
0.4	0.6	0.117	0.165	1.944	1.436	2.408	1.714	0.106	0.625	0.385	0.824	0.088	1.390	0.890	0.898	0.009	0.017	0.600	0.600
0.05	0.95	0.112	0.116	2.484	2.202	3.098	2.714	0.032	0.126	0.436	0.468	0.054	0.217	1.049	1.026	0.010	0.010	0.731	0.706
0.15	0.85	0.101	0.130	2.303	1.983	2.819	2.428	0.047	0.326	0.414	0.570	0.062	0.552	0.964	0.989	0.009	0.012	0.653	0.676
0.25	0.75	0.120	0.144	2.207	1.764	2.734	2.142	0.095	0.525	0.433	0.671	0.078	0.887	0.977	0.953	0.010	0.014	0.681	0.646
0.35	0.65	0.124	0.158	2.002	1.545	2.483	1.857	0.121	0.725	0.43	0.773	0.089	1.222	0.916	0.916	0.009	0.016	0.632	0.615
0.45	0.55	0.113	0.172	1.868	1.326	2.362	1.571	0.154	0.924	0.438	0.874	0.109	1.557	0.919	0.879	0.009	0.018	0.616	0.585

1 = microalgae biomass only, or coal only, 0 = 0 %, 0.1 – 0.45 % = blends, Mg – Fe = Elements in the periodic table, the discard ultra -fine

For each increase in microalgae biomass, Table 3.9, the magnesium content increased by about 0.03 %, phosphorus by about 0.38 % and sulphur by about 0.25 %. This implies that the conversion would be high in blends with more microalgae biomass relative to those with less. Aluminium decreased by about 0.41 % and silicon by about 0.56 %, and if sulphur ignites at about 190 ^{0}C, then an increased content, and particle size could have contributed to the observed spontaneity of coal-microalgae combustion (208). The formation of low melting point metallic sulphates was linked to corrosion (208), (209), which could be a challenge with the increased sulphur content due to microalgae biomass. The potassium content remained constant at about 0.81 % whereas the manganese content moved up by about 00.5 %. The calcium content as well as the iron individually decreased by about 0.015% and 0.015 % with each percent increase in microalgae biomass. The ash was equally examined for the elemental properties and the result is illustrated, Table 3.10.

Table 3.10: Elemental properties of Ash

Some elements in the ash of composites (%)									
% Algae	**Mg**	**Al**	**Si**	**P**	**S**	**K**	**Ca**	**Mn**	**Fe**
0	1.145	23.468	36.914	0.527	4.573	0.784	15.614	0.177	12.362
10	1.014	23.135	36.661	0.705	4.007	0.902	14.625	0.189	14.072
20	1.109	22.905	36.167	1.101	3.893	1.047	14.609	0.194	14.302
30	1.273	22.601	35.213	1.690	3.731	1.327	14.762	0.202	14.510
40	1.393	22.081	34.657	2.27	3.542	1.696	15.004	0.205	14.476
5	1.007	22.843	36.398	0.567	4.317	0.774	15.873	0.190	13.470
15	1.149	21.828	35.538	1.188	3.678	0.974	15.178	0.203	14.994
25	1.285	20.909	34.631	2.173	3.333	1.408	15.676	0.213	15.100
35	1.392	20.256	33.611	2.738	3.232	1.706	16.218	0.224	15.414
45	1.493	19.539	32.355	3.535	2.958	2.150	16.601	0.235	15.871

0 = 100 % coal, Mg – Fe = Elements in the periodic table, note: coal = discard ultra -fine, and contains sand

Table 3.10 shows the percentage of elements (*i.e.* oxides) in the ash residue. An increase in microalgae biomass increased the contents of Mg, K, Ca, Mn, Fe, and P. The quantity of these elements in the ash of "Coalgae®" are higher relative to coal. Ash is composed of oxides, and if MnO_2, Fe_2O_3, CaO etc. are catalytic (210), then microalgae with ash that contains similar oxides also contributed to the catalysis of this coal combustion (211). The decrease in Al, Si, and S content of composite was lower as compared the coal.

3.4 Heat content of Coalgae-microalgae fuel

The ASTM-D5865-07 determination of heat energy properties described in, section 3.4.3 was used to obtain the results, (Table 3.11). The result was compared with higher heating values calculated with the Parikh and Dulong's formula, (appendix Table 10).

Table 3.11: Energy of coal, composites, and microalgae biomass

Algae	**Mass** (g)			**Energy** HHV (MJ/kg)					
(%)	M_1	M_2	M_3	E_1	E_2	E_3	Std	Mean	(±) Uncert
100	0.5003	0.5129	0.5097	22.01	22.33	21.92	0.2122	22.09	0.53
0	0.5222	0.5180	0.5068	20.86	20.93	20.83	0.0503	20.88	0.12
10	0.5275	0.5148	0.5069	20.99	20.97	21.02	0.0212	21.00	0.05
20	0.5141	0.5057	0.5014	21.19	21.18	21.15	0.0194	21.18	0.05
30	0.5008	0.5190	0.5105	21.27	21.15	21.19	0.0606	21.21	0.15
40	0.5134	0.5004	0.5041	21.33	21.55	21.47	0.1118	21.45	0.28
50	0.5056	0.5210	0.5203	21.53	21.59	21.58	0.0322	21.58	0.08

1, 2, 3, = measurements, Std = standard deviation, Uncert = uncertainty, HHV = high heating value.

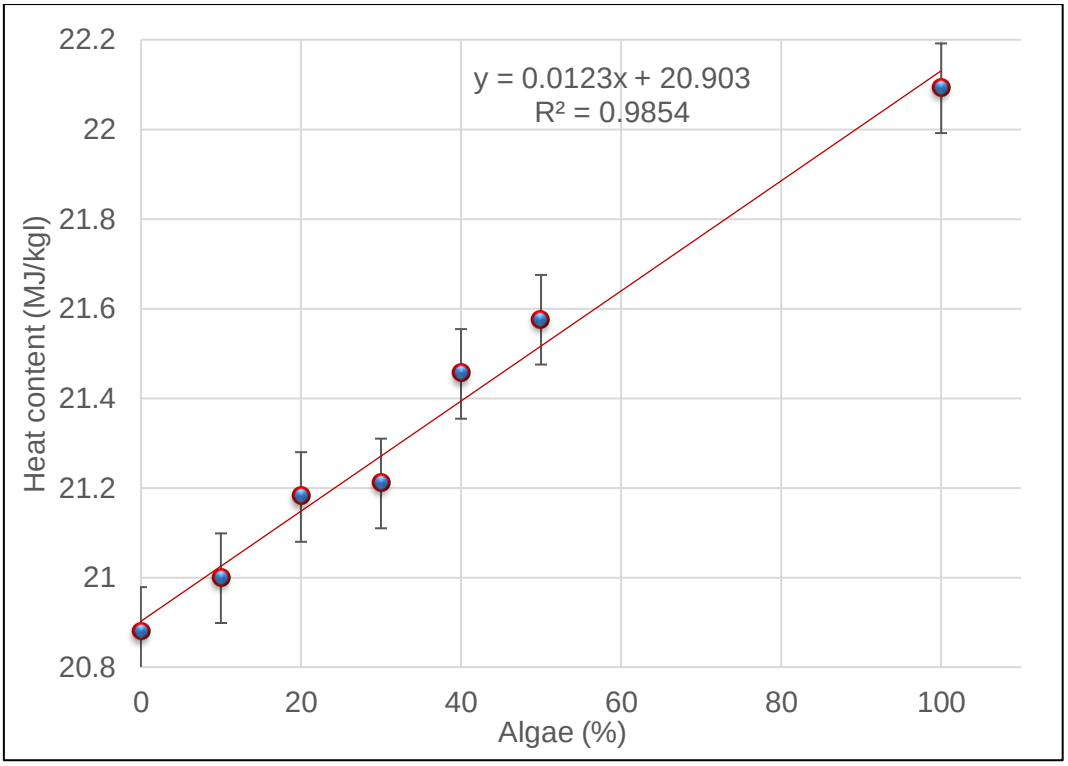

Figure 3.10: Measured Heat value versus algae content

The observed and predicted energy content were compared, Table 3.12, and Figure 3.11.

Table 3.12: Observed and predicted energy of Coal, Microalgae, and blends

Algae (ratio)	**Coal** (ratio)	**Obs. energy** (MJ/kg)	**Pred. energy** (MJ/kg)
0	1	20.88	20.88
1	0	22.09	22.09
0.1	0.9	21.00	21.96
0.2	0.8	21.18	21.84
0.3	0.7	21.21	21.72
0.4	0.6	21.45	21.60
0.5	0.5	21.58	21.48

Obs. = observed values, Pred. = predicted values, Energy = high heating values, HHV

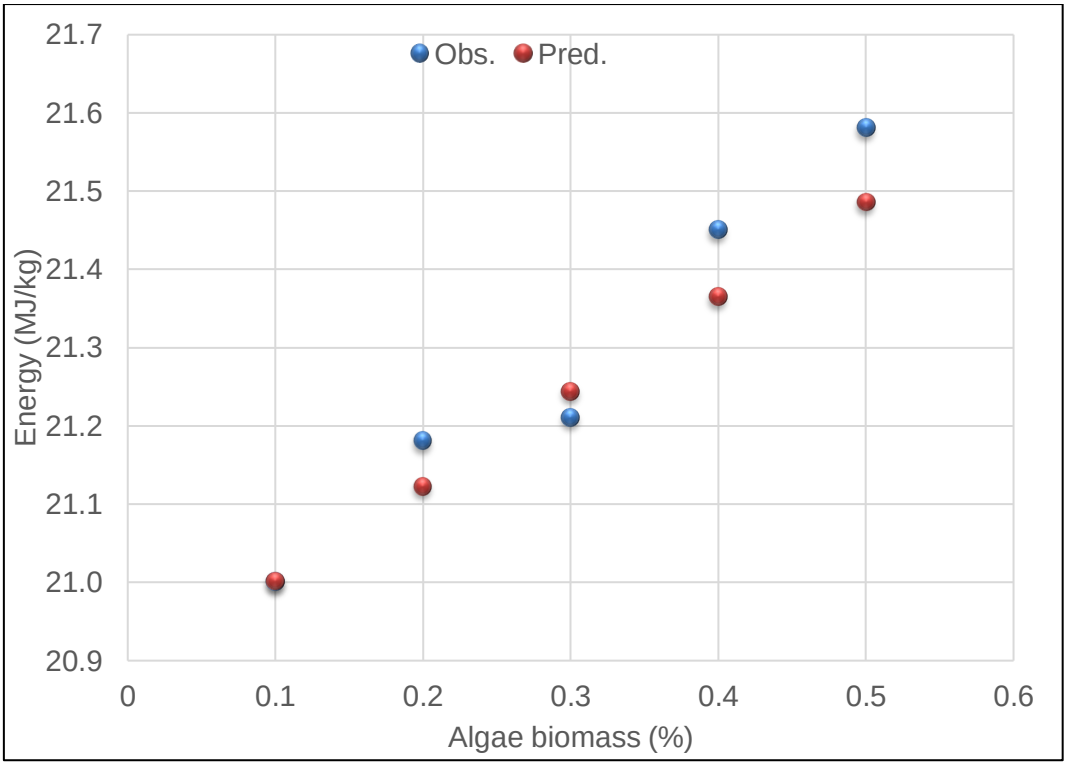

Figure 3.11: Higher heating value of coal, microalgae, and blends

There is no significant difference (paired t-test, p = 0.0801), between the observed and the predicted average high heating value MJ/kg, Figure 3.11, however, each increase in microalgae biomass improves the energy content of the discard ultra-fine coal. The energy value for "Coalgae®" is higher due to microalgae as compared with blends of coal and some biomass, like switchgrass (153). The observed and predicted high heating value (Table 3.12, and Figure 3.11), indicates an increase for each 10 % increase in microalgae biomass. There is an evidence to prove that the heat content increases by about 1.43 %. The model, Figure 3.11 described the observation properly (Corr. R^2 = 96%) at 95 % confidence interval.

3.5 Solid state NMR of Coal and Composites

The result of the solid state nuclear magnetic resonance analysis (section 2.4.5), carried out by the Sasol Laboratory, Stellenbosch University (Table 3.13), indicated that microalgae biomass might have some influence on the structure of coal. The observed fraction of functional groups, points of C-C bonds, and C=C attachment is represented, Table 3.13, below.

Table 3.13: Solid state NMR of coal and Coalgae® (10 % microalgae)

Sample Properties	**Symbol**	**Coal**	**Coalgae®**	**Stdev.**
Fraction Aromatics	f_a	0.79	0.80	0.03
Corrected Fraction Aromatics (excl. CO)	f_a*	0.79	0.75	0.04
Fraction Aliphatic	f_{al}	0.21	0.20	0.02
Fraction Aliphatic C's bonded to Oxygen	f_{al} o	0.00	0.01	0.02
Fraction CO	f_a co	0.00	0.04	0.02
Fraction Phenolics	$f_{a\ P}$	0.06	0.09	0.02
Fraction Alkylated Aromatics	$f_{a\ S}$	0.17	0.17	0.03
Fraction Non-Protonated C's in Aromatic region	f_{al}^{N}	0.55	0.46	0.03
Fraction Protonated C's in Aromatic region	f_{al}^{H}	0.24	0.29	0.03
Fraction Bridgehead C's	f_a^{B}	0.31	0.20	0.04
Fraction Non-Protonated C's + Methyl groups in Aliphatic region	f_{al}^{N*}	0.00	0.00	0.03
Aliphatic $CH+CH_2$	f_{al}^{H}	0.21	0.20	0.02
Mole fraction of Aromatic Bridgehead C's	X_b	0.39	0.27	0.06
Average # of Aromatic C's per cluster	C	19.3	14.1	3.00
	#clusters/100	4.10	5.35	-
# of Attachments per cluster	δ+1	5.8	4.83	-

The fraction of aromatics in the coal, (Table 3.13), increased slightly from 0.79 to 0.80 ± 0.03 with 10 % biomass. About 0.01 fraction of aliphatic carbon may have been involved in bonding though this needs further studies, and the fraction of phenolic group in the coal was raised from 0.06 to 0.09. Though the alkylated aromatics in coal and Coalgae® are the same, fraction of non-protonated C's in aromatic region in coal decreased from 0.55 to 0.46. The fraction of protonated C's in the aromatic region increased from about 0.24 to 0.29. It showed that the amount of hydrogen per aromatic

carbon had increased which appeared to describe a change in structure of coal due to the biomass. Each unsaturated aromatic bond is converted to C=C bonds whereas the bridgehead C's, mole fraction of the aromatic bridgehead C's, and average number of aromatic C's per cluster decreased. It seemed that microalgae biomass slightly altered the structure of coal, however, this requires more information to establish.

3.6 Summary

The average volatile content for linear combination of coal-microalgae biomass was significantly higher (paired t-test, $p = 0.005$) than the observed because of the microalgae biomass. The relative difference between the two averages was 2.38%. Some of the variation in averages suggested interaction between coal and microalgae biomass, though others require further studies to prove. The predicted and observed ash contents were equal (paired t-test, $p = 0.838$), however, more quantity of Coalgae® was consumed relative to coal. A slight difference between the observed and predicted contents of carbon, hydrogen, nitrogen, and sulphur due to measurement error. There is no difference (paired t-test $p = 0.3090$) between the predicted and observed average oxygen.

Chapter 4

4.0 Results and discussion – Combustion and kinetic modelling

This chapter includes the results and discussion of thermogravimetric analysis, kinetics, oxidation models, reaction mechanisms, activation energy and pre-exponential factor analysis for the combustion of coal, microalgae biomass and the blend, “Coalgae®”.

4.1 Thermogravimetric analysis (TGA)

Using the experimental procedure, section 2.4.6, the coal was analysed for thermal properties in air under non-isothermal conditions. The results obtained for coal is given in Table 4.1, mass m equals M, temperature T, dm/dt ~ dM/dT are used.

The mass of coal decreased initially due to dewatering but later increased as it absorbs oxygen for combustion. On ignition, the mass continued to decrease through de-volatilization down to the end of combustion.

Table 4.1: TGA combustion result for coal

100% Eskom Coal (mean), 0 % Blend								
Time (min.)	**Mass** (mg)	**Temp** (^{0}C)	**dm/dt** (mg/K)	**M/M_0**	**T** (K)	**α**	**1/T**	**Y_{CR}**
5.0000	5.1672	40.5460	0.0748	1.0000	313.5467	0.0000	0.0031	-
5.0563	5.1675	40.5500	0.5344	1.0000	313.5500	-7.1E-05	0.0031	-
5.1126	5.1684	40.5516	0.0354	1.0002	313.5517	-0.0003	0.0031	-
5.1689	5.1706	40.6150	0.0171	1.0006	313.6150	-0.0009	0.0031	-
“	“	“	“	“	“	“	“	“

(detail in appendix), dm/dt correlates 99% with dM/dT, Y_{CR} = Coats and Redfern’s model

The results, (Table 4.1) of the combustion of coal gives data of change in mass, temperature, rate dM/dT, mass fraction M/Mo, conversion α, reciprocal of temperature 1/T and Coats and Redfern kinetic model, Y_{CR} as a function of analysis time.

4.1.1 Thermogravimetric analysis of Coal

The thermal process described in Table 4.1, section 4.1 was plotted to obtain the change in mass, TG and the differential DTG for the coal, (Figure 4.1).

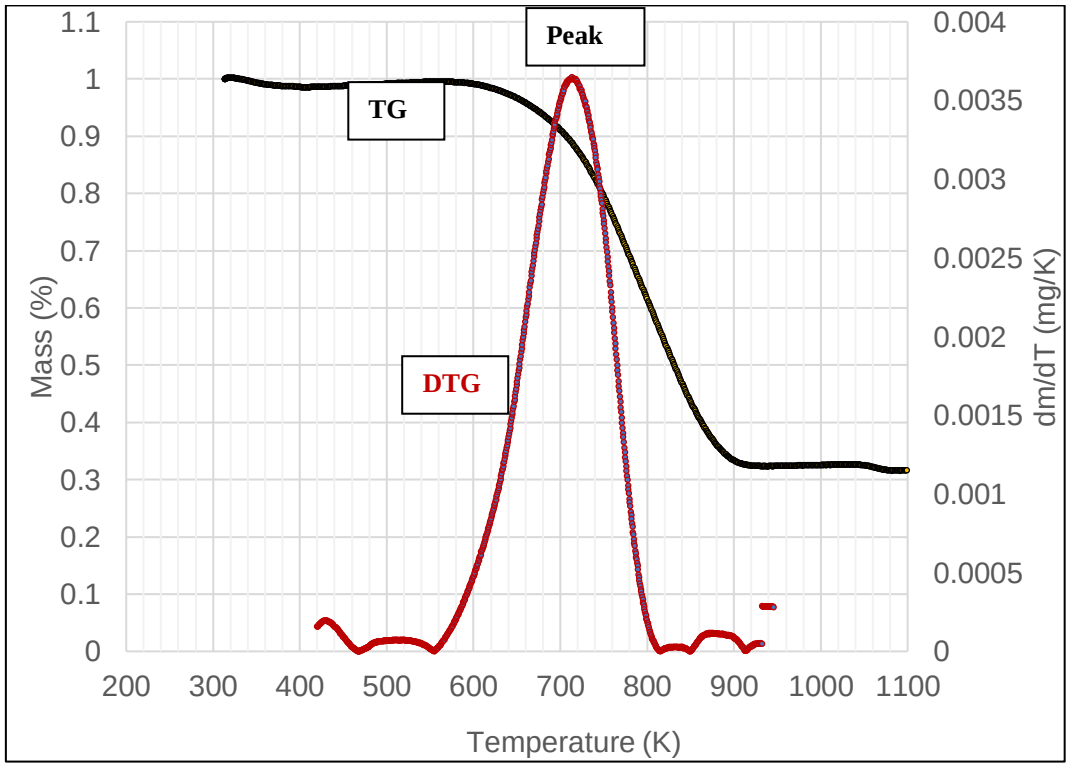

Figure 4.1: Thermograph of coal - TG and DTG

The combustion temperature for the coal analysed as per Table 4.1, which is described (Figure 4.1) reached the peak at ~ 720 K (see detail in appendix table 1). The de-volatilisation stage (A) lies in a short range of between 420 – 550 K which explains the small quantity of volatile matter, (Table 3.4), observed for as compared to other blends. It also explains why stage (A) above for coal is not prominent as compared to other blends, (Figure 4.5 and 4.8a). The combustion of char *i.e.* (stage B) in the graph dominates other processes with the rate of reaction at the peak of the DTG axis (y-axis) approximately 0.0035 mg/K.

4.1.2 Behaviour of Coal, Microalgae, and their blends

With the procedure in section 2.5.6, the behaviour of coal, microalgae, and blends were examined for similarity in combustion trend. The percent rate (dm/dT) for coal was plotted against temperature T and overlaid on similar graph for microalgae biomass. The coal and microalgae biomass, Figure 4.2, showed similar combustion behaviour.

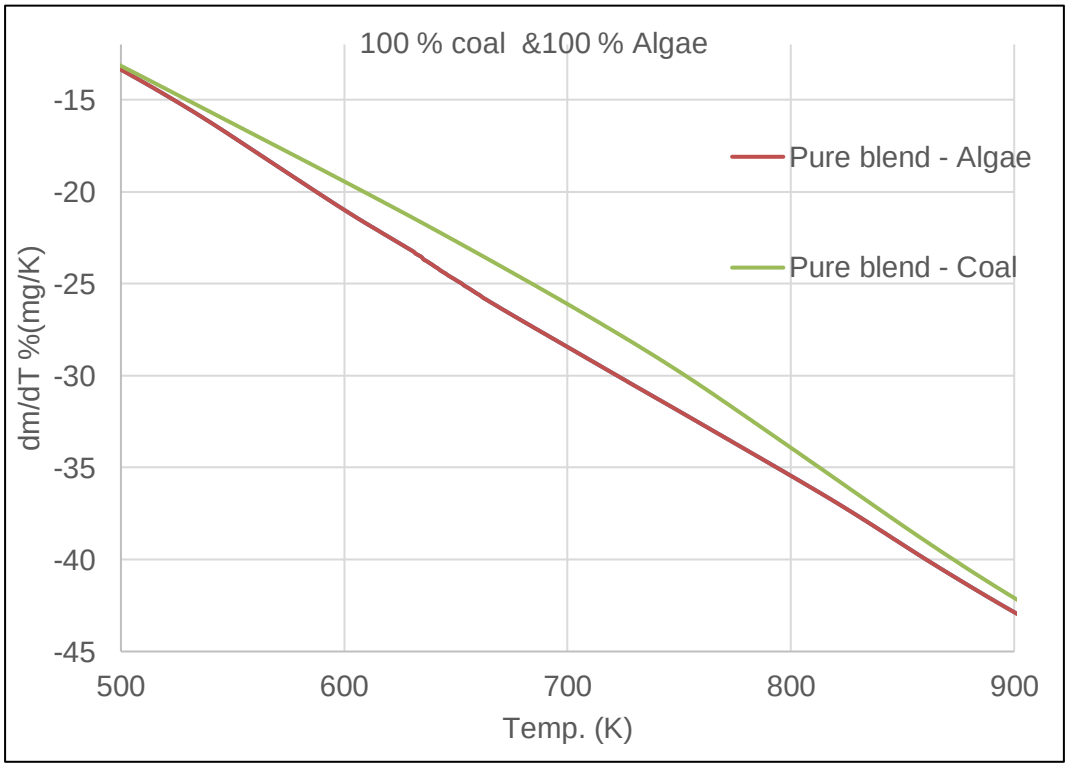

Figure 4.2: The overlay of combustion behaviour of "pure" coal and microalgae

The fusing of trends almost at both ends, (Figure 4.2), showed that the coal and microalgae biomass have similar combustion behaviour. The similarity allowed the materials to interact and be blended. Thus, coal and microalgae biomass were combined. Figure 4.3, for example 70% coal and 30% microalgae blended showed trend neither of coal nor the biomass. The combustion trend indicates an interaction between coal and the biomass.

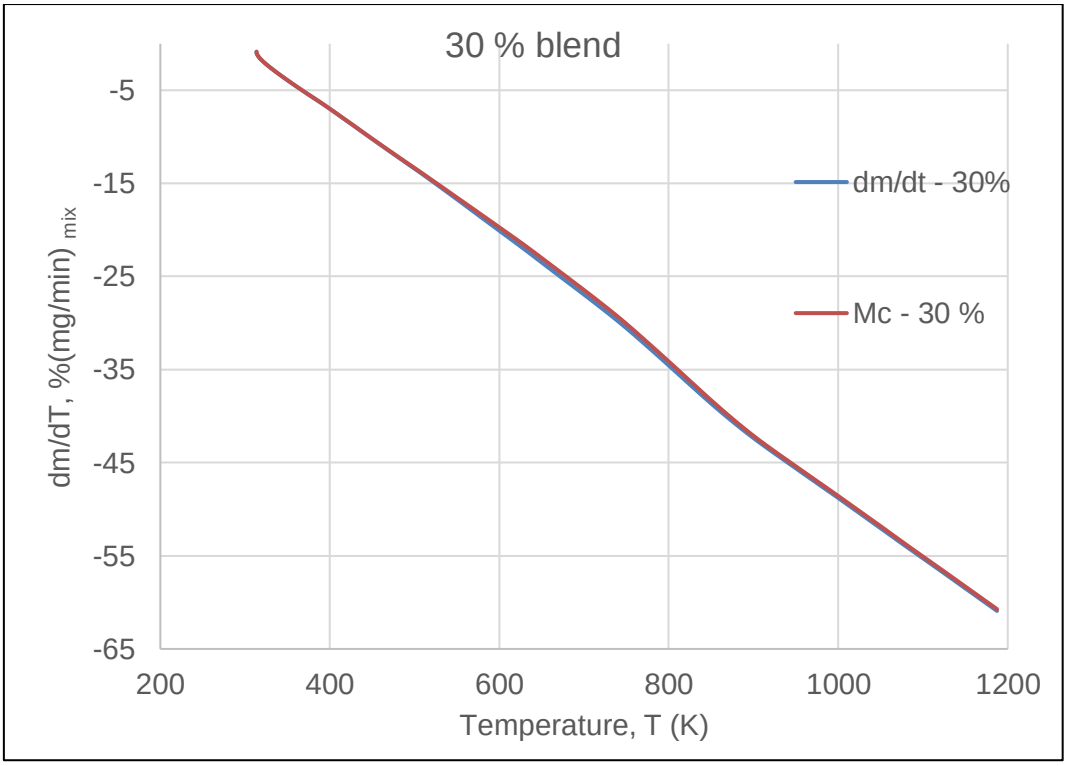

Figure 4.3: The mixture of 70C-30A indicating one thermal event

The rate of combustion *i.e.* (%) decrease in mass of coal per minute due to microalgae biomass for 30 % blend was increased from about -15 to approximately -5, by comparing, Figures 4.2 and 4.3. The increase in rate of combustion of 30 % "Coalgae®" suggests additive behaviour and compatibility. This same additive behaviour was observed for all the coal-microalgae biomass blends but to different extent. It shows that the coal and microalgae biomass interacted as indicated by one thermal profile, Figure 4.3. The overlap reveals that the theoretical 30 % composite is representative of the observed 30 % "Coalgae®". This means that, from the sample preparation result discussed in section 3. 0 and (Table 3.1 - 3.3), blending ~ 35.3 g microalgae biomass slurry of 16.73 % dry solid with ~ 14.7 g wet coal of 94.11 % dry solid produces the 30 % "Coalgae®" equation (4.1),

$$M_c = M_{30\,\%coalgae™} = 0.7x_{coal}.14.7M_{coal} + 0.3y_{algae}.35.3M_{algae} \quad \ldots\ldots\ldots\ldots\ldots\ldots \quad (4.1)$$

Where, M = mass and, x and y = rate.

M_c rate of combustion of composite overlapped with the sum fraction of rate components multiplied by mass confirming that M_c is equal to the sum of components on the left-hand side LHS of equation.

Also, from section 3.5.6 of the experimental procedures, the rate of combustion $\left(\frac{dm}{dt}\right)$ of "Coalgae®" at the maximum temperature must equal the sum of the rates $\left(\frac{dm}{dt}\right)$ for the individual components at maximum temperature multiplied by the fraction of component, for example 30 % is shown in equation (4.2),

$$\left(\frac{dm}{dt}\right) 30\ \%\ \text{Coalgae™} = 0.7x_{coal}.\left(\frac{dm}{dt}\right)_{coal} + 0.3y_{algae}.\left(\frac{dm}{dt}\right)_{algae} \quad \ldots\ldots\ldots\ldots\ldots\ldots\ldots\ldots \quad (4.2)$$

This relationship between theoretical rate, (right hand side of equation) overlaid on observed rate, (left hand side) under standardised temperature of combustion is illustrated in section 4.1.3.

4.1.3 Rate of combustion of Microalgae, Coal and "Coalgae®"

With the procedure in experimental section 2.5.7, the Figures 4.4 – 4.11 was used to compare the theoretical (*i.e.* predicted) and observed combustion rates. The predicted values here are for the discard ultra-fine coal while the observed are for the coal-microalgae composite *i.e.* blends or "Coalgae®". The combustion rate for microalgae biomass, coal, and blends was graphically compared under a standard temperature. The comparison was done by calculating the predicted rate with consideration to a linear combination of rates for the individual material.

The rate of devolatilization and combustion (mg/K) was separated into schemes. The low temperature scheme L, *i.e.* devolatilization or stage A denoted as Y1, and high temperature scheme H, *i.e.* char combustion or stage B denoted as Y2.

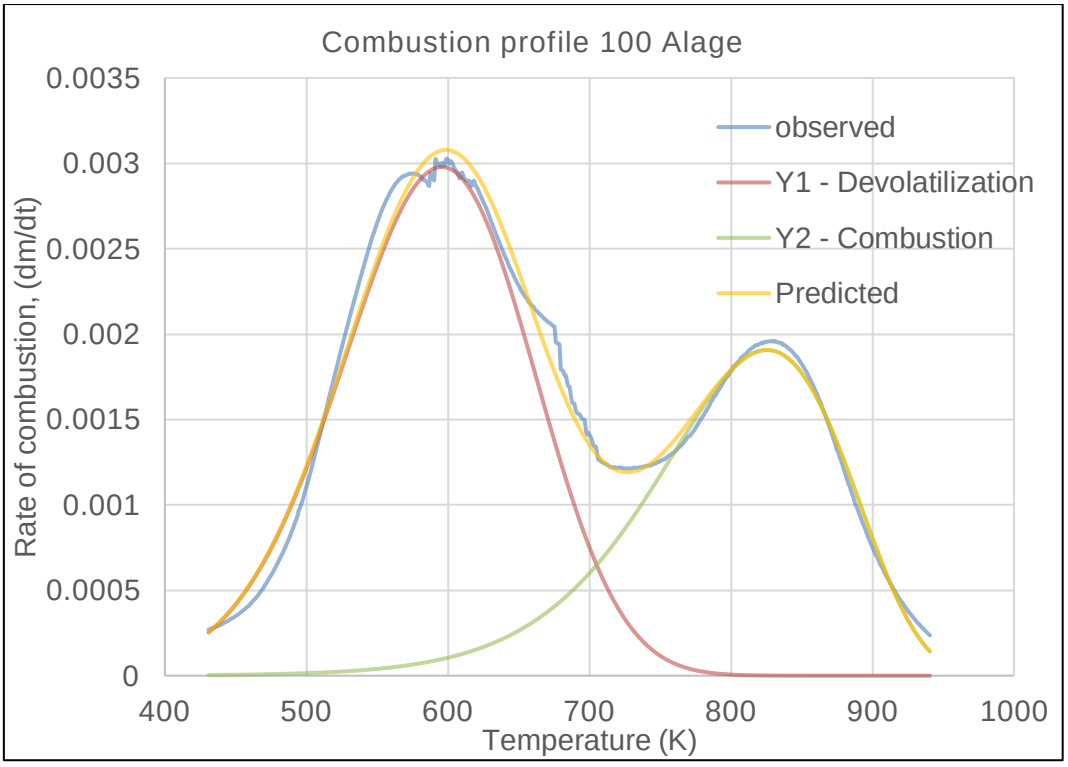

Figure 4.4: The deconvolution for Microalgae showing observed and predicted rate of combustion

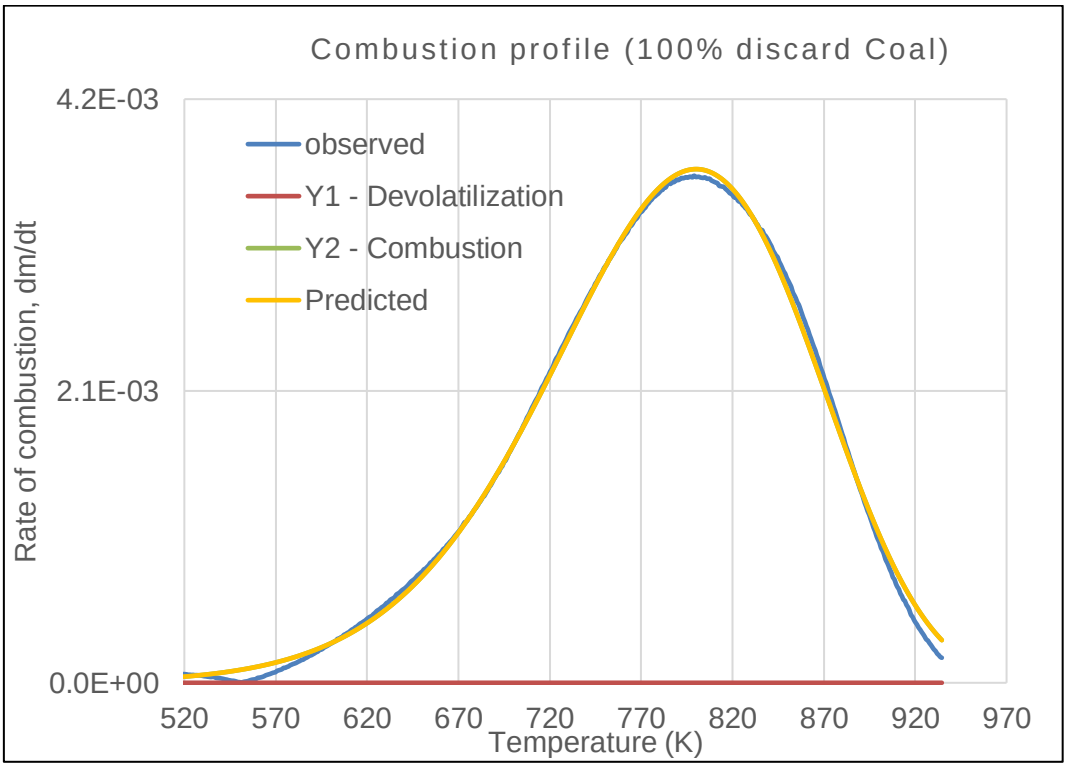

Figure 4.5: The deconvolution for 100 % discard Coal showing observed and predicted rate of combustion

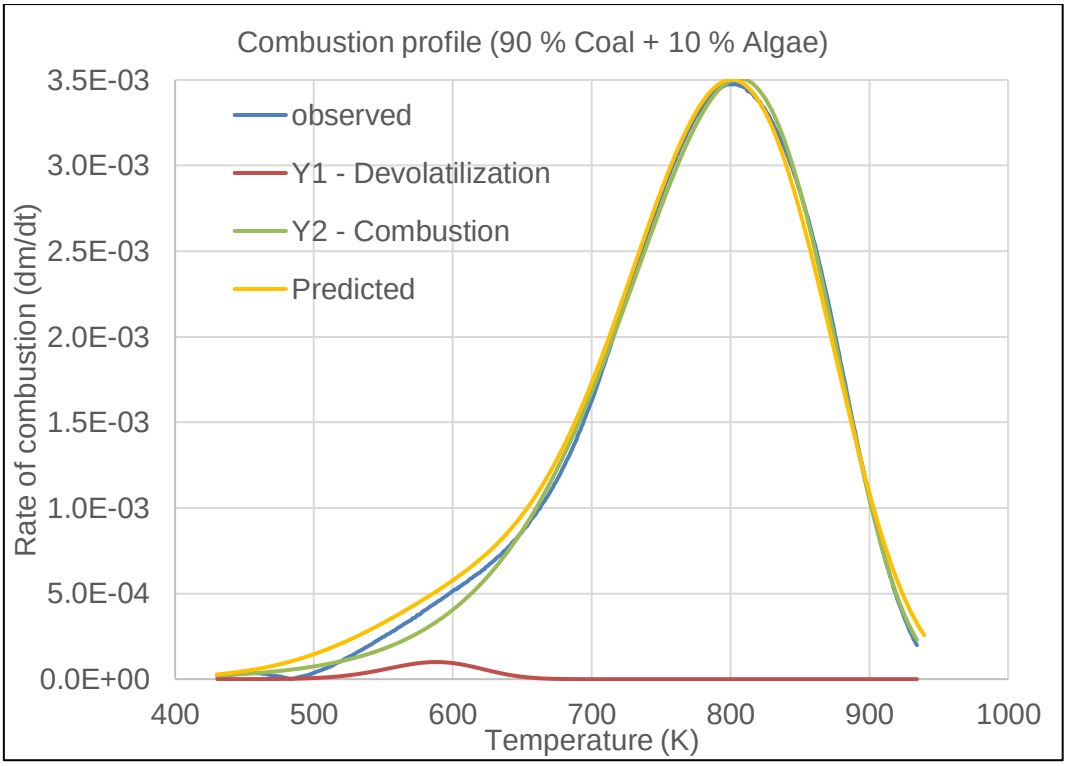

Figure 4.6: The deconvolution for 10 % Coalgae® showing observed and predicted rate of combustion

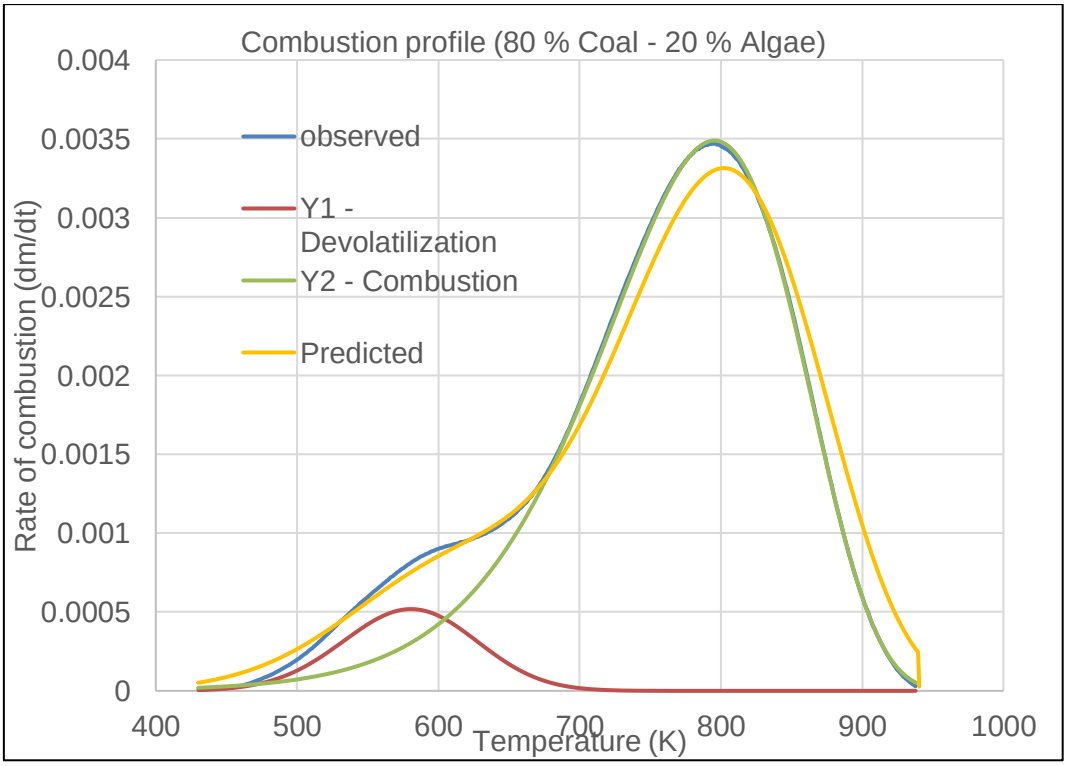

Figure 4.7: The deconvolution for 20 % Coalgae® showing observed and predicted rate of combustion

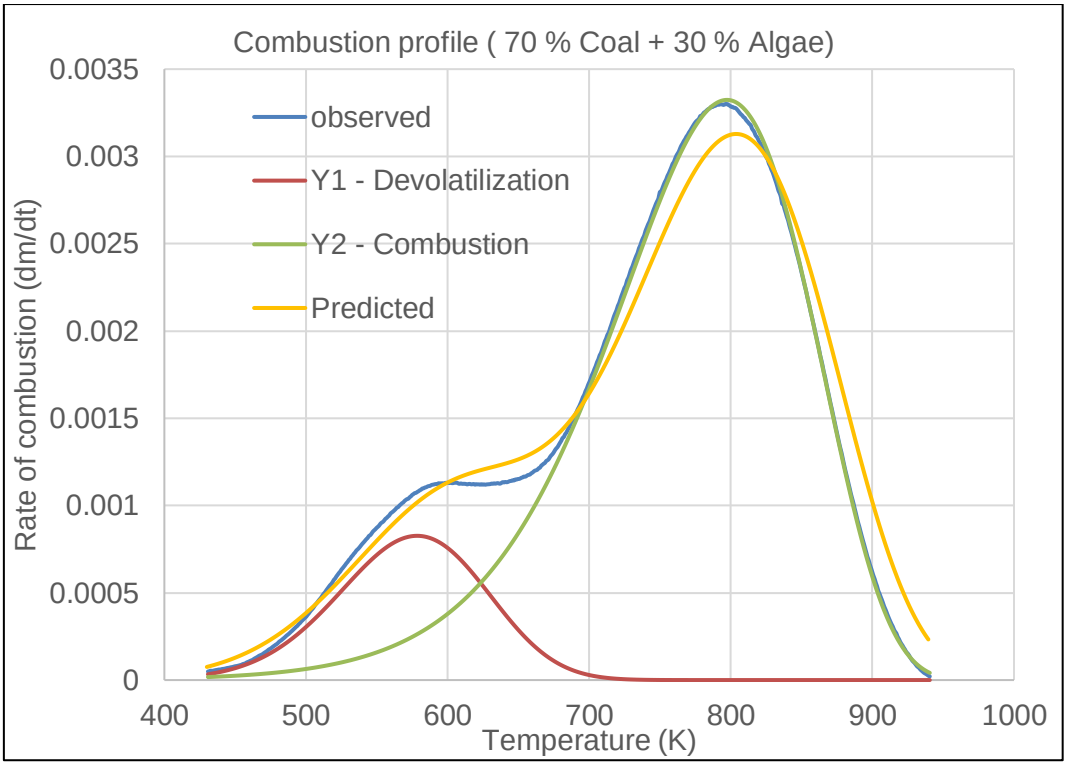

Figure 4.8: The deconvolution for 30 % Coalgae® showing observed and predicted rate of combustion

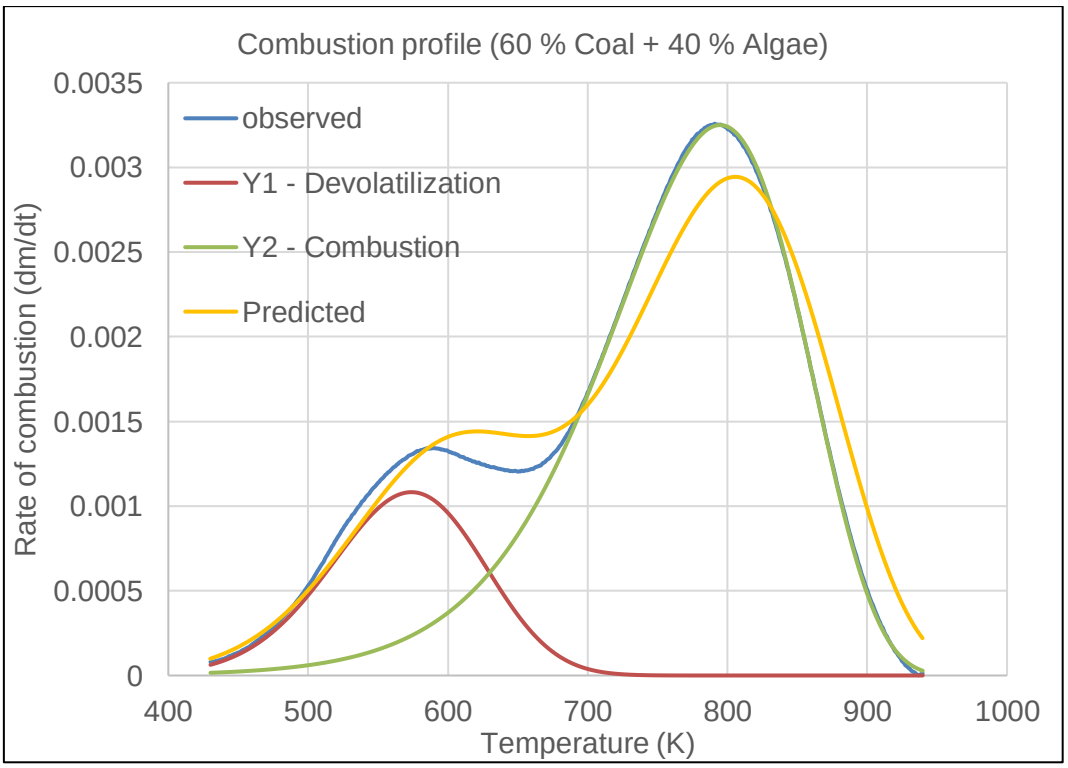

Figure 4.9: The deconvolution for 40 % Coalgae® showing observed and predicted rate of combustion

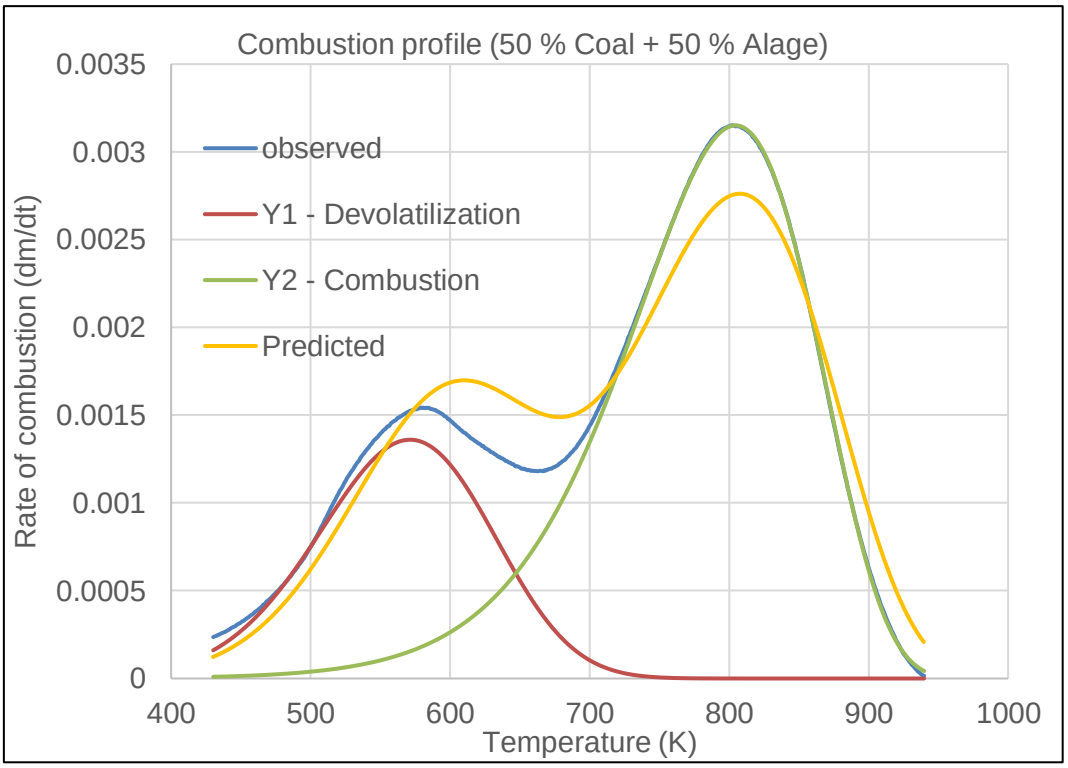

Figure 4.10: The deconvolution for 50 % Coalgae® showing observed and predicted rate of combustion

Table 4.2: Rate and peak temperature for 10 – 50 % "Coalgae®"

%A	Obs. rate (dm/dt)	Theo. rate (dm/dt)	Diff. (%)	SS	Obs. Temp. (K)	Theo. Temp. (K)	Diff. (%)
10	0.0034	0.0035	-0.7	3.26E-06	800.2	800.5	0.0310
20	0.0034	0.0033	4.5	2.53E-05	793.8	802.2	1.0668
30	0.0033	0.0031	5.2	2.72E-05	795.9	804.0	1.0124
40	0.0032	0.0029	9.6	4.23E-05	790.7	805.8	1.8988
50	0.0031	0.0027	12.4	3.50E-05	802.9	807.5	0.5704

Obs. = observed, Theo. = theoretical (predicted), SS = sum of standard residuals, Diff. = difference

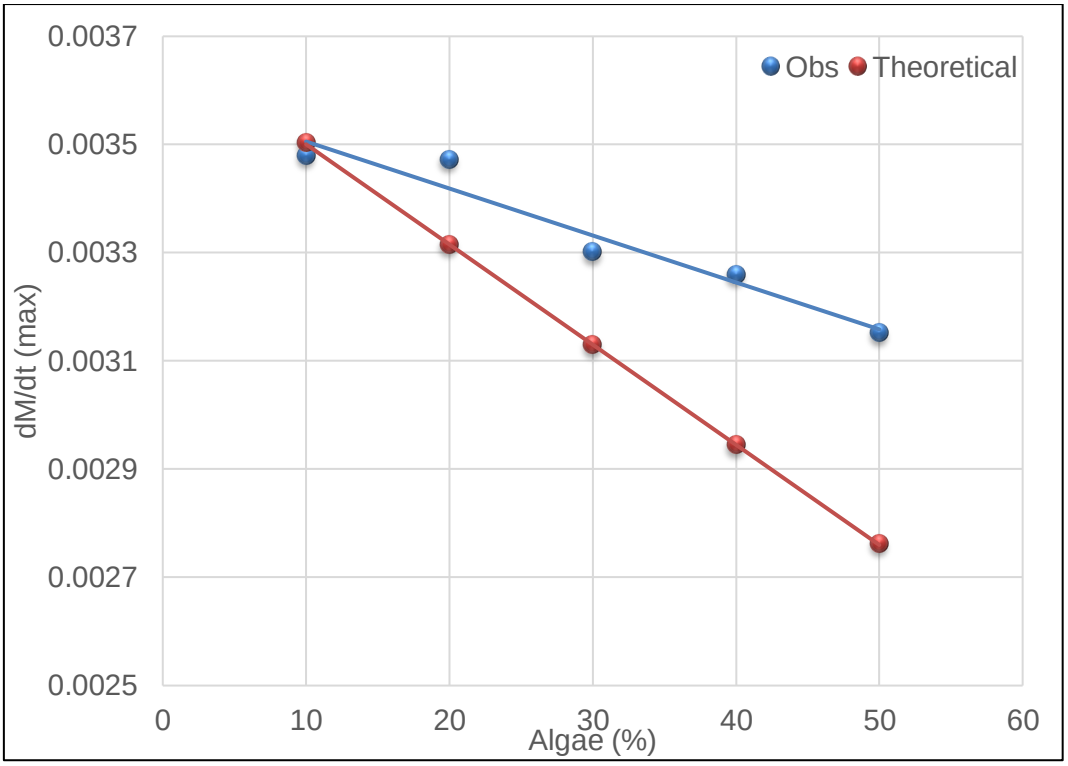

Figure 4.11: Standardized observed and theoretical rate for Coalgae®

This shows the maximum observed and theoretical mass change rates, (Figure 4.11) as a function of increasing microalgae biomass. The combustion rate of composites increased as more microalgae biomass was added. Microalgae biomass is very reactive, and enhanced reactivity of the composites (212) which led to a decreased time of consumption per gram of fuel.

Observed and theoretical rates used in regression analyses to test the differences in gradients are indicated in Table 4.3 below with regression statistics in Table 4.4.

Table 4.3: Observed and theoretical rate used in regression

Experiments (outcomes)	Indicator	Algae (%)	Rate (mg/K)
Obs.	0	10	0.0034
Obs.	0	20	0.0034
Obs.	0	30	0.0033
Obs.	0	40	0.0032
Obs.	0	50	0.0031
Th	1	10	0.0035
Th	1	20	0.0033
Th	1	30	0.0031
Th	1	40	0.0029
Th	1	50	0.0027

Obs. = observed, Th = Predicted or theoretical

Table 4.4: Summary of regression statistics

Summary of ANOVA						
Multiple R	0.94798	**ANOVA**	df	SS	MS	F
R Square	0.89867					
Adjusted R Square	0.86972	Regression	2	4.7151E-07	2.3575E-07	3.1040E+01
Standard Error	0.00009	Residual	7	5.3166E-08	7.5952E-09	-
Observations	10.00000	Total	9	5.2467E-07		-
-	Coefficients	Standard Error	t Stat	P-value	Lower 95%	Upper 95%
Intercept	0.00374	0.00007	53.2262	0.00000	0.00357	0.00391
Indicator	-0.00020	0.00006	-3.6603	**0.00807**	-0.00033	-0.00007
Algae (%)	-0.00001	0.00000	-6.9772	0.00022	-0.00002	-0.00001

df = degree of freedom, SS = sum of standard residuals

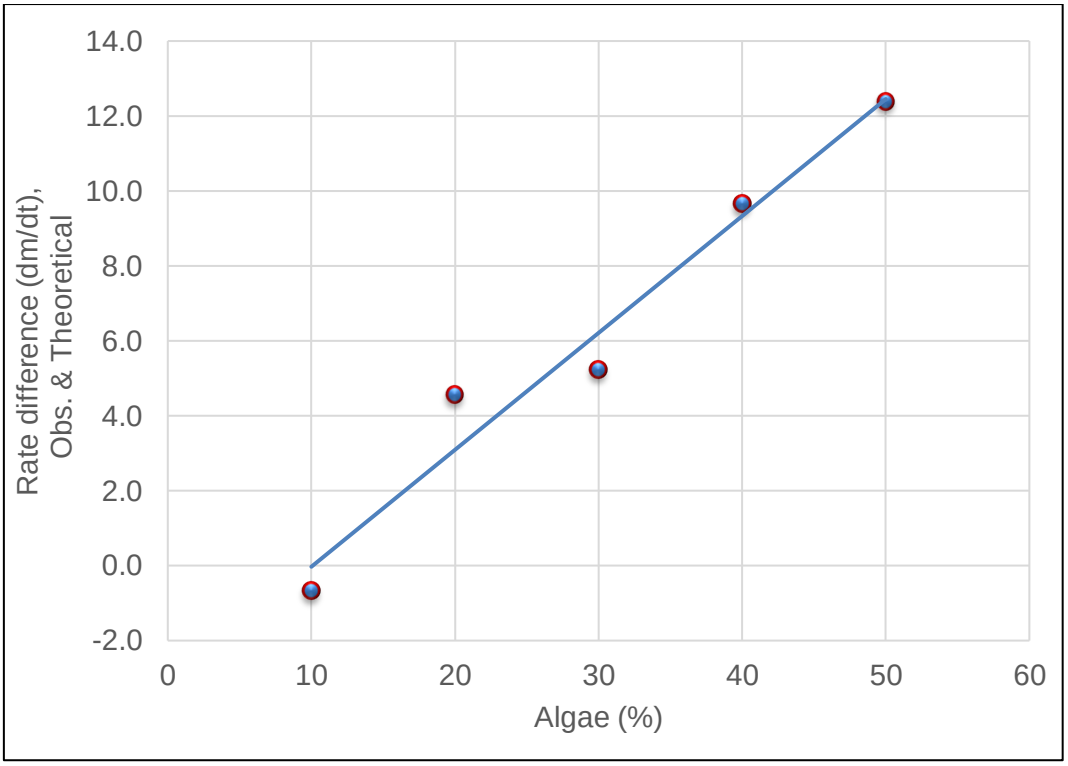

Figure 4.12: Difference between observed and theoretical rate of reaction

Figure (4.12) represents the difference between the observed and theoretical rates of reaction as a function of algae % and Table 4.5 shows the regression output.

Table 4.5: Summary of regression statistics for difference in rate

Regression Statistics		ANOVA				
Multiple R	0.9819	-	df	SS	MS	F
R Square	0.9641	Regression	1	97.3358	97.3358	80.5626
Adjusted R Square	0.9521	Residual	3	3.6246	1.2082	-
Standard Error	1.0992	Total	4	100.9604	-	-
Observations	5.0000	-				
-	Coefficients	Standard Error	t Stat	P-value	Lower 95%	Upper 95%
Intercept	-3.1498	1.15283	-2.73227	0.07180	-6.81867	0.51898
Algae (%)	0.3120	0.03476	8.97567	**0.00292**	0.20137	0.42261

df = degree of freedom, SS = sum of standard residuals

There is enough evidence to prove that there exists significant difference (P-value, 0.0029) between the observed and theoretical rates of combustion. The combustion rate of “Coalgae®” relative to the coal are not the same, Table 4.5.

The average observed rate at peak combustion temperature is significantly higher than the average predicted rate, (paired t-test, p = 0.0475). The difference between the averages is 6.43 %. The rate of reaction for the observed, (Coalgae®) was increased as more of it is consumed under the same condition relative to the predicted (coal) (see later in Figure 4.17). This means improved combustion kinetics, because the maximum time taken for it to oxidize was less compared to coal. An overlay of rate of combustion indicated a different but superior kinetics compared to coal. The blend burns out first relative to parent coal, (Table 1, in appendix), and the rate of combustion increases, Table 4.2 - 4.3, and Figure 4.11. The average predicted combustion temperature at peak is significantly higher than the average observed temperature at peak, paired t-test, p = 0.04022). The difference between the averages is 0.91%. For blends, the coal % reduces and the microalgae composition increases with more influence on the thermal properties *i.e.* "ignition, burnout, peak temperature and reactivity.

4.1.4 Combustion kinetics – Coal

Thermogravimetric profiles are not a direct substitute for kinetic models. This is because models help us to understand the mechanistic pathway and predict important features for combustion reactions.

Using the experimental procedure under section 2.5.8, the kinetic parameters were calculated using Y_O or $Y_{CR,}$ equation (4.3), and the Coats and Redfern kinetic model, (Figure 4.13) below, and (Table 4.2) summarise the result obtained for the discard ultra-fine coal used in this study.

$$y_0 = \ln\left[\frac{1-(1-\propto)^{1-n}}{T^2\,(1-n)}\right] \quad \text{..... (4.3)}$$

Where, y_0 = Coats and Redfern Kinetic model and,

n = order of the reaction,

T = temperature K.

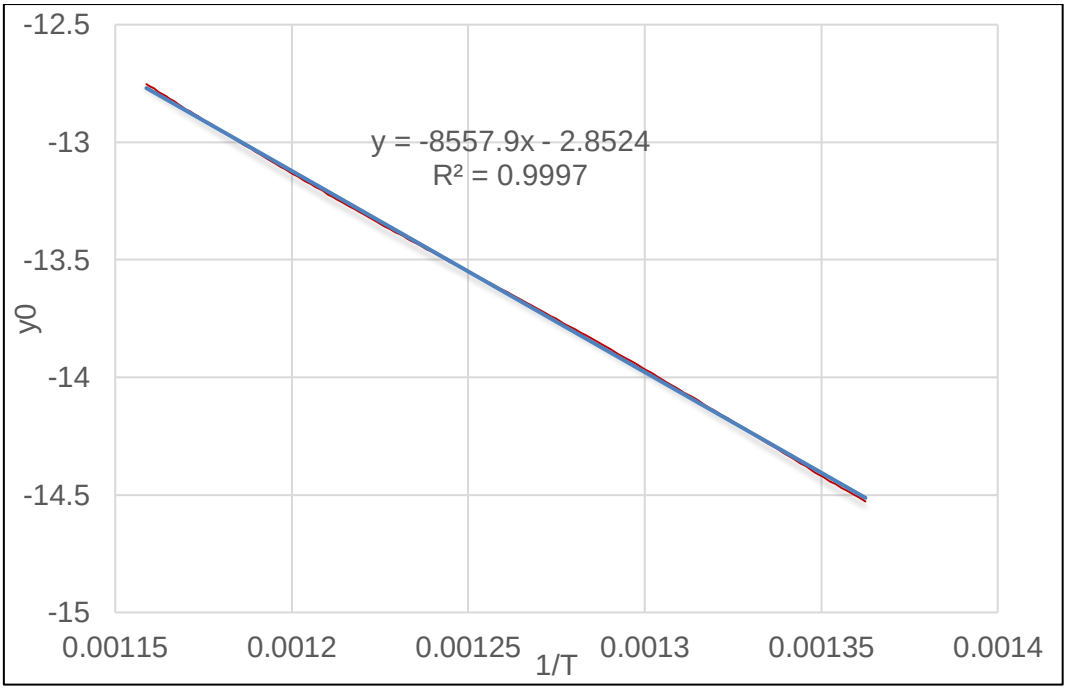

Figure 4.13: Coats and Redfern kinetic model for the discard ultra-fine coal

Based on the Coats and Redferns model y_0 explanation of the combustion of coal, (Figure 4.13) has a single thermal event almost the same as 10 % blend. The model explained about 99 % variation in the kinetics parameters of the coal.

4.1.5 Combustion kinetic parameters of Coal

Table 4.6 indicates the kinetic parameters for the coal based on the preceding model.

Table 4.6: combustion kinetic parameters for discard ultra-fine coal at 95 % C.I

E a (KJ/mol)		**T_{ig} (K)**		**T_{max} (K)**		**DTG_{max} (mg/K)**		**$\Delta t_{1/2}$ (K)**		**S-Value**	
mean	(±)	mean	(±)	mean	(±)	mean	(±)	mean	(±)	mean	(±)
72.2	5.6	694.8	5.1	799.7	4.3	0.0037	0.0002	146.00	8.22	0.797	0.03
H-Value		**gradient**		**Th**		**DTG_{mean}**		**n-order**		**M/Mo**	
0.0100	0.0001	8681.67	671.28	918.33	4.28	0.00097	6.77E-06	1.03	0.02	0.32	0.01

Ea = activation energy, Tig = ignition temperature, Tmax = maximum combustion temperature, DTGmax and DTGmean = maximum and mean of DTG curve, $\Delta t_{½}$ = combustion width, S, and H-values = comprehensive combustion characteristics, Th = burn-out temperature, n -order = reaction index, M/Mo = ash content.

The activation energy of the coal E_a is 72.2 ± 5 kJ/mol, (Table 4.2), close to literature reports (213), (see section 4.7.2). whereas the S-value is 0.797 ± 0.03 and H-value is 0.001 ± 0.0001. Because the S-value of the discard ultra-fine coal is higher than the H-value, as expected of a solid fuel (114), (192), this makes discard acceptable for modification with microalgae biomass. The maximum temperature is 799.7 ± 4.3 K while the reaction order, n = 1.03 ± 0.02 indicates first order. The ash on dry basis Ad, m/m_o is 0.31 ± 0.1mg approximately 27.02 ± 0.03 % (0.297mg) observed in proximate analysis as observed in Table 4.1.

4.2 Thermogravimetric result for Microalgae biomass

With the same non-isothermal TG experimental procedure as described for coal in section 2.4.6 of the experimental section, the result for thermal conversion of microalgae biomass is represented (Table 4.7) below.

Table 4.7: TG and DTG for Microalgae biomass

Algae (means).					**100 %**			
Time (min.)	**Mass** (mg)	**Temp.** ***T*** (^{0}C)	***(dM/dT)***	***M/M₀***	***T*** ***(K)***	α	**1/T**	y_{CR}
5.0400	5.4306	40.5640	0.0641	1.0861	313.5640	-0.0861	0.0031	-
5.0963	5.4308	40.5680	0.1140	1.0861	313.5680	-0.0861	0.0031	-
5.1526	5.4315	40.5740	0.0406	1.0863	313.5740	-0.0863	0.0031	-
5.2089	5.4340	40.6360	0.0199	1.0868	313.6360	-0.0868	0.0031	-

y_{CR} = Coats and Redfern model, (detail in appendix)

There is an increase in original mass of microalgae biomass sample due to the absorption of oxygen (chemisorption) required for combustion. This mass later continues to decrease on until the end of combustion. The mass fraction, M/Mo (%), and dM/dT versus T, and y_0 versus 1/T is detailed under thermograph, Figures 4. 14 and kinetic profile, Figure 4.15.

4.2.1 Combustion of Microalgae biomass

The thermal event of microalgae biomass showed two combustion schemes similar to literature report (128), and labelled A and B (Figure 4.14), which corresponds to the devolatilization and the char combustion respectively.

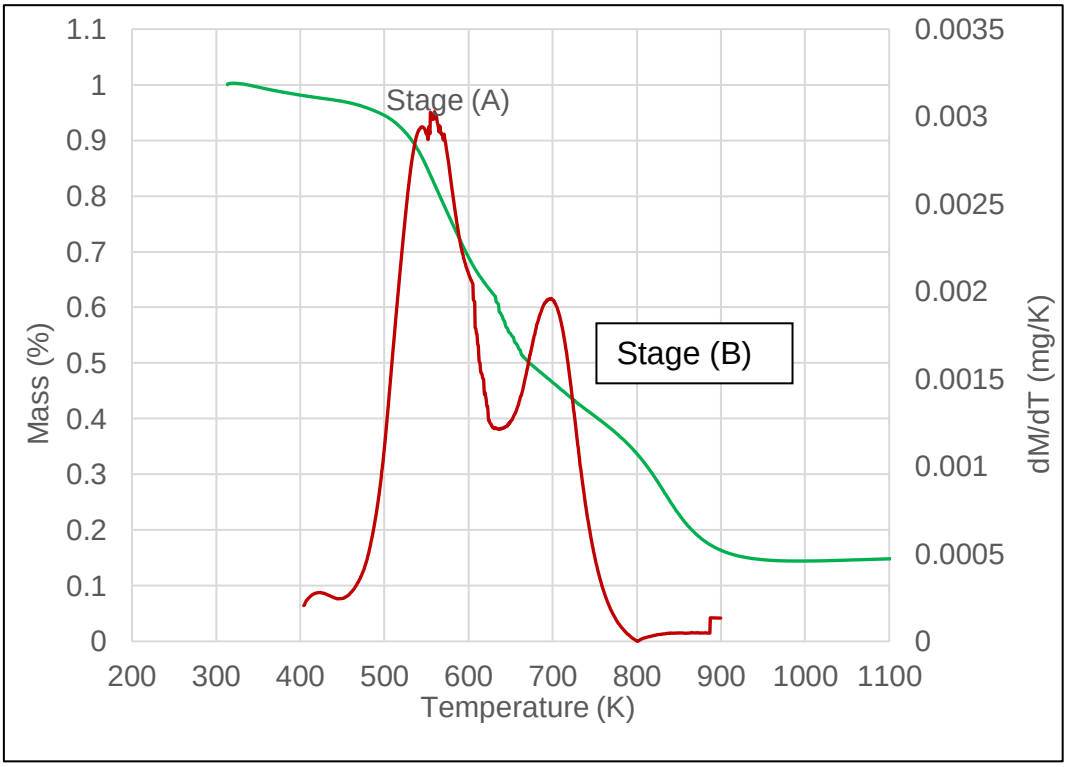

Figure 4.14: Thermograph showing de-volatilization (A) and char combustion (B) of microalgae biomass

The peak temperature is the point at the maximum reactivity in mg/K, and according to Figure 4.14, the peak temperature for the coal was at dm/dt above 0.0035, and that for biomass at 0.003. The peak of stage (A) shows that more volatile was released relative to the coal, (Figure 4.1) with “no” stage A and this agrees with the proximate analysis result, (Table 4.1). The ignition temperature of this biomass lies between 450 – 470 K as compared to coal, Figure 4.1 which is about 500 – 550 K. Microalgae biomass has less fixed carbon, stage (B) relative to coal but the devolatilization started at about 480 K and continued to 700 K. The thermal conversion of microalgae biomass showed a non-linear relationship with temperature change, (Figure 4.15). This was similar to literature report (128) which also showed two combustion steps.

4.2.2 Combustion kinetics of Microalgae biomass

Using the data from section 4.2.1, the Coats and Redfern combustion kinetics model y_{CR}, for microalgae biomass, (Figure 4.14) is shown in (Figure 4.15).

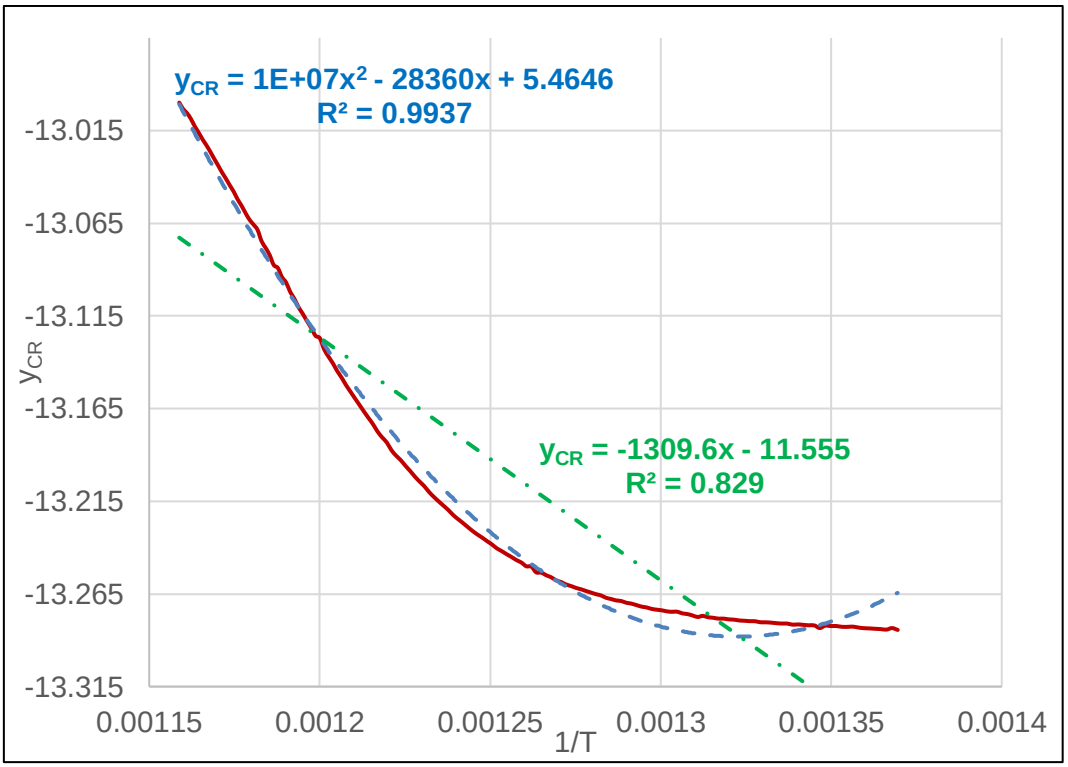

Figure 4.15: Coats and Redfern model for microalgae biomass

From the Coats and Redfern model explanation, (Figure 4.15) the combustion kinetics of microalgae biomass shows that a quadratic model (R^2 = 0.99) provided a better explanation compared to a linear model (R^2 = 0.82). This agreed with the explanation, (Figure 4.14) indicating that microalgae biomass has two thermal events. Thus, stage A and B was separated, (see section 4.6) and further studied for each of coal, microalgae biomass and the blends.

4.2.3 Kinetic parameter for Microalgae biomass

Table 4.8 shows the combustion parameters derived from the Coats and Redfern's kinetic model for 100 % microalgae biomass from (Figure 4.15), section 4.2.2.

Table 4.8: combustion parameters for microalgae biomass

E a mean (kJ/mol)	**T_{ig} Mean** (K)	**T_{max} Mean** (K)	**DTG_{max} Mean** (mg/T)	**DTG_{mean}**	(±)	**Gradient**	**Δ t ½ (K) mean**
235.79 *	497.7	599.3	0.003	0.0012	6.77E-06	28360	179
Th	(±)	**Order** (n)	(±)	**H-value**	(±)	**Ash** (mg)	**S-value mean**
900	4.28	**0.60**	0.02	0.011	0.0001	0.144	1.577

235.79* = calculated using the gradient (Figure 4.15) for non-deconvoluted process

An increase in S-value and a decrease in H-value of a solid fuel, indicates an improvement in the comprehensive combustion characteristics (114), (192). The opposite is true for decreasing comprehensive combustion characteristics. Thus, microalgae biomass of 1.57, (detail in Table 4.8) is superior to coal of 0.79 S-value, (see Table 4.6). The index (order) n, 0.60 shows that the combustion did not follow the first order O1 reaction mechanism as can be seen by the non-linear curve of the Coats and Redfern's description, (Figure 4.15).

4.3. Thermogravimetric analysis of composites

With the non-isothermal TG described in the experimental section 2.4.6, the Table 4.9, shows a typical result for 10 % "Coalgae®".

Table 4.9: TG and DTG result for 10 % "Coalgae®"

90C-10A					**10 %**			
Time (min.)	**Mass** (mg)	**Temp.** T (^{0}C)	**(dM/dT)**	**M /M_0**	**T** (K)	**α**	**1/T**	**y_{CR}**
5.0333	5.1263	40.5566	8.44E-05	1.0000	313.5567	0.0000	0.0031	-
5.0896	5.1262	40.5616	0.0007	0.9999	313.5617	2.01E-05	0.0031	-22.3089
"	"	"	"	"	"	"	"	"
5.1459	5.1269	40.5666	0.0003	1.0001	313.5667	-0.0001	0.0031	-
5.2022	5.1295	40.6266	0.0025	1.0006	313.6267	-0.0009	0.0031	-!

Y_{CR} = Coats and Redferns model, (detail in appendix)

4.3.1 Small scale combustion of “Coalgae®” in TGA

The non-isothermal combustion result, (Figures 4.16 and 4.17), shows an overlay of the small-scale combustion of “Coalgae®” samples relative to coal. The results indicate that the thermograph of “Coalgae®” deviates from that of the original coal as microalgae biomass loading increases.

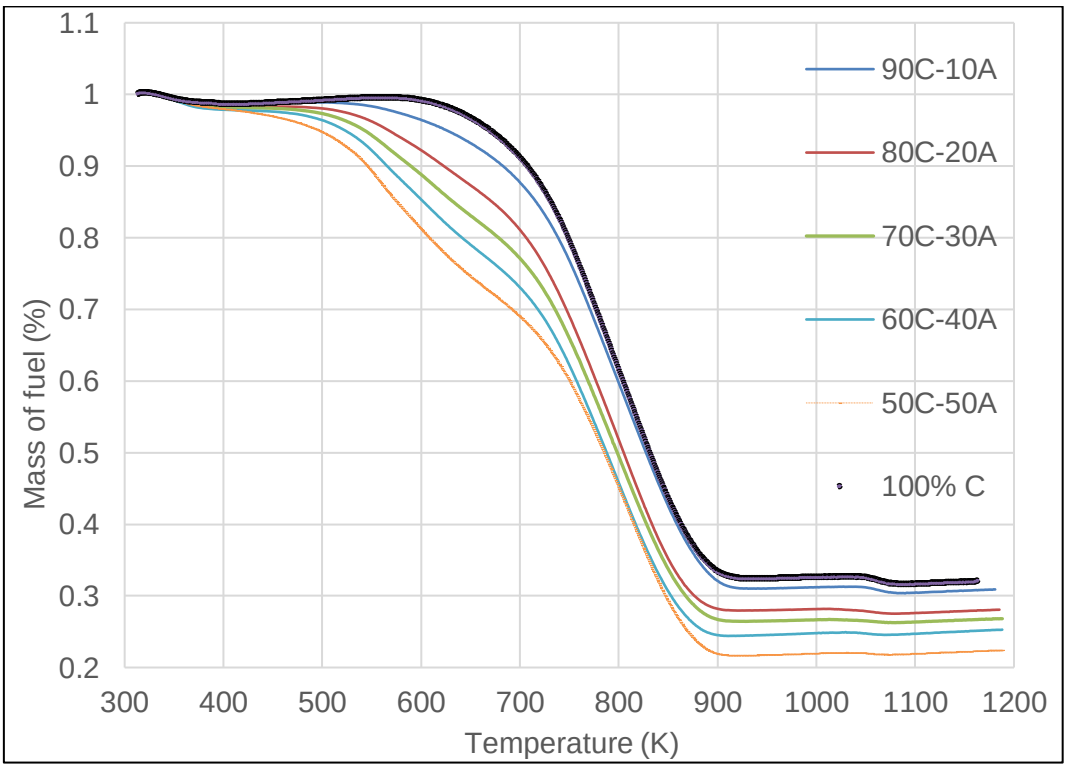

Figure 4.16: Overlay of combustion of composites and coal

From the graph (Figure 4.16), there is an increase in average mass of fuel that combusted as biomass increases from 0 – 50 %. The profiles indicate that for equal mass, the blends finished combusting earlier compared to the original coal where a upper profiles denoted less fuel consumption (136).

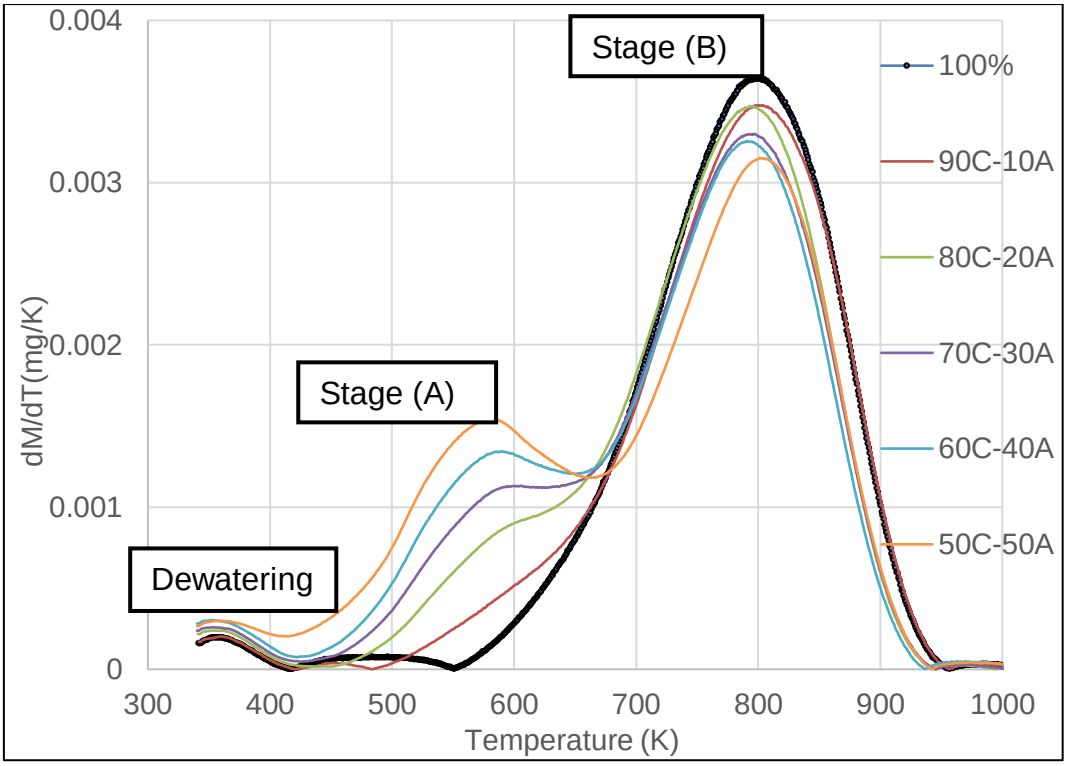

Figure 4.17: Overlay of combustion of composites and coal

The three stages, (Figure 4.17), *i.e.* dewatering, devolatilization (A), and char combustion (B) were observed. These stages show the fuel reactivity, due to the high volatile content of the biomass. The area of curve under stage A is a function of the amount of volatile, while stage B shows the amount of char which depends on the amount of fixed carbon(151). Thus, the graph shows that the amount of volatile increases (peak A) and char decreases (peak B) relative to coal. Only A and B, which are the primary stages of the combustion were considered for analysis. The peak of stage A indicates increase in volatile content while B shows a decrease in the fixed carbon content as temperature increases, and the graph agrees with the earlier observed proximate parameters. After the volatiles are released the combustion of the char/carbon continued to burnout stage. So, the peak temperature is where the maximum "(dm/dt)" combustion rate occurs. The addition of live microalgae biomass to coal influenced the combustion properties of coal. The thermal behaviour of coal, microalgae, and a blend of the two differs.

4.3.2 Pilot combustion of "Coalgae®" in fixed bed reactor

The combustion conditions as described in experimental section 2.4.6, was applied on the large-scale study of Coalgae® in a fixed bed reactor. The bulk or pilot study of the 10 % Coalgae®, as described in section 2.4.7 was carried out at the John Thompson research and development facility (Cape Town). Three distinct phases, (Figure 4.18) like Figure 4.17 described above were observed.

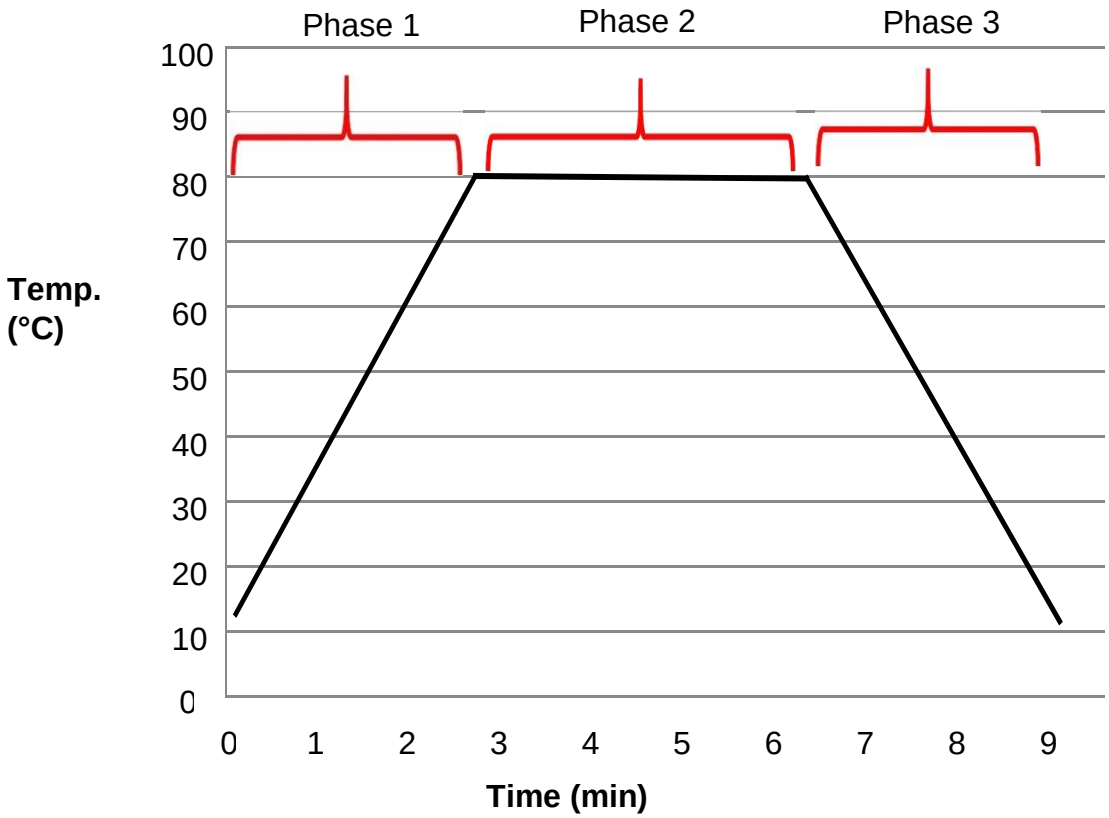

Figure 4.18: The de-water, de-volatile, and stable combustion for 10 % Coalgae®

The phase 1, Figure 4.18, is associated with dewatering, drying, establishing ignition, and de-volatilisation. Phase 2 is the stable combustion associated with a linear relationship with the time and decrease in mass. The phase 3 is related with the char burnout. A comparison of the relationship, (Figure 4.19) between temperature and time of combustion for the coal, Coalgae® and a reference coal are demonstrated in Figure 4.19. The low temperature (pyrolyzed char), product from the same 10 % Coalgae® was introduced for comparison purposes.

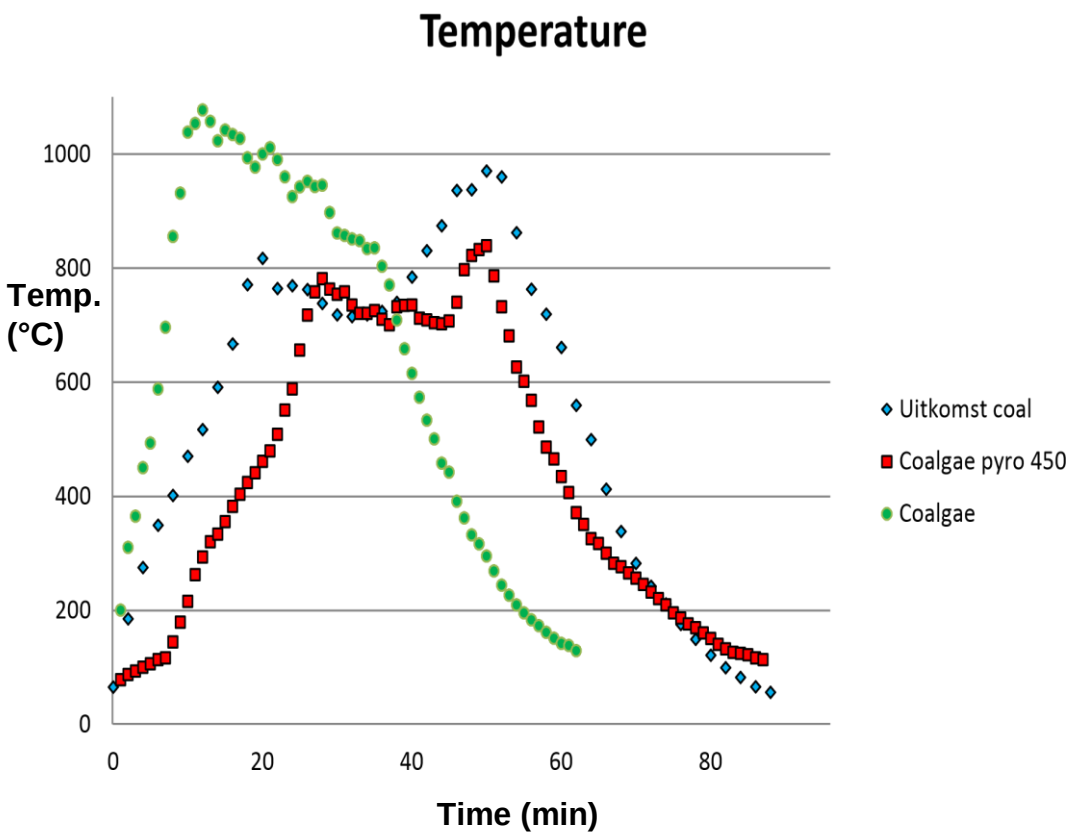

Figure 4.19: Temperature at reactor outlet for fuels with a typical coal as reference.

The thermograph above, (Figure 4.19) displays the difference in temperature for large scale combustion of the reference discard coal, “Coalgae®” and “Coalgae®” pyro 450. Coal and the Coalgae®” pyro 450 char have similar combustion temperature profile. This is due to the coal like nature with an increased carbon content in the Coalgae pyro 450 sample. The rise in temperature is rapid in the 10 % “Coalgae®”, which can be attributed to high volatile content as compared to coal. Coalgae® pyro 450 took longer to ignite with much slower increase in temperature corresponding well to that of typical coal. The reason is due to high carbon and very low volatile matter content of the char. But “Coalgae®” reaches the peak temperature at shortest time compared to both coal, and pyro 450 samples. This is because Coalgae®” follows a different curve, and the temperature peaks after ignition, which later falls gradually. The peak temperature of the “Coalgae®” and “Coalgae®” pyro 450 differs considerably.

The mass loss (kg) with respect to time (min), *i.e.* fuel reactivity in the fixed bed reactor was represented, (Figure 4.20) below.

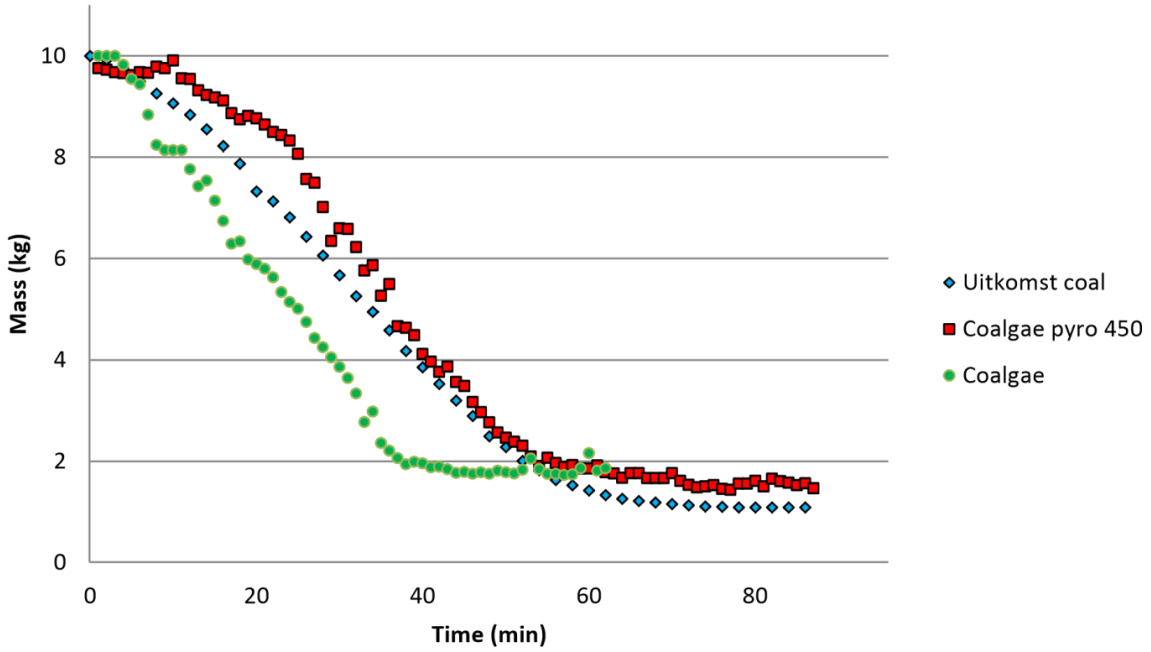

Figure 4.20: Mass reduction for the two fuels vs time with a typical coal as reference.

The mass loss (kg) curve as depicted, Figure 4.20, and like, (Figure 4.16) it showed a quicker initial mass loss for “Coalgae®” when compared to the Coalgae®” pyro 450. This was due to the properties of the fuel/blend that accelerated the combustion and the mass loss (kg). This initial and quicker mass loss accelerate the combustion to reach a stable condition in “Coalgae®” at about 62% earlier than in the case of the “Coalgae®” pyro 450. The combustion (stable) horizontal phase is similar between the two fuels as depicted by the linear gradient, (Figure 4.18), which is like Figure 4.16. During the stable combustion phase, the tests showed a fuel consumption rate of 0.285 kg/min for the “Coalgae®” and 0.232 kg/min for “Coalgae®” pyro 450. This agrees with the rate of combustion, (Table 4.2 and Table 4.3). For the reference coal fuel consumption is 0.176kg/min.

The curve Figure 4.20 illustrates the difference in ash contents, (Table 3.4) in the two fuels compared to typical good quality coal. The coal indicates an ash content of 13.1%. The “Coalgae®” had around 16 - 17% residual mass compared to the 11% residue for the reference coal. The values correspond well to the proximate ash content as determined by laboratory analyses, (section 3.1).

4.3.3 Coal, “Coalgae®” and “Coalgae®” Pyro 450

According to the results in section 4.3.2, “Coalgae®” and “Coalgae®” pyro 450 should combust effectively in a chain grate stoker boiler. The fast ignition and combustion of the “Coalgae®” will allow the stoker speed to be increased which will in turn help with boiler output. The bulk density of the “Coalgae®” is lower compared to coal. Therefore, higher volumes of “Coalgae®” will need to be combusted to achieve the same boiler output compared to coal.

The “Coalgae®” pyro 450 has a similar combustion rate, but the longer ignition time could prevent the stoker speed to be increased sufficiently to achieve full boiler output compared to coal.

The higher combustion temperature of the 10 % “Coalgae®”, Figure 4.19, relative to coal could cause fouling and clinkering, though this depends on the ash fusion temperatures.

Coalgae® and Coalgae® pyro 450 appear to burn much “cleaner” emitting less smoke than coal. A second set of tests is suggested which will include detailed flue gas analyses to compare with a typical coal analysis. It is recommended that a full-scale test on a boiler be done to determine the required ignition time, stoker speed, boiler output and possible clinker formation or fouling. Also, the mechanical handling of the fuel and the effect a coal screw has on the pellets will be observed at the same time.

4.3.4 Combustion kinetics of composites

Using the procedure stated in the experimental details, section 2.5.8 for kinetic modelling Figure 4.21 represents an overlay of the Coats and Redfern model for all the “Coalgae®” sample and the coal between the ignition and burn-out temperatures.

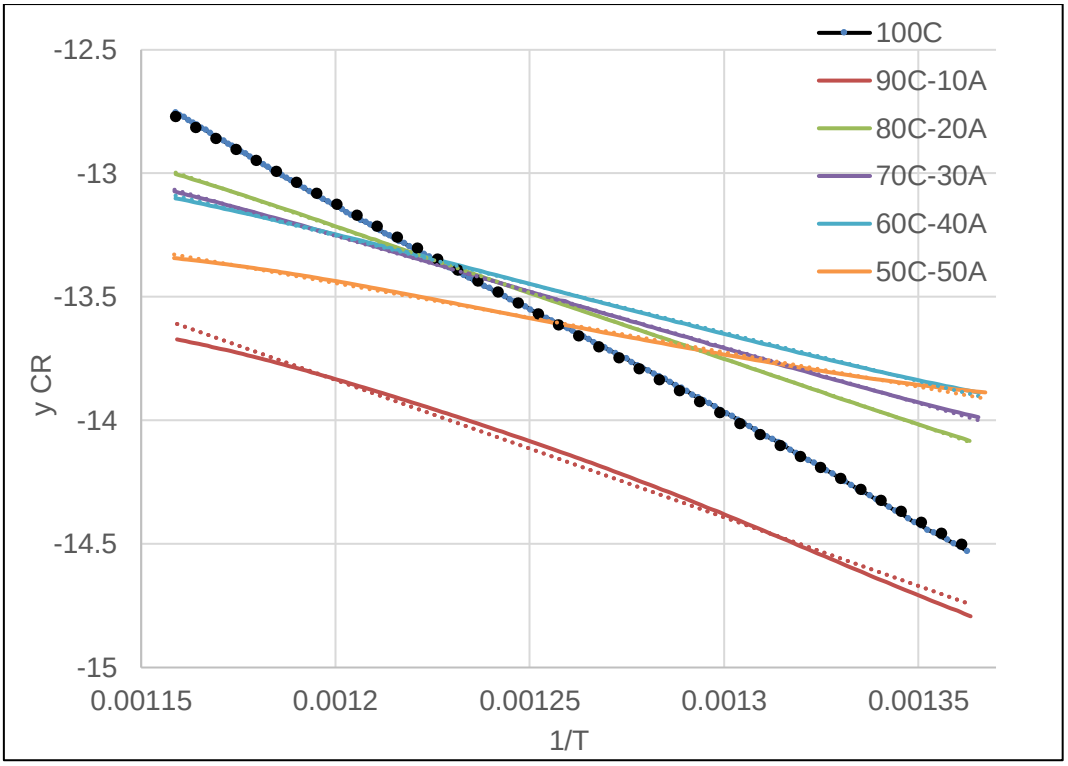

Figure 4.21: Overlay of Coats and Redferns model for composites and coal

The Coats and Redfern model, (Figure 4.21) demonstrates that the combustion kinetics of samples of "Coalgae®" are different from one another as well as from the combustion kinetics of the reference coal. About 99 % of the observed difference in kinetics between ignition and burn out temperatures was explained by each of the linear models. The difference in kinetic model agreed with the overlaid combustion process, (Figure 4.17). The Coats and Redfern explanation of the combustion kinetics of this coal and "Coalgae®" is summarised in, (Table 4.6) below.

Table 4.10: Result of Coats and Redfern model from Tig to T max

Model y_{CR} =	**100C**	**90C-10A**	**80C-20A**	**70C-30A**	**60C-40A**	**50C-50A**
mx	-8557.9x	-5556.7x	-5337.5x	-4510.1x	-3926.4x	-2793.9x
+c	-2.852	-7.168	-6.811	-7.840	-8.540	-10.092
R^2	0.9997	0.9934	1.0000	0.9999	0.9996	0.9979

y_{CR} = Coats and Redfern's model, m = gradient, x = Algae, c = intercept, R_2 = correlation squared

According to Coats and Redfern, (Figure 4.21) the model, (Table 4.10) for 20 % "Coalgae®" provided the most appropriate kinetic description with correlation, R^2 = 1.0000. This information can be related to literature report that successful co-firing requires up to 20 % biomass (13). If at 20 %, co-firing starts to increases boiler efficiency, reduces CO_2, NO_x, SO_x, waste, and fuel cost (13), then the above description, R = 1.000 advised at least 20 % "Coalgae®".

4.4 Coats and Redfern model – 100 % coal versus 10% Coalgae®

The graph below, (Figure 4.22) deduced from section 4. 3.2, shows the kinetic plot for 100 % coal compared to 10 % Coalgae®" only.

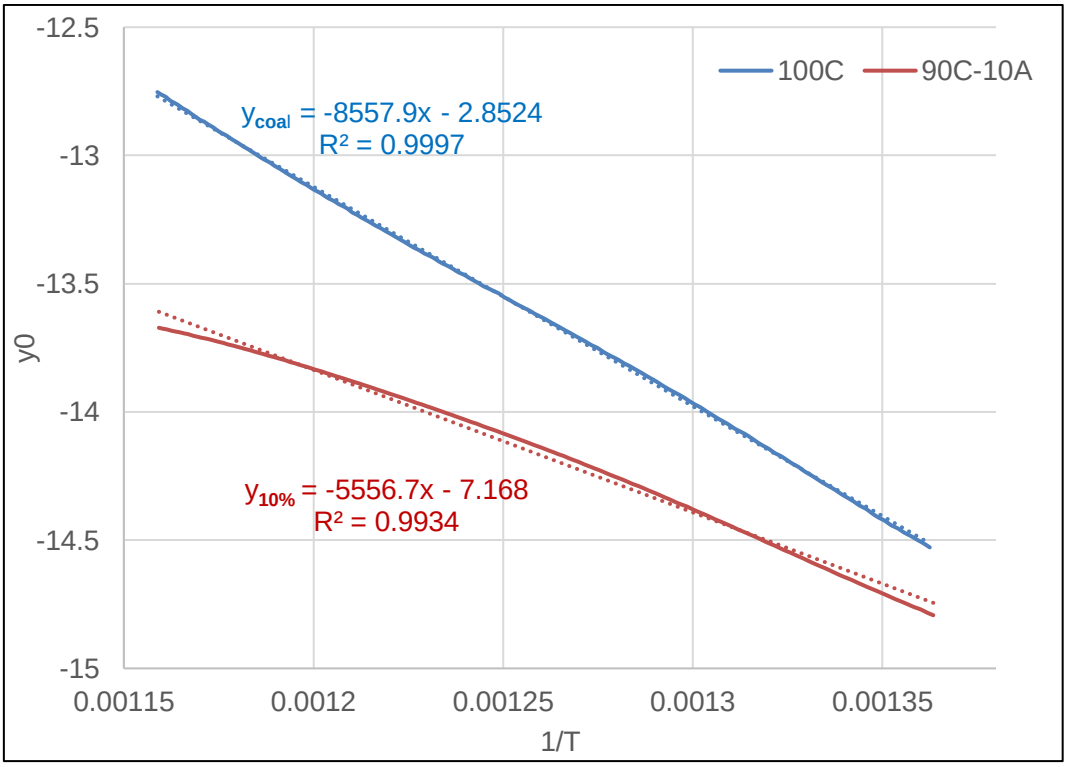

Figure 4.22: Coats and Redfern model for coal and 10 % composites

This model, (Figure 4.22) shows that there is a considerable difference between the combustion kinetics of coal and coal-microalgae blend. Adding 10 % microalgae biomass to coal has a significant kinetic effect indicated by a shift in gradient from 8557.9 to 5556.7, (R^2 = 0.9934) on the combustion of coal. The Coats and Redfern's model may not produce a linear relationship for composites with increase in

microalgae biomass content above 10 %. For this reason, the reaction order for "Coalgae®" samples with more than 10 % microalgae biomass is << n for coal, 1.03 ±0.02, and n for 10 %, 1.26 ±0.07, Table 4.7. Therefore, the reaction mechanisms of all composites with more than 10 % microalgae biomass would be different from the kinetics of 0 % and 10 % (see section 4.6). It corresponds with the literature report stating that addition of biomass to coal changes the oxidation mechanisms (156).

The 10 % microalgae biomass shifted the gradient for coal from 8557.9 to 5556.7, and 99 % of the kinetic effect was described by the model, (R^2 = 0.9934).

4.5 Kinetic parameters for coal and composites

From the calculation described in section 2.4.6 and 2.5.8 of the experimental details, the kinetic parameters were used to obtain the reaction order n, and activation energy E_a, indicated, (Table 4.11) for coal and composites samples using the Coats and Redfern kinetic model.

The model proved that the combustion of coal and 10 % composite has closely related mechanisms with reaction order n ~ 1. The appropriate mechanism for other composites, 20 – 50 % was deduced with oxidation models for solid states reaction.

Table 4.11: The kinetic parameters for Coal and Composites

(Non- de-convoluted combustion process)

Parameters	100C-00A (±)		90C-10A (±)		80C-20A (±)		70C-30A (±)		60C-40A (±)		50C-50A (±)	
E a	72.2	5.6	57.5	11.7	44.4	0.8	37.5	1.8	29.9	1.7	23.2	1.6
m	8681.66	671.28	8774.33	1412.32	5105.66	100.79	4227.16	220.17	3601.50	202.31	2309.5	189.59
T_{ig}	694.80	5.1	684.30	6.7	661.40	1.3	647.1	1.3	634.20	5.4	625.1	2.5
T_{h}	918.33	4.28	906.67	2.71	893.33	10.84	900.00	0.00	890.00	0.00	890.00	0.00
T_{max}	799.70	4.3	800.2	3.0	793.80	3.1	795.9	2.8	790.7	2.8	802.9	3.4
DTG_{max}	0.0037	0.0002	0.0035	0.0001	0.0035	0.0002	0.0033	0.0001	0.0033	0.0001	0.0032	0.0001
DTG_{mean}	0.00096	6.77E-06	0.00097	4.1E-05	0.00099	2.31E-05	0.0009	7.67E-06	0.00102	2.63E-05	0.00106	2.47E-05
$\Delta t_{1/2}$	146	8.22	149	7.89	155	8.5	174	14.69	174	8.82	179	6.67
S	0.797	0.03	0.778	0.02	0.862	0.08	0.875	0.03	0.922	0.06	0.953	0.04
H	0.010	0.0001	0.010	0.0001	0.108	9.6E-05	0.0109	0.0001	0.0109	7.26E-05	0.011	3.66E-05
n	1.03	0.02	1.26	0.75	0.54	0.04	0.46	0.04	0.39	0.04	0.11	0.04
Ash	0.32	0.01	0.30	0.01	0.28	0.01	0.26	0.01	0.24	0.02	0.22	0.02

E a = activation energy, m= gradient, Tig = ignition temp., Th = burn-out, Tmax = maximum temp., Δt1/2 = combustion width, s = s-value, n = reaction order.

The illustration, (Table 4.11), shows the kinetics parameters which include activation energy E_a, gradient m, ignition temperature Tig, burn-out temperature Th, maximum temperature t max, DTG max and mean, width temperature $\Delta t_{½}$, comprehensive combustion index S and H-values and the reaction order n, obtained between ignition Tig and maximum combustion temperatures, Tmax at 95 % confidence interval.

The activation energy E_a decreases with corresponding increase in 10 % microalgae biomass as compared to coal. For every 10 % increase in microalgae biomass the minimum energy required to initiate combustion decreases, (Table 4.11) and (Figure 4.23). This indicates that microalgae biomass can reduce the E_a required to combust coal.

Likewise, the ignition temperature decreases with increase in microalgae biomass. The ignition temperature if likened to the flammability of liquid fuels such as gasoline meaning that for each 10 % increase in microalgae biomass, “Coalgae®” tends to be more flammable. This agreed with the reduced activation energy, (Table 4.11) as biomass increases.

The S-value is a measure of the comprehensive combustion behaviour. High value for Coalgae™ indicates superior reactivity (combustion property) compared to coal (192). There is an improvement, (Table 4.11), in combustion property as mass of microalgae was increased. The fuel properties of composites with high quantity of microalgae tend to be superior to those with low amount of the biomass.

The reaction order, n for 100 % coal *i.e.* 0 % = 1.03 ± 03, and 10 % n = 1.26 ± 0.75, but 20, 30, 40, 50, and 100 % *i.e.* microalgae has the nth order reaction mechanism that must be examined because Coats and Redfern model did not give the precise mechanism ($n<<1$), thus the oxidation mechanisms for solid states must be fitted. The model for coal was linear while microalgae biomass and “Coalgae®” as revealed by the reaction order, n was not linear. This consistent with the stages (A) and (B), (see sections 4.7.1 and 4.7.2) in composites was two separate reaction mechanisms.

The mass fraction, M/Mo represents the mass of ash residue obtained after combustion. There was a progressive decrease i.e. weight loss from 0.31 mg – 0.21 mg mass combusted for 0 – 50 % “Coalgae®” in ash as the mass of microalgae

biomass in composite increases. The observation conforms with the result of the proximate analysis, (Table 3.4).

A graphical description, (Figures 4.23 – 4.26) of the effects of microalgae biomass on combustion parameters of coal are highlighted.

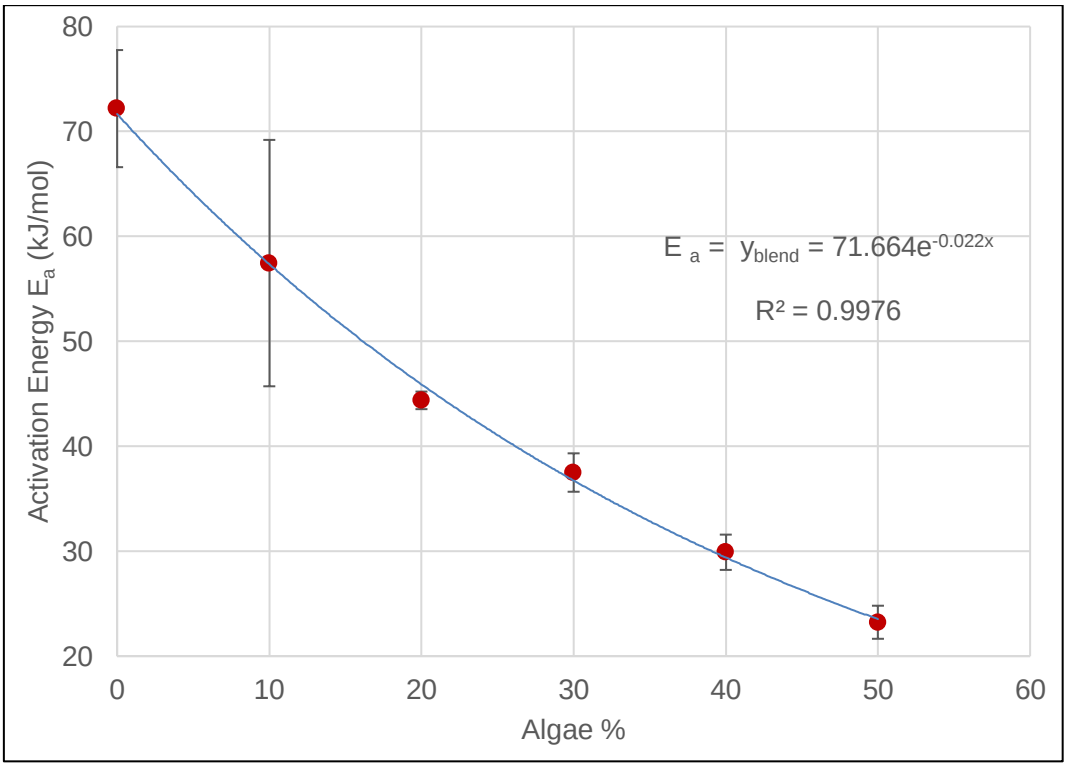

Figure 4.23: The activation energy of composites versus Algae content

From the graph, (Figure 4.23) there is convincing, ($p = 0.00036$) evidence, (Table 4.12) to show that the activation energy decreases exponentially with increasing microalgae biomass. The activation energy $E_{a.}$ decreases by an average of 0.22 kJ/mol exponents for each 10 % increase in biomass. Microalgae biomass promotes the combustion of coal as literatures report states that a reduction in activation energy is characteristic of catalytic activity of an additive (214).

The activation energy, ignition temperature and ash residue were used in regression to deduce, (Table 4.12) the statistical result below.

Table 4.12: Summary of regression statistics

Parameter	Observations	R^2	Std. error	Intercept, c	Gradient, m	P-value
E a	6	0.9689	3.5790	67.985	-0.9552	0.0003
Tig	6	0.9835	3.9703	694.460	-1.4700	0.0001
Ash	6	0.9928	0.0036	0.319	-0.0020	1.9E-05

E a = activation energy, T ig = Ignition temperature, R^2 = correlation squared, m = gradient, c = intercept, std. = standard

There is enough evidence, (Table 4.12) to show that the activation energy, (p = 0.0003), ignition temperature, (p = 0.0001) and ash (p = 1.953 E-05) decreased significantly relative to the coal as more microalgae biomass is added. A comparison of R^2 showed that microalgae biomass reduced the ash content more than it did for the ignition temperature and the activation energy and such has been reported (215).

Nevertheless, the ignition temperature, (Figure 4.24) varies with microalgae biomass in “Coalgae®” as shown graphically.

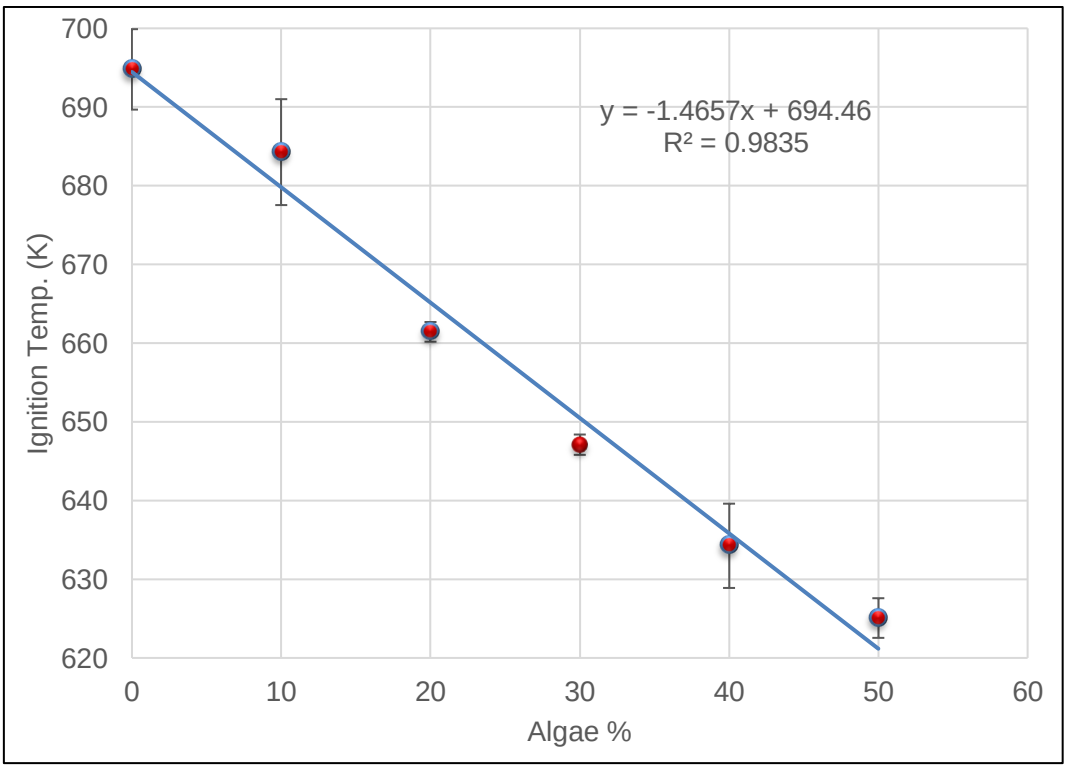

Figure 4.24: The ignition temperature of composites versus Algae content

Also, (Table 4.12 and Figure 4.24) prove that there is a strong evidence to show that ignition temperature decreased with increased microalgae biomass (p = 0.0001). The temperature decreased by an average of 14.6 K for each 10 % rise in microalgae biomass.

The average observed ignition temperature which was determined with the Coats and Redfern model is significantly higher than the predicted ignition temperature, (paired t-test, p = 0.0220). The difference between the average observed and average predicted ignition temperatures is 2.32%.

Figure 4.25 indicates the relationship between microalgae biomass and comprehensive combustion index, S-value.

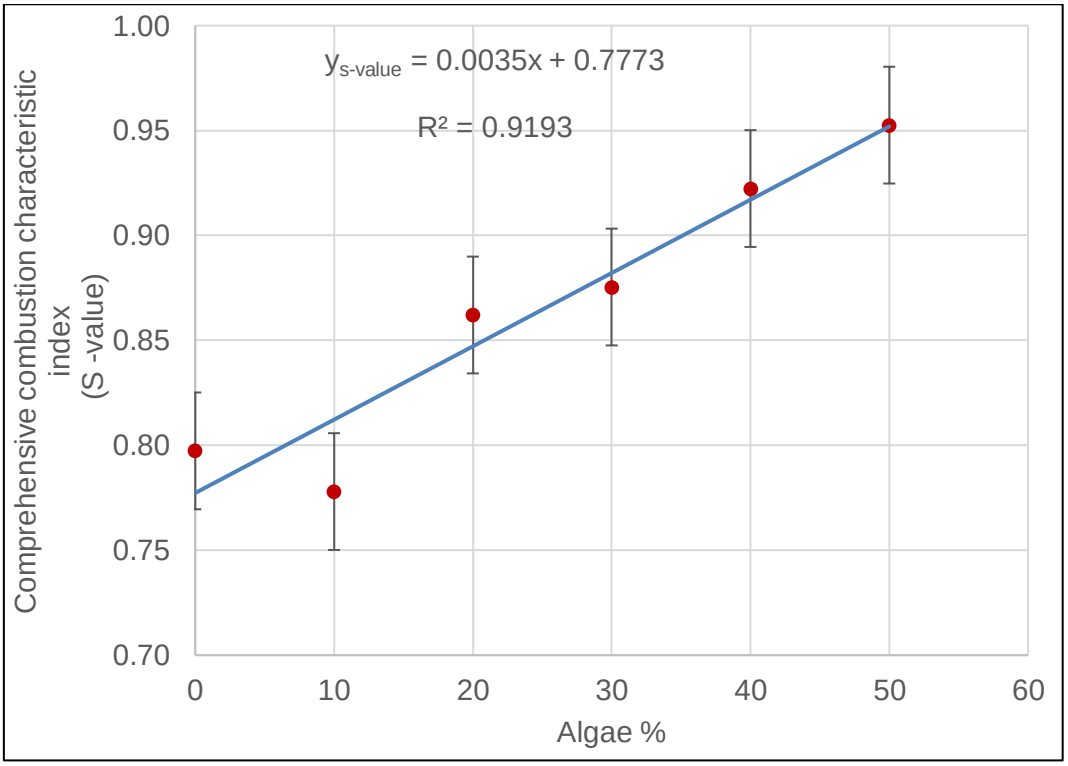

Figure 4.25: The S-value of composites versus Algae content

There is convincing evidence (p = 0.0025), to prove that the S-value increases, (Figure 4.25), with increase in microalgae biomass. At 95 % confidence interval CI, the burning

behaviour significantly improved (S = 0.035) by an average of 0.035 for each 10 % rise in microalgae biomass.

There is an increase in comprehensive combustion characteristic (s-index) which means that composites become more reactive fuel material as compared to the original coal. The increase in S- value could be attributed to the original material which is discard ultra-fine coal, as it has been report that this index increases sharply with low quality coal (216). The index increased with addition of algae which validated the variation in reaction order observed.

The large-scale combustion in a fixed-bed reactor confirmed the simulation of industrial combustion of Coalgae® in the thermogravimetric analyser. The ignition temperature of Coalgae® decreased which implies that the potential to combust becomes high. This explains an improved fuel quality which is confirmed by the reaction order.

The influence of microalgae biomass on order of the reaction, n is illustrated in, (Figure 4.26) below. Based on, (Figure 4.26) the reaction order n, of coal decreases by about 0.21 for each 10 % increase in microalgae biomass. The model explained 82.5 % of the observed differences in reaction order.

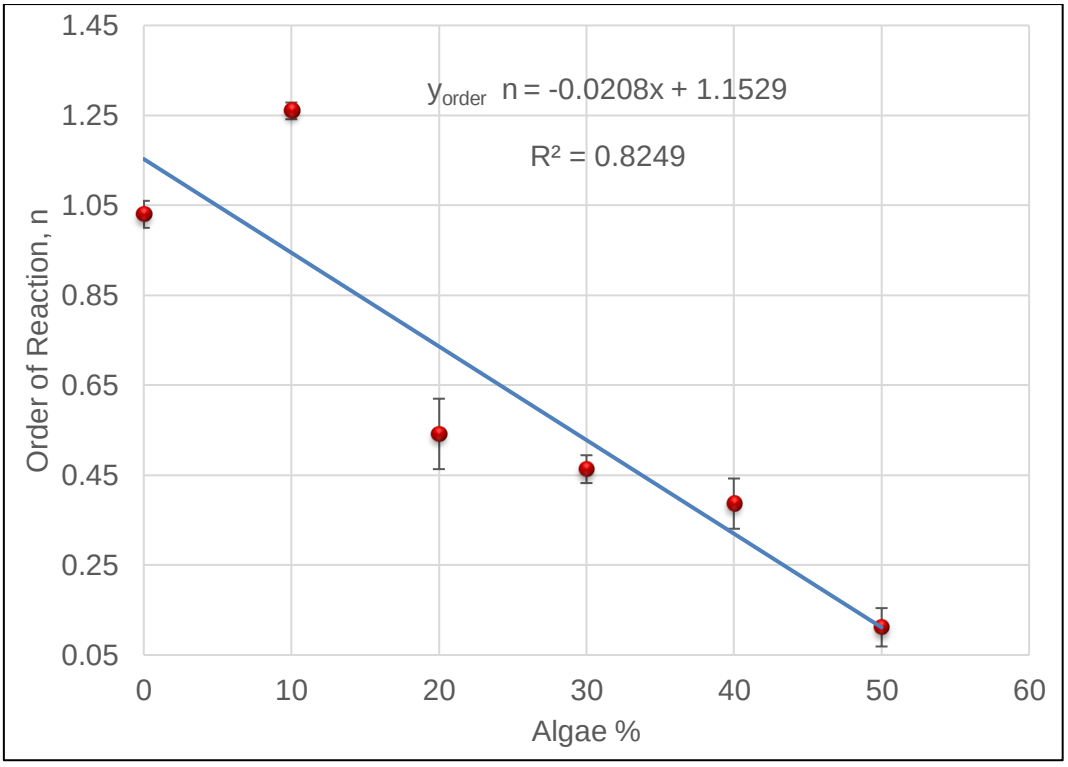

Figure 4.26: The reaction order of composite versus Algae content

As indicated in the graph, (Figure 4.26) above and from regression analyses, there is enough evidence to prove that microalgae biomass significantly decreases reaction order ($p = 0.0122$).

The relationship between the quantity of microalgae biomass in “Coalgae®” and the mass of ash is depicted below in (Figure 4.27). Similarly, the ash decreases but by about 0.02 g for every 10 % increase in microalgae biomass at 95 % confidence interval, CI. About 99.2 % of the total decrease in mass of ash residue was explained the linear model.

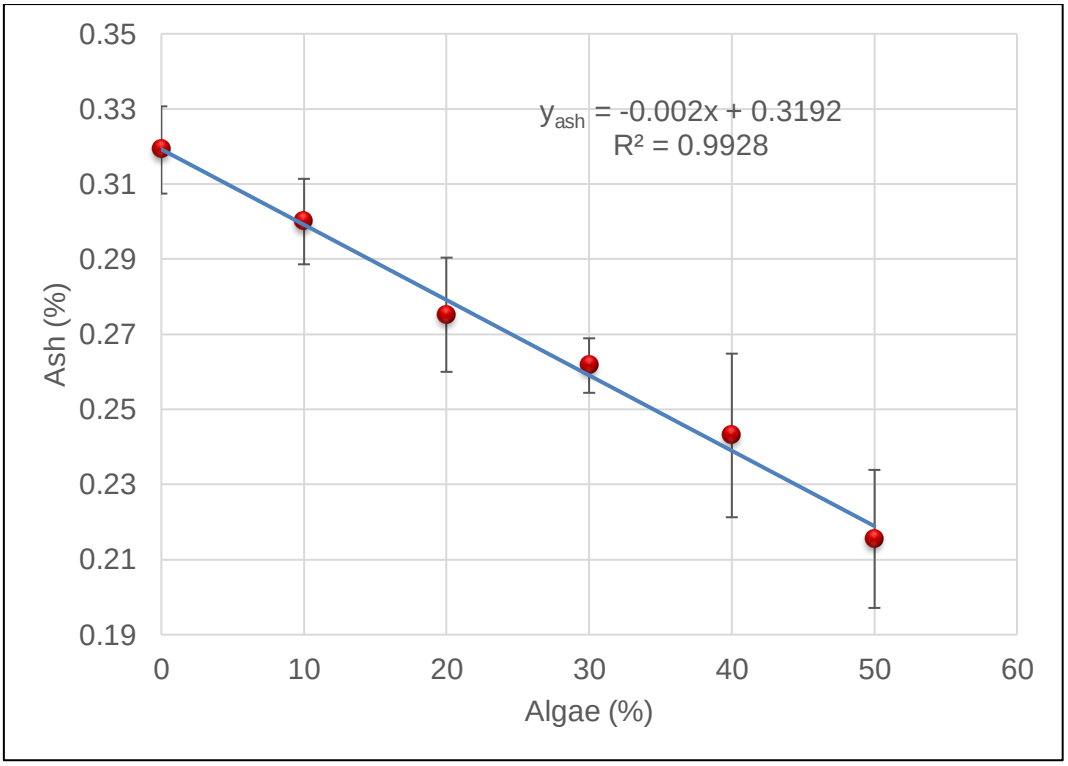

Figure 4.27: Ash residue of composites versus Algae content

From the graph, (Figure 4.27) there is a significant, (p = 1.9E-05) decrease in ash as microalgae biomass increases as expected.

The maximum combustion temperature (T_{max}) varies with microalgae biomass "Coalgae®" as shown, in (Figure 4.28).

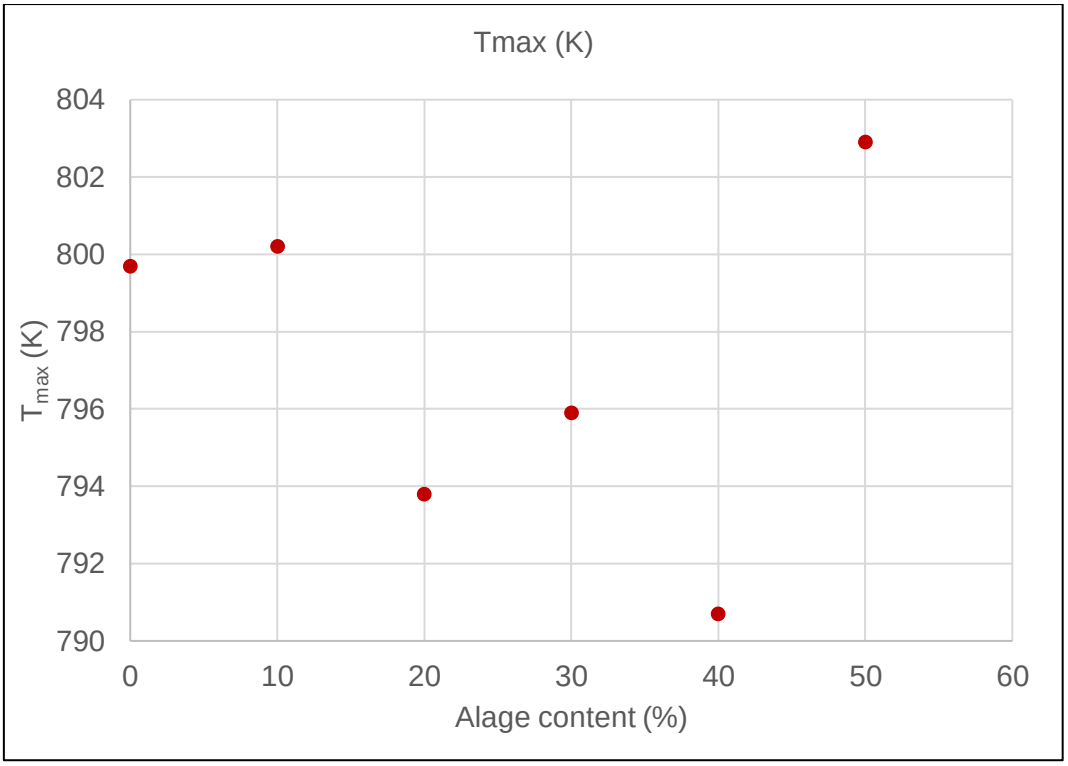

Figure 4.28: Maximum temperature of composites versus Algae content

The T_{max} tends to decrease with more microalgae biomass, however, the trend is not uniform.

On the other hand, the combustion width of “Coalgae®” and microalgae biomass are related as illustrated, in (Figure 4.29).

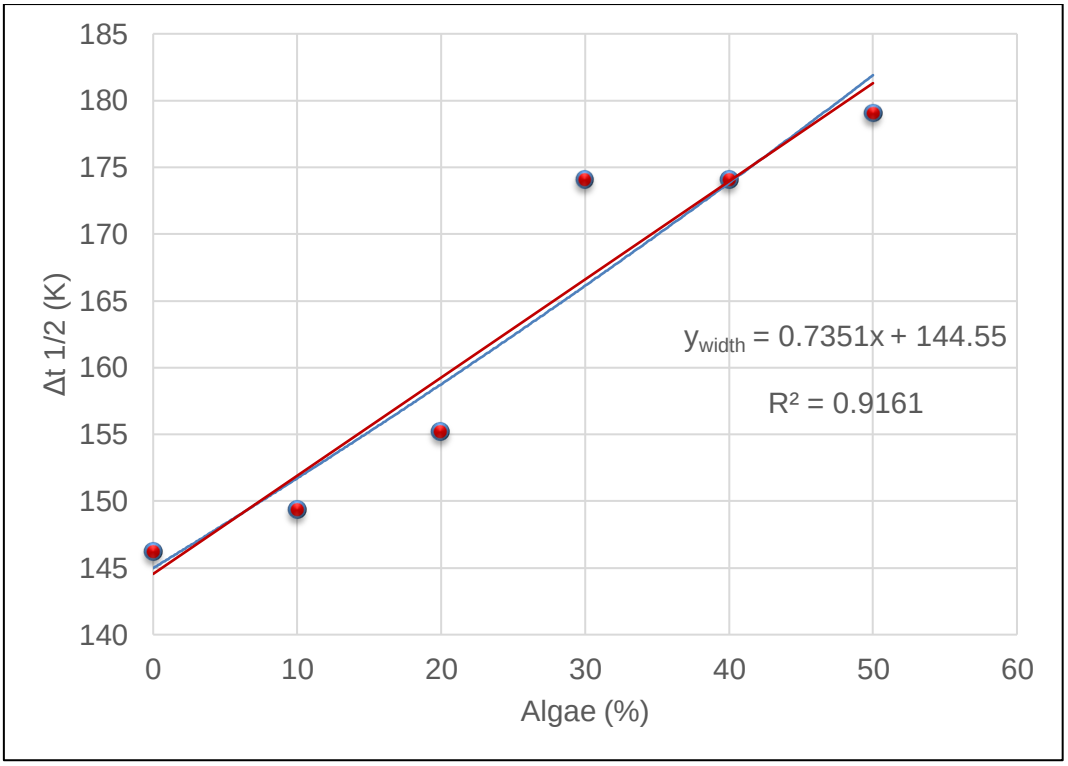

Figure 4.29: The combustion width, Δt ½ of composites versus Algae content

According to this plot, (Figure 4.29) the width shows that the extent of combustion enlarges with an increase in microalgae. About 91 % of the observed width was explained by the model. An increase of 10 % microalgae biomass enlarges combustion width as measured in terms of temperature by about ~ 7.35 K.

4.6 Deconvolution and oxidation mechanisms of composites

In section 4.1.4, 4.2.2 – 4.2.3 and 4.3.2 – 4.5, the combustion kinetics of coal, microalgae biomass and "Coalgae®" were reported as obtained from the Coats and Redfern's model by considering the entire thermal events as one. The experimental procedure in section 2.5.9 was used to deconvolute the overlapped primary reactions into devolatilization and char combustion stages.

The result, (Figures 4.30 – 4.34) of the de-convoluted combustion and the solid states oxidation mechanisms that controls each stage, and the one that controls the entire reaction for each composite are described below.

Oxidation of 0 % or 100C - R2, R3, D1, D3 and O2

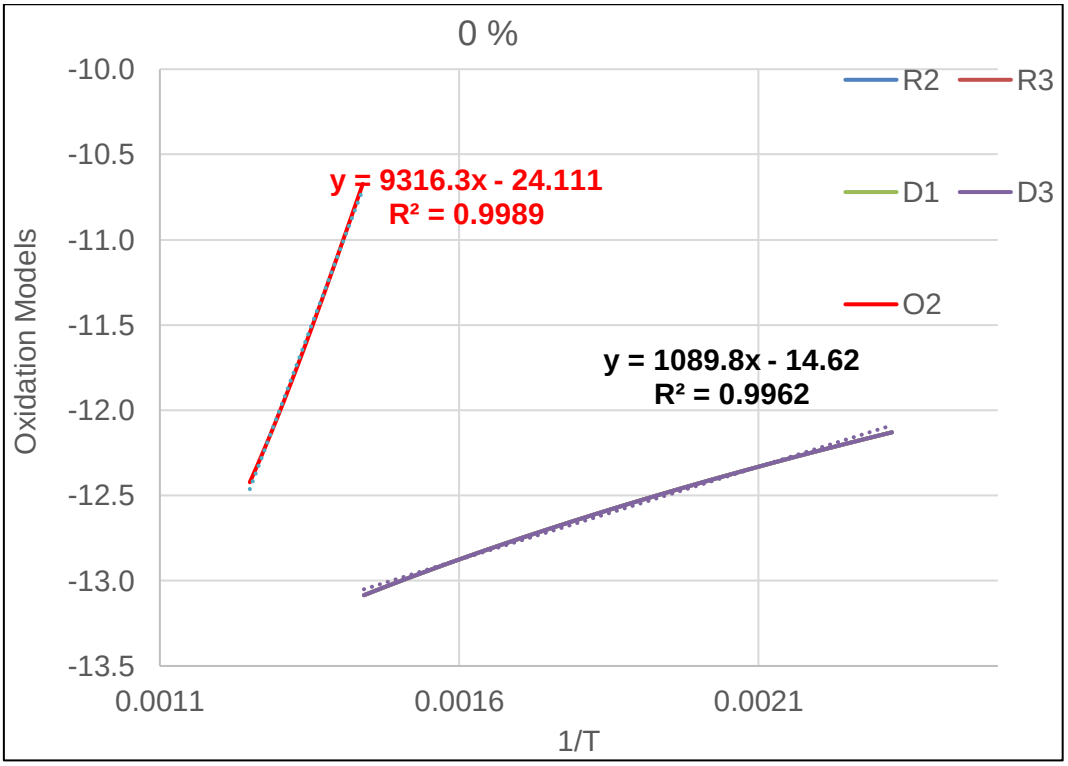

Figure 4.30: The oxidation mechanism for coal – (0 % or 100C)

The graph, (Figure 4.17), showed the solid states oxidation (combustion) models for the coal *i.e.* 0 % or 100C. The combustion of "discard ultra-fine", also referred to as coal was controlled by the second order reaction mechanism O2, contrary to first order, O1, reported for "lump coal" in the literature (156). The 2nd order model defines a reaction with its rate determined by the concentration of two reactants. The concentration of discard ultra-fine coal and its "impurities" controlled the degree of the oxidation. Stage A (de-volatilisation) was to the same extent and simultaneously controlled, (Figure 4.30 and Table 4.13) by contracting area, R2, contracting volume, R3, one-dimensional diffusion, D1 and three-dimensional diffusion, D3. But Lopez-Fonseca et al., 2006, reported that these mechanisms are assumed to govern the conversion model in the combustion of some carbonaceous materials.

The mathematical description for the second order reaction for this coal, 0 % composite is equation (4.4),

$$O2 = (1-\propto)^{-1} = [9316.3]\frac{1}{T} - 24.111 \quad \text{..... (4.4)}$$

The relationship indicated that for each degree in combustion temperature the O2 reaction order, was increased by about 9292.189 (i.e.$9316.3 - 24.111$). The model explains about 99.8 % of the observed increase in oxidation for this coal.

Oxidation of 10 % - R 3, D3, O2

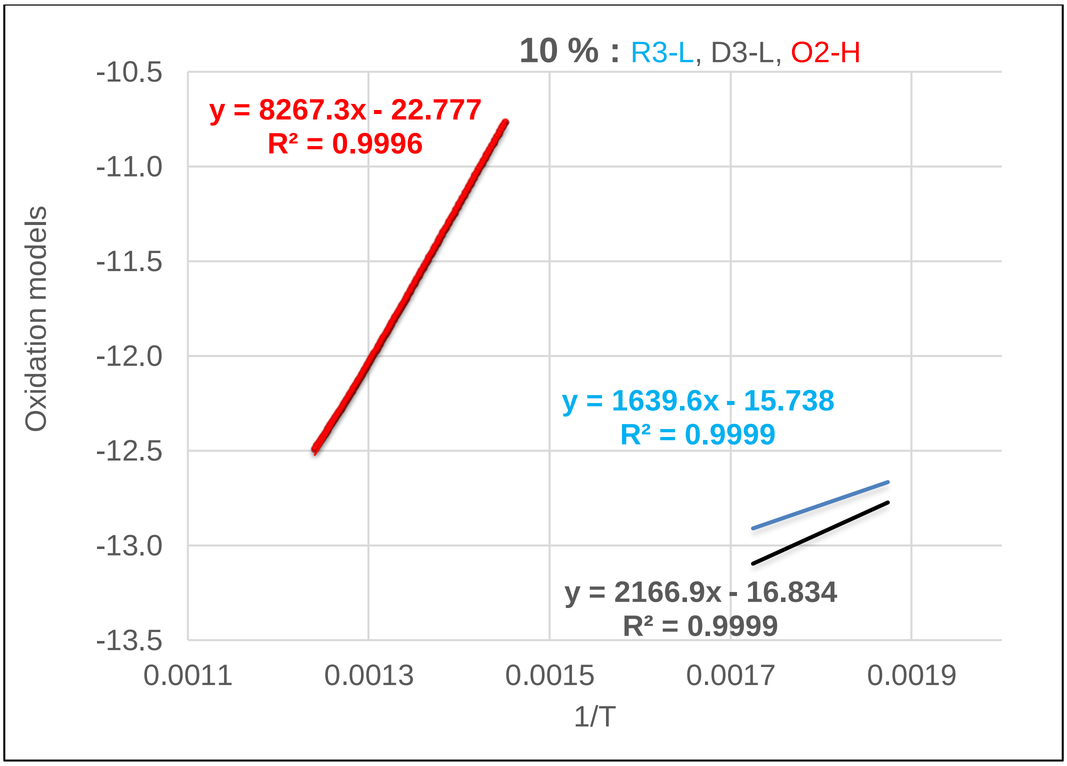

Figure 4.31: The oxidation mechanism for 10 % composite

The oxidation of the low temperature (de-volatilization) stage A, was controlled by R3 and D3. The high temperature stage B, (char) combustion was dominated by second order reaction mechanism, O2, (Figure 4.31). The R3 indicated that there were some spherical molecules, which reacted from the surface inwards during de-volatilization. About 99.9 % of the R3 reaction was described by the mathematical equation (4.5).

$$R3 = 1 - (1-\propto)^{1/3} = [1639.6]\frac{1}{T} - 15.738 \qquad (4.5)$$

For each degree of temperature, the de-volatilization involved phase movement of spherical molecules inwards at about 1623.86 times. Simultaneously, diffusion of these molecules in three dimensions took place, as mathematically described by equation (4.6).

$$D3 = [1-(1-\propto)^{1/3}]^2 = [2166.9]\frac{1}{T} - 16.834 \quad \text{..... (4.6)}$$

The model indicated that 99.99 % of the diffusion of spherical molecules took place in three dimensions at about 2150.07 times per Kelvin.

This char combustion stage B, was controlled by the second order reaction O2, described as equation (4.7).

$$O2 = (1-\propto)^{-1} = [8267.3]\frac{1}{T} - 22.777 \quad \text{..... (4.7)}$$

The second order oxidation reaction O2 took place at about 8244.52 times for each degree Kelvin. Considering the whole oxidation process, i.e. R3 (1623.86), D3 (2150.07) and O2 (8244.52), the second order reaction, O2 was the dominant mechanism. The concentration coal and microalgae determined the rate of oxidation of the entire process.

Oxidation of 20 % - O1, O2

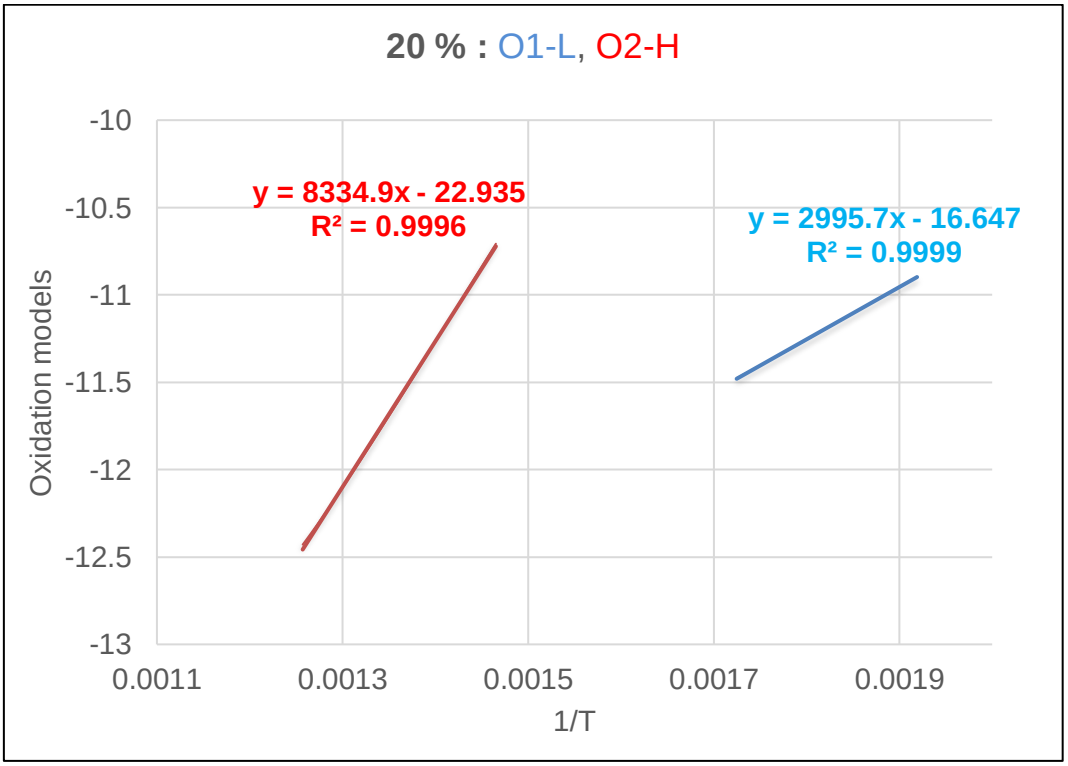

Figure 4.32: The oxidation mechanism for 20 % composite

Also, the graph (Figure 4.32), depicted the stages A and B of 20 % composite. The first order mechanism controlled the stage A while the second order dominated char

combustion stage B. The majority of the homogenous NO_x chemistry takes place in the devolatilization zone (127). From the mechanism, a reduction of NO_x would be expected relative to the coal. The mathematical description of the oxidation in this de-volatilization stage could be given by equation (4.8).

$$O1 = -\ln(1-\propto) = [2995.7]\frac{1}{T} - 16.647 \quad \text{..... 4.8}$$

From equation (4.8), this first order oxidation reaction increased with temperature and the model explained about 99.9 % of the O1 oxidation process for 20 % “Coalgae®”.

The char combustion was controlled by the second order reaction mechanism O2, and about 99.9 % of the observation was described by the model (4.9),

$$O2 = (1-\propto)^{-1} = [8334.9]\frac{1}{T} - 22.935 \quad \text{..... 4.9}$$

From the model, the entire oxidation was favoured by the O2 mechanism which implied an improvement on char combustion per Kelvin.

Oxidation of 30 % - O1, O2

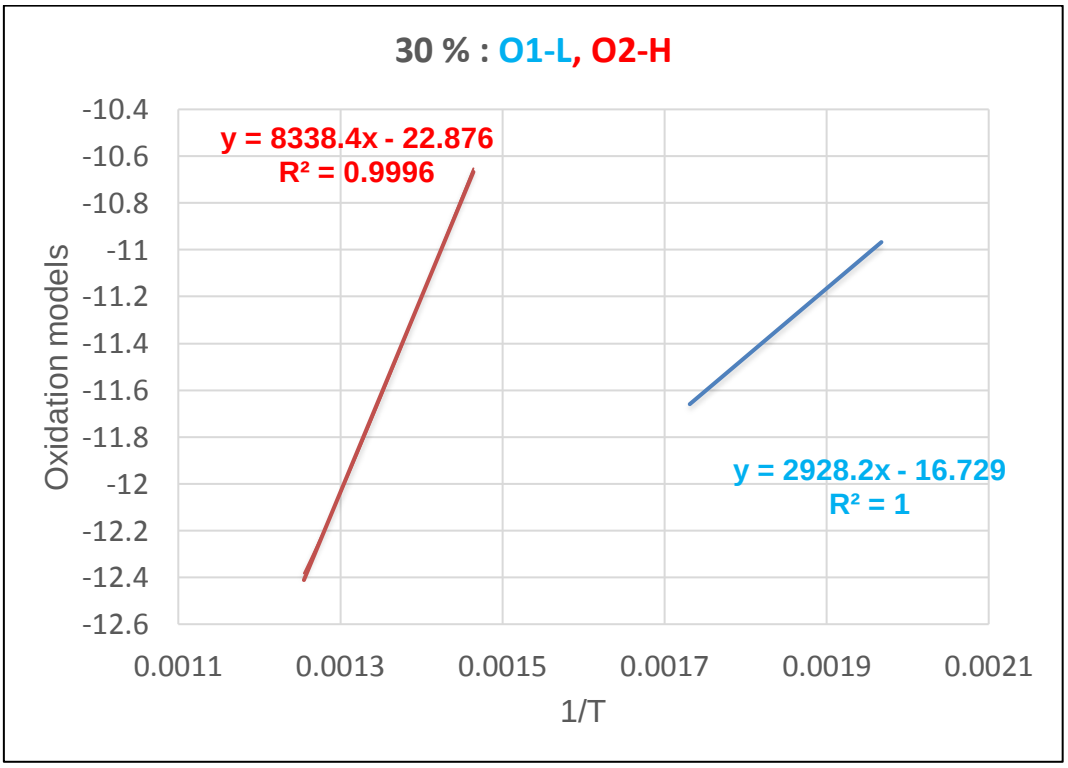

Figure 4.33: The oxidation mechanism for 30 % composites

The graph, (Figure 4.33), showed that de-volatilization of 30 % “Coalgae®” was controlled by the first order reaction mechanism O1. The char combustion was controlled by the second order reaction mechanism O2. The entire devolatilization was first order oxidation reaction (R^2 = 1). The stage A was enhanced to the degree of 2911.47, and stage B to 8315.52 per Kelvin. The entire oxidation process for 30 % was controlled by the second order reaction mechanism.

Oxidation of 40 % - O1, O2

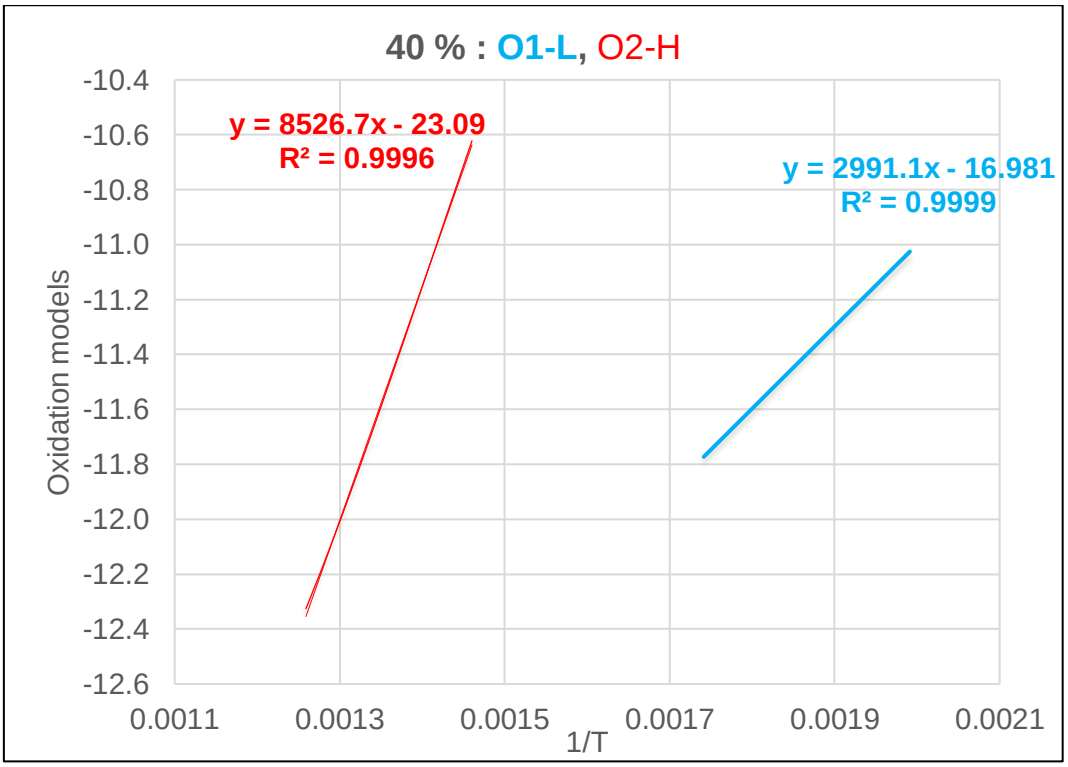

Figure 4.34: The oxidation mechanism for 40 % composite

Like 30 %, the first order reaction mechanism O1, limited the de-volatilization of the 40 % fuel, (Figure 4.34), and the char combustion stage B was controlled by the second order reaction mechanism O2. About 99.9 % of the devolatilization and char combustion was explained by the model. The second order reaction mechanism controlled the entire oxidation process of 40 % composite.

Oxidation of 50 % - O1, O2

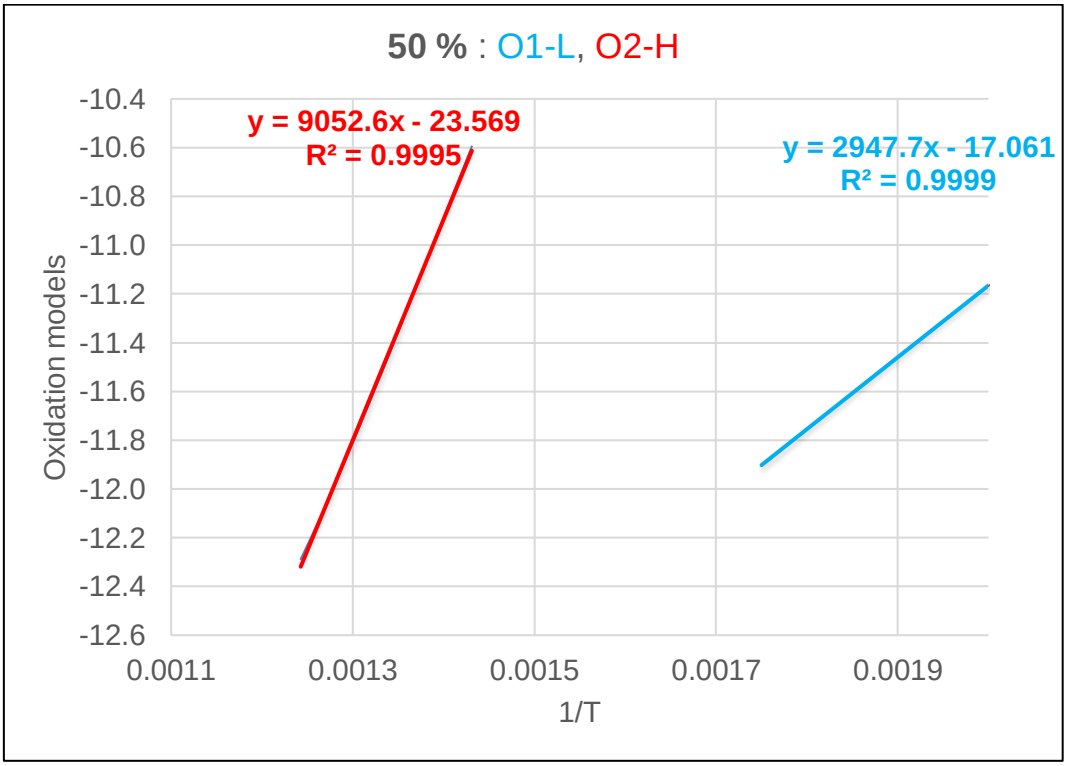

Figure 4.35: The oxidation mechanism for 50 % composite

The graph represented the oxidation mechanism for 50 % coal-50 % microalgae composite, (Figure 4.35). The first order reaction mechanism O1 controlled the low temperature, while the second order O2 controlled high temperature, and the entire oxidation process.

Oxidation of 100 % or 100A – O1, O2

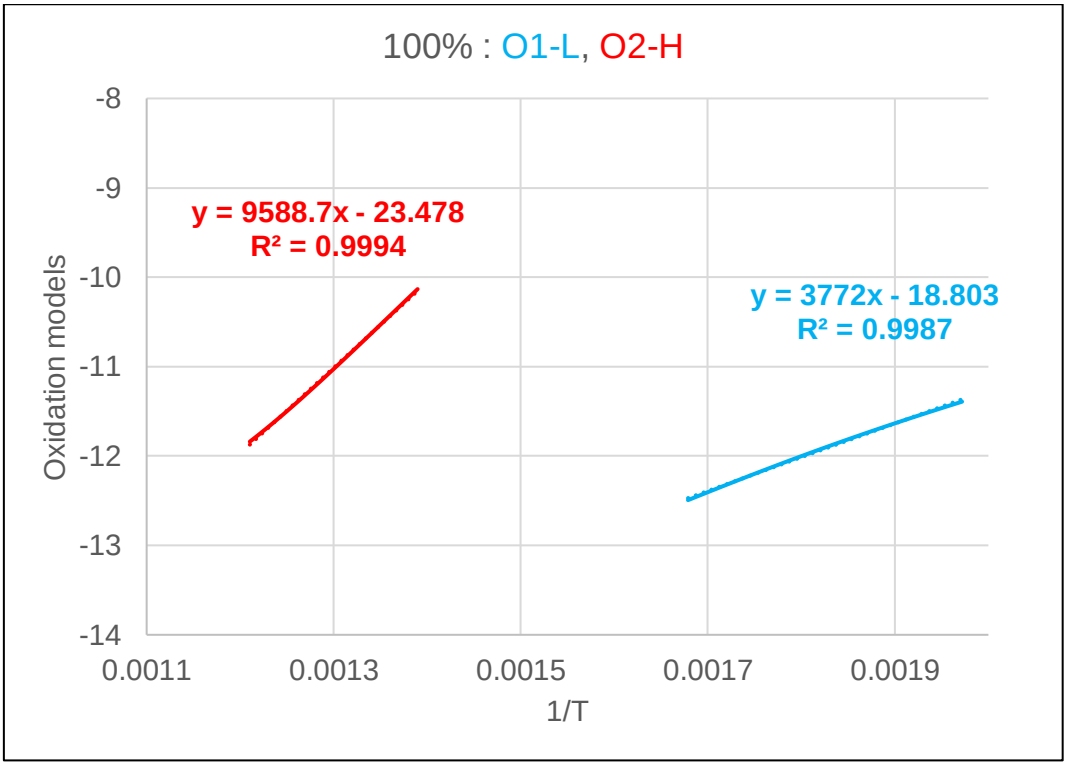

Figure 4.36: The oxidation mechanism for 100 % Algae

The combustion mechanism for the microalgae biomass was shown as above, (Figure 4.36). The first order reaction model, O1 controls the low temperature oxidation (stage A), and about 99.8 % of this observation could be explained by the model. The mathematical description for the oxidations of stage A and B were written as equations (4.10) and (4.11),

$$O1 = -\ln(1-\propto) = [3772]\frac{1}{T} - 18.803 \quad \text{..... 4.10}$$

And

$$O2 = (1-\propto)^{-1} = [9588.7]\frac{1}{T} - 23.478 \quad \text{..... 4.11}$$

The char combustion was limited by the second order reaction mechanism O2. The entire low and high temperature oxidation was determined the second order reaction

mechanism. Because, the extent of O2 reaction, 9565.22 was higher than the O1, 3753.197 per Kelvin.

In summary, microalgae influenced the oxidation mechanism of the discard ultra-fine coal, and the composites. Originally, the coal has no significant devolatilization stage as per the deconvolution. The char combustion of the coal was controlled by the second order reaction mechanism. Microalgae biomass initiated a first order reaction mechanism characterised by the low temperature oxidation and improved the char combustion.

4.7.1 Activation energy of low temperature combustion stage (A)

Using the mathematical procedure in sections 2.5.9 – 2.5.10 of the experimental section, the combustion parameters calculated for each de-convoluted overlapped stages A and B are explained and summarised in this section.

This includes ignition temperature Tig, peak combustion temperatures T p, fuel conversion at peak $\propto_{\mathrm{p}}$, rate of combustion at peak $\left(\frac{\mathrm{d}\propto}{\mathrm{dt}}\right)_{\mathrm{p}}$, reaction mechanism, activation energy E a and frequency factor A.

The stage (A), (Tables 4.13) is the low temperature event **L,** i.e. de-volatilization zone. While stage (B), (Table 4.14) shows the high temperature event **H,** i.e. char combustion.

Table 4.13: Reaction mechanism for combustion stage A of coal, microalgae, and blends

De-convoluted stage A (De-volatilization) = α1										
Composites (Fuels)	**Algae (%)**	**Ignition temp. Tig (K)**	**Temp. at peak T p (K)**	**Conversion at peak α p (mg)**	**Rate at peak d α/dT(p) (mg/K)**	**Reaction Mechanism**	**Corr. sq. R^2**	**Slope m**	**Activation E a (kJ/mol)**	**Frequency Factor c**
Coal	**0**	-	430.47	1.0000	0.0000	**R2, R3, D1, D3**	0.9962	1089.8	**9.06**	**- 14.62**
Algae	**100**	507.15	595.66	0.7358	0.0030	**O1**	0.9987	3772.0	**31.36**	**- 18.80**
90C-10A	**10**	533.49	579.77	0.9954	1.0E-04	**R3**	0.9999	1639.6	**13.63**	**- 15.74**
						D3	0.9999	2166.9	**18.02**	**- 16.83**
80C-20A	**20**	520.57	579.82	0.9695	0.0005	**O1**	0.9999	2995.7	**24.91**	**- 16.65**
70C-30A	**30**	508.63	577.66	0.9441	0.0008	**O1**	1.0000	2928.2	**24.35**	**- 16.73**
60C-40A	**40**	501.70	574.28	0.9213	0.0011	**O1**	0.9999	2991.1	**24.87**	**- 16.98**
50C-50A	**50**	490.19	571.39	0.8897	0.0014	**O1**	0.9999	2947.7	**24.51**	**- 17.06**

The result, Table 4.13, showed the low temperature scheme, stage A oxidation characteristics for coal, microalgae biomass and their blends. There are several chemical reactions, micro-structural changes in the stage A of coal and instantaneous movement as well as transport *i.e.* D1 and D3 of gas molecules through diffusion (156). Also, there are circular disc molecules *i.e.* R2 reacting from the edge inward, and spherical molecules *i.e.* R3 reacting from the surface inward (156). There are movement of an interface at constant velocity which results in the surface of each particle being covered with a layer of the product. The R2 and D3 in10 % sample showed that this blend and coal had close combustion properties. While the O1 in 20 – 50 % blends and microalgae biomass indicates that the rate determining step was the suggested chemical interaction (156).

The ignition temperature T_{ig} showed gradual decrease, (Figure 4.24) with an increase in the quantity of microalgae biomass which agrees well with T_{ig}. The peak combustion temperatures of 10 – 30 % are however similar. In this range, maximum temperature ~ 579.77 – 577.66 K of "Coalgae®" char was achieved.

As more microalgae biomass is loaded, fuel conversion at the peak of combustion temperature, (Table 4.13) increases *i.e*. decrease in mass down the column. The fuel consumption increased from 0.73 mg – 1.00 mg of mass combusted for 0 – 100 % "Coalgae®". Apart from 10 % which we considered characteristically a "transient" material of coal and "Coalgae®", the activation energy for 20 – 50 % in stage A are similar and exists in the range of 24.35 – 24.91 kJ/mol. The decrease in E_a, (Table 3. 16, section 3.5), was due to the reactive microalgae biomass. The de-volatilised molecules from 20 – 50 % have the same combustion properties. The properties are different from volatiles molecules observed for coal and microalgae biomass. This is true as the range, 20 – 50 % is controlled by first order mechanism, O1 which is different from R3 and D3 observed for 10 %. Furthermore, 10 – 50 % composites have the same collision frequency ~ 17. This implies that collision and vibration of molecules for this range is the same. Hence, there is the probability that degree of de-volatilization reaction in "Coalgae®" is different relative to coal with collision frequency of ~ 14.61 and microalgae biomass of ~ 18.80. The de-volatilization reaction in stage (A) is in the order of microalgae biomass > "Coalgae®" > coal.

4.7.2 Activation energy of high temperature combustion stage (B)

The oxidation parameters and activation energy of the high temperature scheme, stage B, (Table 4.14) shows the char combustion properties each of coal, “Coalgae®”, and microalgae biomass respectively due to interactions.

Table 4.14: Reaction mechanism for combustion stage B of coal, microalgae, and blends

De-convoluted stage B (char combustion) = α2										
Composites (Fuels)	**Algae (%)**	**Ignition temp. Tig (K)**	**Temp. at peak T p (K)**	**Conversion at peak α p (mg)**	**Rate at peak d α/dT(p) (mg/K)**	**Reaction Mechanism**	**Corr. sq. R^2**	**Slope m**	**Activation E a (kJ/Mol.)**	**Frequency Factor c**
Coal	**0**	694.85	799.83	0.6119	0.0037	**O2**	0.9989	9316.3	**77.46**	**- 24.11**
Algae	**100**	719.85	826.23	0.7971	0.0019	**O2**	0.9994	9588.7	**79.72**	**- 23.48**
90C-10A	**10**	689.10	806.22	0.5890	0.0035	**O2**	0.9996	8267.3	**68.73**	**- 22.78**
80C-20A	**20**	682.22	795.51	0.6050	0.0035	**O2**	0.9996	8334.9	**69.30**	**- 22.94**
70C-30A	**30**	683.08	796.82	0.6241	0.0033	**O2**	0.9996	8338.4	**69.33**	**- 22.88**
60C-40A	**40**	684.32	794.24	0.6428	0.0032	**O2**	0.9996	8526.7	**70.89**	**- 23.09**
50C-50A	**50**	698.32	804.71	0.6648	0.0032	**O2**	0.9995	9052.6	**75.26**	**- 23.57**

`

The high temperature combustion zone, (Table 4.14) shows the complete combustion of the char. Char is composed of mainly carbon molecules. This can be seen from the similarity in the ignition of coal char ~ 694.85 K as compared to microalgae biomass char ~ 698.32 K.

The ignition temperatures, (Table 4.14) of 10 – 50 % "Coalgae®" are approximately the same (~ 685 K). The temperature is different relative to coal and microalgae biomass. It indicated that this coal and "Coalgae®" had different combustion behaviour. The peak temperature for the (char) combustion stage depicted another similarity for 20 – 40 % with an average value of ~ 795 K. This temperature is smaller as compared to that for coal ~ 800 K, but it has significant impact on the combustion behaviour. It also indicated a different material behaviour, though10 % and 50 % have peak temperatures of ~ 806 K which is higher compared to coal due to the transient nature of these two blends.

However, the conversion (consumption) of char at peak combustion showed significant increase between 10 - 50 % "Coalgae®", i.e. from 0.58 mg – 0.66 mg. This explains the variation in rate of combustion of "Coalgae®" compared to coal. The rate of combustion of "Coalgae®" char differs from coal char, but the char combustion for coal, "Coalgae®", and microalgae biomass is controlled by the second order O2 reaction mechanism. Thus, combusting fuel of equal density one would expect the period of combustion of char in this order, "Coalgae®" > microalgae biomass > coal.

The activation energy showed that "Coalgae®" is more reactive than the discard ultra-fine coal, but less relative to microalgae biomass. Activation energy property is specific to each material. "Coalgae®" samples with 10 – 40 % microalgae had activation energy of about ~ 68.73 – 70.89 kJ/mol. This clearly shows that the char of coal ~ 77.46 kJ/mol, microalgae biomass ~ 79.72 kJ/mol, and the char of "Coalgae®" are different. Due to microalgae biomass, "Coalgae®" required less activation energy of about ~ 68.73 – 70.89 kJ/mol compared to the coal. The combustion of more reactive component (*i.e.* microalgae) released the heat which catalysed the less reactive material (*i.e.* coal) (217), (151). The inorganics of microalgae biomass contributed to catalysing the combustion of this coal. Char contains mainly carbon, but the percent may differ from one material to the other. Thus, char from coal, "Coalgae®", and microalgae biomass have similar properties but are explicitly different, as it has been

reported in literature that biomass char belongs to the most reactive carbon material (159).

The frequency of collisions under the same condition such as time, temperature, space *etc.* are characteristic for molecules. Thus, different molecules collide within themselves at varying rate. The frequency of collision between char molecules of the coal, and char molecules of microalgae biomass are similar ~ 24.11 and 23.48. This indicates comparable char or bonds characteristics. The frequency of collision in coal and the biomass varies though slightly from that of 10 – 50 % "Coalgae®" which falls in the range ~22.78 – 23.57. Thus, if we consider the frequency of collision, the bond between molecules of char of the "Coalgae®" seems to be slightly stronger than bonds in either coal or microalgae biomass, because frequent molecular collision indicates weak bond.

4.7.3 De-convoluted versus single combustion process

The best way to estimate the combustion reactivity of a coal sample is to determine its activation energy (86). Therefore, using the result in section 4.7.1 – 4.7.2 to establish the activation energy of this coal and "Coalgae®" is a superior approach to comparing the reactivity.

The computed activation energy, (Table 4.15) of each "Coalgae®" considered as single thermal event (i.e. the Coats and Redfern's model) was compared with corresponding E_a (i.e. the Frasier-Suzuki de-convolution) of stages A and B, particularly the activation energy of each char.

Table 4.15: Activation energy – de-convoluted versus single combustion process

Process →	Single stage (Coats and Redfern's)		Original data (Non-de-convoluted) stage A	De-convolution Stage A (Low temperature scheme)		De-convolution Stage B (High temperature scheme)		Original data (non-de-convoluted) stage B
Algae (%)	**E a**	**(±)**	**E a 2Stages (Volatiles)**	**E a Stage A**	**Freq. Factor**	**E a Stage B**	**Freq. Factor**	**E a 2Stages (Char)**
0	***72.2***	***5.6***	**-**	**0**	**0.00**	**77.46**	**- 24.11**	**69.58**
10	*57.5*	*11.7*	**-**	18.02	- 16.83	68.73	- 22.78	52.85
20	*44.4*	*0.8*	6.26	24.91	- 16.65	69.30	- 22.94	55.00
30	*37.5*	*1.8*	6.11	24.35	- 16.73	69.33	- 22.88	48.02
40	*29.9*	*1.7*	5.46	24.87	- 16.98	70.89	- 23.09	43.82
50	*23.2*	*1.6*	5.31	24.51	- 17.06	75.26	- 23.57	38.52
100	-	-	**-**	**31.36**	**- 18.80**	**79.72**	**- 23.48**	**-**

The activation energy, $E_{a.}$, (Table 4.15) shows the result obtained using three different approaches to this present combustion kinetics modelling. The first $E_{a.}$ was obtained using Coats and Redfern's method. The second and last $E_{a.}$ was deduced by using ignition T_{ig} and maximum combustion temperature T_h as it is in the original TG data (construction). The third that is stage A and B activation energy E a is the result from the de-convoluted combustion process.

From the Coats and Redfern's model computation, activation energy decreases for each 10 % increase in biomass. The activation energy obtained by construction i.e. reading the ignition and maximum temperature from original data showed that the de-volatilization $E_{a.,}$ lies between 5 – 6 kJ/mol. While the $E_{a.}$ for char combustion is between 38.52 – 52.85 kJ/mol which is less as compared to the coal char 69.58 kJ/mol, which has no microalgae biomass and devolatilization stage A. However, the deconvolution method indicated that activation energy of "Coalgae®" for stage A is between 24.35 – 24.91 kJ/mol except for 10 % with 18.02 kJ/Mol. For char combustion, stage B the activation energy lies between the values of 68.73 – 75.26 kJ/mol which is less as compared with coal char, 77.46 kJ/mol.

This range of activation energy, (Table 4.16), 68.73 – 75.26 kJ/mol in the present research was compared with the values reported in literature.

Table 4.16: The activation energy in literature versus present research

Activation energy Ea. for coal, biomass, and char - kJ/mol					
Materials	**Coal De-volatile**	**Char $_c$**	**Biomass**	**Char $_b$**	**Reference**
Dumped coal fines	~ 0.00	69.58 – 77.46	-	-	Present
Microalgae biomass	-	-	31.36	79.72	Present
Coalgae® fuel	24.35 -24.91	68.73 – 75.26			Present
Cellulose	-	-	48.1 - 282	-	(218)
Hemicellulose	-	-	42.6 - 154	-	(218)
Lignin	-	-	18.1-79.4	-	
Coal - consistent measurements	-	70 - 80	-		(213) (219)
High Vale coal	-	73 ± 0.9	-	-	(213)
Eastern bituminous coal	-	63.8 ± 0.7			(213)
Char	-	105 - 180	-	-	(220)
Char	-	120 - 140	-	-	(221)
Char	144	71.5	-	-	(222)
Chlorella Vulgaris			71	126	(185), (106)
Chlorella Vulgaris	-	-	80.9	135.27	(99) (223) (224)
Scenedesmus almeriensis	-	-	71.3	178.9	
Nannochloropsis gaditana	-		62.9	157.8	
Hard coal	-	115.4	-	-	(159)
Forest residue	-	-	-	130	
Cotton residue	-	-	-	149.9	
Wood	-	145.3	-	-	
Biomass char	-	-	-	114 - 230	(225)

The Table 4.16 shows the comparison of activation energy for coal, biomass, and “Coalgae®”. Activation energy of biomass is due to volatile oxidation while that of coal is due to char oxidation (meaning that oxidation of volatile controls combustion of biomass while oxidation of char controls coal combustion(113). The activation energy obtained using the Frasier-Suzuki deconvolution for microalgae is similar to literature report (106), (148), (224). For coal char it lies in the range reported for coal with consistent measurement (70 – 80), high Vale coal (73 ± 0.9) and char (71.5). The activation energy for “Coalgae®” is less as compared to coal, but it is in the range calculated for coal and the values reported for coal in literature (136).

The slight variation in activation energy of a sample such as coal and coal-microalgae biomass composite could be attributed to heterogeneity of the material and presence of various quantity of minerals. The slight variation repeated itself on the ignition temperature of composites calculated from de-convoluted curves, (Figure 4.37), section 4.8 below for stages A and B as graphically compared.

4.8 Interpretations of kinetic parameters

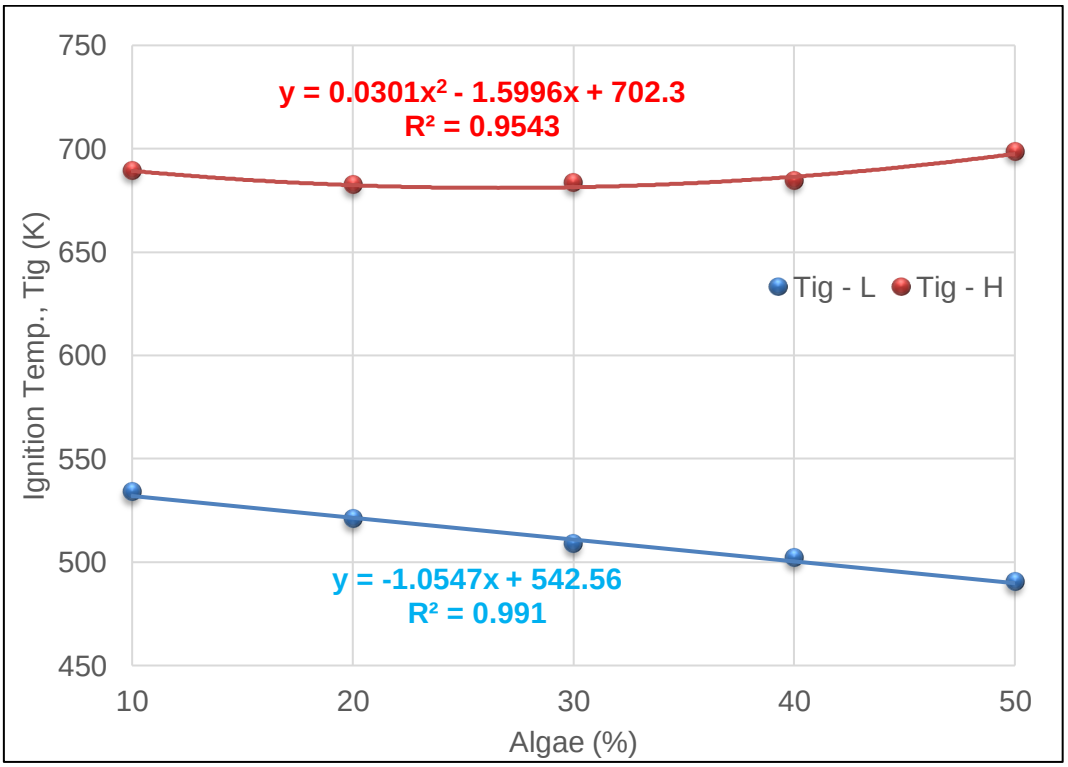

Figure 4.37: The ignition temperature for stages (A) and (B) versus algae (%)

The graph, (Figure 4.37), shows an overlay of ignition temperatures for the low and high temperature combustion stages A and B. It indicates that the Tig for the de-volatilization stage decreased with increase in microalgae which means that the biomass improves ignition (more volatile matters). For 10 – 50 %, the volatile ignition shows a linear relationship that is between 490 – 530 K and about 99 % of this observation (R^2 = 0.991) is explained by the model, while the char ignition is between 680 – 700 K and more consistent than the volatile ignition. The quadratic model represents the mathematical description of char ignition, (4.12).

$$\text{Tig} = 0.0301\text{A}^2 - 1.5996\text{A} + 702.3 \quad \ldots\ldots\ldots\ldots\ldots\ldots\ldots\ldots\ldots\ldots\ldots\ldots\ldots\ldots\ldots\ldots\ldots\ldots \quad (4.12)$$

The small variation in char ignition temperature for 10 – 50 %, (~ 20 K = -253.15 ºC) could be attributed to the biomass and experimental error.

The content of the volatile matter (usually a mixture of low range hydrocarbons and oxygenated compounds) in the fuel/blends will also affect the ignition temperature.

The rate of combustion at peak, (Figure 4.38) for the low temperature stage A changes with microalgae biomass as shown.

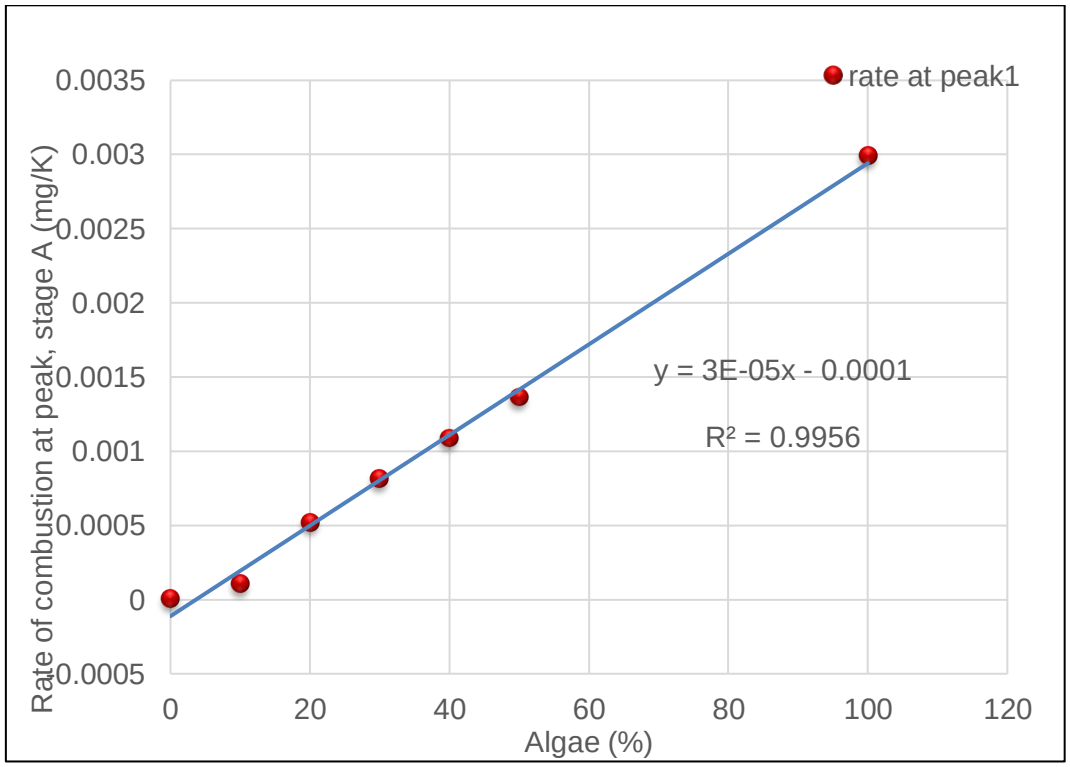

Figure 4.38: The rate of combustion at peak temperature for stage A

The graph, (Figure 4.38) describes the rate of de-volatilization for stage A for corresponding increase in microalgae biomass. Rate at peak combustion is considered as a measure of the rate of reaction. The results proved that rate of combustion reaction increases linearly, indicating substantial improvement in consumption (release of volatile matter) for each composite. The rate of combustion between 10 – 50 % lies in the small range of 9.99E-05 – 0.00135 mg/s or mg/K. The model explained about 99.5 % of the observed rate of devolatilization at peak temperature.

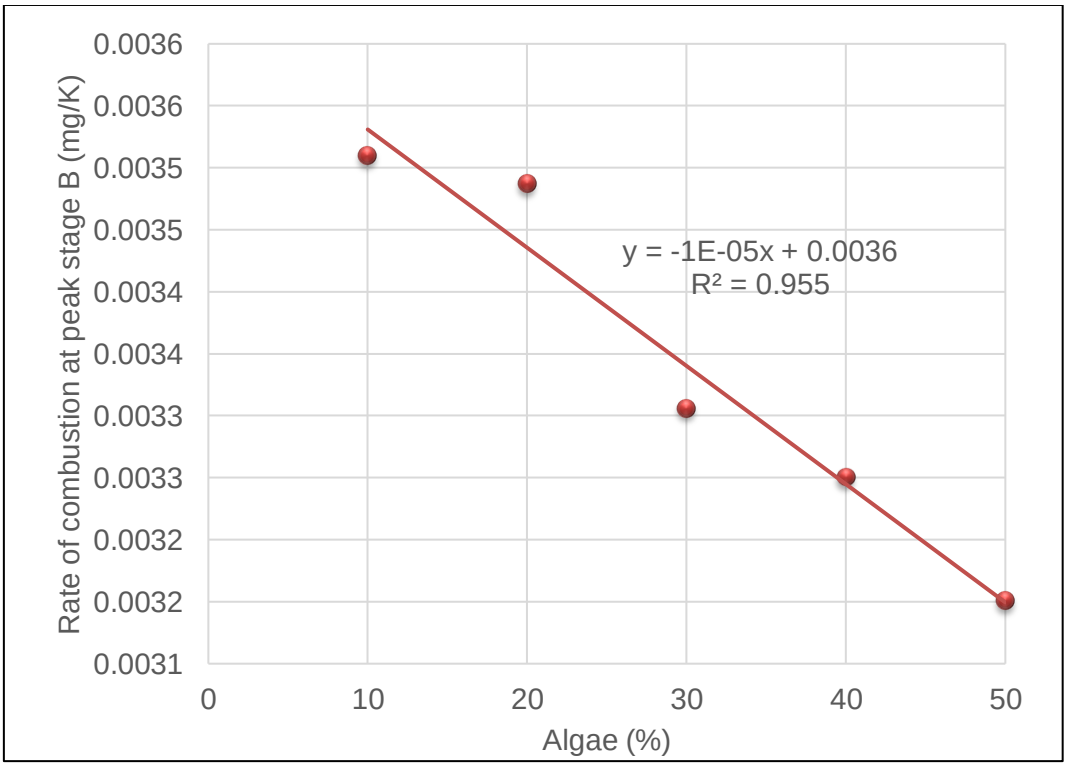

Figure 4.39: The rate of combustion at peak temperature for stage B

The graph, (Figure 4.39), shows the rate of oxidation of the char versus microalgae biomass content. There is minimal decrease in rate of combustion of char, 0.0003 mg/K i.e. (0.0035 – 0.0032) between 10 – 50 %. The more of microalgae biomass added, the lower the rate of char combustion, and 95 % of the model described this process, (Figure 4.39). The decrease in rate of combustion for char of blend was high relative to char of original coal.

In stage A, the conversion at the peak temperature decreases, (Figure 4.40) with more biomass.

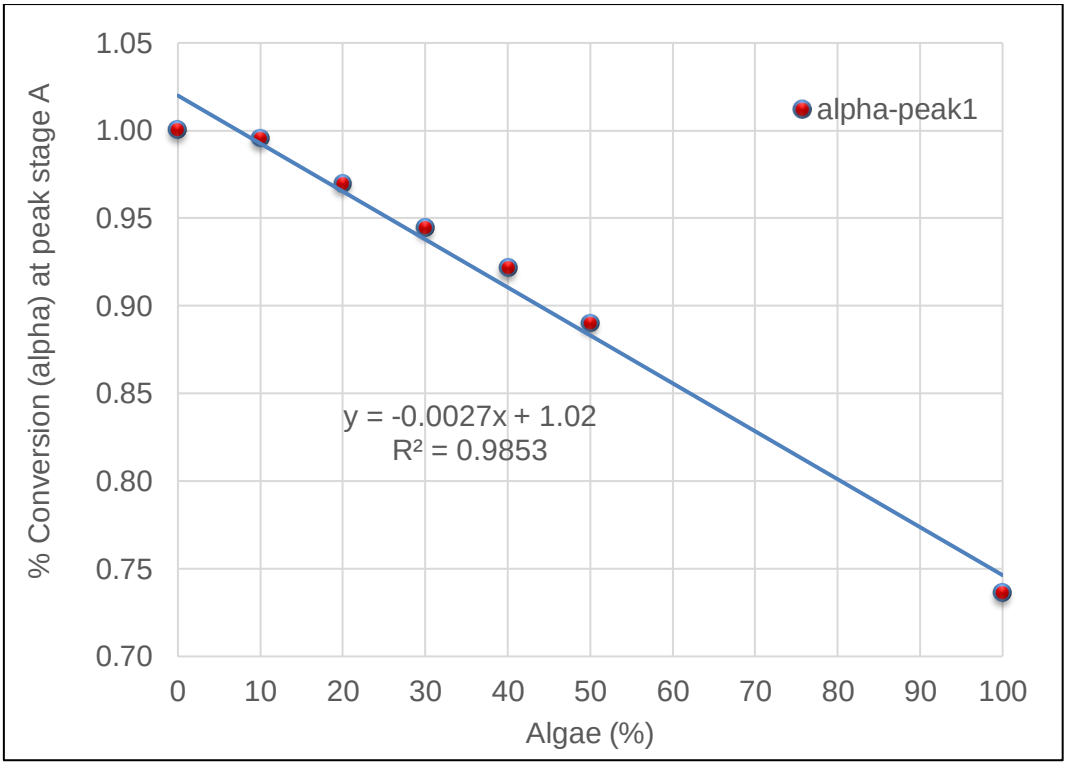

Figure 4.40: Fuel conversion (∝) at peak temperature for stage A

The fuel conversion (consumption) ∝ versus microalgae biomass is highlighted, (Figure 4.40) the graph above. It shows that the quantity of material consumed is increased as compared to the original, i. e. mass << 1 %. There is less (volatiles) residue at peak combustion with increase in biomass. For each 10 % increase in biomass there is a decrease of about 0.027 % in residue at peak combustion. The model explained about 98 % of the increase in consumption of composite at peak.

The reverse is the case for conversion at peak of the high temperature, char combustion stage B as in the chart,

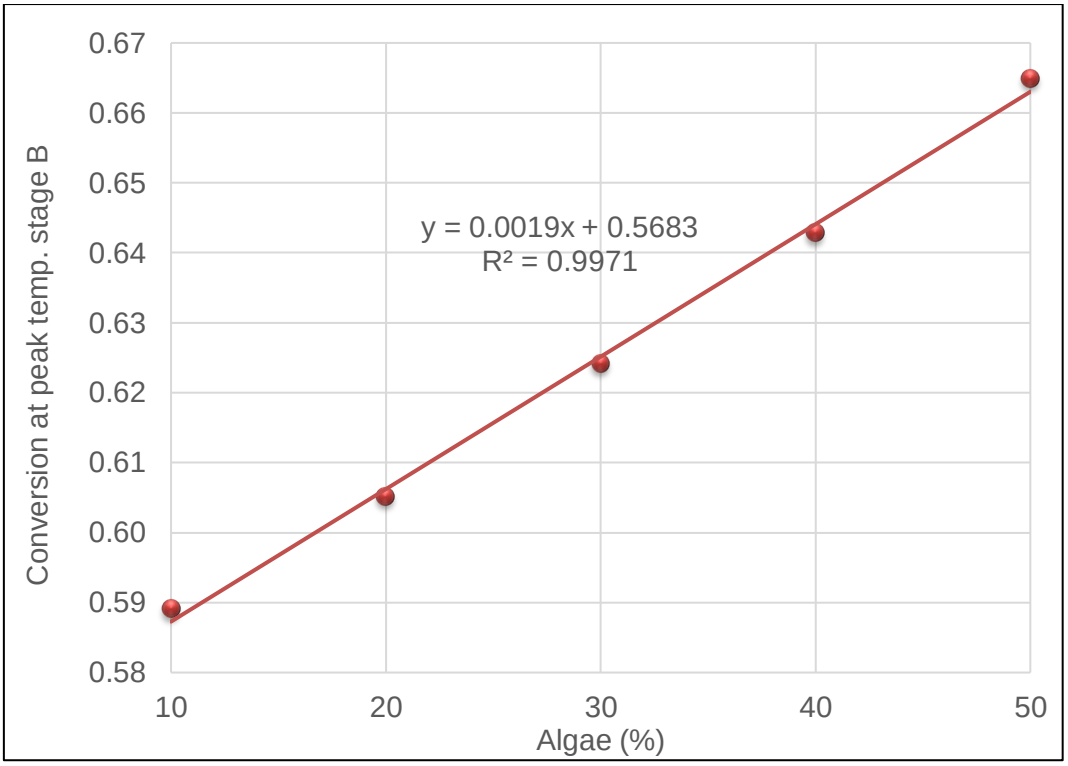

Figure 4.41: Fuel conversion (∝) at peak temperature for stage B

The plot, (Figure 4.41) illustrates the conversion of composites at peak temperature in stage (B). There is a steady increase in oxidation of char at peak temperature with increased in microalgae biomass. For each 10 % of biomass added there is about 0.02 % increase in conversion. The model explained 99 % of the increase in char conversion at peak temperature.

On the other hand, the peak combustion temperatures, (Figure 4.42) for devolatilization stage A is as shown.

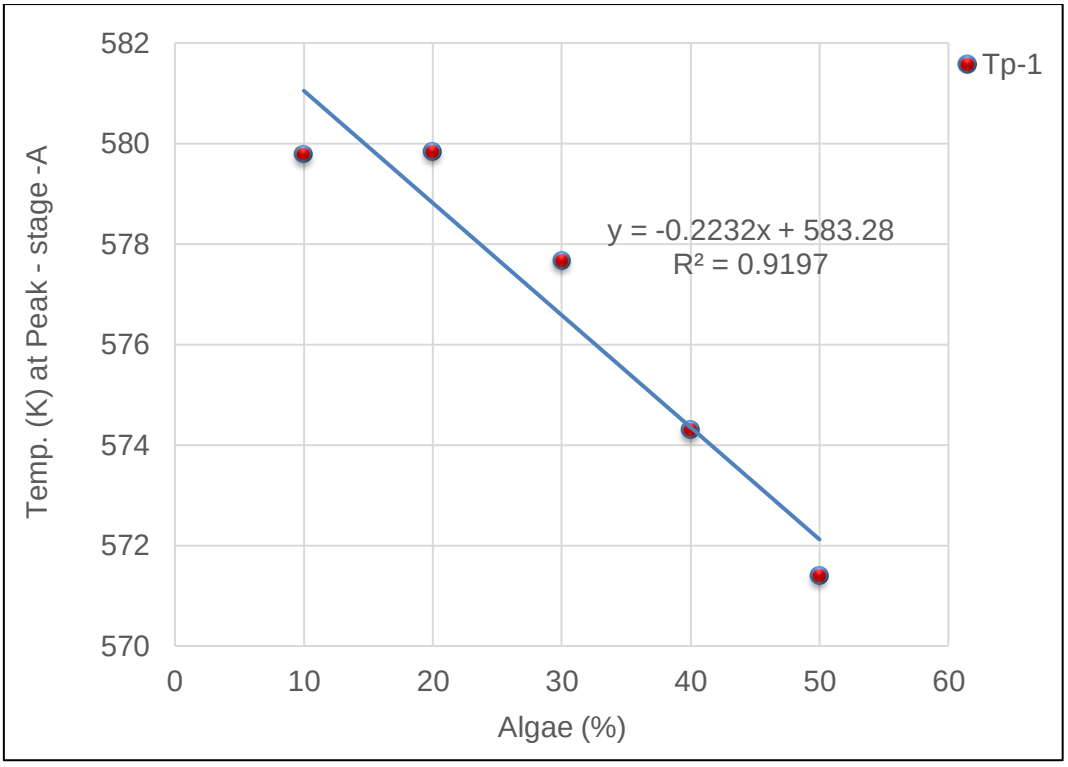

Figure 4.42: The peak combustion temperature for stage A

The illustration above, (Figure 4.42), depicts the peak combustion temperature for "Coalgae®" with increase in microalgae biomass. At the peak of combustion for samples of 10 – 50 %, the temperature lies between 570 – 580 K. The peak temperature decreases in this order, 10 < 20 < 30 < 40 < 50 %. The linear model described about 92 % of drop in peak temperature. There is a decrease of 0.22 Kelvin for every 10 % increase in microalgae at stage A.

Also, (Figure 4.43) below shows the temperature at peak combustion for high temperature stage.

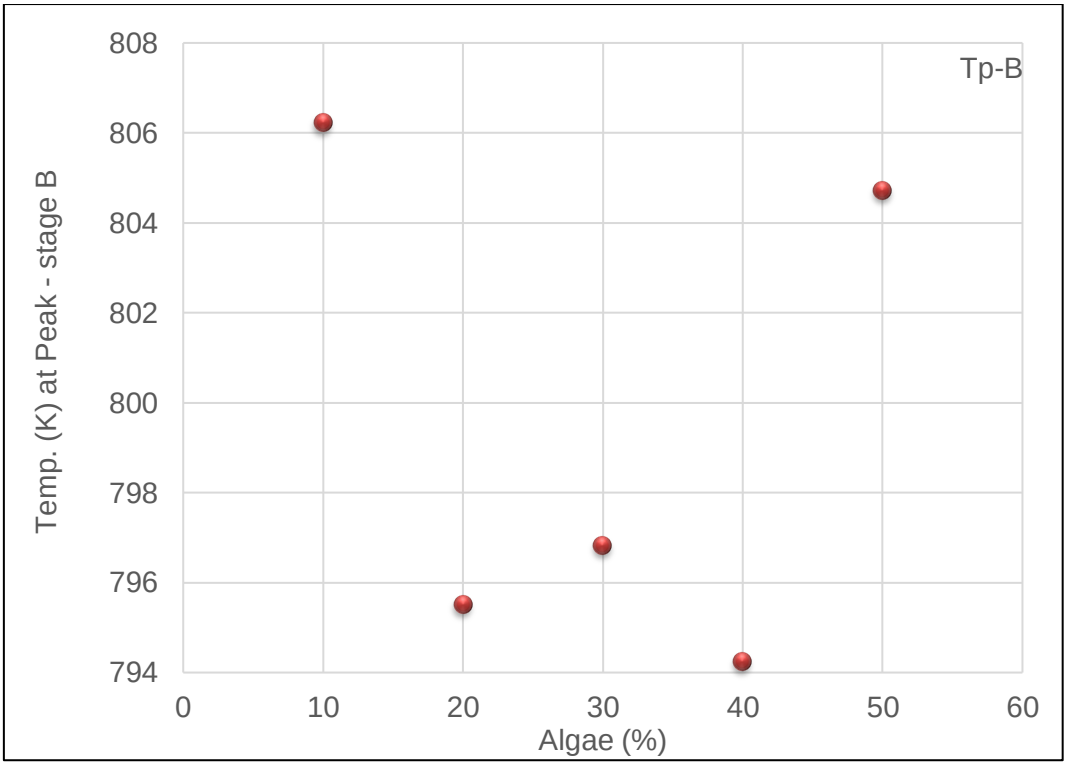

Figure 4.43: The peak combustion temperature for stage B

The Figure 4.43 shows the peak temperature for the combustion of char of the blends. There is no definite pattern in distribution of peak temperature of char combustion. The char has peak temperatures that are different from each other due to the biomass. Char conversion involves a series of heterogeneous reactions in which gaseous reactants are transported from the particle surrounding through the outer boundary layer into the char surface and pores of the particle (226). Lack of visible trend here could be attributed complex heterogeneous reaction in blend. The peaks combustion of all the char of "Coalgae®" are approximately within the same range of temperature. The difference in peak temperature could also be due to experimental error. Thus, a comparison of activation energy would be the best way to differentiate reactivity and explain the observed differences.

The activation energy, $E_{a.}$ obtained with the Coats and Redfern kinetics model and the $E_{a.}$ calculated with the Frasier-Suzuki deconvolution model were related, (Figure 4.44) as described.

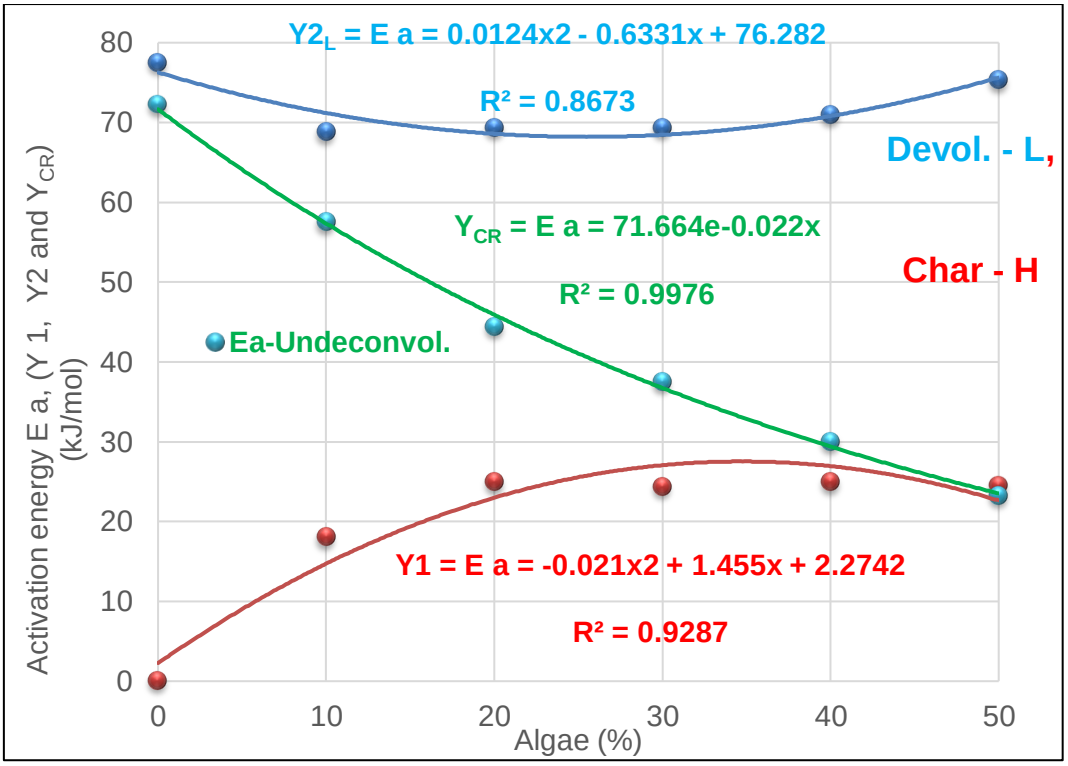

Figure 4.44: The activation energy for stages A, B, and un-deconvoluted event

The plot above, (Figure 4.44) is an overlay of the activation energy in kJ/mol for stages A, B, and the non-de-convoluted combustion process. The difference in activation energy of coal from the investigation conducted by (86), (94), (127) – (165), relative to "Coalgae®", (Figure 4.44) suggests that coal, and "Coalgae®" have different rates of reaction. Activation energy of the un-deconvoluted combustion process calculated with the Coats and Redfern equation lies between the activation energy of the low and high temperature scheme obtained with the Frasier-Suzuki model. This implies that activation energy of the un-de-convoluted process, (Figure 4.44) could be the sum (227) of the activation energies for stages A and B. Thus, for a combustion event that is considered as a single process, the Coats and Redfern model fits properly, as observed in second curve of Figure 4.44. But the Frasier-Suzuki deconvolution fits appropriately when detailed mechanism is required for overlapped combustion events.

The activation energy for low temperature combustion reduces by ~ 0.021 kJ/mol for each unit increase in the percent of biomass. The activation energy for high temperature scheme, *i.e.* char combustion would change by ~ 0.012 kJ/Mol., for each unit increase in microalgae biomass.

The value of frequency factor depends on the structure of material (113). The relationship between frequency factor and quantity of microalgae biomass, (Figure 4.45) in “Coalgae®” is as follows for the low and high combustion schemes.

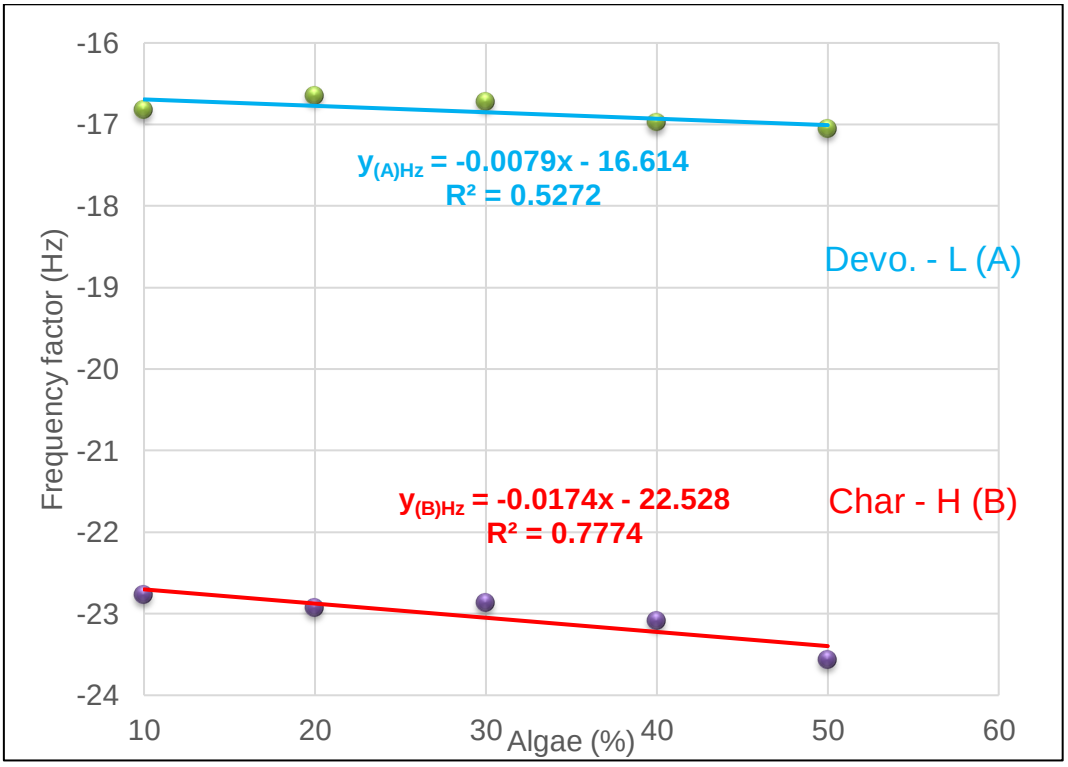

Figure 4.45: The frequency of collision for stages A and B oxidation

The collision of particles in the stage A, (Figure 4.45), is high and above that in stage B. If the rate of collision in stages A and B is written as (A, B), then for 10 – 50 %, we have (-16.9, -22.8), (-16.8, -23.0), (-16.9, -22.9), (-17.0, -23.0) and (-17.0, -23.5) respectively. Therefore, there is greater collision in stage (A) than (B). It means that stage A consists more of gas molecules (volatiles) and B more of solids (*i.e.* carbon). The stage A is homogeneous in gas phase between volatiles and oxygen for, while B is heterogeneous between char (solid) and gas. Thus, oxidation in stage A (de-volatilization) is more spontaneous compared to gradual combustion of char in stage B. Microalgae biomass improves the rate of de-volatilization. This invariably enhances rate of ignition because volatile matter is responsible for fuel ignition.

4.9 Activation energy and interaction between coal and microalgae biomass

The kinetic behaviour of coal-biomass fuel has been indicated by an additive scheme (144). The coal and biomass individually contributed to the mass loss and activation energy, as a weighted fraction of the value of each, equation (4.13), (144).

$$\mathrm{x\ blend}_{\mathrm{predicted}} = (\mathrm{M_{fc}} * \mathrm{x_c}) + (\mathrm{M_{fb}} * \mathrm{x_b}) \quad \text{..... (4.13)}$$

Where, x = fuel properties to be investigated for interaction and,

$\mathrm{M_{fc}}$ and $\mathrm{M_{fb}}$ = weight loss rate of coal and microalgae,

$\mathrm{x_c}$ and $\mathrm{x_b}$ = the mass fraction of coal and biomass in the blend. So, activation energy,

$$\mathrm{Ea\ blend}_{\mathrm{predicted}} = (\mathrm{M_{fc}} * \mathrm{Ea_c}) + (\mathrm{M_{fb}} * \mathrm{Ea_b}) \quad \text{..... (4.14)}$$

Where, Ea = Activation energy of blend and,

$\mathrm{M_{fc}}$ = mass fraction of coal,

$\mathrm{M_{fb}}$ = mass fraction of biomass,

$\mathrm{Ea_c}$ = activation energy of coal,

$\mathrm{Ea_b}$ = activation energy of biomass.

With this, one can confirm if the predicted linear behaviour (E a) equals the observed otherwise there is an interaction (199), (142), (162).

Table 4.17: Observed and predicted E a for coal, microalgae, and blends

Activation energy and frequency of collision for de - convoluted Process									
Fuels		**Stage A (Volatile combustion)**				**Stage B (Char combustion)**			
Algae (ratio)	**Coal** (ratio)	**Obs. E a**	**Pred. E a**	**Obs. (A)**	**Pred. (A)**	**Obs. E a**	**Pred. E a**	**Obs. (A)**	**Pred. (A)**
0	1	0.00	0.00	0.00	0.00	77.46	77.46	-24.11	-24.11
1	0	31.36	31.36	-18.80	-18.80	79.72	79.72	-23.48	-23.48
0.1	0.9	18.02	3.14	-16.83	-1.88	68.73	77.69	-22.78	-24.05
0.2	0.8	24.91	6.27	-16.65	-3.76	69.30	77.91	-22.94	-23.98
0.3	0.7	24.35	9.41	-16.73	-5.64	69.33	78.14	-22.88	-23.92
0.4	0.6	24.87	12.54	-16.98	-7.52	70.89	78.36	-23.09	-23.86
0.5	0.5	24.51	15.68	-17.06	-9.40	75.26	78.59	-23.57	-23.80
Mean		23.33	-	-16.85	-	70.70	-	-23.05	-
Std. deviation		2.9790	-	0.1701	-	2.6715	-	0.3106	-
t - statistics		2.776	-	2.77	-	2.776	-	2.776	-
Uncertainty @ 95% C.I.		3.70	-	0.21	-	3.32	-	0.39	-
E a and (A)		23.33 ± 3.70	-	16.85 ± 0.21	-	70.70 ± 3.32	-	23.05 ± 0.73	-

Obs. = observed, Pred. = predicted, E a = activation energy, A = collision frequency, C.I. = confidence interval

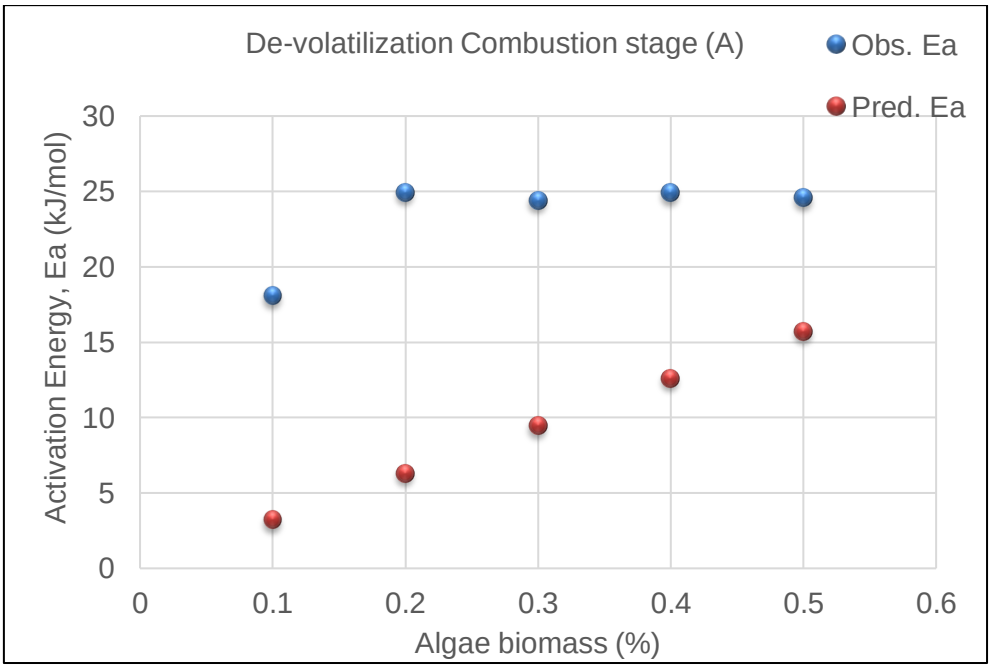

Figure 4.46: Observed and predicted change in activation energy with microalgae for blends at low temperature

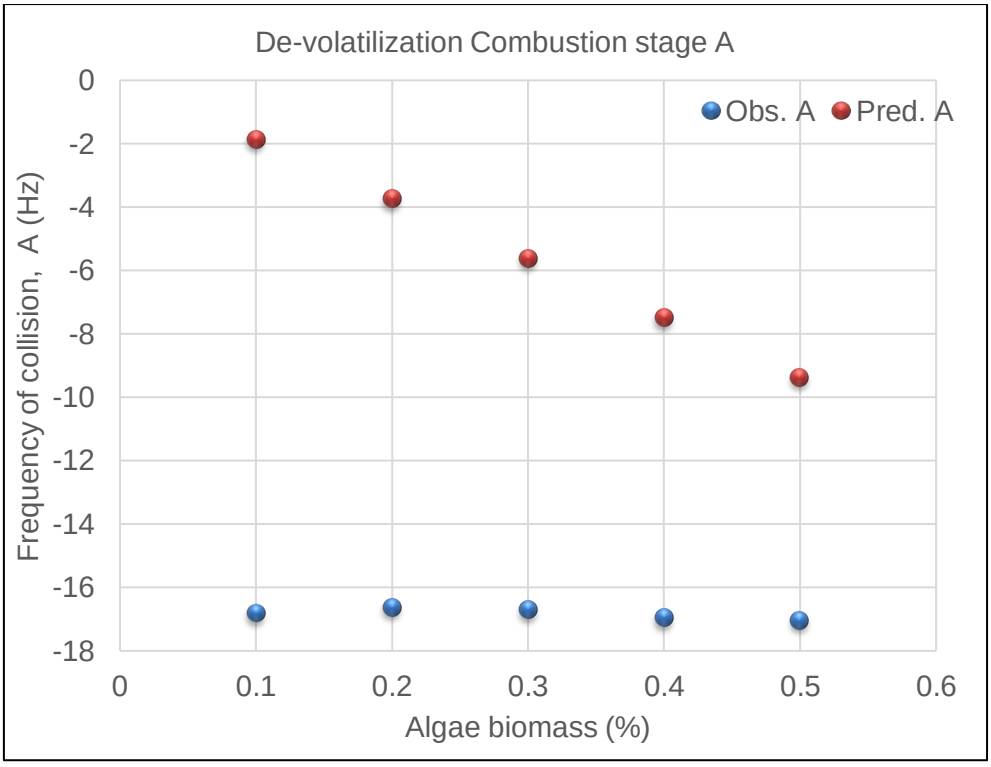

Figure 4.47: Observed and predicted change in collision frequency with microalgae for blends at low temperature

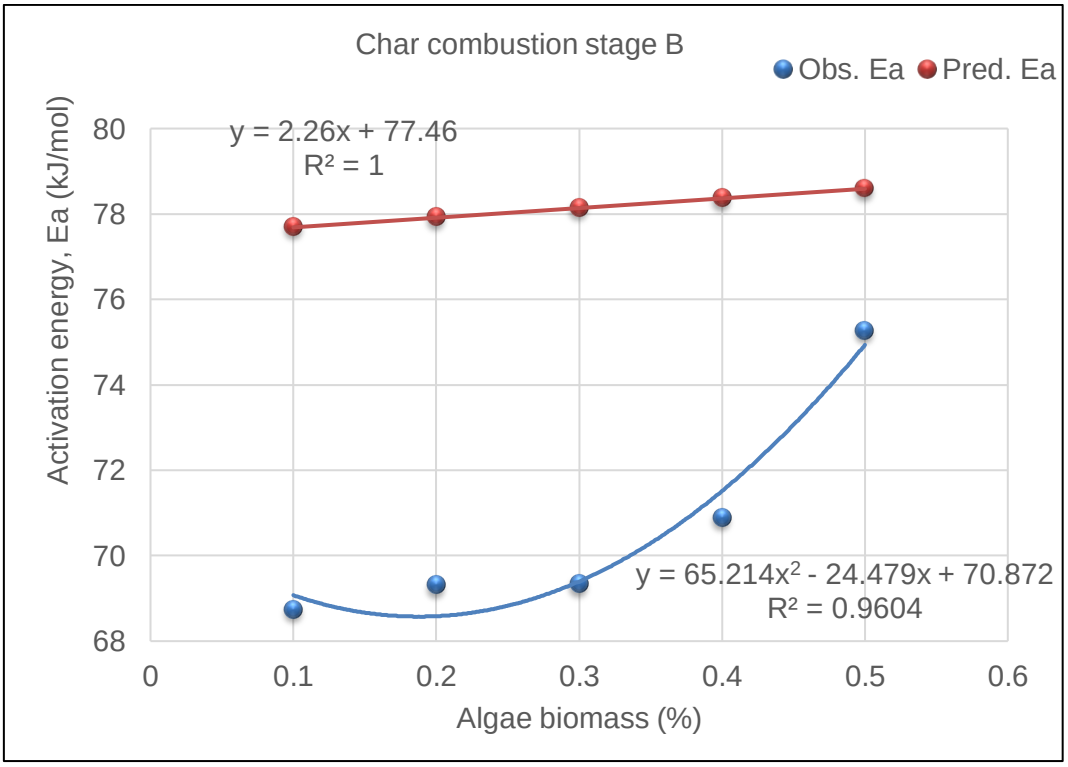

Figure 4.48: Observed and predicted change in activation energy with microalgae for blends at high temperature

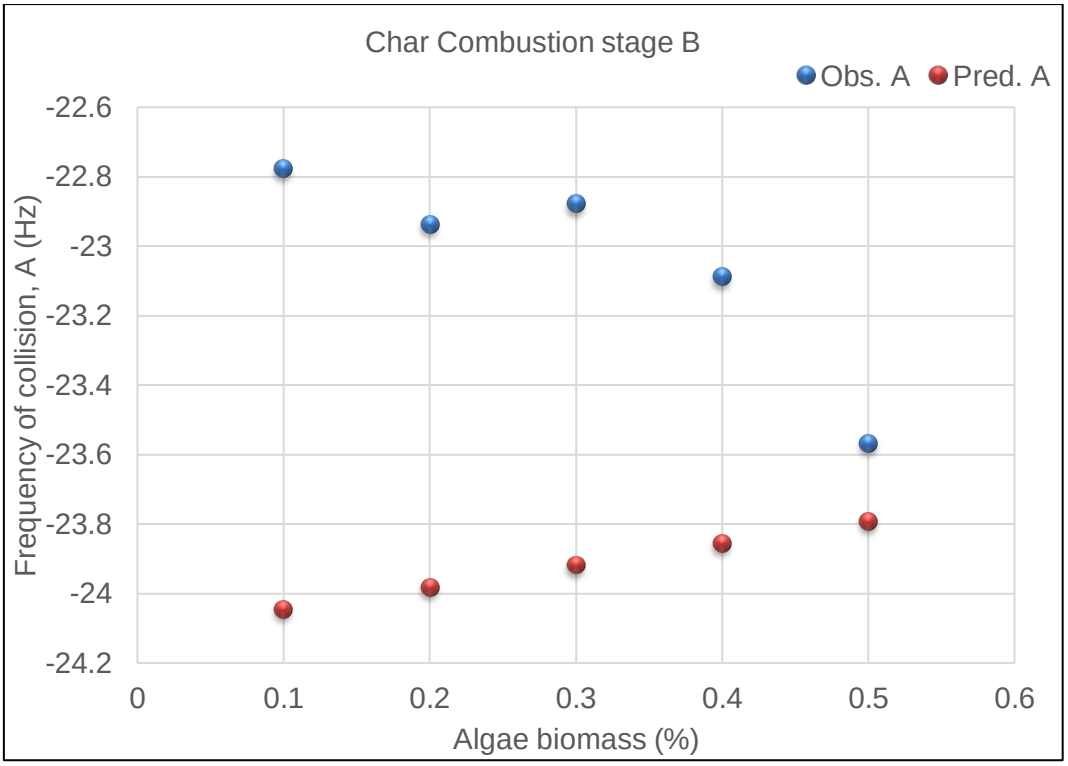

Figure 4.49: Observed and predicted change in collision frequency with microalgae for blends at high temperature

The Table 4.17, and Figures 4.46 – 4.49, show that “Coalgae®” starts to devolatilise at 23.33 ±3.70 kJ/mol and begins to char at 70.70 ± 3.32 kJ/mol, at 95 % confidence interval. The combustion of Coalgae® unlike coal has two thermochemical events due to microalgae biomass. The activation energy of the char combustion of coal, 77.46 ± 5.6 kJ/mol is higher compared to Coalgae®, 70.70 ± 3.32 kJ/mol at 95 % confidence interval. Under the same temperature conditions Coalgae® would char before coal. The difference implies that “Coalgae®” and coal are different fuels, which has unique kinetic properties as confirmed by the interactions in Figures 4.46 – 4.49.

4.10 Summary

“Coalgae®” was significantly different from the usual linear combination of coal and microalgae biomass (E a, p = 0.0570). This explains the de-volatilization which exist in “Coalgae®” unlike the coal, as well as differences in rate of char combustion of both coal and the blends. The observed activation energy from deconvoluted curves for the low temperature scheme is higher than the predicted, Figure 4.46. Furthermore, the observed activation energy for char combustion is lower relative to the predicted, *i.e.* at the high temperature scheme, Figure 4.47. Thus, microalgae co-firing influences

the low temperature scheme, i.e. devolatilization more than char combustion. The difference is evident and significant (p = 0.0570) between the observed and predicted activation energies of char combustion. The activation energy obtained in this study is less than those reported in the literature, Table 4.16, (213), (151). The combustion of coal-microalgae biomass was first investigated as a single thermal event using the Coats and Redferns model, and later deconvoluted using the Frasier-Suzuki model. These showed increase in the s-index and reduction in the activation energy which was similar to literature report (45). Furthermore, a comparison of small and large-scale combustions indicated substantial upgrade relative to the thermal properties of coal. Microalgae biomass enhanced the combustion kinetics and mechanism, served as natural binder, interacted with coal, and improved the oxidation of the blend. The computed reaction order provided details on the combustion properties. Deconvolution and the study of activation energy using the oxidation models provided more details in the understanding of the combustion kinetics of “Coalgae®” as compared to coal.

Chapter 5

5.0 Conclusion and Recommendation

5.1 Conclusions

The combustion of coal-biomass to generate heat and electricity is a well-developed practice. In this research, coal-microalgae composite which was referred to as “Coalgae®” fuel was studied under non-isothermal thermogravimetric combustion conditions. The oxidation kinetics and models for the “Coalgae®” samples were developed and compared to the linearly co-fired coal-microalgae composites, as well as to the coal. On blending, microalgae biomass formed an agglomerate, and during combustion, it interacted in a synergistic manner, catalysed, and upgraded the discard ultra-fine coal, though its exact role on the bonds of the coal was not well understood. The predicted blend (*i.e.* linear combination) of coal and microalgae biomass released 2.38 % volatile matter (paired t-test, p = 0.005), more than the “Coalgae®” at 95% confidence interval. “Coalgae®” had 0.92% fixed carbon (paired t-test, p = 0.039) more than the linear blend. Microalgae biomass supplied a significant amount of the oxygen used for the oxidation of “Coalgae®”, and it appeared that the biomass adsorption onto coal favoured combustion of the fuel. Though the energy content of Coalgae® and the linear blend were not different (paired t-test, p = 0.0801), an increase in the quantity of microalgae biomass increased the energy content per blend. This was accepted because an improvement in energy was not the essence of co-firing, rather to upgrade the combustion kinetics.

The other aspect was the rate of combustion of Coalgae®, which was higher (p – value = 0.0029) relative to the coal, and the linear blend. The rate for Coalgae® at peak combustion was significantly higher (6.43 %, paired t-test, p = 0.0475) than the linear blend. From this and some calculations, it was inferred that the Coalgae® approach to co-firing improved the comprehensive combustion characteristic of the coal. With the ignition temperature, “Coalgae®” was 2.32% higher, (paired t-test, p = 0.0220) than the predicted linear blend, and the ignition property was superior as compared to

the discard coal. The predicted peak combustion temperature for the linear blend was slightly higher than the observed peak for “Coalgae®”, (0.91%, paired t-test, p = 0.04022). There was a heterogenous interaction between the coal, and microalgae biomass at the peak combustion.

For the combustion kinetics, there was a significant decrease in the Coats and Redfern’s kinetic gradient for coal from ~ 8557.9 to ~ 5556.7, at 10 % load level due to the microalgae biomass. The combustion kinetics was upgraded as described by the model, (R^2 = 0.9934), and 20 % of microalgae biomass loaded appeared to be the best fit for the “Coalgae®” approach to co-firing. The activation energy of the linear blend was considerably (p = 0.0570) different from that of “Coalgae®”. The “Coalgae®” fuel devolatilised at 23.33 ±3.70 kJ/mol, charred at 70.70 ± 3.32 kJ/mol relative to the coal that had char activation energy of 77.46 ± 5.6 kJ/mol. Thus, “Coalgae®” is more reactive relative to the original ultra-fine coal at 95 % confidence interval. It was found from the combustion deconvolution process that the microalgae biomass initiated substantial devolatilization reaction to the coal which was characterised by first order reaction mechanism. The char combustion of “Coalgae®” and coal were controlled by the second order reaction mechanism.

The entire oxidation of discard ultra-fine was coal limited by second order reaction mechanism. However, the concentration of coal and “impurities” controlled its degree of oxidation. The oxidation of 10 % fuel was from the surface inwards, in phases and in three dimensions during devolatilization. The oxidation of microalgae biomass, and 20 – 50 % “Coalgae®” in the low temperature stage was limited by first order reaction mechanism, and a decrease in NO_x could be possible for the composites. The char oxidation for 20 – 50 % “Coalgae®” fuel was controlled by the second order reaction mechanism. The second order reaction mechanism also limited the entire (low and high temperature) oxidation for each fuel, and microalgae biomass was responsible for the low temperature stage in the composites. The small-scale combustion properties of Coalgae® was also comparable to the pilot scale. From these, the research established that the treatment of ultra-fine coal with live microalgae improved the combustion behaviour of the composites to an extent greater than what was expected from a simple linear combination of coal and the dry microalgae biomass. Finally, “Coalgae®” exhibited superior oxidation relative to the regular combination of coal and dry microalgae biomass, which supported the overall hypothesis.

5.2 Recommendations for further studies

The hypothetical linear combination model for coal and dry microalgae biomass does not provide an appropriate kinetic description for the combustion of “Coalgae®”. Therefore, the following has been identified and recommended for further studies.

- There is the need to develop a model that would describe the combustion of “Coalgae” to facilitate the acceptance of this fuel for power production.

- A study is recommended to evaluate if microalgae has any impact on the structure of coal, and to examine the secondary reactions during the combustion of Coalgae®.

- The “bonding” if there is any formed by the interaction of coal and microalgae biomass needs to be investigated. This will advise on the by-products of the combustion and provide detailed knowledge on the control of CO_2, CO, CH_4, NOx, and SOx emissions.

- On preparation, microalgae biomass requires handling and management of voluminous amount of water; thus, a rapid and efficient dewatering process must be considered.

- The research approach is proposed to include the reclamation of low and high-grade discard ultra-fine, and utilization of lump coal resources. Therefore, pre-cleaning of the discard ultra-fine coal may be considered.

- Large-scale production of microalgae biomass using the flue gas from “Coalgae®” is recommended to support a continuous industrial process, and CO_2 reduction cycle on an economy of scale.

- The mechanical stability of “Coalgae®” pellet as compared to commercial coal briquette should be evaluated. This would add knowledge to the transportation and storage planning associated with the fuel.

- The health outcome of using “Coalgae®” and its char as domestic fuel with respect to respiratory diseases needs to be studied.

- “Coalgae®” should be fired in a coal power station to evaluate its large-scale performance, and technical challenge associated with its combustion prior to commercialization.

References

1. Verma M, Loha C, Nath A, Kumar P. Drying of biomass for utilising in co-firing with coal and its impact on environment – A review. Renew Sustain Energy Rev [Internet]. Elsevier Ltd; 2017;71(February 2015):732–41. Available from: http://dx.doi.org/10.1016/j.rser.2016.12.101
2. Cornejo P, Flores M, Gordon A, García X. A modeling approach to co-firing biomass / coal blends in pulverized coal utility boilers : Synergistic effects and emissions profiles. Energy. 2017;120:663–74.
3. Agbor E, Zhang X, Kumar A. A review of biomass co-firing in North America. Renew Sustain Energy Rev. 2014;40:930–43.
4. Shahbaz M, Kumar A, Nasir M. The effects of financial development, economic growth, coal consumption and trade openness on CO2 emissions in South Africa. Energy Policy [Internet]. Elsevier; 2013;61:1452–9. Available from: http://dx.doi.org/10.1016/j.enpol.2013.07.006
5. Tas BE. A novel coal additive from microalgae produced from thermal power plant flue gas. J Clean Prod. 2016;133:1086–94.
6. Ritchie J, Dowlatabadi H. The 1000 GtC coal question : Are cases of vastly expanded future coal combustion still plausible ? Energy Econ [Internet]. Elsevier B.V.; 2017;65:16–31. Available from: http://dx.doi.org/10.1016/j.eneco.2017.04.015
7. Dmitrienko MA, Nyashina GS, Strizhak PA. Major gas emissions from combustion of slurry fuels based on coal , coal waste , and coal derivatives. J Clean Prod [Internet]. Elsevier Ltd; 2018;177:284–301. Available from: https://doi.org/10.1016/j.jclepro.2017.12.254
8. Wang C, Liu Y, Jin X, Che D. Effect of water washing on reactivities and NO x emission of Zhundong coals. J Energy Inst [Internet]. Elsevier Ltd; 2016;89(4):636–47. Available from: http://dx.doi.org/10.1016/j.joei.2015.06.002
9. Munawer ME. Human health and environmental impacts of coal combustion and post-combustion wastes. J Sustain Min [Internet]. Elsevier Ltd;

2017;xxx:1–10. Available from: https://doi.org/10.1016/j.jsm.2017.12.007

10. Scheffknecht G, Al-makhadmeh L, Schnell U, Maier J. Oxy-fuel coal combustion — A review of the current state-of-the-art. Int J Greenh Gas Control. 2011;16–35.
11. Buhre BJP, Elliott LK, Sheng CD, Gupta RP, Wall TF. Oxy-fuel combustion technology for coal-fired power generation. 2005;31:283–307.
12. Jones JM, Ross AB etal. Organic carbon emissions from the co-firing of coal and wood in a fixed bed combustor. Fuel [Internet]. 2017;195:226–31. Available from: http://dx.doi.org/10.1016/j.fuel.2017.01.061
13. Demirbas A. Sustainable cofiring of biomass with coal. Energy Convers Manag. 2003;44(9):1465–79.
14. Sahu SG, Chakraborty N, Sarkar P. Coal – biomass co-combustion : An overview. Renew Sustain Energy Rev. 2014;39:575–86.
15. Lempp P. Biomass Co-firing Technology Brief [Internet]. IEA-ETSAP and IRENA. 2013. Available from: www.irena.org/publications cited 2015.05.019
16. Kati Veijonen, Pasi Vainikka TJ and EA. Biomass Co-firing : An efficient way to reduce greenhouse gas emissions. European Bioenergy Networks (EUBIONET). 2003.
17. Baxter L. Biomass-coal Co-combustion : Opportunity for Affordable Renewable energy. Fuel. 2005;84:1295–302.
18. Roni MS, Chowdhury S, Mamun S, Marufuzzaman M, Lein W, Johnson S. Biomass co-firing technology with policies, challenges, and opportunities: A global review. Renew Sustain Energy Rev [Internet]. Elsevier Ltd; 2017;78(January):1089–101. Available from: http://dx.doi.org/10.1016/j.rser.2017.05.023
19. Zeelie et al. Carbonaceous Fines Beneficiation Using Micro-Algae and Related Processes [Internet]. South Africa: US Patent; US Patient 13/818,287, 2013. Available from: http://www.google.com/patents/US20130199087. [cited 2013.05.009]
20. Agrawal A, Chakraborty S. A kinetic study of pyrolysis and combustion of microalgae Chlorella vulgaris using thermo-gravimetric analysis. Bioresour

Technol. Elsevier Ltd; 2013;128:72–80.

21. Charles K. Westbrook, William J. Pitz MM. Combustion and Pyrolysis Chemistry (CPC): Kinetic Modelling [Internet]. Mechanism Development. 2015 [cited 2015 Jun 7]. Available from: https://cpc.kaust.edu.sa/Pages/kinetic-modelling.aspx. 2015.01.006

22. Brennan L, Owende P. Biofuels from microalgae — A review of technologies for production , processing , and extractions of biofuels and co-products. Renew Sustain Energy Rev. 2010;14:557–77.

23. Ejesieme V. Evaluating the effect of microalgae biomass on the combustion of coal [Internet]. 2014. 77 p. Available from: http://opac.seals.ac.za/search. 2015.12.004

24. Lin Q, Wang S, Liang Y, Song S, Ren T. Analytical prediction of coal spontaneous combustion tendency: Velocity range with high possibility of self-ignition. Fuel Process Technol [Internet]. Elsevier B.V.; 2017;159:38–47. Available from: http://dx.doi.org/10.1016/j.fuproc. 2016.09.027

25. Su H, Zhou F. Effects of oxygen supply on low-temperature oxidation of coal : A case study of Jurassic coal in Yima , China. Fuel [Internet]. Elsevier Ltd; 2017;202:446–54. Available from: http://dx.doi.org/10.1016/j.fuel. 2017.04.055

26. Wu Z, Yang W, Yang B. Thermal characteristics and surface morphology of char during co-pyrolysis of low-rank coal blended with microalgal biomass : E ff ects of Nannochloropsis and Chlorella. Bioresour Technol [Internet]. Elsevier; 2018;249(August 2017):501–9. Available from: http://dx.doi.org/10.1016/j.biortech.2017.09.196

27. More and cleaner energy | Shell Global [Internet]. 2017. Available from: http://www.shell.com/energy-and-innovation/the-energy-future/more-and-cleaner- energy.html [cited 2017.05.024]

28. Longwell J.P, E.S. Rubin JW. Coal: Energy for the future. Prog Energy Combust Sci. 1995;21(95):269–360.

29. Fernando R. Cofiring high ratios of biomass with coal. CCC/194 ed. IEA Clean Coal Centre; 2012. Available from: www.usea.org/sites/defaults/files/012012/co-firing [cited 2016.06.028]

30. Gao Y, Tahmasebi A, Dou J, Yu J. Combustion characteristics and air pollutant formation during oxy-fuel co-combustion of microalgae and lignite. Bioresour Technol [Internet]. Elsevier Ltd; 2016;207:276–84. Available from: http://dx.doi.org/10.1016/j.biortech.2016.02.031

31. Giostri A, Binotti M, Macchi E. Microalgae co-firing in coal power plants : Innovative system layout and energy analysis. Renew Energy [Internet]. Elsevier Ltd; 2016;95:449–64. Available from: http://dx.doi.org/10.1016/j.renene.2016.04.033

32. Tahmasebi A, Asyraf M, Yu J, Bhattacharya S. Thermogravimetric study of the combustion of Tetraselmis suecica microalgae and its blend with a Victorian brown coal in O2/N2 and O2/CO2 atmospheres. Bioresour Technol [Internet]. Elsevier Ltd; 2013;150:15–27. Available from: http://dx.doi.org/10.1016/j.biortech.2013.09.113

33. Chen C, Ma X, He Y. Co-pyrolysis characteristics of microalgae Chlorella vulgaris and coal through TGA. Bioresour Technol [Internet]. Elsevier Ltd; 2012;117:264–73. Available from: http://dx.doi.org/10.1016/j.biortech.2012.04.077

34. Johnston CMT, Kooten GC Van. Economics of co-fi ring coal and biomass : An application to Western Canada. Energy Econ [Internet]. Elsevier B.V.; 2015;48:7–17. Available from: http://dx.doi.org/10.1016/j.eneco.2014.11.015

35. Ren Q, Zhao C. Evolution of fuel-N in gas phase during biomass pyrolysis. Renew Sustain Energy Rev [Internet]. Elsevier; 2015;50:408–18. Available from: http://dx.doi.org/10.1016/j.rser.2015.05.043

36. Maciejewska A, Veringa H, Sanders J, Peteves SD. Co-firing of biomass with coal: Constraints and role of biomass pre-treatment [Internet]. EU 22461 E. Netherlands; 2006. Available from: http://ie.jrc.ec.europa.eu

37. Pokothoane PS. Analysis of Co-firing Biomass with South African Coal in Pulverised Coal Boilers. [Internet]. 2010. Available from: http://wiredspace.wits.ac.za/handle/10539/9744

38. De S, Assadi M. Impact of cofiring biomass with coal in power plants – A techno-economic assessment. Biomass and Bioenergy [Internet]. Elsevier Ltd; 2009;33(2):283–93. Available from:

http://dx.doi.org/10.1016/j.biombioe.2008.07.005

39. Hein KR., Bemtgen J. EU clean coal technology — co-combustion of coal and biomass. Fuel Process Technol [Internet]. 1998;54(1-3):159–69. Available from: http://www.sciencedirect.com/science/article/pii/S0378382097000672

40. Ulloa CA, Gordon AL, García XA. Thermogravimetric study of interactions in the pyrolysis of blends of coal with radiata pine sawdust. Fuel Process Technol [Internet]. Elsevier B.V.; 2009;90(4):583–90. Available from: http://dx.doi.org/10.1016/j.fuproc.2008.12.015

41. Alam F, Mobin S, Chowdhury H. Third generation biofuel from Algae. Procedia Eng [Internet]. Elsevier B.V.; 2015;105(Icte 2014):763–8. Available from: http://dx.doi.org/10.1016/j.proeng.2015.05.068

42. Dandan Chen, Zengyi Ma JY. Renewable and sustainable energy review. Renew Sustain Energy Rev [Internet]. Elsevier; 2017;68(October 2016):410–31. Available from: http://dx.doi.org/10.1016/j.rser.2016.10.001

43. Zhou C, Liu G, Wang X, Qi C. Co-combustion of bituminous coal and biomass fuel blends : Thermochemical characterization , potential utilization and environmental advantage. Bioresour Technol [Internet]. Elsevier Ltd; 2016;218:418–27. Available from: http://dx.doi.org/10.1016/j.biortech.2016.06.134

44. Pérez A, Calero M, Ronda A. Kinetic analysis of pyrolysis and combustion of the olive tree pruning by chemical fractionation. Bioresour Technol [Internet]. Elsevier; 2018;249(August 2017):557–66. Available from: http://dx.doi.org/10.1016/j.biortech.2017.10.045

45. Wang G, Zhang J, Shao J, Liu Z, Zhang G, Xu T, et al. Thermal behavior and kinetic analysis of co-combustion of waste biomass / low rank coal blends. Energy Convers Manag [Internet]. Elsevier Ltd; 2016;124:414–26. Available from: http://dx.doi.org/10.1016/j.enconman.2016.07.045

46. Liu Z, Hu W, Jiang Z, Mi B, Fei B. Investigating combustion behaviors of bamboo, torrefied bamboo, coal and their respective blends by thermogravimetric analysis. Renew Energy [Internet]. Elsevier Ltd; 2016;87:346–52. Available from: http://dx.doi.org/10.1016/j.renene.2015.10.039

47. Demirbas A. Combustion characteristics of different biomass fuels. Prog Energy Combust Sci [Internet]. 2004;30(2):219–30. Available from: http://www.sciencedirect.com/science/article/pii/S0360128503000789 [cited 2016.09.012]

48. Neminda B, Gan S, Eastwick C, Kiat H. Biomass as an energy source in coal co-firing and its feasibility enhancement via pre-treatment techniques. Fuel Process Technol [Internet]. Elsevier B.V.; 2017;159:287–305. Available from: http://dx.doi.org/10.1016/j.fuproc.2017.01.029

49. Goerndt ME, Aguilar FX, Skog K. Drivers of biomass co-firing in U.S. coal-fired power plants. Biomass and Bioenergy [Internet]. Elsevier Ltd; 2013;58:158–67. Available from: http://dx.doi.org/10.1016/j.biombioe.2013.09.012

50. Mehmood S, Reddy B V, Rosen MA. Energy Analysis of a Biomass Co-firing Based Pulverized Coal Power Generation System. Sustainability [Internet]. 2012;4:462–90. Available from: www.mdpi.com/journal/sustainability [cited 2015.08.013]

51. Sebastián F, Royo J, Gómez M. Cofiring versus biomass-fired power plants : GHG (Greenhouse Gases) emissions savings comparison by means of LCA (Life Cycle Assessment) methodology. Energy [Internet]. Elsevier Ltd; 2011;36(4):2029–37. Available from: http://dx.doi.org/10.1016/j.energy.2010.06.003

52. Vassilev S V, Vassileva CG, Vassilev VS. Advantages and disadvantages of composition and properties of biomass in comparison with coal : An overview. Fuel [Internet]. Elsevier Ltd; 2015;158:330–50. Available from: http://dx.doi.org/10.1016/j.fuel.2015.05.050

53. Mckendry P. Energy production from biomass (part1): overview of biomass. Bioresour Technol [Internet]. 2002;83(July 2001):37–46. Available from: http://www.sciencedirect.com/search [cited 2017.02.007]

54. Momeni M. Fundamental Study of Single Biomass Particle Combustion. Aalborg University, Denmark; 2012.

55. Chen C, Ma X, Liu K. Thermogravimetric analysis of microalgae combustion under different oxygen supply concentrations. Appl Energy [Internet]. Elsevier Ltd; 2011;88(9):3189–96. Available from:

http://dx.doi.org/10.1016/j.apenergy.2011.03.003

56. Cai J, He Y, Yu X, Banks SW, Yang Y, Zhang X, et al. Review of physicochemical properties and analytical characterization of lignocellulosic biomass. Renew Sustain Energy Rev. 2017;76(October 2016):309–22.

57. Basu P, Butler J, Leon MA. Biomass co-firing options on the emission reduction and electricity generation costs in coal-fired power plants. Renew Energy [Internet]. Elsevier Ltd; 2011;36(1):282–8. Available from: http://dx.doi.org/10.1016/j.renene.2010.06.039

58. Saidur R, Abdelaziz EA, Demirbas A, Hossain MS, Mekhilef S. A review on biomass as a fuel for boilers. Renew Sustain Energy Rev [Internet]. Elsevier Ltd; 2011;15(5):2262–89. Available from: http://dx.doi.org/10.1016/j.rser.2011.02.015

59. Arias B, Pevida C, Rubiera F. PJ. Effect of biomass blending on coal ignition and burnout during oxy-fuel combustion. Fuel [Internet]. 2008;87(12):2753–9. Available from: http://www.sciencedirect.com/science/article [cited 2016.04.014]

60. Martins AA, Caetano NS, Mata TM. Microalgae for biodiesel production and other applications : A review. Renew Sustain Energy Rev. 2010;14:217–32.

61. Rodriguez LC, May B, Herr A, Connell DO. Biomass assessment and small scale biomass fired electricity generation in the Green Triangle , Australia. Biomass and Bioenergy [Internet]. Elsevier Ltd; 2011;35(7):2589–99. Available from: http://dx.doi.org/10.1016/j.biombioe.2011.02.030

62. Cambero C, Sowlati T. Assessment and optimization of forest biomass supply chains from economic , social and environmental perspectives – A review of literature. Renew Sustain Energy Rev [Internet]. Elsevier; 2014;36:62–73. Available from: http://dx.doi.org/10.1016/j.rser.2014.04.041

63. Smith, K.L., Smoot, L.D., Fletcher, T.H. and Pugmire RJ. The Structure and Reaction Processe of Coal. Luss D, editor. 1994.

64. Jiang X, Chen D, Ma Z, Yan J. Models for the combustion of single solid fuel particles in fluidized beds: A review. Renew Sustain Energy Rev [Internet]. Elsevier; 2017;68(October 2016):410–31. Available from:

www.elsevier.com/locate/rser [cited 2017.03.016]

65. Sami M, Annamalai K, Wooldridge M. Co-firing of coal and biomass fuel blends. Progess Energy Combust Sci [Internet]. 2001;27:171–214. Available from: http://www.sciencedirect.com/science/article [cited 2016.07.001]

66. Schobert HH, Song C. Chemicals and materials from coal in the 21st century. Fuel. 2002;81:15–32.

67. Wang H, Dlugogorski BZ, Kennedy EM. Coal oxidation at low temperatures : oxygen consumption , oxidation products , reaction mechanism and kinetic modelling. Progess Energy Combust Sci. 2003;29:487–513.

68. Williams A, Pourkashanian M, Jones JM. Combustion of pulverised coal and biomass. Progess Energy Combust Sci. 2001;27:587–610.

69. Balmer M. Household coal use in an urban township in South Africa. 2012;18(3):27–32.

70. Yohe R. GS. Oxidation of Coal [Internet]. Urbana, Illinois; 1958. Available from: http://archive.org/details/oxidationofcoal207yohe [cited 2017.02.012]

71. Jenkinsa BM, Baxterb LL, Miles Jr TR, Miles TR. Combustion properties of biomass. Fuel Process Technol [Internet]. 1998;54(1-3):17–46. Available from: http://www.sciencedirect.com/science/article [cited 2017.03.004]

72. Bacchi RDA. Best Practice Guidelines for Combustion Modeling. 2013 ESSS Conference & Ansys users Meeting. Atibaia, SP - Brasil; 2013.

73. Smith D, Stephenson P, Williams A, M. Gharebaghi, R. Irons, R. Porter RTJP etal. Combustion modelling opportunities and challenges for oxy-coal carbon capture technology. Chem Eng Res Des [Internet]. Institution of Chemical Engineers; 2010;89(9):1470–93. Available from: http://dx.doi.org/10.1016/j.cherd.2010.11.010

74. Chung (Peter) Chieh. Chemical Kinetics Lecture Note, PPT [Internet]. Reif JHE-S, editor. University of Waterloo; Available from: https://www.slideserve.com/tybalt/chemical-kinetics-lecture-notes-edited-by-john-reif-from-ppt-lectures-by [cited 2014.05.011]

75. Vallance C. Reaction Kinetics [Internet]. 1-31 p. Available from: www.vallance.chem.ac.uk/pdfs/kineticslectureNotes [cited 2014.04.029]

76. Behrens M. Solid State Kinetics: Lecture Series. Hetrogenous Catalysis. Berlin, Germany; 2006.

77. Palma CF. Modelling of tar formation and evolution for biomass gasification : A review. Appl Energy [Internet]. Elsevier Ltd; 2013;111:129–41. Available from: http://dx.doi.org/10.1016/j.apenergy.2013.04.082

78. Hall SL, East A. Chemical Kinetics: Lecture Note CHEM 1001 3.0 Section N [Internet]. Available from: www.chem.yorku.ca/profs/krylov/ [cited 2014.05.009]

79. Wallington TJ, Kaiser EW, Farrell JT. Automotive fuels and internal combustion engines : a chemical perspective. 2006;(1974):335–47.

80. IDC Technologies. Coal classification [Internet]. p. 1–7. Available from: www.idc-online.com/technical_references/pdfs/chemical_engineering/Coal.pdf

81. Maffei T. Kinetic Model of Coal Combustion. Politecnico Di Milano; 2013.

82. Vassilev S V, Baxter D, Andersen LK, Vassileva CG, Morgan TJ. An overview of the organic and inorganic phase composition of biomass. Elsevier Ltd; 2012;94:1–33.

83. Bunt JR, Neomagus HWJP, Botha AA, Waanders FB. Reactivity study of fine discard coal agglomerates. J Anal Appl Pyrolysis [Internet]. Elsevier B.V.; 2015;113:723–8. Available from: http://dx.doi.org/10.1016/j.jaap.2015.03.001

84. Raheem A, Azlina WAKGW, Tau YH, Danquah MK. Thermochemical conversion of microalgal biomass for biofuel production. Renew Sustain Energy Rev. 2015;49:990–9.

85. Fluri TP. The potential of concentrating solar power in South Africa. Energy Policy [Internet]. Elsevier; 2019;37(12):5075–80. Available from: http://dx.doi.org/10.1016/j.enpol.2009.07.017

86. Munzhedzi R, Sebitosi AB. Redrawing the solar map of South Africa for photovoltaic applications. Renew Energy. 2009;34:165–9.

87. Borowitzka MA. Commercial production of microalgae : ponds, tanks, tubes and fermenters. J Biotechnol [Internet]. 1999;70(1-3):313–21. Available from: http://www.sciencedirect.com/science/article/pii/S0168165699000838 [cited 2017.02.007]

88. Altech. Algae - The Growth Platform [Internet]. Altech Animal Nutrition, Animal

Feed Supplements, Animal Health. 2016 [cited 2017 Mar 16]. Available from: http://www.alltech.com/future-of-farming/algae-the-growth-platform [cited 2017.03.016]

89. Aslam A, Thomas-hall SR, Aziz T, Schenk PM. Selection and adaptation of microalgae to growth in 100 % unfiltered coal-fired flue gas. Bioresour Technol [Internet]. Elsevier Ltd; 2017;233:271–83. Available from: http://dx.doi.org/10.1016/j.biortech.2017.02.111

90. Horsman M, Wu N, Lan CQ, Dubois-calero N. Biocatalysts and Bioreactor Design. Biotechnol Prog. 2008;(1):815–20.

91. Brown MR, Jeffrey SW, Volkman JK, Dunstan GA. Nutritional properties of microalgae for mariculture. Aquaculture [Internet]. 1997;151(1-4):315–31. Available from: http://www.sciencedirect.com/science/article/pii/S0044848696015013 [cited 2017.02.007]

92. Lorenz RT, Cysewski GR. Commercial potential for Haematococcus microalgae as a natural source of astaxanthin. Trends Biotechnol [Internet]. 2000;18(4):160–7. Available from: http://www.sciencedirect.com/science/article/pii/S0167779900014335 [cited 2017.02.007]

93. Olaizola M. Commercial development of microalgal biotechnology : from the test tube to the marketplace. Biomol Eng [Internet]. 2003;20(4-6):459–66. Available from: http://www.sciencedirect.com/science/article/pii/S1389034403000765 [cited 2017.02.007]

94. Olaizola M. Commercial production of astaxanthin from Haematococcus pluvialis using 25 , 000-liter outdoor photobioreactors. J Appl Phycol [Internet]. 2000;12(3-5):499–506. Available from: https://link.springer.com/article/10.1023/A:1008159127672?LI=true [cited 2017.02.007]

95. He L, Subramanian VR, Tang YJ. Experimental analysis and model-based optimization of microalgae growth in photo-bioreactors using flue gas. Biomass and Bioenergy [Internet]. Elsevier Ltd; 2012;41(314):131–8. Available from:

http://dx.doi.org/10.1016/j.biombioe.2012.02.025

96. Spolaore P, Joannis-cassan C, Duran E, Isambert A, Génie L De, Paris EC. Commercial Applications of Microalgae. J Biosci Bioeng [Internet]. 2006;101(2):87–96. Available from: http://www.sciencedirect.com/science/article/pii/S1389172306705497 [cited 2017.02.007]

97. Eitner J. Microalgae – produced on a commercial scale - Fraunhofer-Gesellschaft [Internet]. ACHEMA. 2015 [cited 2016 Dec 5]. Available from: https://www.fraunhofer.de/en/press/research-news/2015/June/microalgae-produced-on-a-commercial-scale.html [cited 2016.12.005]

98. ECN Phyllis classification [Internet]. 2018 [cited 2018 Mar 12]. Available from: https://www.ecn.nl/phyllis2/Browse/Standard/ECN-Phyllis#microalgae [cited 2018.03.012]

99. Valverde JL. Kinetic analysis and thermal characterization of the microalgae combustion process by thermal analysis coupled to mass spectrometry. Appl Energy [Internet]. Elsevier Ltd; 2014;114:227–37. Available from: http://dx.doi.org/10.1016/j.apenergy.2013.09.055

100. Raheem A, Prinsen P, Vuppaladadiyam AK, Zhao M, Luque R. A review on sustainable microalgae based biofuel and bioenergy production: recent developments. Clean Prod. Elsevier Ltd; 2018;

101. Filippis P De, Caprariis B De, Scarsella M, Verdone N. Double Distribution Activation Energy Model as Suitable Tool in Explaining Biomass and Coal Pyrolysis Behavior. Energies. 2015;8:1730–44.

102. Murray KE, Shields JA, Garcia ND, Healy FG. Productivity , carbon utilization , and energy content of mass in scalable microalgae systems. Bioresour Technol [Internet]. Elsevier Ltd; 2012;114:499–506. Available from: http://dx.doi.org/10.1016/j.biortech.2012.03.012

103. Norsker N, Barbosa MJ, Vermuë MH, Wijffels RH. Microalgal production — A close look at the economics. Biotechnol Adv [Internet]. Elsevier Inc.; 2011;29(1):24–7. Available from: http://dx.doi.org/10.1016/j.biotechadv.2010.08.005

104. Alvarez P, Salgueiro, J.L, Perez, L., Cancela. A., Sanchez, A., Ortiz L. Total Use of Microalgae as Feedstock for Biodiesel and Pellet Production. Int J Environ Resour. 2016;10(4):637–44.

105. Ben-iwo J, Manovic V, Longhurst P. Biomass resources and biofuels potential for the production of transportation fuels in Nigeria. Renew Sustain Energy Rev [Internet]. Elsevier; 2016;63:172–92. Available from: http://dx.doi.org/10.1016/j.rser.2016.05.050

106. Plis A, Lasek J, Skawi A. Kinetic analysis of the combustion process of Nannochloropsis gaditana microalgae based on thermogravimetric studies. J Anal Appl Pyrolysis. 2017;127(August):109–19.

107. Filippis PDE, Caprariis BDE, Scarsella M, Verdone N. Double Distribution Activation Energy Model for microalgae pyrolysis. Recent Adv Energy, Environ Financ Plan [Internet]. 2014;68–73. Available from: http://www.wseas.us/e-library/conferences/2014/Florence/DEEE/DEEE-07.pdf [cited 2016.11.021]

108. Ververis, C., K.Georghiou., D. Danielidis. etal. Cellulose , hemicelluloses , lignin and ash content of some organic materials and their suitability for use as paper pulp supplements. Bioresour Technol. 2007;98:296–301.

109. Peterson. Fine coal Filtration [Internet]. Filter Applications. Available from: http://www.petersonfilters.com/filter-applications/fine-coal-filtration [cited 2016.06.006]

110. Bada SO, Falcon RMS, Falcon LM, Makhula MJ. Thermogravimetric investigation of macadamia nut shell, coal, and anthracite in different combustion atmospheres. J South African Inst Min Metall. 2015;(August):741–6.

111. Kucukvar M, Tatari O. A comprehensive life cycle analysis of co fi ring algae in a coal power plant as a solution for achieving sustainable energy. Energy [Internet]. Elsevier Ltd; 2011;36(11):6352–7. Available from: http://dx.doi.org/10.1016/j.energy.2011.09.039

112. Zeng T, Weller N, Pollex A, Lenz V. Blended biomass pellets as fuel for small scale combustion appliances : Influence on gaseous and total particulate matter emissions and applicability of fuel indices. Fuel [Internet]. 2016;184:689–700. Available from: http://dx.doi.org/10.1016/j.fuel.2016.07.047

113. Goldfarb JL, Liu C. Bioresource Technology Impact of blend ratio on the co-firing of a commercial torrefied biomass and coal via analysis of oxidation kinetics. Bioresour Technol [Internet]. Elsevier Ltd; 2013;149:208–15. Available from: http://dx.doi.org/10.1016/j.biortech.2013.09.053

114. Niu S, Han K, Lu C. Characteristic of coal combustion in oxygen / carbon dioxide atmosphere and nitric oxide release during this process. Energy Convers Manag [Internet]. Elsevier Ltd; 2011;52(1):532–7. Available from: http://dx.doi.org/10.1016/j.enconman.2010.07.028

115. Kirtania K, Bhattacharya S. Pyrolysis kinetics and reactivity of algae e coal blends. Biomass and Bioenergy [Internet]. Elsevier Ltd; 2013;55:291–8. Available from: http://dx.doi.org/10.1016/j.biombioe.2013.02.019

116. Eltra GmbH. Thermogravimetric Analyzers Specialists for Elemental Analysis [Internet]. Germany; 2014. p. 1–46. Available from: www.eltra.org [cited 2017.06.006]

117. Andre Klostermeier. Quality Control of Coal with Elemental Analyzers [Internet]. 2013. Available from: www.eltra.org [cited 2017.06.006]

118. Shaha A.K. Combustion and Fuel Engineering. Bureau of Energy Efficiency; p. 1–28. Available from: www.pcra.org [cited 2016.09.011]

119. ASTM. ASTM D7582 - 15 Standard Test Methods for Proximate Analysis of Coal and Coke by Macro Thermogravimetric Analysis [Internet]. Available from: https://www.astm.org/Standards/D7582.htm [cited 2015.03.016]

120. Apaydin-varol E, Pu E. Slow pyrolysis of pistachio shell. Fuel. 2007;86:1892–9.

121. ASTM- Standard Test Method for Heat of Combustion of Liquid Hydrocarbon Fuels by Bomb Calorimeter (Precision Method). Designation: D4809-09a (June 23, 2012). 2012;4809.

122. Vario EL Cube, elementar-the legend newly defined [Internet]. 2013. Available from: www.elementar.de. [cited 2014.07.014]

123. Mathieu D. PANalytical Epsilon 5 XRF spectral acquisition , processing and reporting. Ottawa, ON K1A 0H3; 2013.

124. PANalytical. Epsilon 3 Automation - Flexible and safe automation for process control [Internet]. The Netherlands; Available from:

www.panalytical.com/epislon3xautomation [cited 2016.06.008]

125. Panalytical. IMPROVE Standard Operating Procedure for the X-Ray Fluorescence Analysis of Aerosol Deposits on PTFE Filters (with PANalytical Epsilon 5) SOP 301 [Internet]. 2014. Available from: http://airquality.crocker.ucdavis.edu/files/9014/5774/5516/SOP_301_X-Ray_Fluorescence_Analysis.pdf [cited 2016.06.008]

126. Wilk M, Magdziarz A, Gajek M, Zajemska M, Jayaraman K. Combustion and kinetic parameters estimation of torrefied pine , acacia and Miscanthus giganteus using experimental and modelling techniques. Bioresour Technol. 2017;243:304–14.

127. Toftegaard MB, Brix J, Jensen PA, Glarborg P, Jensen AD. Oxy-fuel combustion of solid fuels. Prog Energy Combust Sci [Internet]. Elsevier Ltd; 2010;36(5):581–625. Available from: http://dx.doi.org/10.1016/j.pecs.2010.02.001

128. Gai C, Liu Z, Han G, Peng N, Fan A. Combustion behavior and kinetics of low-lipid microalgae via thermogravimetric analysis. Bioresour Technol [Internet]. Elsevier Ltd; 2015;181:148–54. Available from: http://dx.doi.org/10.1016/j.biortech.2015.01.045

129. Kanervo J. Kinetic Analysis of Temperature Programmed Reactions. Helsinki University of Technology; 2003.

130. Villaseñor J, Sánchez P, Valverde JL. Thermogravimetric – mass spectrometric analysis of lignocellulosic and marine biomass pyrolysis. Bioresour Technol [Internet]. Elsevier Ltd; 2012;109:163–72. Available from: http://dx.doi.org/10.1016/j.biortech.2012.01.001

131. Wagner NJ. The characterization of weathered discard coals and their behaviour during combustion. Fuel [Internet]. 2008;87(8-9):1687–97. Available from: http://www.sciencedirect.com/science/article/pii/S0016236107004231 [cited 2017.03.005]

132. Widmann G. Interpreting TGA curves [Internet]. 2001. Available from: www.masontechnology.ie/x/Usercom_13.pdf [cited 2017.03.007]

133. Jayaraman K, Versan M, Gokalp I. Thermogravimetric and mass spectrometric

(TG-MS) analysis and kinetics of coal-biomass blends. Renew Energy [Internet]. Elsevier Ltd; 2017;101:293–300. Available from: http://dx.doi.org/10.1016/j.renene.2016.08.072

134. Yu D, Chen M, Wei Y, Niu S, Xue F. An assessment on co-combustion characteristics of Chinese lignite and eucalyptus bark with TG – MS technique. Powder Technol [Internet]. Elsevier B.V.; 2016;294:463–71. Available from: http://dx.doi.org/10.1016/j.powtec.2016.03.016

135. Maiti S, Dey S, Purakayastha S, Ghosh B. Physical and thermochemical characterization of rice husk char as a potential biomass energy source. Bioresour Technol. 2006;97:2065–70.

136. Sahu SG, Sarkar P, Chakraborty N, Adak AK. Thermogravimetric assessment of combustion characteristics of blends of a coal with different biomass chars. Fuel Process Technol [Internet]. Elsevier B.V.; 2010;91(3):369–78. Available from: http://dx.doi.org/10.1016/j.fuproc.2009.12.001

137. Hao Z, Yang B, Jahng D. Combustion characteristics of biodried sewage sludge. Waste Manag [Internet]. Elsevier Ltd; 2018;72:296–305. Available from: https://doi.org/10.1016/j.wasman.2017.11.008

138. Fern C, Fierro J, Cara J, Martínez O, S ME. Oxy-combustion of corn, sunflower, rape and microalgae bioresidues and their blends from the perspective of thermogravimetric analysis. Energy. 2014;74:845–54.

139. Vamvuka D, Sfakiotakis S. Thermochimica Acta Combustion behaviour of biomass fuels and their blends with lignite. Thermochim Acta [Internet]. Elsevier B.V.; 2011;526(1-2):192–9. Available from: http://dx.doi.org/10.1016/j.tca.2011.09.021

140. Wang Z, Hong C, Xing Y, Li Y, Feng L, Jia M. Combustion behaviors and kinetics of sewage sludge blended with pulverized coal : With and without catalysts. Waste Manag [Internet]. Elsevier Ltd; 2018;xxx:xxx – xxx. Available from: https://doi.org/10.1016/j.wasman.2018.01.002

141. Garcia-maraver A, Perez-jimenez JA, Serrano-bernardo F. Determination and comparison of combustion kinetics parameters of agricultural biomass from olive trees. Renew Energy [Internet]. Elsevier Ltd; 2015;83:897–904. Available from: http://dx.doi.org/10.1016/j.renene.2015.05.049

142. Celaya AM, Lade AT, Goldfarb JL. Co-combustion of brewer' s spent grains and Illinois No . 6 coal : Impact of blend ratio on pyrolysis and oxidation behavior. Fuel Process Technol [Internet]. Elsevier B.V.; 2015;129(6):39–51. Available from: http://dx.doi.org/10.1016/j.fuproc.2014.08.004

143. Sima-ella E, Yuan G, Mays T. A simple kinetic analysis to determine the intrinsic reactivity of coal chars. Fuel. 2005;84:1920–5.

144. Yangali P, Celaya AM, Goldfarb JL. Co-pyrolysis reaction rates and activation energies of West Virginia coal and cherry pit blends. J Anal Appl Pyrolysis [Internet]. Elsevier B.V.; 2014;108:203–11. Available from: http://dx.doi.org/10.1016/j.jaap.2014.04.015

145. Karimian M, Schaffie M, Hassan M. Determination of activation energy as a function of conversion for the oxidation of heavy and light crude oils in relation to in situ combustion. J Therm Anal Calorim [Internet]. Springer Netherlands; 2016;125(1):301–11. Available from: "http://dx.doi.org/10.1007/s10973-016-5439-1

146. Álvarez A, Pizarro C, García R, Bueno JL, Lavín AG. Determination of kinetic parameters for biomass combustion. Bioresour Technol. 2016;216:36–43.

147. Syed S, Qudaih R, Talab I, Janajreh I. Kinetics of pyrolysis and combustion of oil shale sample from thermogravimetric data. Fuel [Internet]. Elsevier Ltd; 2011;90(4):1631–7. Available from: http://dx.doi.org/10.1016/j.fuel.2010.10.033

148. Plis A, Lasek J. Thermochemical and kinetic analysis of the pyrolysis process in Cladophora glomerata algae. J Anal Appl Pyrolysis. 2015;115(July 2012):166–74.

149. Vamvuka D, Sfakiotakis S, Saxioni S. Evaluation of urban wastes as promising co-fuels for energy production – A TG / MS study. FUEL [Internet]. Elsevier Ltd; 2015;147:170–83. Available from: http://dx.doi.org/10.1016/j.fuel.2015.01.070

150. Karimian M, Scha M, Hassan M. Estimation of the kinetic triplet for in-situ combustion of crude oil in the presence of limestone matrix. Fuel. 2017;209(July):203–10.

151. Varol M, Atimtay AT, Bay B, Olgun H. Investigation of co-combustion

characteristics of low quality lignite coals and biomass with thermogravimetric analysis. Thermochim Acta [Internet]. Elsevier B.V.; 2010;510(1-2):195–201. Available from: http://dx.doi.org/10.1016/j.tca.2010.07.014

152. Ali SAM, Razzak SA, Hossain MM. Apparent kinetics of high temperature oxidative decomposition of microalgal biomass. Bioresour Technol [Internet]. Elsevier Ltd; 2015;175:569–77. Available from: http://dx.doi.org/10.1016/j.biortech.2014.10.109

153. Liu X, Chen M, Wei Y. Kinetics based on two-stage scheme for co-combustion of herbaceous biomass and bituminous coal. FUEL [Internet]. Elsevier Ltd; 2015;143:577–85. Available from: http://dx.doi.org/10.1016/j.fuel.2014.11.085

154. Kök M V. Thermal Analysis Applications In Fossil Fuel Science. Literature survey. J Therm Anal Calorim [Internet]. 2002;68(3):1061–77. Available from: https://link.springer.com/article/10.1023/A:1016119428815

155. Khawam A, Flanagan DR. Solid-State Kinetic Models : Basics and Mathematical Fundamentals. J Phys Chem [Internet]. 2006;110(35):17315–28. Available from: https://cdn-pubs.acs.org/doi/10.1021/jp062746a [cited 2014.05.021]

156. Gil M V, Casal D, Pevida C, Pis JJ, Rubiera F. Thermal behaviour and kinetics of coal / biomass blends during co-combustion. Bioresour Technol [Internet]. Elsevier Ltd; 2010;101(14):5601–8. Available from: http://dx.doi.org/10.1016/j.biortech.2010.02.008

157. Lu H, Robert W, Peirce G, Ripa B, Baxter LL. Comprehensive Study of Biomass Particle Combustion. Energy & fuels. 2008;22(4):2826–39.

158. Kumar A, Gupta P, Goyal T, Kumar R. Modelling of pyrolysis of coal – biomass blends using thermogravimetric analysis. Bioresour Technol [Internet]. 2008;99(17):8022–6. Available from: http://www.sciencedirect.com/science/article/pii/S0960852408002903 [cited 2014.04.029]

159. Kastanaki E, Vamvuka D. A comparative reactivity and kinetic study on the combustion of coal – biomass char blends. Fuel [Internet]. 2006;85(9):1186–93. Available from: http://www.sciencedirect.com/science/article/pii/S0016236105004461 [cited

2014.04.029]

160. Otero M, Sánchez ME, Gómez X. Co-firing of coal and manure biomass: a TG-MS approach. Bioresour Technol. Elsevier Ltd; 2011 Sep;102(17):8304–9.

161. Sharara M, Sadaka S. Thermogravimetric Analysis of Swine Manure Solids Obtained from Farrowing , and Growing-Finishing Farms. 2014;(March):75–86.

162. Lin Y, Ma X, Yu Z, Cao Y. Investigation on thermochemical behavior of co-pyrolysis between oil-palm solid wastes and paper sludge. Bioresour Technol [Internet]. Elsevier Ltd; 2014;166:444–50. Available from: http://dx.doi.org/10.1016/j.biortech.2014.05.101

163. Niu SL, Lu CM, Han KH, Zhao JL. Thermogravimetric analysis of combustion characteristics and kinetic parameters of pulverized coals in oxy-fuel atmosphere. J Therm Anal Calorim. 2009;98(1):267–74.

164. Vossoughi S, El-Shoubary Y. Kinetics of Crude Oil Coke Combustion. Soc Pet Eng [Internet]. 1989;83:201–6. Available from: https://www.onepetro.org/conference-paper/SPE-16268-MS [cited 2016.04.025]

165. Shawalliah S, Abd N, Ismail K, Bahari A, Abd Z. Investigation on thermochemical behaviour of low rank Malaysian coal , oil palm biomass and their blends during pyrolysis via thermogravimetric analysis (TGA). Bioresour Technol [Internet]. Elsevier Ltd; 2010;101(12):4584–92. Available from: http://dx.doi.org/10.1016/j.biortech.2010.01.059

166. Ozbas KE, Kök M V., Hicyilmaz C. Comparative kinetic analysis of raw and cleaned coals. J Therm Anal Calorim. 2002;69(2):541–9.

167. Korkut Açıkalın. Pyrolytic characteristics and kinetics of pistachio shell by thermogravimetric analysis. J Therm Anal Calorim [Internet]. 2012;109(1):227–35. Available from: http://akademiai.com/doi/abs/10.1007/s10973-011-1714-3

168. Tonbul Y. Pyrolysis of Pistachio shell as a Biomass. J Therm Anal Calorim [Internet]. 2008;91(2):641–7. Available from: https://link.springer.com/article/10.1007/s10973-007-8428-6 [cited 2015.12.022]

169. Vuthaluru H. Investigations into the pyrolytic behaviour of coal/biomass blends

using thermogravimetric analysis. Bioresour Technol. 2004 Apr;92(2):187–95.

170. Liang XH, Kozinski JA. Numerical modeling of combustion and pyrolysis of cellulosic biomass in thermogravimetric systems. 2000;79(0016).

171. Safi MJ, Mishra IM, Prasad B. Global degradation kinetics of pine needles in air. Thermochim Acta. 2004;412(1-2):155–62.

172. Chen G, Ma X, Lin M, Lin Y, Yu Z. Study on thermochemical kinetic characteristics and interaction during low temperature oxidation of blended coals. J Energy Inst [Internet]. Elsevier Ltd; 2015;88(3):221–8. Available from: http://dx.doi.org/10.1016/j.joei.2014.09.007

173. House JE. Principles of Chemical Kinetics.pdf. 1977. 244 p.

174. Ozbas KE, Kök M V, Hicyilmaz C. Comparative Kinetic Analysis of raw and cleaned coals. 2002;69:541–9.

175. Mehta SK, Kaur R, Singh S. Thermogravimetric evaluation of decomposition kinetics of metal surfactant complexes. J Therm Anal Calorim. 2012;107(1):69–75.

176. Cai J, Liu R. Kinetic Analysis of Solid-State Reactions : A General Empirical Kinetic Model. 2009;3249–53.

177. Luangkiattikhun P, Tangsathitkulchai C, Tangsathitkulchai M. Non-isothermal thermogravimetric analysis of oil-palm solid wastes. Bioresour Technol. 2008;99:986–97.

178. Vyazovkin S, Wight CA. Model-free and model-fitting approaches to kinetic analysis of isothermal and nonisothermal data. 1999;341:53–68.

179. Grierson S, Strezov V, Ellem G, Mcgregor R, Herbertson J. Thermal characterisation of microalgae under slow pyrolysis conditions. J Anal Appl Pyrolysis. 2009 May;85(1-2):118–23.

180. Aboulkas A, El harfi K, El bouadili A. Kinetic and mechanism of Tarfaya (Morocco) oil shale and LDPE mixture pyrolysis. J Mater Process Technol. 2008 Sep;206(1-3):16–24.

181. Vyazovki S. WC. Isothermal and non-isotherm al kinetics of therm ally stimulated reactions of solids. Int Rev Phys Chem. 1998;17(3):407–33.

182. Sciazko M. Application of Solid State Kinetics to Coal Pyrolysis Reaction [Internet]. Available from: http://home.agh.edu.pl/~lstepien/Gasification/Lectures/L8-3.pdf [cited 2017.05.012]

183. Šesták J. Rationale and fallacy of thermoanalytical kinetic patterns. J Therm Anal Calorim. 2011 Dec 21;110(1):5–16.

184. Guo J, Lua AC. Kinetic study on pyrolytic process of oil-palm solid waste using two-step consecutive reaction model. Biomass and Bioenergy. 2001;20:223–33.

185. López-González D, Fernandez-Lopez M, Valverde JL S-SL. Thermogravimetric-mass spectrometric analysis on combustion of lignocellulosic biomass. Bioresour Technol. 2013;143:562–74.

186. Perejón A, Sánchez-jiménez PE, Criado JM, Pérez-maqueda LA. Kinetic analysis of complex solid state reactions. A new deconvolution procedure. J Phys Chem. 2011;115 (8):1780–91.

187. Vaimakis TC. Thermogravimetry (TG) or Thermogravimetric Analysis (TGA). J Anal Appl Pyrolysis [Internet]. 2015;1–15. Available from: https://www.researchgate.net/publication/287813187 [cited 2017.03.024]

188. Tait B. Techno-Economics of Microalgae to Coalgae ®. Port Elizabeth; 2014.

189. James G S. Handbook of Coal Analysis. New Jersey: John Willey & Sons Inc.; 2005. 2005 p.

190. Panalytical. EPSILON 3 XLTechnical specification [Internet]. AA Almelo; 2003. Available from: http://www.analytical.ru/epsilon3xl.pdf [cited 2015.06.012]

191. Baysal M, Yürüm A, Burçin Y, Yürüm Y. Structure of some western Anatolia coals investigated by FTIR , Raman , C solid state NMR spectroscopy and X-ray diffraction. Int J Coal Geol. 2016;163:166–76.

192. Xiumin J, Chuguang Z, Jianrong Q, Jubin L, Dechang L. Combustion Characteristics of Super Fine Pulverized Coal Particles. Energy & fuels. 2001;15:1100–2.

193. Valverde JL. Pyrolysis , combustion and gasification characteristics of Nannochloropsis gaditana microalgae. Bioresour Technol [Internet].

2013;130:321–31. Available from: http://dx.doi.org/10.1016/j.biortech.2012.12.002

194. Wang Y, Song Y, Zhi K, Li Y, Teng Y, He R, et al. Combustion kinetics of Chinese Shenhua raw coal and its pyrolysis carbocoal. J Energy Inst [Internet]. Elsevier Ltd; 2017;90(4):624–33. Available from: http://dx.doi.org/10.1016/j.joei.2016.04.011

195. Makhula M.J., Bada S.O., Falcon R.M.S., Falcon L.M. Thermogravimetric investigation of macadamia nutshell, coal, and anthracite in different combustion atmospheres. J South African Inst Min Metall [Internet]. 2015;115:17159. Available from: http://dx.doi.org/10.17159/2411-9717/2015/V115N8A10

196. Shawalliah S, Abd N, Ismail K. Combustion characteristics of Malaysian oil palm biomass, sub-bituminous coal and their respective blends via thermogravimetric analysis (TGA). Bioresour Technol [Internet]. Elsevier Ltd; 2012;123:581–91. Available from: http://dx.doi.org/10.1016/j.biortech.2012.07.065

197. Huang L, Liu J, He Y, Sun S, Chen J, Sun J, et al. Thermodynamics and kinetics parameters of co-combustion between sewage sludge and water hyacinth in CO2/O2 atmosphere as biomass to solid biofuel. Bioresour Technol [Internet]. Elsevier Ltd; 2016;218:631–42. Available from: http://dx.doi.org/10.1016/j.biortech.2016.06.133

198. Xie W, Huang J, Liu J, Zhao Y, Chang K, Kuo J, et al. Assessing thermal behaviors and kinetics of (co-) combustion of textile dyeing sludge and sugarcane bagasse. Appl Therm Eng [Internet]. Elsevier Ltd; 2018;131:874–83. Available from: https://doi.org/10.1016/j.applthermaleng.2017.11.025

199. Kastanaki E, Vamvuka D, Grammelis P, Kakaras E. Thermogravimetric studies of the behavior of lignite-biomass blends during devolatilization. Fuel Process Technol. 2002;78:159–66.

200. Kastanaki E, Vamvuka D. A comparative reactivity and kinetic study on the combustion of coal – biomass char blends. Fuel. 2006;85:1186–93.

201. Gil M V, Riaza J, Álvarez L, Pevida C, Pis JJ, Rubiera F. Kinetic models for the oxy-fuel combustion of coal and coal/biomass blend chars obtained in N2 and

CO2 atmospheres. Energy [Internet]. Elsevier Ltd; 2012;48(1):510–8. Available from: http://dx.doi.org/10.1016/j.energy.2012.10.033

202. Al-qayim K, Nimmo W, Hughes K, Pourkashanian M. Kinetic parameters of the intrinsic reactivity of woody biomass and coal chars via thermogravimetric analysis. Fuel [Internet]. Elsevier; 2017;210(April):811–25. Available from: http://dx.doi.org/10.1016/j.fuel.2017.09.010

203. Dhyani V, Bhaskar T. A comprehensive review on the pyrolysis of lignocellulosic biomass. Renew Energy [Internet]. Elsevier Ltd; 2017;(xxx):1–22. Available from: http://dx.doi.org/10.1016/j.renene.2017.04.035

204. Liu K. Characterization of ash in algae and other materials by determination of wet acid indigestible ash and microscopic examination. Algal Res [Internet]. Elsevier; 2017;25(April):307–21. Available from: http://dx.doi.org/10.1016/j.algal.2017.04.014

205. Ullah H, Liu G, Yousaf B, Ubaid M, Abbas Q. Combustion characteristics and retention-emission of selenium during co-fi ring of torrefied biomass and its blends with high ash coal. Bioresour Technol [Internet]. Elsevier; 2017;245(August):73–80. Available from: http://dx.doi.org/10.1016/j.biortech.2017.08.144

206. Yang Z, Zhang Y, Liu L, Wang X, Zhang Z. Environmental investigation on co-combustion of sewage sludge and coal gangue : SO2, NOx and trace elements emissions. Waste Manag [Internet]. Elsevier Ltd; 2016;50(x):213–21. Available from: http://dx.doi.org/10.1016/j.wasman.2015.11.011

207. Schweinfurth BSP. An Introduction to Coal Quality. The National Coal Resource Assessment Overview. U.S. Geological Survey, Reston, Virginia: 2009; 2009. p. 16.

208. Cheng J, Zhou J, Liu J, Zhou Z, Huang Z, Cao X, et al. Sulfur removal at high temperature during coal combustion in furnaces : a review. 2003;29:381–405.

209. Stanger R, Wall T. Sulphur impacts during pulverised coal combustion in oxy-fuel technology for carbon capture and storage. Prog Energy Combust Sci [Internet]. Elsevier Ltd; 2011;37(1):69–88. Available from: http://dx.doi.org/10.1016/j.pecs.2010.04.001

210. Ma B, Li X, Xu L, Wang K, Wang X. Investigation on catalyzed combustion of high ash coal by thermogravimetric analysis. Thermochim Acta. 2006;445:19–22.

211. Vassilev S V, Baxter D, Andersen LK, Vassileva CG. An overview of the chemical composition of biomass. Fuel [Internet]. Elsevier Ltd; 2010;89(5):913–33. Available from: http://dx.doi.org/10.1016/j.fuel.2009.10.022

212. Ã CW, Wang F, Yang Q, Liang R. Thermogravimetric studies of the behavior of wheat straw with added coal during combustion. Biomass and Bioenergy. 2009;33:50–6.

213. Murphy JJ, Shaddix CR. Combustion kinetics of coal chars in oxygen-enriched environments. Combust Flame. 2006;144:710–29.

214. Kök M V, Acar C. Kinetics of Crude Oil Combustion. J Therm Anal Calorim. 2006;83:445–9.

215. Riaza J, Gil M V, Álvarez L, Pevida C, Pis JJ, Rubiera F. Oxy-fuel combustion of coal and biomass blends. Energy [Internet]. Elsevier Ltd; 2012;41(1):429–35. Available from: http://dx.doi.org/10.1016/j.energy.2012.02.057

216. Moon C, Sung Y, Ahn S, Kim T, Choi G, Kim D. Effect of blending ratio on combustion performance in blends of biomass and coals of different ranks. Exp Therm Fluid Sci [Internet]. 2013;47:232–40. Available from: http://dx.doi.org/10.1016/j.expthermflusci.2013.01.019

217. Farrow TS, Sun C, Snape CE. Impact of biomass char on coal char burn-out under air and oxy-fuel conditions. Fuel [Internet]. Elsevier Ltd; 2013;114:128–34. Available from: http://dx.doi.org/10.1016/j.fuel.2012.07.073

218. Legemza J, Findora L. Thermal degradation and kinetic study of sawdusts and walnut shells via thermal analysis. J Therm Anal Calorim. 2016;125(2):689–94.

219. Yang W, Wang H, Zhang M, Zhu J, Zhou J, Wu S. Fuel properties and combustion kinetics of hydrochar prepared by hydrothermal carbonization of bamboo. Bioresour Technol [Internet]. Elsevier Ltd; 2016;205:199–204. Available from: http://dx.doi.org/10.1016/j.biortech.2016.01.068

220. Hurt RH, Calo JM. Semi-global Intrinsic Kinetics for Char Combustion Modeling. Combust Flame. 2001;125(3):1138–49.

221. Russell N V. Development of TG measurements of intrinsic char combustion reactivity for industrial and research purposes. Fuel Process Technol [Internet]. 1998;57(2):113–30. Available from: https://www.sciencedirect.com/science/article/pii/S0378382098000770 [cited 2016.09.011]

222. Ahn DH, Gibbs BM, Ko KH, Kim JJ. Gasification kinetics of an Indonesian sub-bituminous coal-char with CO 2 at elevated pressure. Fuel [Internet]. 2001;80(11):1651–8. Available from: https://www.sciencedirect.com/science/article/pii/S0016236101000242 [cited 2016.09.011]

223. Xu Q, Li J, Xie A. Kinetic studies on combustion of microalgae under different oxygen concentrations. Materials for Renewable Energy and Environment (ICMREE), 2013 International Conference [Internet]. Chengdu, China: IEEE; 2014. p. 1–5. Available from: http://ieeexplore.ieee.org/stamp/stamp.jsp?tp=&arnumber=6893672 [cited 2018.01.023]

224. Tang Y, Ma X, Lai Z. Thermogravimetric analysis of the combustion of microalgae and microalgae blended with waste in N2/O2 and CO2/O2 atmospheres. Bioresour Technol [Internet]. Elsevier Ltd; 2011;102(2):1879–85. Available from: http://dx.doi.org/10.1016/j.biortech.2010.07.088

225. Williams A, Jones JM, Ma L, Pourkashanian M. Pollutants from the combustion of solid biomass fuels. Progess Energy Combust Sci. 2012;38(2):113–37.

226. Guedea I, Pallarès D, Díez LI, Johnsson F. Conversion of large coal particles under O2/N2 and O2/CO2 atmospheres — Experiments and modeling. Fuel Process Technol [Internet]. Elsevier B.V.; 2013;112:118–28. Available from: http://dx.doi.org/10.1016/j.fuproc.2013.02.023

227. Jia, C., Wang, Q., Ge J et al. Pyrolysis and combustion model of oil sands from non-isothermal thermogravimetric analysis data. J Therm Anal Calorim. 2014;116(1073):10973.

Appendix

(The raw data for this research is organised separately on CD due the volume)

A – Figures

Chapter 2

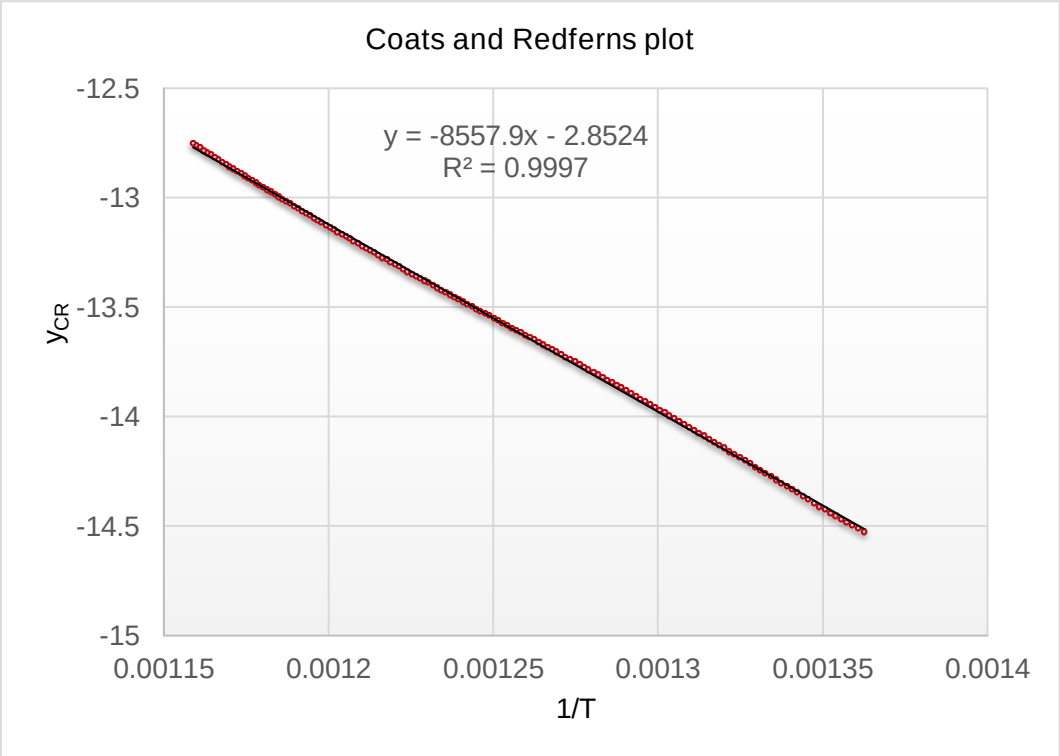

Figure 1: Coats and Redfern kinetics – coal

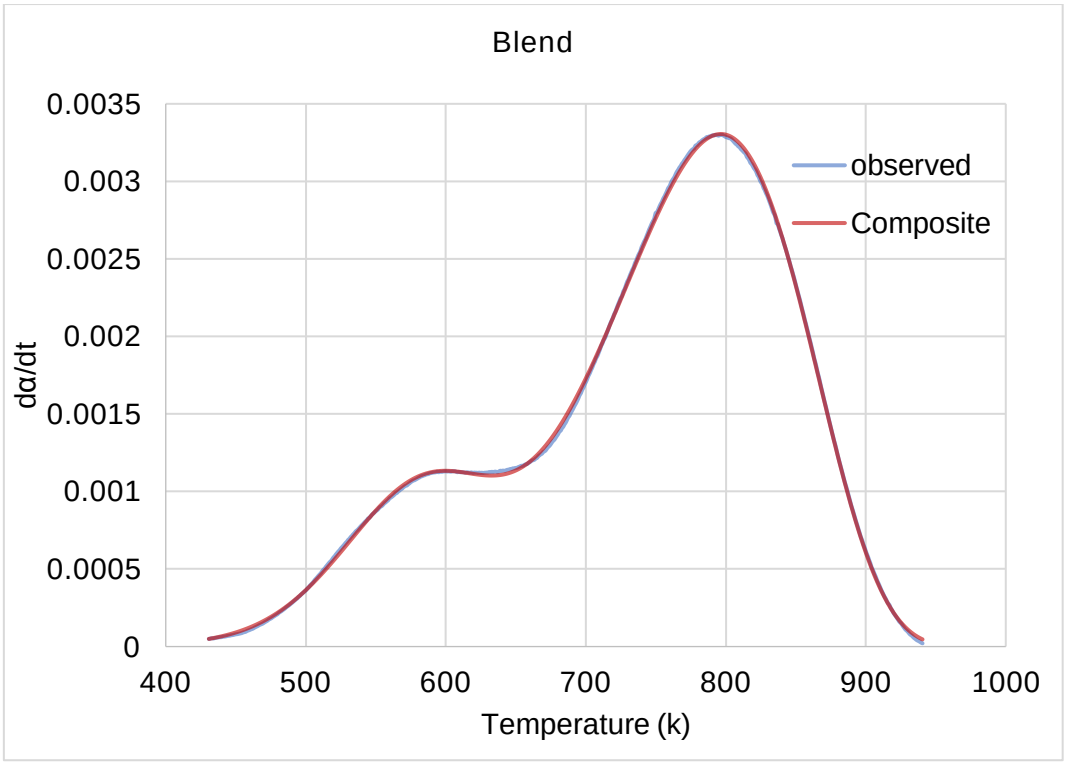

Figure 2: Typical DTG combustion

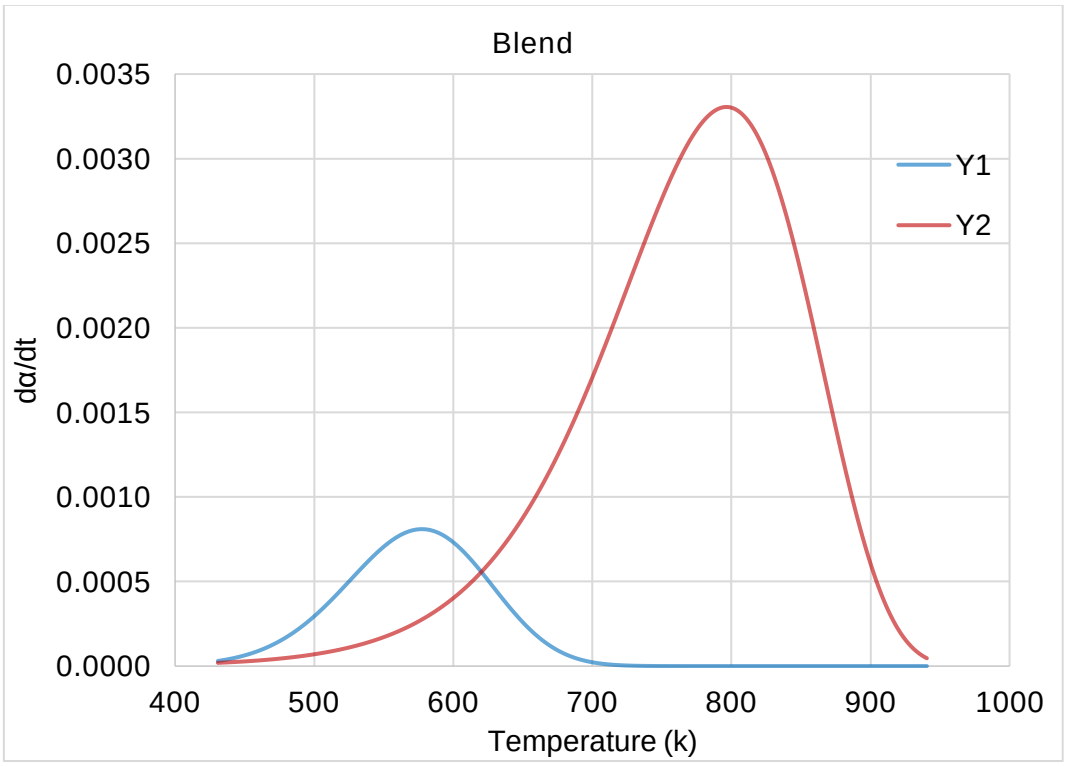

Figure 3: Typical deconvolution of combustion

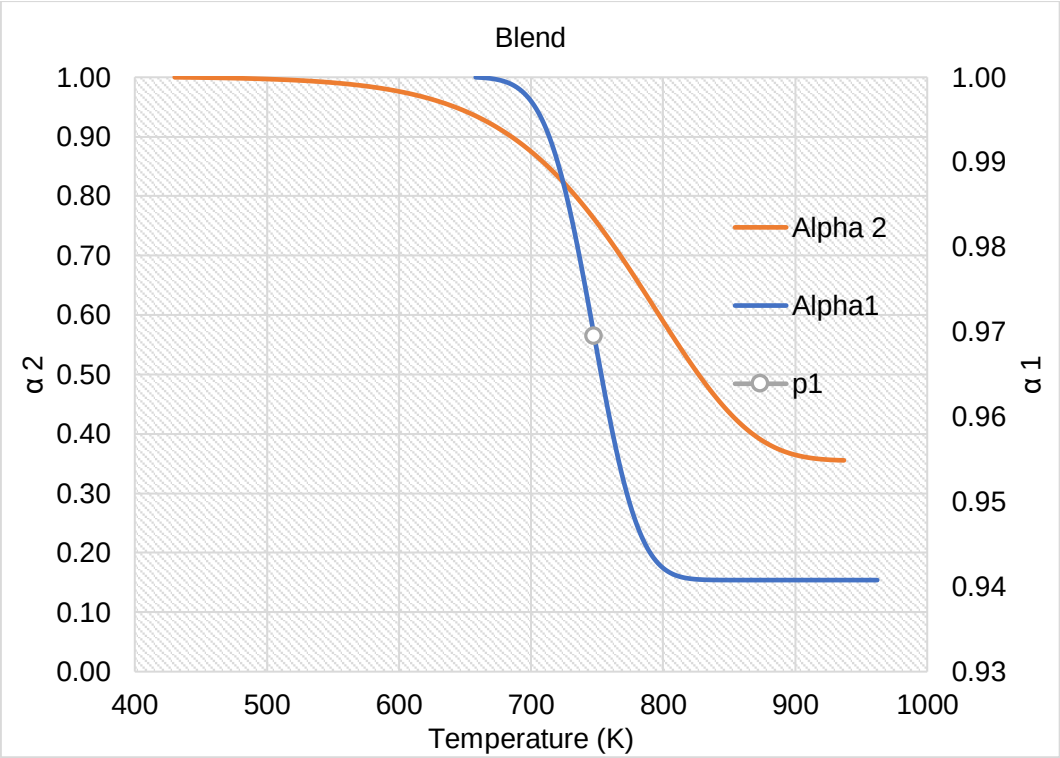

Figure 4: Areas under low and high combustion

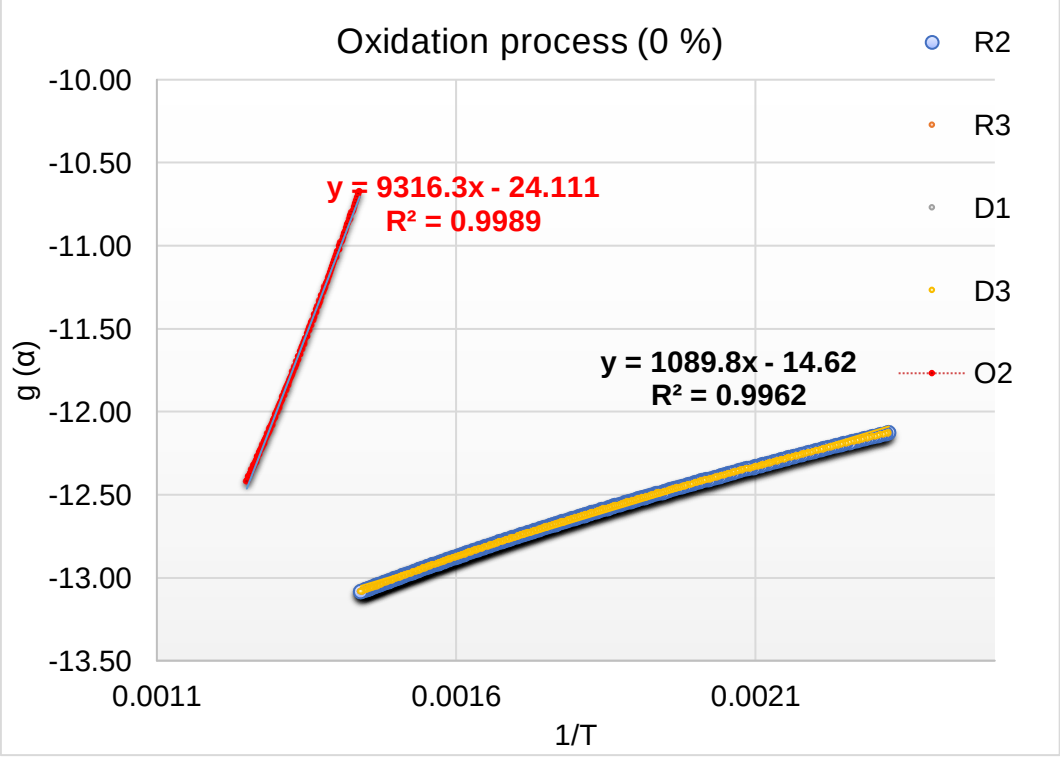

Figure 5: Mechanisms – Low and high temperature schemes

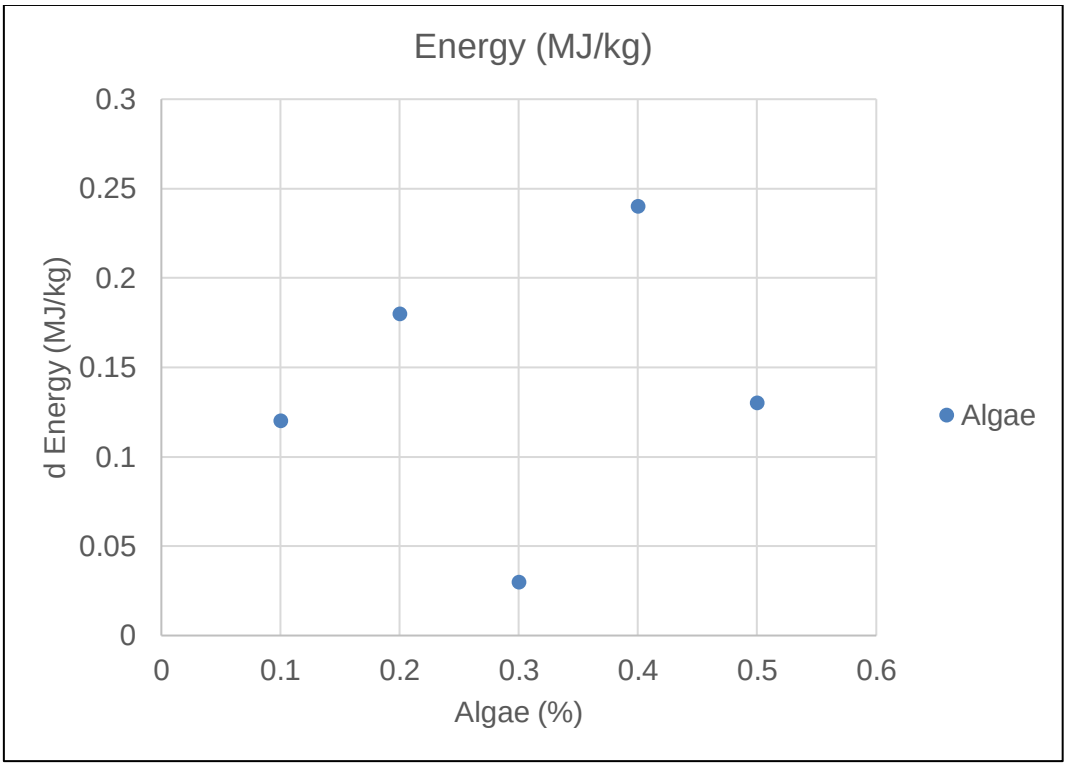

Figure 7: Change in heat energy with increase in algae biomass

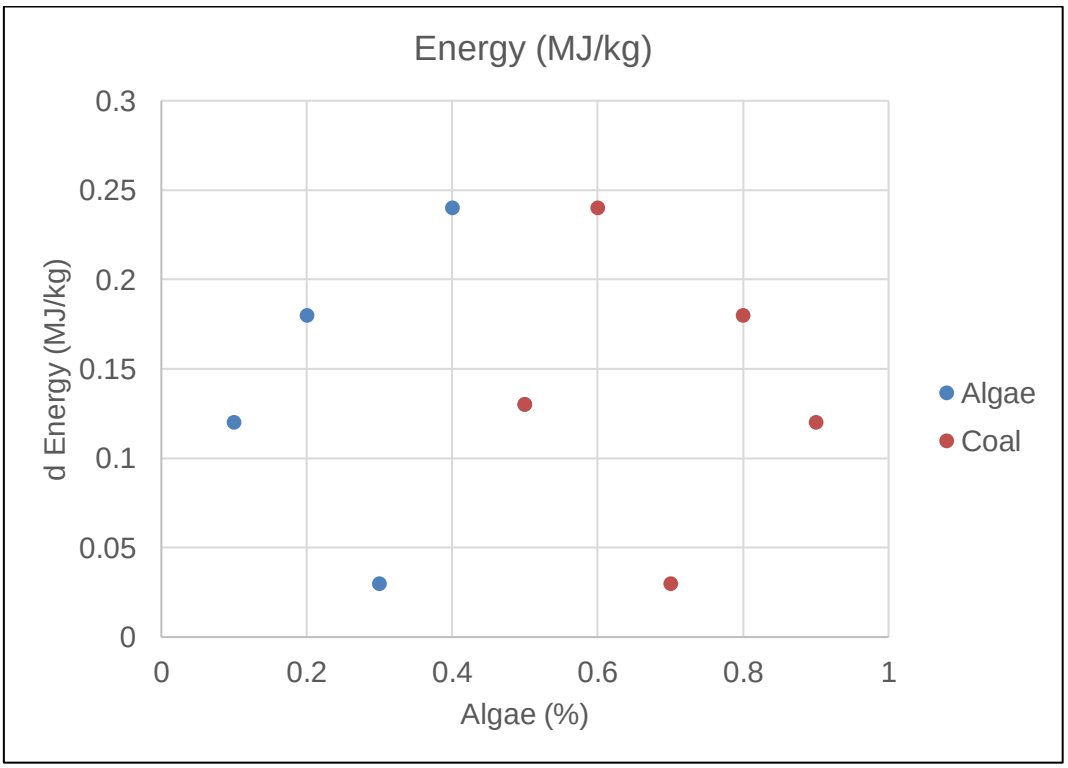

Figure 7: Change in heat energy with increase in algae and coal

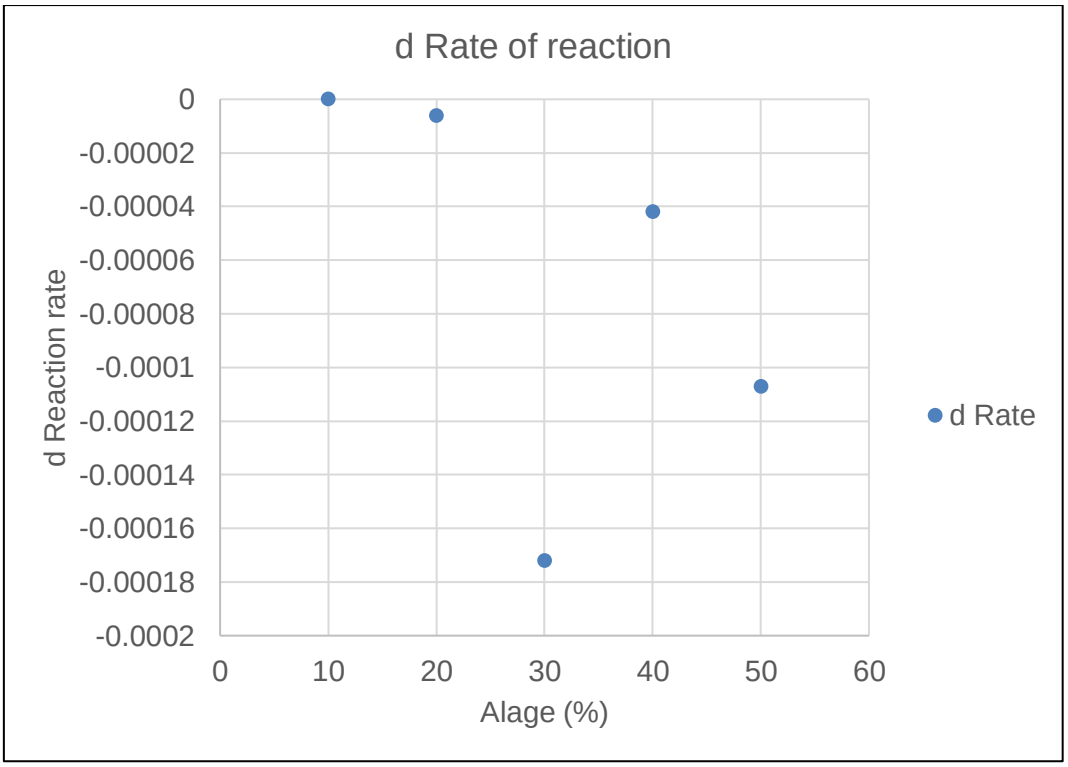

Figure 8: Change in rate of reaction with increase in algae biomass

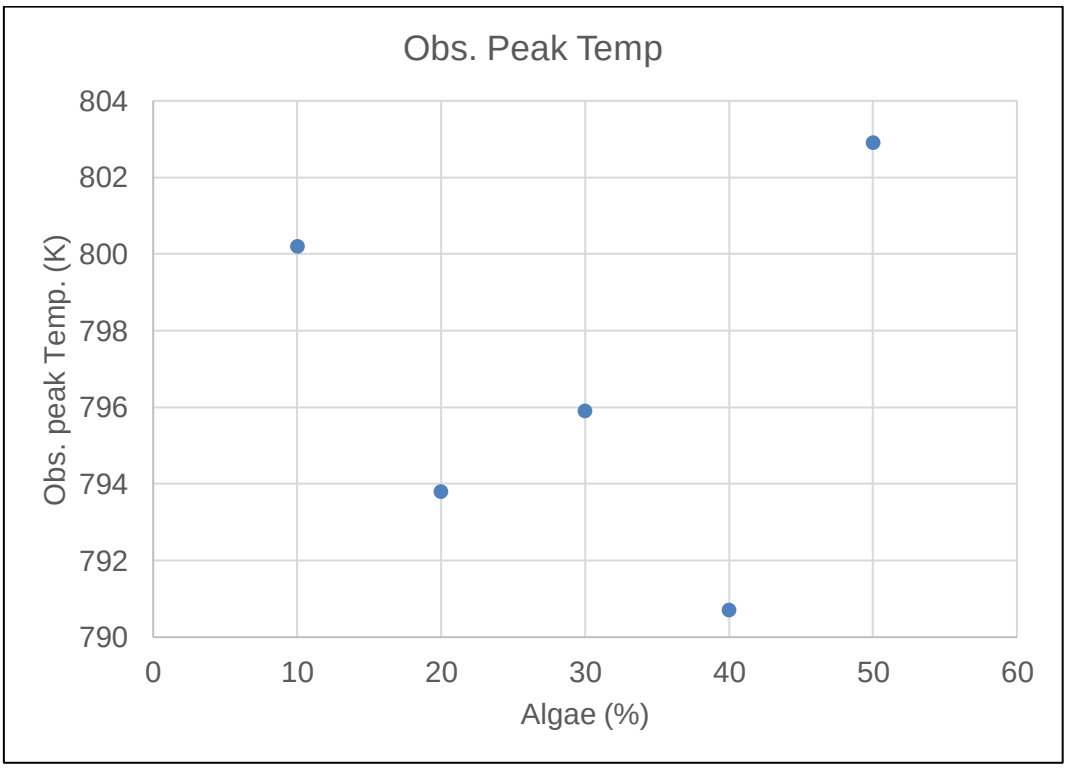

Figure 9: Observed peak combustion temp. with increase in algae biomass

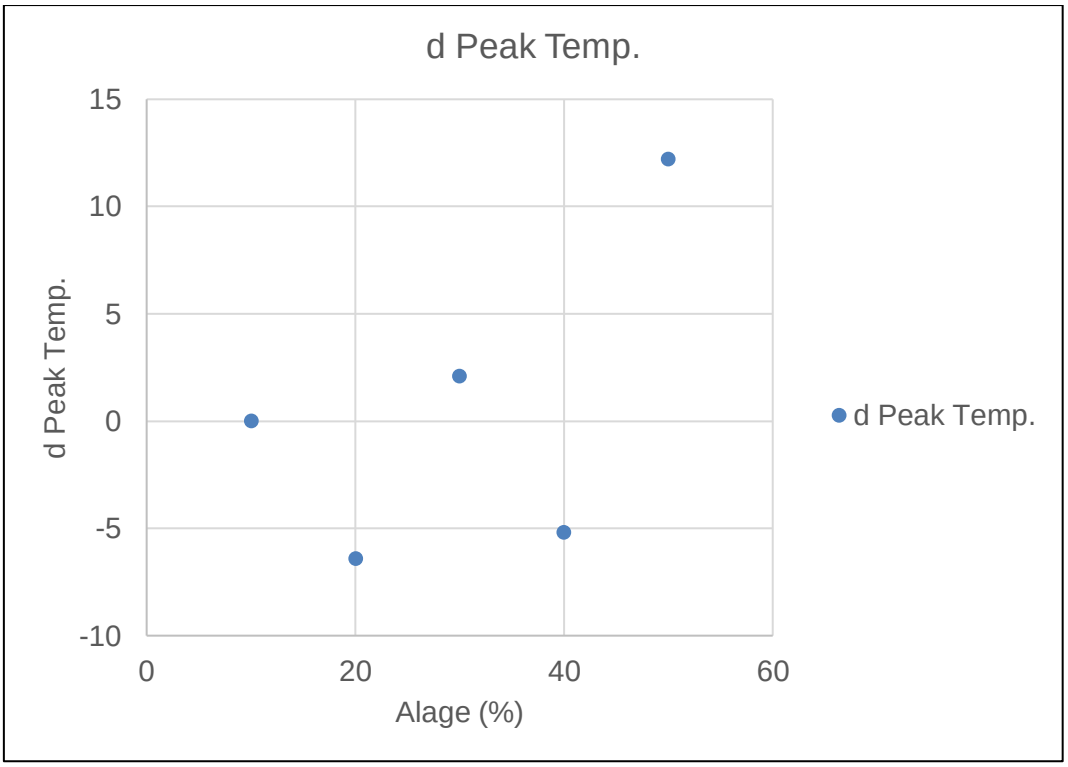

Figure 10: Change in peak combustion temp. with increase in algae biomass

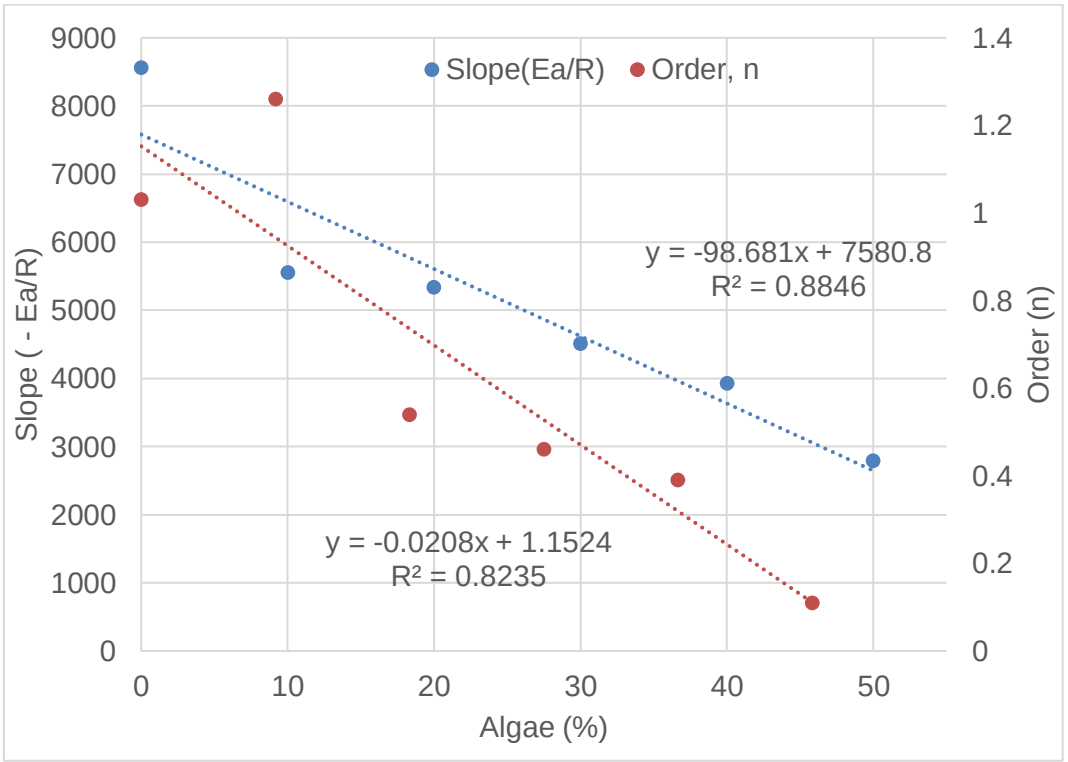

Figure 11: Change in slope and reaction order with increase in algae biomass

B – Tables

Chapter 2

Table 1: combustion parameters

Parameters	***E a***	***m***	***Tig***	***Th***	***Tmax***	***DTG max***	***DTG mean***	***Δ t 1/2***	***S***	***H***	***n***	***Ash***
100C-00A	*72.2 ± 5.6*	*8681.66 ± 671.28*	*694.80± 5.1*	*918.33 ± 4.28*	*720.00 ± 4.3*	*0.0037 ± 0.0002*	*0.00096 ± 6.77E-06*	*146 ± 8.22*	*0.797 ± 0.03*	*0.010 ± 0.0001*	*1.03 ± 0.02*	*0.3191 ± 0.0116*

Table 2: Combustion parameters

Combustion Parameters											
Gradient	E a **(kJ/mol)**	$T_{i\,g}$ **(K)**	T_h**(K)**	t_{max} **(K)**	DTGmax	DTG mean	Δ T ½ **(K)**	***S***	H	n	M/Mo (ash) mg
8558	71.15	694.7	920	799.0	0.0036	0.0010	147.59	**0.791**	0.011	1	0.319

Table 3: TG and DTG data

90C-10A, 10 %									
Time (**min.**)	**Mass** (mg)	**Program Temp.** (^{0}C)	**Sample Temp.** ***T*** (^{0}C)	**(dm/dT)**	**m/m_0**	**T (K)**	α	**1/T**	**Y CR**
5.03333	5.126371	40	40.55667	8.44E-05	1	313.5567	0	0.0031	#NUM!
5.08965	5.126299	40.84479	40.56167	0.000717	0.9999	313.5617	2.01E-05	0.0031	-22.3089

Table 4: Theoretical and observed rates of combustion

%A	Observed rate (dm/dT)	Theoretical rate (dm/dT)	Difference (%)	SS	Observed Temp (K)	Theoretical Temp (K)	Difference (%)
10	0.003478	0.003502	-0.7	3.26E-06	800.2	800.5	0.031033

Table 5: Deconvolution and area under curve

T (K)	1/T	(dm/dT)	Combustion stages	Y1	Y2	Area under stages	DA1	DA2	Conversion per stage	α1	α2
430.425	0.0023	1.265E-05		9E-08	2E-05		8E-08	2E-05		8E-08	2E-05
,,	,,	,,		,,	,,		,,	,,		,,	,,
950.610		2.657E-05		6E-210	7E-05		-3E-207	-4E-02		9E-03	6E-01

Table 6: Oxidation model g $(\propto)$ *examined for* Y_1 *and* Y_2

O1	O2	O3	R 2	R 3	D1	D2	D3	D4
-16.3520	0.0000	0.0000	-17.0452	-17.4607	-32.7040	-33.3829	-34.9214	#NUM!
,,	,,	,,	,,	,,	,,	,,	,,	,,
-4.7581	0.0086	0.0172	-5.4534	-5.8682	-9.5247	-10.2150	-11.7363	#NUM!

Table 7: Mechanism – low temperature

De-convoluted stage A, Y1 = α1, De-volatilization										
Composites (Fuels)	**Algae (%)**	**Ignition temp. Tig (K)**	**Temp. @ peak T p (K)**	**Conversion @ peak α p (mg)**	**Rate at peak d α/dT(p)**	**Reaction Mechanism**	**Corr. sq. R^2**	**Slope m**	**Activation E a (KJ/Mol.)**	**Frequency Factor c**
100C-00A	**0**	-	430.47	1.0000	0.0000	***R2, R3, D1, D3***	0.9962	1089.8	**9.06**	**-14.62**

Table 8 Mechanism – high temperature

De-convoluted stage B, Y2 = α2, Char combustion										
Composites (Fuels)	**Algae (%)**	**Ignition temp. Tig (K)**	**Temp. at peak T p (K)**	**Conversion @ peak α p (mg)**	**Rate at peak d α/dT(p)**	**Reaction Mechanism**	**Corr. sq. R^2**	**Slope m**	**Activation E a (KJ/Mol.)**	**Frequency Factor c**
100C-00A	**0**	694.85	799.83	0.6119	0.0037	***O2***	0.9989	9316.3	**77.46**	**-24.11**

Table 9 Activation energy – stages A and B

(%) Algae	**Mechanism**	**Stage (A) Devolatilization**				**Stage (B) Char combustion**			
(%)	Model g(α)	Corr. (R^2)	Slope (m)	Act. Energy E a	Intercept (c)	Corr. (R^2)	Slope (m)	Act. Energy E a	Intercept (c)
0 (Coal)	**O1**	**0**	**0**	**0.0000**	**0**	**0.9982**	**-8917.3**	**72.5333**	**-2.3808**
	O2	0	0	0.0000	0	0.4873	-4843.2	39.3946	-5.353
	O3	0	0	0.0000	0	0.5521	-11134	90.5640	4.4876
	R 2	0	0	0.0000	0	0.9882	-0.0024	0.0000	3.00E-06
	R 3	0	0	0.0000	0	0.9882	-0.0016	0.0000	2.00E-06
	D1	0	0	0.0000	0	0.9655	-14157	115.1530	2.5986
	D2	0	0	0.0000	0	0	0	0.0000	0
	D3	0	0	0.0000	0	0.0393	78.425	-0.6379	-13.776
	D4	0	0	0.0000	0	0.8182	1737.5	-14.1328	-2.7803

Table 10 Calculated Energy (HHV) values

Microalgae		Blend	Parikh etal		Dulong's	Microalgae continued		Blend	Parikh etal		Dulong's
		Sample	**HHV (MJ/kg)**	**Fuel ratio**	**HHV (MJ/kg)**			**Sample**	**HHV (MJ/kg)**	**Fuel ratio**	**HHV (MJ/kg)**
Algae		*100A*	17.02	0.21	21.3	45	13.5401	*55C-45A*	19.67	1.47	21.5
(%)		*100A*	17.02	0.21	19.3	55	18.0821	*45C-55A*	19.62	1.34	21.8
Label	**Actual**	*100C*	19.99	2.04	22.5	10	2.0531	*90C-10A*	**19.85**	1.91	**22.7**
0	0.0311	*100C*	**19.99**	2.04	**22.1**	20	4.6351	*80C-20A*	19.85	1.86	21.7
10	2.0531	*90C-10A*	**19.96**	1.98	**22.7**	30	7.7771	*70C-30A*	19.89	1.78	21.8
20	4.6351	*80C-20A*	19.82	1.86	23.2	40	11.4791	*60C-40A*	19.92	1.65	22.5
30	7.7771	*70C-30A*	19.88	1.74	21.1	5	0.9721	*95C-05A*	19.94	1.97	22.4
40	11.4791	*60C-40A*	19.85	1.65	21.6	15	3.2741	*85C-15A*	19.85	1.89	22.2
5	0.9721	*95C-05A*	19.95	2.03	22.1	25	6.1361	*75C-25A*	19.74	1.71	21.3
15	3.2741	*85C-15A*	19.92	1.89	22.3	35	9.5581	*65C-35A*	19.74	1.60	21.9
25	6.1361	*75C-25A*	19.82	1.75	21.6	45	13.5401	*55C-45A*	19.57	1.44	21.1
35	9.5581	*65C-35A*	19.79	1.62	21.8	55	18.0821	*45C-55A*	19.50	1.32	22.5

Chapter 3

Table 10: Change in kinetics as described by Coats and Redfern's model

Coalgae kinetic parameters deduced from Coats-Redfern and Arrhenius Equations							
Order		Fuels		Rate of Reaction	(E a/R)	Freq. of collision	Corr. Sq.
		Algae	**Coal**	Response	Slope (m)	Intercept (c)	
(n)	(±)	(%)	(%)	y =	(-m) x	(-c)	**(R^2)**
1.03	± 0.02	0	1	Faster	8557.9	2.8524	0.9997
1.26	± 0.75	0.10	0.9	Fastest	5556.7	7.168	0.9934
0.54	± 0.04	0.20	0.8	Fast	5337.5	6.8113	1
0.46	± 0.04	0.30	0.7	slow	4510.1	7.8407	0.9999
0.39	± 0.04	0.40	0.6	slower	3926.4	8.5401	0.9996
0.11	± 0.04	0.50	0.5	slowest	2793.9	10.092	0.9979

E a = activation energy, R = universal gas constant

NELSON MANDELA
UNIVERSITY

DECLARATION BY CANDIDATE

NAME: ___EJESIEME OBIALO VITUS_____

STUDENT NUMBER: ____211266744_____

QUALIFICATION: _PhD CHEMISTRY_____

TITLE OF PROJECT: AN INVESTIGATION OF THE COMBUSTION KINETICS OF COAL-MICROALGAE COMPOSITE

_____

_____

DECLARATION:

In accordance with Rule G5.6.3, I hereby declare that the above-mentioned treatise/ dissertation/ thesis is my own work and that it has not previously been submitted for assessment to another University or for another qualification.

SIGNATURE: _____  **_____**

DATE: _____03/09/2018_____